Tension on a stretcher: mechanical and morphological characteristics of canvas paintings supports

Iaccarino Idelson, A.

DOI
10.4233/uuid:f6cb374e-5095-45be-a705-561e675011f0

Publication date
2025

Document Version
Final published version

Citation (APA)
Iaccarino Idelson, A. (2025). *Tension on a stretcher: mechanical and morphological characteristics of canvas paintings supports*. [Dissertation (TU Delft), Delft University of Technology]. https://doi.org/10.4233/uuid:f6cb374e-5095-45be-a705-561e675011f0

Important note
To cite this publication, please use the final published version (if applicable).
Please check the document version above.

Tension on a stretcher: mechanical and morphological characteristics of canvas paintings supports

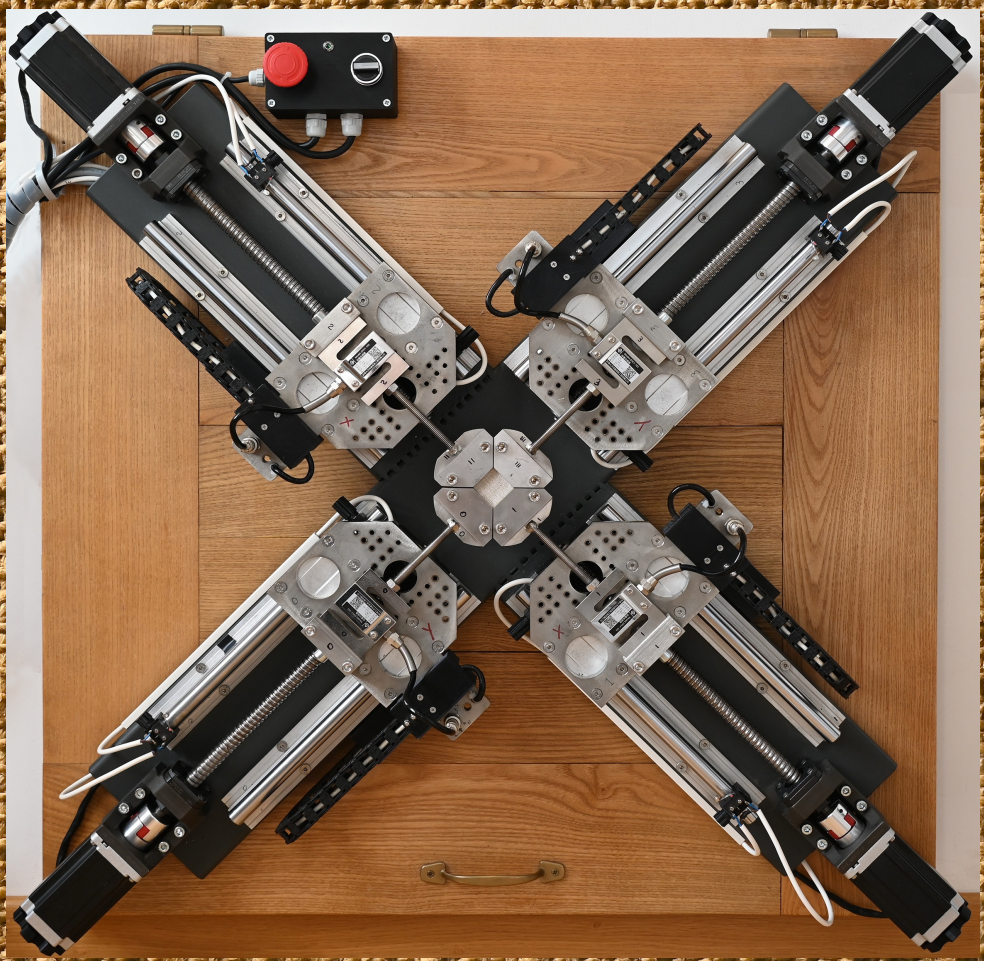

Antonio Iaccarino Idelson

Propositions

Accompanying the dissertation

Tension on a stretcher: mechanical and morphological characteristics of canvas paintings supports

by

Antonio Iaccarino Idelson

1. Until now, the high structural variability of historical textiles has hindered the ability of researchers to obtain measurable data on their morphology.

2. Biaxial tensile testing of historical textiles is necessary to reproduce their loading conditions and behavior on the painting's stretcher.

3. The value of tension of a painting on its stretcher is one of the most influential parameters on its conservation, but it is almost impossible to measure it in standard museum conditions.

4. Recurring characteristics in the structure of historical textiles allow a high degree of confidence in the identification of the warp and weft directions when a selvedge is not available.

5. The method of calculation of the elastic module of a textile woven in natural fibers is the prerogative of the engineer doing the work.

6. The value of tension of a painting on its stretcher is the second most influential parameter affecting its conservation after the painting's value.

7. Open-source hardware is more valuable than patenting research innovations.

8. Differences between civilizations spark philosophical debates that lead to Enlightenment in both conservation and aerospace engineering.

9. In the future the construction of mechanical testing machines will be the core business of a painting conservator.

10. A lot of industrial experience is needed to complete a PhD in 4 years.

These propositions are regarded as opposable and defendable, and have been approved as such by the promotor Dr. R. M. Groves and the Co-Promotor Dr. ir. O. K. Bergsma.

Stellingen

1. Onderzoekers worden belemmerd door de grote structurele variabiliteit van historisch textiel in het verkrijgen van meetbare gegevens over hun morfologie.

2. Biaxiale trektesten van historisch textiel zijn nodig om de belasting condities op en het gedrag van het spieraam van schilderijen te reproduceren.

3. De waarde van de trekspanning op het spieraam van een schilderij is een van de meest invloedrijke parameters voor de conservering ervan, maar het is bijna onmogelijk om dit te meten in standaard museumomstandigheden.

4. Terugkerende kenmerken in de structuur van historisch textiel maken een hoge mate van vertrouwen mogelijk in de identificatie van de schering- en inslagrichting wanneer een zelfkant niet beschikbaar is.

5. De berekeningsmethode van de elasticiteitsmodulus van een textiel geweven van natuurlijke vezels is het voorrecht van de ingenieur die het werk uitvoert.

6. De waarde van de trekspanning van een schilderij op zijn spieraam is na de waarde van het schilderij de meest invloedrijke parameter die de conservering beïnvloedt.

7. Open-source hardware is waardevoller dan het patenteren van innovaties uit onderzoek.

8. Verschillen tussen beschavingen leiden tot filosofische debatten die leiden tot verlichting in zowel conservering als luchtvaart- en ruimtevaarttechniek.

9. In de toekomst zal de bouw van mechanische testmachines de kernactiviteit zijn van een schilderijenrestaurator.

10. Er is veel industriële ervaring nodig om een PhD in 4 jaar af te ronden.

Tension on a stretcher: mechanical and morphological characteristics of canvas paintings supports

Dissertation
for the purpose of obtaining the degree of doctor
at Delft University of Technology
by the authority of the Rector Magnificus, Prof.dr.ir. T.H.J.J. van der Hagen,
chair of the Board for Doctorates
to be defended publicly on
Monday 15 September, 2025 at 10:00 o'clock

by
Antonio IACCARINO IDELSON,

Master of Arts in Conservation and Restoration, Istituto Centrale per il Restauro, Rome Italy

This dissertation has been approved by the promotors.

Composition of the doctoral committee:

Rector Magnificus chairperson

Dr. R. M. Groves, Delft University of Technology, promotor

Dr. ir. O. K. Bergsma Delft University of Technology, copromotor

Independent members:

Prof. dr. ir. R. Benedictus	Delft University of Technology
Prof. dr. E. Bosco	Eindhoven University of Technology
Prof. dr. Ł. Bratasz	Polish Academy of Sciences, Poland
Dr. E. Richardson	Rochester Institute of Technology, USA
Prof. dr. N. F. Shahidzadeh	University of Amsterdam

Reserve member:

Prof. dr. ir. R. A. Alderliesten	Delft University of Technology

ISBN 978-94-6518-129-5

A digital copy is available at

https://doi.org/10.4233/uuid:f6cb374e-5095-45be-a705-561e675011f0

Table of contents

Chapter 1 Introduction 11

Chapter 2 Description of the field, literature review and aims of the research 19

2.1 Materials and treatments 19

2.1.1 The yarns 20

2.1.2 The canvas 20

2.1.3 The role of the sizing and preparation layers 23

2.1.4 The stretchers and their evolution 25

2.1.5 Structural treatments and the lining of paintings 27

2.2 Measuring and choosing the value of tension 29

2.2.1 Boundaries for the choice of tension 31

2.2.2 Early phases in the collection of data on the mechanical behavior of canvas painting materials 33

2.3 Loads and mechanical properties 35

2.3.1 Studies in crack formation 35

2.3.2 About the mechanical characterization of the materials of canvas paintings 37

2.3.3 Extracting the materials properties from mechanical testing 38

2.3.4 Degree of conservation of the fibers affecting materials properties 38

2.3.5 Nanoindentation and microscale testing 39

2.4 The central goals of this research 40

2.5 Methodology 42

2.6 Case studies in conservation practice allowing the progress of the research 43

2.6.1 Rembrandt's The Night Watch at the Rijksmuseum Amsterdam 43

2.6.2 A painting by Tiepolo at the Louvre Museum 44

2.7 Summary 45

Chapter 3 Quantitative morphological description of the canvas structure 47

3.1 Introduction and general definitions 47

3.1.1 Aims of the research 51

3.1.2 The specimens object of the research 51

3.1.3 Sample preparation and statistical data collection 53

3.2 Measuring procedures 56

3.2.1 Weight and thickness of the canvas, thread-count and yarn linear density 56

3.2.2 Identification of fibers 57

3.2.3 pH measures 57

3.2.4 Yarn width assessment 58

3.2.5 Twist 59

3.2.6 Description of the method for twist measurements in historical textiles 60

3.2.7 Crimp 62

3.2.8 Description of the method for crimp measurements in historical textiles 65

3.2.9 Yarn thickness measurement 66

3.3 Experimental results 67

3.3.1 Weight and thickness of the canvas, thread-count, fiber identification and pH 67

3.3.2 Yarn width, thickness and Z axis compression 69

3.3.3 Measures of Twist Per Meter 75

3.3.4 Measures of crimp % 79

3.3.5 Crimp value 81

3.4 Discussion 82

3.4.1 Characteristics allowing the identification of warp and weft without a selvedge 82

3.4.2 Warp and weft correlations in literature 84

3.5 Conclusions and future work 85

Chapter 4 Design and construction of testing devices 87

4.1 The construction of a biaxial tester 88

4.1.1 The need for a custom designed biaxial tensile tester *88*
4.1.2 The biaxial tensile tester in context *88*
4.1.3 General requirements for tensile testing of canvas paintings samples *91*
4.1.4 Samples dimensions *92*
4.1.5 Testing loads, speeds and run limitations *92*
4.1.6 Testing procedures *93*

4.2 Mechanical design **94**
4.2.1 Concept *94*
4.2.2 Mechanical construction *96*
4.2.3 Description of the motion actuators *98*
4.2.4 The load cells and clamping devices *100*
4.2.5 The end stops *102*

4.3 Electronic design **103**
4.3.1 The electronics *103*
4.3.2 Software development *104*
4.3.3 Machine controller firmware *105*
4.3.4 Pre-tensioning algorithm *106*
4.3.5 PC software development *106*
4.3.6 File format *108*

4.4 Build instructions **109**
4.4.1 Construction of the steel cross *109*
4.4.2 Perforation of the structure for fixing the actuators *109*
4.4.3 Test the assembly of the actuators and powder coat the structure *109*
4.4.4 Installation of the cables and of the actuators *110*
4.4.5 Construction of the sample clamps *110*
4.4.6 Construction of the box for the electronics *110*
4.4.7 The box for the switches *111*

4.5 Operating instructions **111**

4.5.1 Clamping the sample *111*

4.5.2 Test procedures tips *112*

4.6 Validation and characterization **113**

4.6.1 Displacement of the carriages *113*

4.6.2 Load cells data *113*

4.7 Results **114**

4.7.1 Pre-tensioning *114*

4.7.2 Biaxial and uniaxial tensile tests *115*

4.7.3 Peel tests *117*

4.8 The open-source format **117**

4.9 Design and construction of a portable uniaxial tester **118**

4.10 Design and construction of a Displacement Tester and hand-held probe **121**

4.11 Conclusions **123**

Chapter 5 Biaxial tensile testing of the historical textiles and correlations with morphology **125**

5.1 Introduction and general parameters **125**

5.1.1 Preliminary considerations about samples dimensions *126*

5.1.2 Comparing test results obtained using two sample dimensions *127*

5.1.3 Considerations about testing speed *132*

5.2 Calculating the E modulus of the set of samples **133**

5.2.1 The tensile modulus of a canvas *133*

5.2.2 A review of the approaches to the loading area for stress in textiles *136*

5.2.3 The method developed to calculate the loading section area of the samples *138*

5.2.4 The "object related" and the material E modulus values for the set of samples *140*

5.3 The E modulus values in the conservation science literature **142**

5.3.1 Early studies *142*

5.3.2 More recent studies *145*

5.4 Analysis of the biaxial testing data of the set of specimens **149**

5.4.1 Correlation with the warp and weft directions *149*

5.4.2 E modulus and crimp *150*

5.4.3 E modulus and twist *150*

5.4.4 E modulus decreasing after A *151*

5.4.5 Very low warp modulus *152*

5.4.6 High modulus textiles *154*

5.4.7 The tensile modulus correlated to textile morphology *156*

5.4.8 Uniaxial or biaxial testing and ratio between weft and warp E moduli *163*

5.4.9 Tensile modulus and fiber, pH and age of the textile *164*

5.4.10 Additional biaxial tests performed on four naturally aged paintings *167*

5.5 Conclusions and future work **167**

Chapter 6 Construction and testing of a mockup to investigate the mechanical behavior of a wax-resin lined painting **169**

6.1 The use of mockups **169**

6.1.1 Definition of the elastic moduli and characterization of the materials *171*

6.2 Materials and methods **172**

6.2.1 The naturally aged painting *172*

6.2.2 The wax-resin lining of the mockup painting *173*

6.2.3 The tensile tests *174*

6.2.4 The new flexural testing tower and the flexural tests *175*

6.2.5 The tensile and flexural moduli *176*

6.3 Results and discussion **177**

6.3.1 Morphological data on the textiles *177*

6.3.2 Tensile response of the materials under biaxial and uniaxial testing *178*

6.3.3 The lining canvas *179*

6.3.4 The effect of wax-resin on the lining canvas 181

6.3.5 The naturally aged painting 182

6.3.6 Mechanical response of the mockup and calculation of its elastic moduli..... 182

6.3.7 Calculation of the loaded section area of the mockup 184

6.4 Conclusions and future work 186

Chapter 7 Investigating the mechanical behavior of *The Night Watch* 187

7.1 Introduction..... 187

7.2 The choice of an elastic system for the structural conservation of The Night Watch 187

7.3 The elastic strainer for The Night Watch 190

7.4 Displacement testing of The Night Watch 192

7.5 Conclusions..... 197

Chapter 8 Conservation treatment of Tiepolo's "Juno in the clouds", assisted by structural testing, at the Louvre Museum Paris..... 199

8.1 Introduction 199

8.2 The painting and its conservation needs 199

8.2.1 The possibility of using a rigid panel 200

8.2.2 The need for a new lining 201

8.3 Introduction to the lining method and to treatment reproducibility..... 201

8.3.1 The first phase of the structural intervention..... 202

8.3.2 The support fabric 203

8.4 Mechanical tests on the materials 204

8.4.1 tensile tests 204

8.4.2 The cold and dry lining method, characterized by peel tests..... 207

8.5 The elastic system..... 211

8.6 Conclusions 214

Chapter 9 Conclusions and future work 215

9.1 Conclusions 215

9.2 Future work 220

10 Glossary of engineering terms used in the text 223

11 Glossary of textile definitions used in the text 225

12 Acknowledgments 227

13 Curriculum Vitae 229

Appendix 1 The full tables of the mechanical and morphological data collected on the set of 26 specimens 231

Appendix 2 Additional tensile test data 259

2.1 Individual yarn tests, correlated to uniaxial and biaxial tests of the same textile .. 259

2.2 Tests performed at different speeds 274

Appendix 3 An optical method for the determination of twist in yarns (1973) 279

Appendix 4 Design file and bill of materials for the biaxial tester 289

Design files summary 289

Bill of materials summary 289

LITERATURE REFERENCES 291

Chapter 1 Introduction

Paintings on canvas are among the most widespread forms of art [Torrioli, 1990], to the point that the term “canvas” is often used as a synonym[1] for “painting” in the common language. The origins of the technique can be traced back to early times in human history and technological development, as textiles have been produced since the neolithic period [Bender Jørgensen et al., 2023]. Recent research in the early stages of mankind demonstrates with increasing evidence that textile production has been a key technology for the early *homo sapiens* before the last migrations out of Africa as early as 70k years ago, and it seems very likely that it played a key role in the environmental adaptation and survival during cold periods, as *Sapiens* dispersed in Africa in changing climatic niches for at least 120k years [Hallett et al., 2025]. The *Neanderthals* adapted to cold environments well before *Sapiens*, and it is to no surprise that similar evidence is now being found also within their technological skills [Hardy et al., 2020]. Evidence of spinning and dyeing of plant fibers have been found in paleolithic settlements, as the Dzudzuana cave in Georgia, where Evidence of spinning and dyeing of flax fibers dated at about 32k years ago was found [Kvavadze et al., 2009] and [Bar-Yosef et al., 2011].

The origins of painting on textiles may be related to body painting [Biddle, 2007], and the reasons for the success of the use of textiles as a support for painting reside in the fact that textiles were among the most widely available artifacts (along with pottery) and were destined to have multiple uses, including decoration. Paintings on canvas are documented in Roman texts like Pliny the elder’s Natural History (1st c. AD), and early examples have survived in Egyptian archaeology, from the 1st millennium BC painted funerary shrouds found on the mummies, to the Fayum portraits[2] (2nd and 3rd c. AD) [Doxiadis, 2000]. Early examples have also been documented in India [Guy and Britschgi, 2011] and China[3], but the conservation of organic materials poses a limit to their survival other than in burials or particularly dry environments. Painting on pottery is generally considered to be one of the first developments of artistic expression in painting after cave art, as many examples survive from very early times[4] because they are not sensitive to moisture and biological deterioration. However, painting on textiles required a simpler technology than fired clay and was therefore probably more widespread, although the

[1] https://www.merriam-webster.com/thesaurus/canvas

[2] These were painted on wood, as portraits of the living person that were inserted in the mummy after the death, or directly on the mummy bandages, in memory [Torrioli, 1990].

[3] https://en.wikipedia.org/wiki/Chinese_painting

[4] Corpus Vasorum Antiquorum ("corpus of ancient vases"; abbreviated CVA) is an international research project for documentation of ancient ceramics started in 1923. It covers a compendium of more than 100,000 vases located in collections of 26 participating countries. https://www.cvaonline.org/cva/browse

material record of painted canvases is now more limited due to their deterioration in archaeological contexts. In the Pompeii wall paintings, that survived the 79 AD eruption thanks to their inorganic nature, we find depictions of painters at work on a canvas nailed on a wooden stretcher, in a manner that is almost indistinguishable from contemporary practices [Coarelli, 2002].

The flexible and low weight support allowed the painting to adapt to different shapes, to be hung to decorate interiors, to be used as a banner. Assembling textiles by stitching allowed producing very large paintings, and in the 1st c. AD Pliny the elder describes[5] a colossal portrait on linen canvas of the emperor Nero, measuring 120 feet. In 1550, Vasari[6] notes that: "*Men, in order to be able to carry paintings from town to town, have found the convenience of painted canvases, as those that weigh little, and when rolled up are easy to transport. […] because this way seemed easy and comfortable, not only small paintings were made to be carried around, but also altar paintings and other very large works of art […] where the size of the panels does not reach, the size and comfort of the canvases will serve".* Another important reason for the success of the technique is the lower the cost of the support if compared with panel paintings. Archival researches [Bourriot, 1998] found that canvas was 4 to 10 times cheaper than wooden panels. The object of the present study is therefore deeply rooted in human civilization and plays a key role in aesthetics, cultural heritage and in the economy of art.

As a technological artifact, a painting on canvas is made of a textile that receives the preparation and paint layers while being kept flat thanks to the tension assured by the presence of a rigid wooden structure. The fact that the textile is kept more or less free from deformations plays a role in the perception of the painted image that evolved over the centuries. In his canvas painting "The Art of Painting" J. Vermeer[7] depicts the gentle undulations and vertical folds formed in the map hanging in the background of the composition, proving that these were not considered an aesthetic problem or a matter of neglect, as otherwise they would have been hidden so as not to disturb the elegance of the depicted scene. Undulations were perceived as inherent to the nature of the materials, and the viewer was able to interpret them without significantly diminishing the perception of the image, as demonstrated by the Gestaltpsycologie, and analyzed in [Capriotti, 2004]. The need for a faultlessly flat surface became more stringent during the 18th century, when Neoclassicism imposed rigorous geometries, clear precise lines,

[5] Natural History, book XXXV, chapter 33.
[6] Vasari, G., *Introduzione alle tre arti del disegno, cioè architettura, pittura e scoltura*, Cap XXIII. Translation by the author.
[7] c. 1662–1668, Kunsthistorisches Museum, Vienna

and well-defined forms. This is probably even more important in the contemporary aesthetics, in which images are most often mediated by the flat screens of digital devices.

The qualities of the stretcher and the possibility of changing or improving the tension of the canvas have evolved in parallel, also following the evolution of the restoration and conservation techniques. Lining, in particular, is a technique that allows the painting to return to its original, undeformed state [Hackney, 2020]. The technique became well established during the second half of the 17th century, and, since then, the flatness of the painting became a bigger concern for restores, owners and the other stakeholders [Capriotti, 2004]. The introduction of stretchers that may be expanded in the corners to increase tension and reduce the visibility of the formations of the canvas has been a game changer with a very significant impact on the conservation of the paintings [Buckley, 2007]. Distortions in the painting's planarity impact on its aesthetic appreciation, but they are also related to its structural integrity, and to the insurgence of cracks in the preparation and paint layers. Crack formation is directly connected with the distribution and the value of the forces acting within the painting in its relation with the stretcher [Roche, 1993]. A crack occurs when a material is subjected to forces that exceed its ultimate load, and the distribution of cracks within a painting tells the story of the stresses that have occurred during the painting's conservation history [Keck, 1969]. Changes in environmental values change the mechanical characteristics and the dimensions of the materials, and subsequently the stresses they are submitted to [Mecklenburg, 2021]. In particular, the amplitude of the variations of environmental temperature and relative humidity, and their speed, are key factors to the insurgence of cracks and deformations in canvas paintings [Michalsky, 2016].

Conservation science studies have focused on these problems since very early times [Cardinali et al., 2007], and the field of mechanical studies in paintings conservation is deeply related to the understanding and quantification of those forces. Conservation techniques aim at changing the painting and its structure as little as possible, while trying to mitigate risks. It is therefore a continuous negotiation between intervening on the artifact and intervening on the environment. Obtaining stable values in the environment is often a complex issue, especially in historical buildings, and requires important financial and infrastructural resources [Michalsky, 2005]. The stabilization of the environment can also be treated at a local level in the proximity of the painting, with the use of enclosed framing, backing boards [Sozzani, 1997] and showcases [Padfield and Borchersen, 2007]. Treatments on the painting, on the other side, include the consolidation of unstable or fragile areas, and the use of elastic tensioning systems [Iaccarino Idelson, 2005] to avoid the buildup of forces to reach critical values or the ultimate load of the materials [Hagan, 2023].

The constituent materials of canvas paintings have the relatively unpredictable nature of historical artifacts that have been produced from a variety of raw materials and with a range of manufacturing techniques. The simplest part is the stretcher, because wood is a relatively homogeneous material that has been characterized in good detail for construction engineering studies. The paint layers, the main object of the creative work of the artist, are extremely variable in binders, pigments, additives, coatings, and thickness, even at a short distance within the same painting. The elastic modulus and the ultimate load of the paint layers can differ by two or three orders of magnitude for the same binding media, i.e., linseed oil or other, because of the interaction with the different pigments and because of aging [Hagan et al., 2015]. In order to understand the factors that cause such variations, and in order to measure the mechanical characteristics of the different paint layers with a reasonable level of repeatability and standardization, hardly any alternative exists to working with new materials to produce specimens that need to be left to naturally age in the laboratory environment [dePolo et al, 2021]. This is because any attempt to obtain artificially aged samples (especially for oil bound paints) leads to the different chemical reactions from those happening within natural aging conditions and time. This has led to the collection of reference data since the 1980s, that has proven to be useful for predictive simulations, though of course the materials and condition of a real painting are hard to replicate in a digital simulation model [Colville et al., 1982; Young and Hagan, 2008]. The textile receives and supports the paint layers, it is the core of the structure and has great influence on the appearance and mechanical characteristics of the painting as a whole. The mechanical characterization of naturally aged textiles is made complex due to the variability of the materials, as compared to those of modern industrial textile, and by the unpredictability of the degradation processes that the painting has undergone during the centuries. Moreover, the availability of testing samples is very scarce and it is in clear conflict with the conservation of a painting, as mechanical testing can be a destructive practice.

A general description of the field is given in chapter 2, where the aims and structure of this research are also defined. This thesis focuses on the mechanical characterization of samples of historical textiles from canvas paintings, with the aim of building up a collection of data, to understand their material behavior. The choice to focus on naturally aged historical textiles is based on the absence of comparable data in the literature, and on the availability of a relatively large number of specimens due to the author's practice in the profession of conservator. The research is therefore based on the need to describe the materials to be tested, in order to obtain data allowing correlations to be made between morphological characteristics and mechanical behavior, and on the testing procedures and methods. The data obtained is contextualized and made available for comparative studies and predictive simulations.

The set of information required in textile engineering for a quantitative morphological description is quite wide [Pierce, 1937; Behera et al., 2010], ranging from the weight and dimensions of the yarns, the number of twists they have acquired in the spinning process; the description of the woven structure including the number of yarns, the % of crimp, the thickness and the weight of the textile. Yet, modern industrial textiles can be sampled with virtually no limitations, which is not possible with historical materials. In conservation studies, only a small fraction of this data is available, and the remaining are difficult to obtain and very rarely used. Since this severely limits the understanding of historical structures, this research focused on organizing and establishing a protocol of non-destructive or minimally invasive methods for the observation and quantitative description of the morphology of textiles, compatible with the study of historical specimens, as we will see in chapter 3. Analysis of the resulting organized wealth of data allowed correlations to be made between the warp and weft directions and a range of specific features. The correlations, found on a heterogeneous set of textiles, provided useful tools for identifying the weft direction from the warp direction in a canvas when a selvedge is not available.

The response of a textile sample to tension is needed to make predictions about its behavior and to compare it with other textiles or materials. Tensile tests are usually performed using uniaxial testing machines, where the sample is a strip of fabric stretched between two clamped areas at the ends [Hagan, 2023], repeated in the warp and weft directions. The intertwined yarns follow an undulated path in the textile, and when subjected to tension, they need to de-undulate before showing the full tensile response [Roche, 2003]. When the yarns in one direction are subjected to tension, they tend to a straight, fully stretched, configuration, while the ones in the orthogonal direction become more undulated. The phenomenon is called “crimp transfer”, and plays an important role in the definition of the tensile response of a textile. When both directions are subjected to tension simultaneously, in biaxial loading conditions or testing, the tensile response shown by the material is different because of the interaction of the two orthogonal sets of yarns. In real-life loading conditions tension in a textile are normally biaxial, though not necessarily symmetric, mathematical corrections need to be introduced to calculate the biaxial response from uniaxial testing [Chiriboga, 2013].

In order to directly measure biaxial loading tensile data on the historical samples object of testing, a new device was designed and constructed by the author in collaboration with prof. Miguel Sanchez from the Polytechnic University of Valencia, Spain, as described in chapter 4. The device has miniature clamps and high definition in the readings of displacement and force, allowing the testing of very small samples, as the size of the material that can be made available for testing historical textiles is small by definition. However, tests still need to be performed at the macro scale (10 mm x 10 mm sample area), in order to keep a direct correlation with the actual original object. Testing

the samples after having characterized their morphology allowed comparisons to be made and correlations with their structure. This also introduces the perspective of possible future studies in parallel with the data available in literature on modern textiles, as very little is available on historical materials. The different methods used to evaluate the section actually responding to the tension, i.e., that of the fibers alone without the empty spaces normally present in the woven structure, were analyzed. A method was chosen and adopted for the set of samples described in this study, allowing the mechanical data to be used for predictive digital simulations, described in chapter 5.

The mockup of a wax resin lined 17th c. painting was built and described in chapter 6. This was done to obtain otherwise inaccessible information about the mechanical behavior of a similar painting, and inspiration was driven from *The Night Watch* which has a wax-resin lining dating from 1975, because of the wealth of knowledge available about the precious painting. The mock-up was tested as a whole and each layer individually, and the data showed that the tensile response of the materials is compatible with the tension chosen for a painting like *The Night Watch* on its new elastic strainer, indicating no risk to its structural integrity. The tensile and flexural elastic moduli were elaborated, and as such values are unprecedented in the conservation science literature for a lined painting structure, solutions were proposed to define the loading area in its cross-section. Further research is needed, and the data in chapter 5 suggests a direction.

Two major field studies are also part of this research.

In chapter 7, the study of Rembrandt's *The Night Watch* at the Rijksmuseum Amsterdam involved the study of its structure through non-destructive mechanical tests. A custom-built displacement tester (described in chapter 4) was used to measure the response of the painting to forces that caused it to be displaced out of plane while under the known value of tension on the elastic strainer. The painting's behavior in such a controlled setting is also a form of non-destructive mechanical testing, that may eventually be integrated into a FEM model and used to elaborate the values of tensile and flexural moduli intended as an engineering method to solve to solve the multivariable equation required to determine the painting's elastic moduli is also more explicit.

In chapter 8, the complete structural treatment of a detached wall painting by Tiepolo at the Louvre Museum, is described. Each step of the intervention, and the materials used, made the object of mechanical testing and characterization, allowing an uncommonly high level of understanding. The new lining canvas was chosen for its high elastic modulus and isotropic behavior in the plane, and is subjected to known forces within the elastic tensioning system. The lining was carried out with repeatable procedures and quantified materials and methods, and the force of adhesion obtained was measured with peel tests on a mockup. This allowed verifying that the force is

appropriate for the conservation and long-term structural integrity of the painting, and that the adhesion will be fully reversible at the time of the future interventions.

Chapter 2 Description of the field, literature review and aims of the research

Outline of the chapter

2.1 Materials and treatments
- 2.1.1 The yarns
- 2.1.2 The canvas
- 2.1.3 The role of the sizing and preparation layers
- 2.1.4 The stretchers and their evolution
- 2.1.5 Structural treatments and the lining of paintings

2.2 Measuring and choosing the value of tension
- 2.2.1 Boundaries for the choice of tension
- 2.2.2 Early phases in the collection of data on the mechanical behavior of canvas painting materials

2.3 Loads and mechanical properties
- 2.3.1 Studies in crack formation
- 2.3.2 About the mechanical characterization of the materials of canvas paintings
- 2.3.3 Extracting the materials properties from mechanical testing
- 2.3.4 Degree of conservation of the fibers affecting materials properties
- 2.3.5 Nanoindentation and microscale testing

2.4 The central goals of this research

2.5 Methodology

2.6 Case studies in conservation practice allowing the progress of the research
- 2.6.1 Rembrandt's The Night Watch at the Rijksmuseum Amsterdam
- 2.6.2 A painting by Tiepolo at the Louvre Museum

2.7 Summary

2.1 Materials and treatments

The structure of a traditional painting on canvas can be simplified to a small number of elements: the design layers, including the ground, paint layers and varnish; the sizing layer, that makes the connection with the canvas; the canvas support and a wooden structural reinforcement [Buckley, 2007]. The description of the materials starts from the way the fibers are arranged by spinning to create a yarn, and then woven into a textile. The textile is stretched to receive the preparation and paint layers, and it continues its life in connection with a stretcher. These will also be described, though the preparation and paint layers will be treated only at a very general level because the focus in this study

is on the textile and on its tensile behavior. The following sections will address in detail the structure of the textile and its tension on stretcher.

2.1.1 The yarns

Yarns in painters' canvases have historically been made from flax and hemp cellulose fibers, less commonly cotton and other fibers [Torrioli, 1990]. Spinning the fibers with hand spindles to hold the fibers together produced the yarns, what made the fibers suitable for weaving. During the spinning process, a selected quantity of fibers from the bundle are twisted in a helical structure running around the neutral axis of the yarn. Fibers located on the periphery of the yarn are bent and must follow a longer path than those in the center, thus generating a centripetal pressure that provides cohesion; moreover, proximity increases friction between them [Pierce, 1937]. This simple process, which has been known since the early Neolithic times [Burke, 2010], makes it possible to produce strong yarns from relatively short fibers (Figure 1). Increasing the quantity of fibers in the yarn, the distance from the neutral axis of the peripheral fibers is longer, and the length of their helical path increases. If too much twist is given, i.e., too many turns in a given length of yarn, tension at the periphery makes the yarn stiff and susceptible to mechanical deterioration. Conversely, low twist yarns are more flexible and fluffier, useful for making soft, warm clothing, but have low tensile strength [Barella et al., 1980]. The "optimum twist" [Neckář and Das, 2019] will be higher in thinner yarns, and in traditional hand spinning, where the number of fibers is not constant along the yarn [Kania, 2010], the sections with fewer fibers are thinner and have more twist than the thicker ones.

Figure 1 Image of a twisted yarn in flax fibers. (photo credit: Antonio Iaccarino Idelson)

2.1.2 The canvas

Weaving techniques are based on the use of a loom in which a set of parallel yarns, the warp, is divided into groups that are alternately lifted to open the "warp shed" and allow

other yarns, the weft, to pass through, creating the woven structure of the textile. The simplest pattern, one warp for one weft thread, is called plain (or flat) weave. Many other variations are possible, where the threads alternate in different patterns, to obtain fabrics with different mechanical or aesthetic characteristics [Cieta, 2020], but these exceed the focus of this thesis. Fabrics also differ in the density of the yarns (thread count), which implies a more or less open or tight structure. Canvases used for painting have different thread counts, from a minimum of around 7 per centimeter to a maximum that can exceed 30. The diameter of the yarns used for weaving, and their twist affect the mechanical properties of the fabrics as well as their thickness. In Figure 2 we see three examples of plain weave textiles, all at the same scale 10x10 mm (warp is vertical). The first, *a*, is tightly woven and has a high thread count, 31.3x29 yarns/cm; *b* and *c* have very similar thread count (9x7 and 9x9 yarns/cm), but *b* appears tightly woven because yarns are thicker; *c* is a typical loose textile, originally woven to sieve cheeses, but also used for painting, or for lining canvas paintings.

a) *b)* *c)*

Figure 2 Same scale images (10 x 10mm) of 3 textiles, (n. 18; 4 and 24 in Appendix 1) (photo credit: Antonio Iaccarino Idelson)

When the warp shed is closed over the weft yarn, the other set of parallel warps are lifted to create the interlaced structure and allow a new weft to be inserted. Each weft is a fulcrum, deflecting the course of the warp yarns, which take on a wavy shape. The weft yarns are also deformed by the thrust of the warps, and friction locks their acquired shapes making them become permanent. The undulated paths reduce their free length, and the dimensions of the textile are therefore smaller than those of the yarns used to produce them during weaving [Textile terms and definitions, 1975]. The difference in length, named crimp, is about the value of 10% of the length of the textile, and varies with weaving technique, dimensions of the yarns and thread count. If warp and weft are the X and Y axis in the plane of the textile, the pressure generated between yarns is mostly on the Z axis, orthogonal to the plane of the textile, therefore the original circular section of the free yarns becomes crushed into an elliptical one (see chapter 3, Figure 20). Yarns with low twist tend to become almost like flat ribbons, while a high twist

reduces their availability to adapt their shape, and the elliptical section stays closer to a circle.

The quantity of contact surface between the yarns determines the level of their interaction, and a textile in which the empty space between the yarns is very small, like in Figure 2*a*, has highly interconnected yarns. For vegetable fibers, the moisture related behavior has close analogies to that of wood. Therefore, when environmental humidity increases, they increase their diameter and their dimensions change more radially than longitudinally [Yamamoto et al., 2001]. Yarns, made of spun cellulose fibers, increase their diameters with increasing environment humidity, causing the swelling of the textile. The transverse swelling of the fibers is an order of magnitude higher than the longitudinal one, and increasing the pressure along the Z axis on the surrounding yarns results in the contraction of the textile. In Figure 3 [Bilson, 1996], in which the dashed portion of the neutral axis of the yarn, undergoing neglectable dimensional change, we see the effect of transverse swelling in causing the contraction of the textile. The shrinkage of tightly woven textiles produces high contraction forces, that are smaller when the yarns are spaced, as in 2*c*.

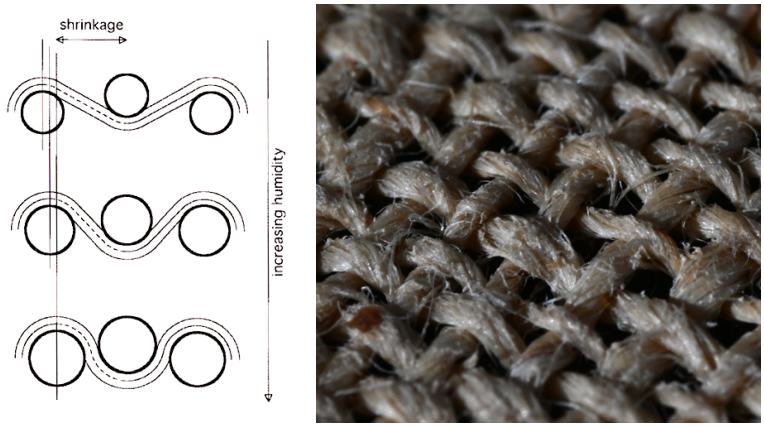

Figure 3 Mechanism of canvas shrinkage during humidification swelling of the fibers, from [Bilson, 1996]. Highly spaced yarns cause less contraction in the textile upon humidification (photo credit: Antonio Iaccarino Idelson)

When the perimeter of a canvas is connected to a wooden structure, the shrinkage implies an increase of tension due to the restrained dimensions (Figure 4). Wetting a restrained canvas causes slippage in the fibers and a permanent increase of its dimensions when returning to normal humidity conditions. Therefore, if before wetting it were stretched taut on the stretcher, most of the initial tension will be lost. The role of the expansion of the wood in the stretcher is limited to the outward expansion from the fixed points in the corner joints, and its contribution to the increase of canvas tension is not very relevant.

2.1.3 The role of the sizing and preparation layers

Sizing has the primary function of making the canvas a less absorbent and more homogeneous support for the ground and paint layers, reducing the drainage of the binding media [Hackney, 2020]. A layer of sizing is typically made of a water dispersion of animal glues, that are mostly made of collagen proteins, long chain fibrous structures that show important dimensional variations and changes in the mechanical properties with environmental humidity [Bridarolli et al., 2022]. The typical traditional procedure for the construction of a canvas painting starts by "sizing" the stretched canvas with a water-based solution of animal glue. As we have seen, wetting with water results in a substantial loss of tension due to its permanent extension. However, the animal glue in the solution undergoes a significant contraction upon drying, which reestablishes the tension in the canvas [Mecklenburg, 2007]. In Figure 4 [Iaccarino Idelson, 2021] we see the tensions generated within a restrained canvas: the initial tension, set to 2 N/cm, proves to be too high for the canvas to maintain over time, that slowly reaches an equilibrium point at the plateau of about 1.7 N/cm because of creep; the water-based solution of size causes an abrupt rise of tension to about 3 N/cm; liquid water reduces friction among the fibers, further promoting their slippage, and tension falls to about 0.6 N/cm during the drying process, in this case after about 9000 seconds; when the water content becomes low enough to allow the contraction of the glue, the tension in the system is gradually restored and reaches values that can exceed the 1.7 N/cm plateau (in the weft direction we see 2.6 N/cm), because tension is now due to the glue film. Such description has the important implication that wetting the canvas again, or increasing relative humidity, the tension in the system will be reduced.

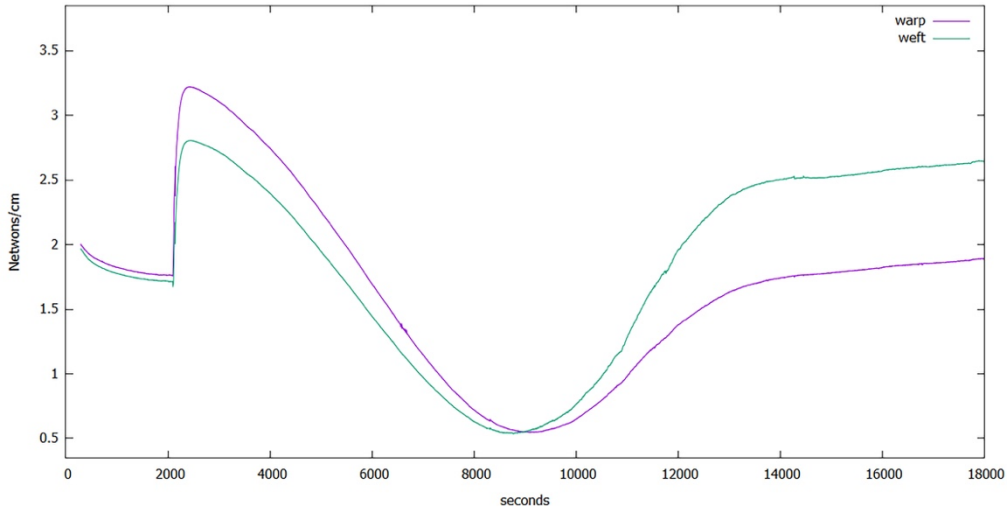

Figure 4 Biaxial tension plot of a constrained linen canvas being wet with size and let dry in a 50% relative humidity environment [Iaccarino Idelson, 2021]

From every point of view, including the mechanics of the painting, the preparation and paint layers play the fundamental role. The preparation is used to obtain a substrate suitable to receive the painting, and its surface texture regularizes that deriving from the structure of the textile [Stols-Witlox, 2017; Hackney, S. 2020]. The materials and methods used for the ground layer are already part of the painting technique, and its color is often visible between the brush strokes and can appear through the transparency of the thinner paint layers. "Priming is a color laid on the cloth, &c. previous to those which are to form the picture"[8]: the binding media used for it, the porosity obtained with the charges, the pigments and the surface treatments determine the degree of drainage from the paint layers, influencing their gloss and appearance. The ground is often the thickest layer above the canvas, and it has independent mechanical characteristics, though these are always deeply connected to those of the paint layers. A thorough description of the complex correlations between paint and preparation layers goes beyond the scope of this study, but an eloquent example can be seen in Figure 5, from [Iaccarino Idelson, 2012]. The reddish oil bound preparation layers are visible in the painted composition of this 16th century Italian painting, and are severely cracked because of the dimensional changes induced in the earth colors by environmental factors. At the center of the image an area can be seen where basic lead white was used to paint a grey and white band. Lead irons migrated from the very thin paint layer to the preparation, allowing for deeper polymerization of the oil that changed its mechanical structure [Tumosa and Mecklenburg, 2005]. Oil bound films containing lead ions show much smaller dimensional changes with variations of environmental humidity, and they have higher Elastic Modulus and ultimate load [Mecklenburg, 2007].

[8] Anonymous. Compendium of Colours, 1808. From: Stols Witlox, 2017, pages 223 and 334.

Figure 5 Red oil based preparatory layer containing earth colors, cracked and failed where the lead white did not stabilize it migrating from the thin overlaying paint layers, from [Iaccarino Idelson, 2012]

2.1.4 The stretchers and their evolution

The first stretchers were made of wooden elements connected in the corners and, in case of need, crossbars or corner crossbeams could be added as reinforcements. Such structures have fixed dimensions and are technically defined as "strainers" [Buckley, 2007]. The interaction between the canvas and the wooden structure has been an object of interest and investigation since early times, and the way the tension of canvas is achieved has evolved over the last three centuries. The first mention of the expandable stretches appears[9] in the 1757 "Dictionnaire" by Antoine Pernety [Pernety, 1757]. Although the author does not hint to restoration practices, it seems most likely that such stretchers were first created as tools for restorers, to be used during lining or consolidation treatments. Since the stress related problems first appear in the corner areas, the use of corner expansion stretchers seemed to be useful in solving the problem by increasing the tension where it seemed to be most needed. However, corner expansion increases the local concentration of the forces that cause the damage in the painting it is intended to resolve; therefore, the distortions are only temporarily removed, and the tension is cyclically increased. The use of a hammer to key out the corners was

[9] « On a inventé depuis peu une manière de faire des châssis qu'on appelle châssis à clefs ; ils sont préférables en tout aux anciens châssis, parce qu'au moyen des clefs, on tend la toile plus fortement, & toutes les fois que la sécheresse la relâche. Ces clefs se mettent dans tous les coins d'assemblage, et aux bouts de traverse ».

considered a dangerous and uncomfortable operation, which led to the search for alternative solutions.

The first stretchers with spring-loaded corners appeared as early as the mid-19th century, in a commercial attempt to solve this problem[10]. The springs, which are hidden in the stretcher bars, needed to be small, and stiff enough to overcome the high friction that occurs in the corner joints. The first known patent of a stretcher for canvas paintings in which the corner keys are substituted with springs, meant to expand the stretcher automatically, dates to 1866 (US patent n. 58.154, Sept. 18, 1866, by J.E. Todd) [Buckley, 2007]. Corner expansion obtained with springs hidden in the stretcher bars proved to be dangerous because the springs need to be small and to provide a great amount of expansion force. Therefore, if the relaxation of the painting allows the opening of the stretcher, its contraction is neither able to overcome friction nor to compress the springs, resulting in stress concentrations that exceed the painting's yield and failure point, as seen in the composition of images in Figure 6 from [Iaccarino Idelson, 2009].

Figure 6 Damages to a painting mounted on a Wright and Gardner elastic stretcher in 1884, from [Iaccarino Idelson, 2009]

A turning point in the evolution of the connection between the canvas painting and its stretcher happened in 1953 at the Istituto Centrale per il Restauro in Rome. A new

[10] The USA Patent Office is a valuable source of information. Among the first, we find in Sept. 18, 1866 the patent n. 58154 by J. E. Todd; some exemplars of the Jan 19, 1875 patent n. 159012 by J.P. Wright and D.W. Gardner have survived until the late 20th c.

approach was devised, based on the idea of separating the function of holding the painting in the space (as with a strainer) from that of providing it with tension. The result was that of freeing the painting from tacks or staples and connecting it to springs placed on the reverse of a strainer with rounded edges [Carità, 1957]. The method allowed the painting to move, adapting its dimensions to the changing environment, thanks to this simple switch in the approach to the functions of the supporting structure, and thanks to the liberation from fixtures along the edges. The method solved the problem of stress concentration in corners, Figure 7, as demonstrated in [Accardo et al., 1992]. Berger [Berger, 1984] proposed a mixed solution, which has hardly had any follow-up. The author proposed the conservation of original strainers and stretchers, by simply rounding their edges and adding springs on the back, using a measured value of tension for the painting [Iaccarino, 1996].

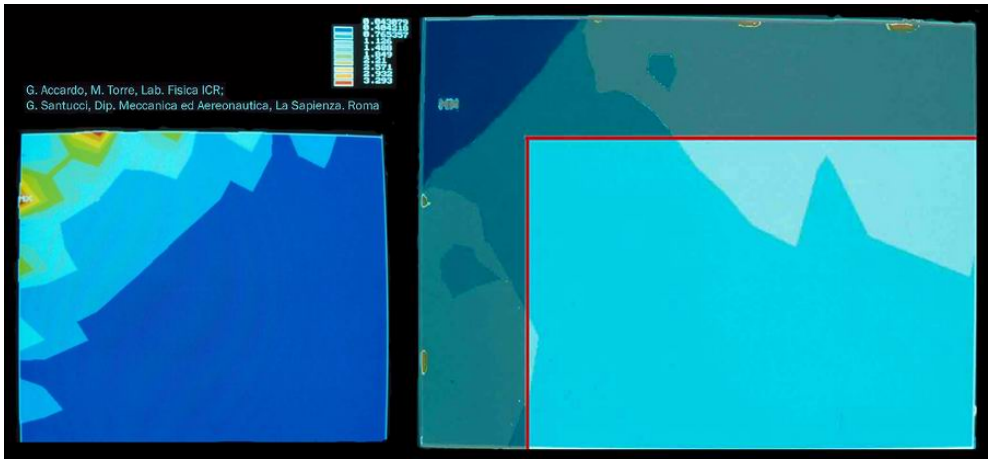

Figure 7 The 1992 FEM representing the tension distribution in the corner of painting on a key expansion stretcher (left) and on a strainer with rounded profiles (right). The canvas exceeding the red line is the lining canvas folded on the back to meet the spring system [cred. Mauro Torre].

2.1.5 Structural treatments and the lining of paintings

Used to improve the adhesion of the paint layers to the canvas and the planarity of the painting, impregnation treatments were relatively common and are documented[11] since the early 17th c. Lining, the addition of a second canvas to the rear of the painting in order to reinforce it, repair structural damage and re-establish the adhesion of the paint layers, is a likely ancient practice, appearing in written documents since the mid-17th

[11] T.T. de Mayerne describes in 1632 (Manuscript Ms. Sloane 2052 f.5v) a consolidation method based on repeated applications of fish glue through the painted canvas.

century[12]. Percival-Prescott proposed a connection between the expected life-span of the painting before major conservation issues appeared, and the stabilization of the lining technique in Venice "towards the end of the 17th century, roughly 150 years after the introduction of oil painting on canvas technique" [Percival-Prescott, 1974]. The adhesive was obtained from animal glues and cereal flours, in different proportions and with a variety of additives, and the use of the "paste glue" was shared all over Europe for centuries. In the 1840s, the wax-resin method was introduced in the Northern Europe [Te Marvelde, 2001], where the paste glue was more problematic because it offered a favorable substrate for microbial growth in humid environments. The other advantage being that of not requiring water-based treatments, the method became a new standard. Its many drawbacks, including the severe alteration of the materials and the risks of darkening the original colors and of the alteration of the surface texture, caused the surge of a need for alternatives to traditional methods since the 1960s. At the 1974 Greenwich Conference on comparative lining techniques [Villers, 2003 **(b)**], new lining methods were tested and introduced in the conservation practice.

Berger [Berger, 1970] proposed a new adhesive named BEVA, based on industrial formulations that emulated the wax-resin mixtures but using hydrocarbon waxes and synthetic resins. This allowed the conservation practice to follow the traditional approaches with a reduction of the risks of color saturation if compared with natural wax-resin mixtures. The material offers more flexibility in practical applications, requires a slightly lower temperature, and can also be used diluted in solvents. The use of synthetic materials, like polyester and glass fiber canvases, Mylar sheets, vacuum pumps and hot tables, that became progressively more widespread in the conservation of canvas paintings since the late 1960s, allowed the use of BEVA in many different variations. BEVA was a commercial success and, to date, has almost replaced the traditional method.

Mehra proposed to use acrylic emulsions that where already on the market, tested and approved by the conservation community. His approach was that of dividing the different phases of the structural treatment, such as consolidation, reduction of the deformations, and adhesion of the new canvas (the actual lining), proposing dedicated methods and materials for each. He aimed for the elimination of the heat to reactivate the adhesive, thus using cold methods that either involve the use of the fresh emulsion or its reactivation with a solvent [Mehra, 1972]. He was a promoter of the cold suction table, that allowed a reduction of the moisture content during treatments, while keeping the painting under a homogeneous pressure. Mehra also used peel tests to compare the

[12] Among the oldest documented paste glue linings, we find that done in 1672 by Carlo Maratti on the "Natività della Vergine" by Annibale Carracci, now at the Louvre Museum [Conti, 1988].

adhesion obtained with different variations of the method and also bending tests to define the stiffening of the painting after the lining [Mehra, 1975]. He tackled the problems connected with reversibility and with the addition of weight due to the adhesive and the new canvas [Mehra, 1981]. Phenix and Hedley used peel tests on mockups for the solvent reactivation of an acrylic adhesive [Phenix and Hedley, 1984], to define which was the most promising method to achieve homogeneous reactivation and good bond strength. Similar comparations were carried out for heat reactivated adhesives [Katz, 1985]. A comprehensive timeline of the developments of structural conservation methods at the turn of the millennium is found in [Ackroyd, 2002].

A well-known declination of Mehra's methods, named "mist lining" [Van Och and Hoppenbrouwers, 2003], was developed at the SRAL Maastricht. The method proposes an efficient solution for the solvent reactivation of dry acrylic emulsions, allowing the use of much smaller quantities of solvent if compared with the previous attempts [Phenix and Hedley, 1984]. It combines the use of low-pressure envelopes (an easy-to-use, low-cost version of the cold suction table) and the application of adhesive by spraying onto the lining canvas, with an innovative method of distributing the solvent vapors to reactivate the lining adhesives. This brought Mehra's methods into more widespread use, making them more accessible to the conservation community and less confined to research and educational institutions. The Mist lining procedure is based on a blend of acrylic emulsion adhesives, Plextol K360, whose very low glass transition temperature (-9°C) makes it tacky on contact when dry, and Plextol D540, with a Tg of 29°C. This blend of 7 parts K360 and 3 parts D540 was replaced in 2020 by a 50% blend of K360 and D512 (Tg: 26°C) [Arvind, 2021]. Applications to paintings destined for the Mediterranean climate required eliminating the Plextol K360 because it melting point 40°C is too low for the hot season. A modified approach was devised for the hot climates [Iaccarino idelson et al., 2018], using only Plextol B500 as the adhesive and MEK vapors for its reactivation in a vacuum bag instead of a low-pressure envelope. Peel tests were performed with different amounts of the adhesive and the solvent used for its reactivation in a sealed vacuum envelope, which allows quantitative control of the vapors involved in the process [Iaccarino Idelson and Garofalo, 2019]. Research into lining techniques continues, but no matter what method is used, one aspect is common to all when it comes to understanding the mechanics of a painting. When a new canvas is added to the original, the painting is able to withstand higher tensions than ever before, because of its new sandwich structure.

2.2 Measuring and choosing the value of tension

A probably unexpected side effect of the use of accessible, visible springs, instead of springs hidden in the structure of the stretcher, was the possibility of measuring the force used for the tension of a painting. Knowing the number of springs and their elastic constant, the measure of their elongation allowed calculating the force acting on a

stretch of perimeter. The value of the force used for a painting was published for the first time in [Carità, 1955], when a low tension was needed (1,36 N/cm) for a detached wall painting transferred on canvas. During the 1990 restoration of the painting by Caravaggio[13] "St. Jerome Writing", the value of 6 N/cm was chosen [Accardo et al., 1991]. In 1993, for a painting with similar dimensions and lining methods, the much lower tension of 2,6 N/cm was deemed sufficient [Iaccarino, 1996]. The value of the tension on a painting can be calculated through springs elongation, and the research carried out at the Laboratorio di Restauro di Viterbo in the years 2000-2003, focused on the correlation of the quantified tension with the behavior of a painting [Iaccarino Idelson, 2004 (b)]. The measurement of the tension of paintings when still on their original stretcher[14] was also part of the research. The traditional method of evaluating and judging the tension of a painting is to press a hand on the surface to feel its response. An analogue procedure was used to measure tension, applying a known value of force on the surface and measuring the corresponding displacement. In order to obtain the data, pressure was applied with a simple hand-driven device that also measured the data. A first test was performed on the paintings still on their stretchers, describing the plot of their response to an out-of-plane force under the unknown tension value. The paintings were then placed on a temporary strainer equipped with load cells to measure tension and select pre-determined tension values[15]. The force/displacement tests were repeated with increasing tensions and the plots were compared with the first measurements. The weighted mean of the overlapping sections allowed a quantification of the initial unknown tension, finding for the three paintings the values of 1.5 N/cm, 2.6 N/cm and 3.4 N/cm[16]. The plots describing the response of the paintings were analyzed to study how the displacement was reduced by increasing tension on the stretcher, finding a threshold value identified by a bend in the slope of the plot (Figure 8). After this, the

[13] The method was applied to Caravaggio's paintings in St. John's co-cathedral at Valletta, Malta, in 1954 [Carità, 1957] and on many other masterpieces until 1960, when it was abandoned because of a change in the Institute's management. It came back to the attention of the Laboratory of Physics at Istituto Centrale per il Restauro in 1989 when Caravaggio's St. Jerome writing was stolen and returned to Rome for a new conservation treatment.

[14] As it is virtually impossible to insert force sensors at the interface between the stretcher and the canvas, a direct measurement of the tension of a painting mounted on its stretcher has never been obtained. Within the framework of that project, the information was intended to provide a reference for the choice of tension. Tension was measured for three paintings on their stretchers.

[15] The paintings were required to be removed from their stretchers for scheduled conservation treatments.

[16] The three paintings are at the Museo Civico di Viterbo. "Il sacrificio di Polissena", by D. Corvi, 1785, 170x220 cm with a double canvas paste lining, was found to have the tension value of 3.4 N/cm; "S. Crispino" by unknown painter, 1806, 97 x 73 cm with a double canvas paste lining, had a tension of 2.6 N/cm; "Fra' Vincenzo Fani", by an 18th c. unknown painter, 126 x 95 cm on a single canvas paste lining, had a tension of 1.5 N/cm.

displacement vs tension tends to a constant value and therefore, if the tension is further increased, the resistance of the painting to displacement does not improve accordingly. For this reason, the threshold located between 2 and 2.5 N/cm was defined the "Maximum Useful Tension" (MUT), because tension above this value is not useful to improve the tautness of the painting [Iaccarino Idelson and Torre, 2004]. On the other hand, as the goal of correctly stretching the painting is achieved, providing more than the MUT would result in "useless" additional stress that may induce mechanical damage. Interestingly, Stefan Michalski found numerous other cases in which a tension threshold of about 2.5 N/cm corresponds to an optimal effectiveness in containing out-of-plane deformations in paintings and membranes [Michalski, 2021].

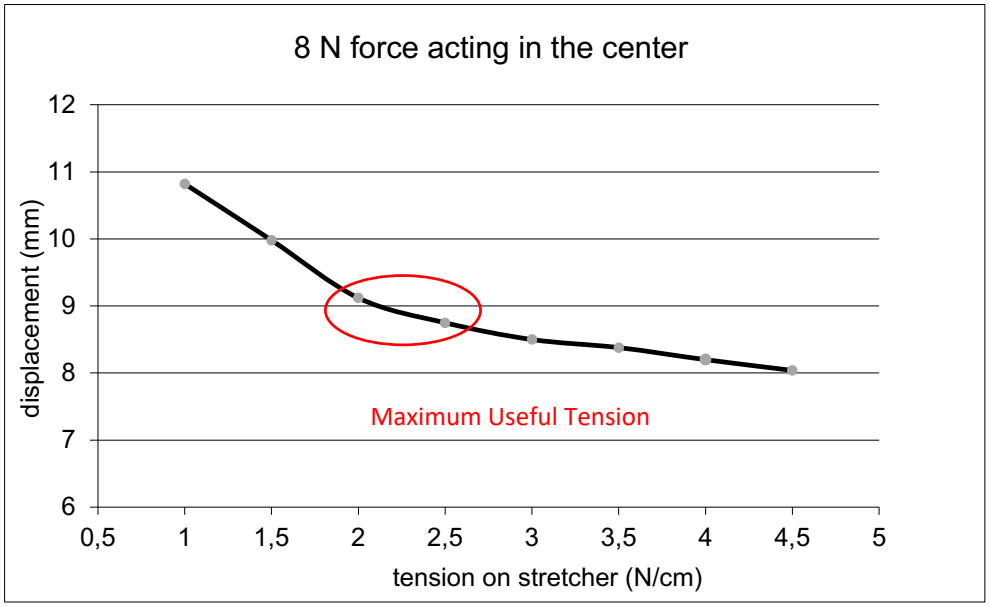

Figure 8 The influence of tension on the displacement of the painting decreases at MUT value, from [Iaccarino Idelson and Torre, 2004]

2.2.1 Boundaries for the choice of tension

A survey involving 106 mid-career paintings conservators[17] recorded the value of tension they judged correct for the same mockup painting [Iaccarino Idelson, 2009]. Results show explicit trends: traditional liners chose values above 4 N/cm; conservators

[17] The survey was carried out between 2004 and 2006 by Antonio Iaccarino Idelson and Carlo Serino, with the participation of Mauro Torre and Giorgio Capriotti. The mockup reproduced a modern, unlined painting measuring 1 x 1m.

specializing in contemporary art chose values below 1 N/cm; the large majority (80.2%) chose values between 0.8 N/cm and 3.1N/cm. The weighted mean of choices, divided in intervals of 0.3 N/cm, was 1.7N/cm (Figure 9). This suggests that most conservators based their choice on an experience-based awareness of the MUT, preferring values below 2.5 N/cm. Such values are also in agreement with previous research, as Gustav Berger suggested that conservators intuitively choose tensions between 2 and 3 N/cm [Berger and Russel, 1990], and Alain Roche, who based his research on the reference value of 2 N/cm [Roche, 1993; Roche, 2016]. A low elastic constant of the springs[18] is crucial [Nimmo et al., 1996; Iaccarino, 1996; Iaccarino Idelson, 2005; Mecklenburg, 2021] because it allows the springs to adjust their elongation to that of the painting with a small change in force. When the painting contracts, the springs will extend, but the force applied to the painting will only have a small increase.

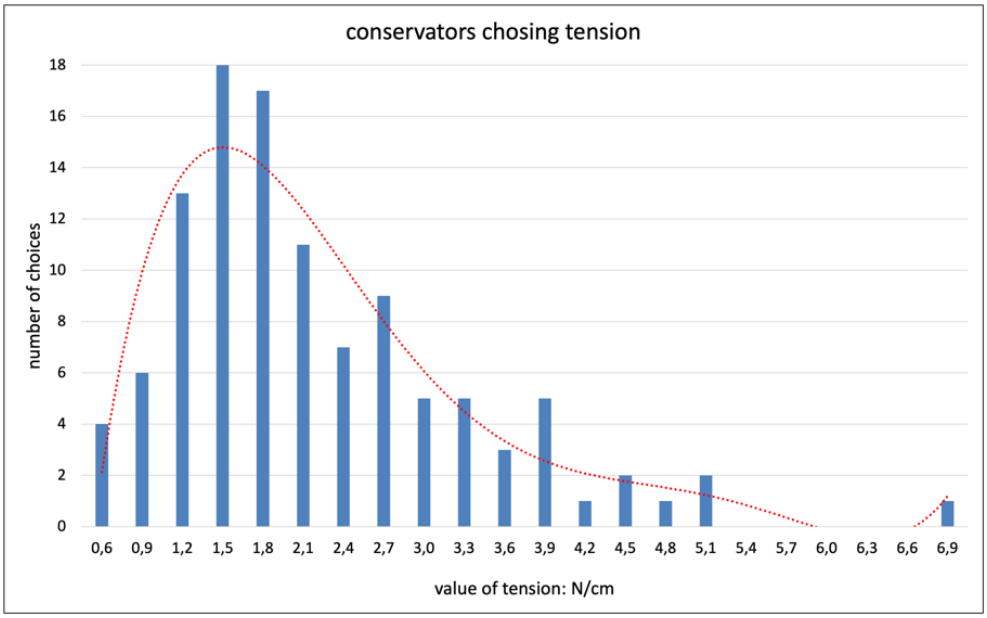

Figure 9 Tension chosen for the same mockup painting by 106 Italian conservators, from [Iaccarino Idelson, 2009]

Several hundred paintings have been stretched according to these principles since the late 1990s in Europe, the USA and Latin America, and low elastic constant springs allow

[18] The "spring constant", or "k" in the Hooke law $F=\boldsymbol{k}\Delta l$ represents the stiffness of the spring because it describes the quantity of elongation undergoes to provide a given force. A small value of *k* describes a spring that requires a great force to elongate.

paintings to experience substantial environmental changes, as in the case of the three large format paintings by J. Miró "Peintures murales pour un temple", exhibited in a hall with extreme RH variations and showing neither deformation nor new cracks for 10 years [Iaccarino Idelson et al., 2019]. Extremely fragile artifacts, such as the early 16th-century double-sided banner painted on silk by Sodoma [Ciatti et al., 2009], have been stretched on long springs with a low elastic constant for almost 20 years, showing no out-of-plane deformation nor damage. The largest wax-resin lined canvas painting in the Rijksmuseum, "The Battle of Waterloo", by J. W. Pieneman[19], measuring 566 x 823 cm, with an estimated weight of at about 100 kg, was mounted in 2012 on a strainer with cylindric profiles turning on ball bearings [Sozzani et al., 2013]. The elastic system kept a good balance of forces, and has prevented the insurgence of any distortion with the tension of 3.2 N/cm, higher than the MUT because it is an oversize and extremely heavy painting. The choice was based on previous experience and the Rijksmuseum conservators involved in the project were satisfied with the chosen tension on the basis of the feel of the painting to the touch, being close to what is expected when stretching a canvas with a traditional approach[20].

Measured values of tension, chosen in consideration of their characteristics, have allowed the safe conservation of the paintings for decades, and have reduced new cracks formation in the pictorial layers, as shown by Alain Roche for a large painting by O. Debré on elastic tension since 2002 [Roche, 2016]. The tension values used for different categories of paintings were summarized in 2021 at an Expert meeting of the Getty Conserving Canvas Initiative [Iaccarino Idelson and Serino, 2021]. During the same meeting, Marion Mecklenburg confirmed that such values are in the safe region for similarly categorized paintings, according to his research [Mecklenburg, 2021].

2.2.2 Early phases in the collection of data on the mechanical behavior of canvas painting materials

The role of conservation-related sciences in the care of museum objects has been continuously increasing since the late 19th century. In 1930, under the auspices of the *Office International des Musées,* the "Conférence Internationale pour l'étude des méthodes scientifiques appliquées à l'éxamen et à la conservation des oeuvres d'art" was held in Rome. The Conference was dedicated to the study and diffusion of the scientific methods and technologies allowing deeper knowledge of the materials and of the artists techniques that could influence their conservation [Cardinali et al., 2007].

[19] The 1824 painting by J.W. Pieneman is at the Rijksmuseum Amsterdam, inv. n. SK-A-1115.
[20] Laurent Sozzani, Lisette Vos, Anna Krekeler, Erika Smeenk-Metz, Ige Verslype.

The introduction of engineering studies in the conservation of canvas paintings started around the mid 20th century, although the interest for the understanding of the causes of their degradation, and attempts to find solutions are documented from much earlier times. An example is in the work of Roberto Carità, an art historian with an engineering background who proposed the above-mentioned elastic tension systems [Carità, 1955], while he worked at Istituto Centrale per il Restauro in Rome until 1960. During the same years, the ICOM Commission for the Care of Paintings asked Dr Christian Wolters, director of the laboratory of the Bayerische Staatsgemaldesammlungen in Munich, to prepare a study on the supports of canvas paintings, and the 1960 number was dedicated to "The care of paintings: fabric paint supports" [Wolters, 1960]. This contributed to bringing the structural treatments on canvas paintings to the general attention of the conservator-restorers community, since at that time these were still delegated to the specialized figure of the liner, who was not a restorer but a technician. In 1969 Giovanni Urbani, in collaboration with the ICOM Commission for the Care of Paintings, started the research described in "Propositions pour un programme de recherches sur la conservation des peintures sur toile" [Urbani, 1969]. The objective was to provide reproducible material science data that could be used to support conservation choices. Preliminary results were presented at the ICOM CC Madrid Conference in 1972 [Conti and Tassinari, 1972], where usual lining canvases were described for their creep. The overall outcome of this research was the 1973 book[21] "Problemi di Conservazione" [Urbani, 1973], that saw a close collaboration with textile engineers Enzo Tassinari, Walter Conti and Ennio Sorta, from the SNAM Textile Research Center in Milan. Tassinari focused on the mechanical characterization of lining canvases, and on their tension during lining [Tassinari, 1973 **(a)**; Tassinari, 1973 **(b)**]. Together with Conti, they studied their creep under cycling tensions [Conti and Tassinari, 1973 **(a)**], and proposed an optical method for the determination of twist in the yarns of a painted canvas [Conti and Tassinari, 1973 **(b)**], which will be further developed in chapter 3. Another study deserving attention is that of Sorta, who suggested measuring the elastic modulus of a canvas painting, considered as a whole, a composite material, by means of the speed of an elastic wave [Sorta, 1973], as we will see in chapter 4. Sorta proposed the use of a commercial device, the "Dynamic Modulus Tester"[22], what was done a few years later in textile engineering studies [Blyth and Postle, 1979], to measure the elastic modulus for different kinds of textiles.

---

[21] A collection of 36 essays and papers by 48 authors, on the most sensitive conservation subjects (canvas, panel and wall paintings, stone, glass, metals, ceramics and paper artifacts) analyzed with a scientific and technological approach. Holographic techniques and thermal images, at the time new in conservation, were also introduced

[22] In 1973 it was produced by the Morgan Inc., today the Lawson Hemphill Inc. produces a similar device, the LH 551 DMT.

The 1974 Greenwich Conference on Comparative lining techniques, was a watershed for the structural conservation of canvas paintings, and its chair Westby Percival-Prescott reported that: "Testing of materials, and mechanical aspects of lining procedures (still in the early stages in this field) were dealt with by Tassinari (Italy) in the Physical characteristics of canvases" [Percival-Prescott, 1975]. Tassinari's work [Tassinari, 1974] produced a durable echo in the conservation community and appeared in the list of references of later researchers for a decade. After Greenwich, Gerry Hedley, a civil engineer with a training in conservation working at the Courtauld Institute of Art, presented at the 1975 ICOM-CC in Venice an influential, early study "Some empirical determinations of the strain distribution in stretched canvases", in which he used a visual method for the localization and quantification of the tension-related strain in a canvas [Hedley, 1975 **(a)**]. This paper may be considered to be among the antecedents for the FEM based simulations, as it uses engineering tools for the description of strains within the surface of the painting. Caroline Villers introduction[23] to the 2003 print edition [Villers, 2003 **(a)**] of the papers from the Greenwich Conference is a perfect conclusion for the description of the state of the art in the 1970s. "*In 1969 at the ICOM-Committee for the Care of Paintings Triennial Meeting in Amsterdam, Professor Urbani presented an influential paper calling for a systematic program of review of lining practice, especially the physical and chemical relationships between the constituents of the lining and the original materials of the painting; […] Urbani had initiated an investigation on the structural and mechanical properties of canvas "in line with the most up-to-date findings of the science of materials" and Tassinari explicitly discussed the use of a scientific model for solving problems […] Berger, Hedley, Mehra and Tassinari, among others, promoted an entirely new way of evaluating the performance of lining materials in relation to the original painting, and in the 1980s Mecklenburg's work extended the materials science aspects of this approach to the mechanics of the painting composite.*"

2.3 Loads and mechanical properties

2.3.1 Studies in crack formation

Studies on crack formation in historical paintings aim at reconstructing the causes that led the paint layers to develop cracks by analyzing their directions and patterns. This does not provide a quantification of the forces but estimations of the distribution and local concentration of stresses within the painting during its conservation history by looking at their effects. Cracks are perpendicular to the force vector and their presence proves that forces exceeding the material's ultimate load were reached [Keck, 1969; Mecklenburg, 1982; Karpowicz, 1990]. This approach also provides information about

[23] Pages XII-XV.

the material characteristics of different mixtures of pigments and binders, as some will develop more cracks than others, or will show different plastic deformations before the cracks appear. Their localization and shape provide data about the causes of the forces, which originated within the paint and preparation layers, in the sizing layer or in the canvas on stretcher.

The stretcher is a rigid structure providing spatial reference to the painting by imposing a constraint to the canvas, and plays a very an important role in crack formation. The level of tension and the forces that develop between painting and stretcher with environmental changes, have been studied since the 1980s [Berger, 1981; Mecklenburg, 1982; Russel and Berger, 1982; Accardo, et al. 1992] and research provided an insight into the mechanics of the relationship. Alain Roche studied the influence of the connection of the painting on stretcher, by comparing crack formation on mockups on different stretchers in presence of environmental changes, demonstrated that the presence of springs to mitigate stress buildup allowed a significative reduction of crack formation, from 22,24% to only 0,92% of the painting's surface [Roche, 1993]. Analyzing the case study of a large contemporary art canvas painting (6 x 2 m) by O. Debré, he demonstrated that after changing the stretcher with an elastic strainer with low elastic constant springs in 2002, crack formation had not progressed further [Roche, 2016]. The presence of microcracks in the paint layers allowed the study of the behavior of the fibers in the yarns of the textile used for painting in presence of environmental changes [Scharf et al., 2021].

Modeling paint layer cracks allows their causes to be studied, and FEM simulations can provide detailed understanding of their formation and progress. As we will see, the choice of the input mechanical data to implement the FEM model is always a key issue. In [Giorgiutti-Dauphiné and Pauchard, 2016], mechanical data was obtained through micro-indentation on a mixture of stiff and deformable colloidal particles on a non-porous substrate, providing the elastic modulus and the time for stress relaxation for visco-elastic systems. A different approach was followed in [Roche and Soldano, 2018] who used data derived from dried paint samples constrained during environmental variations (as in [Lee et al., 2022]) and mechanically tested for the ultimate load, to determine the safe environmental values and the amplitude of their fluctuations. Alain Roche also developed a dedicated program, "*e.PRI*" [24] evaluating a "risk index" on the basis of a 6-12 months record of environmental data of the exhibition space for a specific painting, proposing recommendations for safe environmental values.
An interesting example is found in [Lee et al., 2022] where numerical modelling of the behavior of an oil painting on canvas is used to simulate and analyze its behavior under

[24] https://www.larcroa.fr/e-pri-e-painting-risk-index/

desiccation, aiming to isolate the role of the glue size layer in determining corner bulging and crack formation. The glue sizing, oil-bound preparation, and paint layers elastic modulus are modeled starting from Mecklenburg's tests on restrained samples of the materials. The canvas and wooden strainer were modeled from literature data. The role of the glue size is demonstrated, as the presence of animal glue causes the reduction of the painting's dimensions, and the deformation (lateral torsional buckling) of the wooden strainer reduces the stresses in the paint and preparation layers and therefore crack formation.

2.3.2 About the mechanical characterization of the materials of canvas paintings

The elastic modulus describes the response of a homogeneous material to a tensile force acting along its length, and is the ratio of the stress (force per unit area) applied to the object and the resulting axial strain (deformation) in the linear elastic region of the material. The definition itself implies a difficulty in applying this fundamental parameter to the constituent materials of paintings on canvas, which are not homogeneous materials, and have extremely variable morphology and compositions. Even the definition of a linear elastic region can be controversial, and the stress-strain curve is not directly comparable to that of standard engineering materials, as it is often divided into regions corresponding to a stepwise adaptation of the material to increasing load. It is nevertheless commonly used for the study of historical materials because it provides a very useful approximation allowing comparisons and predictive simulations to be made.

Among the data characterizing a textile, the value of crimp, representing the degree of undulation of the yarns, plays a key role in the tensile response. When subjected to tension, yarns undergo a "de-crimping" phase, in which the fibers will only partially respond to tension [Roche, 2003]. The amount of twist also describes the tensile response of the yarn, because it determines fiber cohesion. The sizing layer makes a significant contribution to the structure of the painting, as animal glues have a high modulus of elasticity at low relative humidity. However, their modulus decreases very rapidly with water content [Janas et al., 2022; Bridarolli et al., 2022].

The elastic modulus of preparation and paint layers is determined by the type of seeds used to produce the oil (such as flax, poppy or others) and even more by the interaction with the pigments bound in it, which leads to the formation of paint films with very different reactions to tension and environmental changes [Mecklenburg, 2007]. The available data come from the work of researchers who have physically tested samples of paint layers. The main difficulty in performing such tests lies in the preparation of the samples, since the paint layers are usually applied to a permanent support (a canvas with a layer of glue), which must not be present in the sample in order to be able to separate its behavior during the test. Paint materials must be applied at a constant thickness to a non-absorbent support that will not adhere to them during the considerable time

required for the film to mature and set. In addition, their mechanical properties change over time as polymerization or other curing processes in the binder progress. Most of the available data on mechanical behavior comes from the work of Mecklenburg [Mecklenburg, 2007], Hagan [Hagan et al., 2015], Roche [Roche, 2016], and a limited number of other researchers who were concerned with making samples, allowing them some setting time, and testing them under certain environmental conditions. Similar procedures only allowed the testing of new or relatively young samples of paint layers, since thermal or other artificial aging processes do not reproduce natural aging, but only provide stiffer materials with little connection to the original [Erhardt et al., 2000]. A lively public debate on the use of aging protocols of the materials used in [Carr et al., 2003] to mimic the mechanical behavior of a "typical 19th-century English painting" can be found in the letters to the editor in Vol. 49 (2004) of Studies in Conservation. In addition, the degree of structural homogeneity of the paint film is variable, and in addition to age cracks, discontinuities, agglomeration of materials, and air bubbles are often present. Alain Roche modeled the form of such discontinuities extracted from cross sections and used them to predict the failure mechanisms in paint layers [Roche, 2016].

2.3.3 Extracting the materials properties from mechanical testing

Mechanical testing provides information about the object with all its complexity and the uneven distribution of the loading sections within the structure. In the case of a canvas, the directions of the yarns and the empty spaces between the fibers that constitute them introduce variables that depend on each single case, thus making the comparison between different textiles not as straightforward as it may seem. For this reason, different methods have been developed over the years to extract the materials properties from each specific test [Mecklenburg et al., 1991; Young, 1996 a; Chiriboga, 2013; Maraghechi et al., 2023 a], in order to obtain information that is as independent as possible from the overall structure.

2.3.4 Degree of conservation of the fibers affecting materials properties

Natural fibers are subject to degradation, mostly due to depolymerization that causes shortening of the cellulose chains. Degradation implies a reduction of the mechanical properties and affects the conservation of the artifact. The analysis of the degree of polymerization of the cellulose of a textile has been used as a quantitative argument to define the actual need for a lining treatment for a painting [Scicolone et al., 1996] and [Timar-Balazsy and Eastop, 1998]. The relation between the Degree of Polymerization of the supports of canvas paintings has been used, setting a limit DP value of about 600 to assess the need for treatments or to elaborate about their structural stability. The viscometric method used for the determination of the DP is laborious and requires the careful extraction of contaminants (sizing among others), and requires the use of a relatively large sample. Such characteristics have often questioned its reliability because

the yarns used to measure it are typically extracted from the tacking margin, where they are freely accessible. Still, the forms of degradation are very different from those encountered in the painted areas, that may actually be more degraded because of the migration of acidic materials from the painting. Still, the unpainted textile along the tacking margin may also have important degradation, accumulated because of different causes. The correlation between DP and pH has been investigated [Oriola et al., 2014] and [Oriola et al., 2015], remarkable works that have seen the analysis of considerable numbers of samples. Such correlation underpins the effect of acidic degradation (due to environmental or intrinsic factors) is a key factor for the reduction of the Degree of Polymerization of the cellulose fibers, setting the limit at about pH 5. Techniques aiming at the definition of the degree of cellulose depolymerization and degradation of the textile to inform conservation treatments have advanced and evolved [Bräunig et al., 2023] and have been applied to archaeological artifacts [Reynaud et al., 2020]. The use of Raman spectroscopy to determine the crystallinity of the cellulose can be used for both the identification of the fibers [Garside and Wyeth, 2003] and the definition of their state of conservation and expected mechanical performance [Edwards et al., 2006].

2.3.5 Nanoindentation and microscale testing

Nanoindentation [Lukomski et al., 2022] is the frontier tool to obtain mechanical data on historical materials with a very high definition, such as the individual layers of the painting in a cross section, requiring only extremely small samples. The main problem is the interpretation of the data, because the technique provides the correlation between the force acting on the sample causing the indentation, and the depth and shape of such permanent deformation. The interpretation of the mechanical data derived from nanoindentation and its calibration is at present the object of different working groups, that are proceeding in different research directions. On one side we see the method used to evaluate the mechanical properties of contemporary art materials [Almasian et al., 2021]. On the other side we see the use of nanoindentation on cross sectional paint samples of materials that can also be tested as free film samples to obtain standard reference values [Freeman et al., 2019]. The goal of this research direction is to find ways to interpret the mechanical evaluations from nanoindentation in order to provide data usable in predictive FEM simulations. In [Fujisawa and Lukomski, 2019] nanoindentation procedures are analyzed in order to clarify the correlation between the viscoelastic painting material and the constraint offered by the much stiffer embedding material in a cross section. In [Tiennot et al., 2020], nanoindentation is used on samples of a reproduction and of an historical painting, proposing a protocol that allows their mechanical characterization. In [Lukomski et al., 2022] a review discusses nanoindentation studies of artists' paints carried out over the last two decades. Their analysis of experimental and theoretical works focuses on understanding the limitations of the technique and developing strategies to overcome them. These include evaluating the influence of sample preparation and material heterogeneity on the results obtained,

as well as establishing correlations between micro/nano-scale and macro-scale mechanical parameters.

A different approach, testing cellulose fibers at the micro-scale, is found in [Maraghechi et al., 2023 **(a)**], based on in-situ micro-tensile testing combined with optical profilometry. Micro-scale testing allows reducing the sample size to dimensions that may be considered compatible with sampling from an historical artifact. Like nanoindentation, the correlation with the macro-scale, that of the historical artifact, is not always straightforward.

2.4 The central goals of this research

As we have seen, the knowledge of the mechanical properties of canvas paintings is mostly based on tests performed on new materials or on materials that have undergone the relatively short natural aging process that corresponds to part of an individual researcher's professional life. Very little data is available on naturally aged, historical materials, and over time research has focused primarily on the paint and preparation layers. The canvas support of paintings has not been thoroughly analyzed and, for conservation uses, textiles have been studied mostly when dealing with the industrial ones used for lining paintings [Young and Jardine, 2012]. Knowledge of traditional hand-woven textiles is very limited, even from the point of view of their description, because most of the methods used to analyze modern textiles cannot be applied to the historical ones. Furthermore, the variability of historical textiles is much higher than that of the modern ones, and statistical relevance is of greater importance. For these reasons, most of the research carried out on the description of canvas paintings supports is dealing with only very few data even in very deep studies [Vandivere et al., 2019]. The availability of specimens that can be analyzed and tested is a real bottleneck, and an in-depth study of the canvas supports of paintings is urgently needed in order to reduce the level of approximation that characterizes the field.

Another level of the problem is the availability of testing machines for the small samples that can be obtained from historical materials. The normal loading condition for a textile is that of a tension applied simultaneously in the two axes (warp and weft), although not necessarily with perfect symmetry. Biaxial lading becomes crucial when describing the tensile response of a textile, because any load applied in one of the two axes will be affected by the loading condition of the other, and a certain degree of “stiffness transfer” will always take place. Since biaxial machines are extremely rare in conservation science, and usually do not allow the testing of small samples, tensile testing of textiles is normally based on a single axis, repeated for warp and weft. These provide values that need to be mathematically corrected [Chiriboga, 2013], especially when performed on textiles that do not carry thick preparation and paint layers that may become predominant in the overall response of the composite material, and this introduces an

unpredictable level of error. Biaxial tensile tests provide instead data that is dependent only on the test conditions, such as speed and environmental parameters. From the point of view of the predictive engineering simulations, it must be emphasized that the raw data from mechanical test describe the behavior of the material as an object with a set of complex features and characteristics. In order to allow comparisons between different materials, as we have seen, it becomes necessary to calculate the actual loading section area of the material [Mecklenburg et al., 1991]. The methods used to do this have evolved over the decades [Young, 1996 **(a)**; Chiriboga, 2013; Maraghechi et al., 2023 **(a)**], but they are still an open subject because they clearly depend on the quantification of the morphological description of the textile, which is to date incomplete and inaccurate.

The focus of this research is to fill the gaps in both the morphological description of the historical textiles and in their biaxial tensile testing. Mechanical testing of the original materials needs to be preceded by a detailed description of their morphological and material properties, in order to establish correlations between the two levels of characterization. On the one hand, this helps to understand the role of each in ensuring or limiting the stiffness and ultimate load of the textile, and on the other hand, it could be used to make predictions that could reduce the need for physical testing when a treatment decision is required. From the point of view of material properties, the aim is also to organize the data in such a way as to increase the possibility of carrying out simulations that provide reliable quantitative predictions.

For the first time a complete protocol is proposed here, that grants a quantitative description of an historical textile, i.e., providing measures for most of the data required in textile engineering studies about industrial textiles and allowing comparisons to be made. Thanks to the author's position of senior paintings conservator, and to the collaboration of colleagues, a large number of historical specimens have been collected. These were morphologically analyzed in deep detail, and correlations became possible with the warp and weft directions of the textile that ensure a high probability in their identification, also when a selvedge is not available.

Multiple samples from each specimen were subjected to biaxial tensile testing using a dedicated tensile machine that was designed and built for the task. The data will allow correlations to be made with their morphological data and with the loom directions, providing a more robust understanding of the structure of an historical textile. Based on the quantitative description of the morphology of the specimens, a method has been developed to calculate their effective loading area, allowing predictive simulations.

2.5 Methodology

As seen in the literature review, research on the mechanical aspects of the conservation and treatment of canvas paintings is scattered in many different directions. My first action is to analyze and focus on the information that seems most relevant for understanding the morphological and mechanical characterization of the textiles used as support for canvas paintings. Particular attention will be paid to all the measurable data and to the methods used to obtain them.

From a group of 86 naturally aged specimens, 22 plain canvas weave specimens are selected from those with a selvedge. Twelve of these are from paintings with known historical provenance (dating from 1728 to the 1950s) and represent a relatively homogeneous group of mid- to late-19th-century French artworks, then paintings from other contexts, lining and loose lining canvases between the 18th and 19th centuries. Four modern canvases complete the set, both as a link to industrial textiles and because they allow the unlimited sampling needed to calibrate some of the observational procedures.

The observation protocol defined during the research is intended to provide quantitative data for most of the characteristics observed and considered necessary in the textile industry, with the sole exception of the linear density. The exception is due to the fact that the standard reference value is the “Tex”, a direct measure of linear density corresponding to the weight in grams of 1000 m of yarn, while the length of the free yarns available from the samples, in the range of a few centimeters, is insufficient to allow a reasonable accuracy at the same scale. Therefore, the decision was made to measure the density of the textile and not that of the single yarns. Some of the data will be measured as the weighted mean of all the yarns visible in the sample area (such as yarn width and twist), while others represent the simple mean of the highest number of observations possible, 15 for textile thickness, 9 for yarn width, twist and thread count, 4 for textile density, 3 for the crimp and the thickness of the yarns. Correlations will be established between different features and the warp and weft directions, to allow an estimation of the weaving direction when a selvedge is not available.

A biaxial tensile tester designed and built to measure the tensile response of small samples will be used for the 26 specimens. The machine is completely open source, and all design data made available online, in the hope that more machines providing similar measurements will soon be available in the conservation field.

Three to five samples from each of the 26 specimens will be biaxially tested under identical conditions. The secant tensile modulus of all specimens will be calculated at 4 strain values, chosen to allow comparisons between specimens and correlations with morphological characteristics. A very low strain secant modulus is intended to simulate

the response of the textile under a tension comparable to the standard conservation conditions; the second value is intended to describe the decrimping phase (the reduction of the yarns undulation) of the textiles' tensile behavior, for the specimens that will show one; the third value is relatively high, corresponding to the straight line behavior of most textiles, and is intended to match the standard values used in literature to calculate the "general E modulus" of the textiles; the last strain value is intended to be close to the ultimate elongation, therefore it may also turn out useful to compare the ultimate load.

The quantitative morphological description of the textiles will provide all the data needed to evaluate the influence of specific features on the mechanical response. The data will also be used to calculate the loading section of the textiles, using a procedure defined by an equation that takes into account the key features of their different structures.

2.6 Case studies in conservation practice allowing the progress of the research

Two case studies are presented in this thesis, in which the procedures and techniques developed during the research proved useful for the conservation and treatment of paintings in museums. In particular, the work done for Rembrandt's *The Night Watch* at the Rijksmuseum Amsterdam will provide important advances in the understanding, or at least useful preliminary testing, about the use of the theoretical the loading section for the calculation of the tensile and flexural moduli of the layered structure of a lined painting.

2.6.1 Rembrandt's *The Night Watch* at the Rijksmuseum Amsterdam

The Night Watch was installed in March 2022 on a new elastic strainer with a known value of tension and its structure was studied through non-destructive mechanical tests. A custom-built displacement tester was used to measure the response of the painting to forces that caused it to be displaced out of plane while under the known value of tension on the elastic strainer. The painting's behavior in such a controlled setting is also a form of non-destructive mechanical testing, that may eventually be integrated into a FEM model and used to elaborate the values of tensile and flexural moduli intended as an engineering method to solve to solve the multivariable equation required to determine the painting's elastic moduli is also more explicit.

The mockup of a wax resin lined 17th c. painting, inspired to *The Night Watch* because of the wealth of knowledge available about the precious painting, intended as a research object, will be used for testing to determine the mechanical behavior of a similar painting.

Biaxial and uniaxial tensile tests performed on the individual layers and the complete mockup will describe tensile behavior, and the influence of the lining adhesive will also be studied. Flexural tests will be performed on samples of the complete structure of the mockup, using a dedicated custom-built additional tool on the biaxial tester.

The described research on the mockup allows a problem to be faced that appears to be unconventional in the FEM simulations of canvas paintings, that is, modeling the behavior of a lined painting. The definition of the flexural modulus on the basis of experimental data has been attempted before only for the completely different case of a very thin and flexible painting mockup [Chiriboga, 2013]. This was an unlined modern canvas, with extremely thin preparation and paint layers, that could be rolled in the "heart loop test" without being damaged, and clearly a very low flexural modulus was measured. The mockup will be stiff enough to allow using a standard 3-point bending test. The only other reference found in the literature is about panel paintings [Young et al., 2002], and the parameters involved in the calculation of the flexural modulus and in the definition of the loading section are an open subject for relevant studies.

A Displacement Tester (a custom-made device described in chapter 4) will be used to apply a force to the rear of the painting (as in the flexural tests) and measure its displacement. The 48 locations offered by the stretcher's geometry will produce an overall understanding of the painting's resistance to displacement. The tests, repeated after the painting is mounted on the elastic strainer with a known value of tension, may then be simulated in the FE model. The approach will allow further investigating about the values of the tensile and flexural moduli, evaluating the correspondence between the experimental values and the simulation. In perspective, the same model may allow an indirect measurement of the tension the painting had on the 1975 stretcher at the moment when the first set of displacement tests were carried out (January 2022).

2.6.2 A painting by Tiepolo at the Louvre Museum

The structural treatment carried out by the author on the painting and on the re-functionalization of the existing strainer for the elastic tension will be outlined, to represent the extent to which the application of measured procedures can influence the conservation choices. A mockup will be used to represent all the layers in the stratigraphy of the painting for biaxial and uniaxial tensile tests to evaluate the level of anisotropy of its response in warp and weft, and to compare the E modulus of the materials with that of the lining canvas. The lining method, used since 2012 with measured quantities of the adhesive and of the solvent used for its reactivation, allows previsions to be made about the force that would have been obtained in the adhesive joint, thanks to a reference database. These will be verified with peel tests performed on the mockup, lined simultaneously with the painting.

2.7 Summary

The main focus of this thesis will be the study of the morphological and mechanical characteristics of the 26 textiles object of investigation. The first effort will be that of organizing a set of procedures to provide quantitative information about the morphology of the yarns and of the interlaced structures of plain weave canvases. Quantitative data is needed for comparative studies, but also to establish correlations with the tensile response of the textiles, which will also be quantified with the use of the dedicated tensile tester described in chapter 4. The values of 4 secant tensile moduli, calculated along the 26 stress-strain plots will be analyzed and compared with the data derived from literature.

The use of elastic tensioning systems allows the value of the paintings' tension on stretcher to be known with precision, and this was done by the author on several hundreds of paintings during the last 30 years. The knowledge of the forces allows the evaluation of their effects on the painting, and considerations about the perspectives of its structural integrity within a specific environment. The use of this approach will be described for two case studies, Rembrandt's *The Night Watch* at the Rijksmuseum Amsterdam and a detached wall painting by Tiepolo at the Louvre Museum Paris. The case studies, outstanding masterpieces in extraordinary museum contexts, are very different and offer possibilities for better understanding the mechanics of the paintings and the issues of structural conservation.

Chapter 3 Quantitative morphological description of the canvas structure

Outline of the chapter

3.1 Introduction and general definitions
- 3.1.1 Aims of the research
- 3.1.2 The specimens object of the research
- 3.1.3 Sample preparation and statistical data collection

3.2 Measuring procedures
- 3.2.1 The weight and thickness of the canvas, the thread-count and yarn linear density
- 3.2.2 Identification of fibers
- 3.2.3 pH measures
- 3.2.4 Yarn width assessment
- 3.2.5 Twist
- 3.2.6 Description of the method for twist measurements in historical textiles
- 3.2.7 Crimp
- 3.2.8 Description of the method for crimp measurements in historical textiles
- 3.2.9 Yarn thickness measurement

3.3 Experimental results
- 3.3.1 Weight and thickness of the canvas, thread-count, fiber identification and pH
- 3.3.2 Yarn width, thickness and Z axis compression
- 3.3.3 Measures of Twist Per Meter
- 3.3.4 Measures of crimp %
- 3.3.5 Crimp value

3.4 Discussion
- 3.4.1 Characteristics allowing the identification of warp and weft without a selvedge
- 3.4.2 Warp and weft correlations in literature

3.5 Conclusions and future work

3.1 Introduction and general definitions

The structure and morphology of the textiles used as supports for historical canvas paintings is known with surprisingly little detail when compared to the possibilities and requirements of the textile industry [Pierce, 1937; Neckář and Das, 2018]. This is largely due to the fact that it is not as easy to take samples from a historical artifact as it is from a new industrial product, and also because the support of canvas paintings is typically impregnated with foreign substances. Nevertheless, such difficulties have led to a kind of resignation in conservation science, as if further data were simply impossible to obtain.

In the course of this study, organizing a set of protocols allowing the quantification of morphological parameters for the description of historical textiles proved to be a powerful tool, providing observations with a repeatable basis. Quantification allows the

study of individual parameters and structures, and new possibilities are opened for the correlation with their mechanical response. The characteristics of warp and weft yarns in canvas paintings can be described using a systematic approach to their structural analysis, with reference to the methods used in textile engineering. In this study novel methods will be used to measure crimp, twist, yarn width and thickness, and the process will investigate the possibility to identify warp and weft directions when a selvedge is not available. Thread count, thickness, weight, and pH of the textile will also be measured on 26 samples, most of which were taken from historical paintings of known provenance. The study will allow for a deeper understanding of the making of a traditional textile and will provide interpretations for the structural organization of fibers in historical woven structures. These insights will also be useful for technical art history and to support conservation decisions.

In addition to obtaining a better understanding of the structure of the historical canvases used for painting and lining, this study provides measurable data that will allow the comparison of different textiles and open possibilities for their analysis using textile engineering methods. The information will be collected in a reference database with the aim of establishing correlations between specific characteristics of the interlacing yarns with the mechanical behavior of the textile in tensile tests. The description of a woven structure in the textile industry is based on a set of fundamental data, that are needed to characterize it, to make predictions about its structural behavior [Pierce, 1937; Behera et al., 2010], and to allow comparisons between different fabrics. The usual information required includes:

- the thickness of the textile,
- weight/m^2 of the textile,
- the type of woven structure (plain weave or other),
- the type of fiber,
- the number of yarns/cm,
- the diameter of the yarns,
- their weight per unit of length,
- the percentage of crimp the yarns undergo during weaving,
- the number of twists per unit of length during the spinning process.

When describing a historical textile, the only data usually available are the type of weave, the thread-count and the nature of the fibers. The pH and the degree of polymerization of the cellulose, which are not often needed in the textile industry, are sometimes measured in conservation as indicators of degradation processes and are used for treatment decisions [Maraghechi et al., 2023 b]. Most other measurements are complicated by the variability of historical materials and their limited availability for sampling. The presence of sizing and paint layers is an additional limitation, particularly

influencing the measurements of the weight and thickness of the textile. The weight of the yarn per unit length, although a fundamental piece of information in the textile industry, is very difficult to obtain in the field of conservation due to the unavailability of clean yarns of sufficient length[25], as we have seen in chapter 2, but this information can be considered of secondary importance for historical textiles if other descriptors are available.

The diameter of a yarn can only be measured before weaving, as yarns acquire an elliptical shape during the process. The observation of historical artifacts requires two measurements to provide the axes of its elliptical section: the yarn width within the Cartesian plane of the textile, and the yarn thickness. The width of historical yarns is very uneven along their length when compared to industrially spun yarns, making it more complex to provide a repeatable value [Berry et al., 1978]. Non-destructive observations of images in the XY plane of the textile allow width to be measured with a statistical approach, while yarn thickness, which is only visible in the Z plane, requires invasive observations and is therefore more limited.

Twist and crimp values are of paramount importance to the textile industry in understanding the properties and performance of a textile, and their quantification has been a subject of study since the early 20th century, and have always made the object of textile technology studies [Pierce, 1937; Mertova et al., 2016; Neckář and Das, 2018]. The capability to quantify them for historical textiles would allow a much deeper understanding of their mechanical properties and behavior, thus improving the possibilities for their conservation. In particular, for textiles that are not constrained by foreign materials such as sizing, preparation, or paint layers, knowledge of the crimp and twist in the yarns is also relevant from the point of view of the treatment choices, as both affect their mechanical resistance. Quantitative data describing historical textiles [Iaccarino Idelson et al., 2025 **(a)**] allow morphological comparisons and the use of statistics, and will hopefully improve the robustness of conservation strategies.

Detailed technological descriptions of ancient textiles including twist and crimp measurements are rare. In [Berry et al., 1978] they were made possible by applying the engineering approach to an exceptionally rich archaeological find. The standard method of measuring twist in a yarn is to untwist it and count the number of turns required to

[25] The standard reference is the Tex, a direct measure of linear density of the yarn providing the weight in grams per 1 kilometer of yarn. Industrial yarns are weighed when rolled on bobbin, a simple operation with the additional advantage of lowering the error due to the length of the sample. When dealing with historical textiles, the length of the yarns available for weight measurement are often no more than a few centimeters and they are often contaminated with substances that affect their weight.

revert the fibers to their original state, parallel to the yarn axis [Saville, 1999]. In most cases, this is not applicable to historical textiles, because the yarns are too fragile to withstand such mechanical manipulation or are impregnated with substances that would not allow it [Conti and Tassinari, 1973 **(b)**]. Observation based methods are used to measure the "twist angle", as described in handbooks [Seiler-Baldinger, 1996], papers [Rouba, 1992], archaeological reports [Ostergard, 2004] and in studies dedicated to thread-by-thread tear mending [Flock, 2020 **(a)**]. However, the twist angle is a semi-qualitative value as the actual number of twists per meter in a yarn, obtained through the correlation of the angle with the width of the yarn, is not provided. A method that allows a correlation between the twist angle and the actual count of the twists per unit of length to be made [Conti and Tassinari, 1973 **(b)**, **see Appendix 3**] has never been used in conservation science before the present study, and its application is published in [Iaccarino Idelson et al., 2025 **(c)**]. Similarly, the standard method for measuring crimp is also mechanical, based on uncrimping the yarn by pulling it straight to calculate the difference in length, and this is also not possible for naturally aged textiles. The path the yarn travels in the textile can be calculated by analyzing its waveform in the cross section of the fabric [Mertova et al., 2016] or by observing the image of individual yarns [Young and Jardine, 2012], because geometrical simplifications provide reliable data for modern, regular textiles. An alternative optical method is based on drawing a line on the neutral axis of the yarn using specialized software [Kolcavova Sirkova and Vysanska 2012]. This approach was found to be the most suitable for describing irregular crimp configurations and was used for the study of historical yarns [Iaccarino Idelson et al., 2025 **(a)**].

The most comprehensive descriptions available for the canvas supports of paintings are obtained from the analysis of radiographs and provide information on the position, direction, and frequency of the yarns [van de Wetering, 1997; Johnson, et al., 2013; Noble et al., 2018]. In the textile industry, automated methods to obtain the thread count from the image of a textile are being developed [Pan, et al. 2015; Aldemir, et al., 2018]. Although very useful for industrial inspection, or for technical art history, the methods do not provide all the quantitative data needed for the structural characterization of historical textiles. The need for such information becomes stringent when trying to find correlations between the mechanical behavior of historical textiles under tensile testing and their morphological features. In preparing this chapter, the decision was made to apply the basic technological definitions listed above to historical artifacts, in order to test the limits of objective knowledge[26].

[26] A paper describing the general methodology for structural and morphological characterization of warp and weft yarns in canvas paintings has been accepted and is currently undergoing peer review [Iaccarino Idelson et al., 2024]

3.1.1 Aims of the research

The methodological study proposed here aims at a systematic approach to the structural analysis of the canvas painting supports with reference to textile engineering methods. As we have seen in the definition of the goals of this research, this is the fundamental level of understanding of historical textiles that needs to be addressed to obtain a set of quantitative data to be used as a reliable base for further studies. Such an opening would expand the possibilities for understanding their mechanical behavior, allow predictions about deterioration processes, and improve the assessment of conservation conditions. The individual characteristics, such as yarn width and thickness, twist, crimp, and even the thickness and weight/m^2 of the textile, present specific difficulties when dealing with a sample that is highly variable, limited in quantity, degraded, and contaminated. The organization of simple statistical methods for data collection is also a relevant subject, since the goal is to allow comparisons.

Twist and crimp are the result of the way the fibers have been modified from the original bundle to shape the textile; therefore, the standard measurement methods are based on mechanically reversing these deformations until they return to their initial unorganized state [Booth, 1968; Saville, 1999; Czaplicki, 2006]. When testing naturally aged canvases, the availability of samples of suitable dimensions is a major limiting factor. In addition, naturally aged yarns are fragile and would break before the mechanical processes required for the measurement are complete. Furthermore, in a painted canvas, the yarns are locked into three-dimensional structures, and unwinding or decrimping them is simply not an option [Conti and Tassinari, 1973 (b)]. Therefore, data on these two key parameters are typically unavailable for the characterization of historical textiles and the canvases that support paintings. The development of methods to measure these two fundamental variables on complex ancient textiles, knowing that methods were not available, and are urgently needed.

The quantification of the morphological characteristic of historical textiles will allow using reproducible definitions. These are will help identify recurring characteristics that can provide a degree of confidence in the identification of warp and weft yarns when a selvedge is not available. Since the mechanical behavior of the textile is different in the two directions [Young and Hibberd, 1999], this is also an urgent need, and their identification can be relevant for conservation and research purposes [Rouba, 1980; Noble et al., 2018].

3.1.2 The specimens object of the research

The need for this study arose when approaching the mechanical examination of a group of specimens with uniaxial and biaxial tensile tests using a dedicated device designed and built by the author, described in chapter 4 and published in [Iaccarino Idelson et al.,

2023]. A group of "plain weave" fabrics[27] without paint layers was selected, all of which have a selvedge to ensure that warp and weft can be reliably identified. Most of the specimens (22 out of 26) are historical and therefore naturally aged, some with known provenance, date, and artist. These were extracted from paintings (dating from 1728 to the 1950s) during past conservation treatments; 12 of them represent a relatively homogeneous group of mid-to-late 19th century French artworks. Lining and loose lining canvases between the 18th and 19th centuries[28], and 4 modern canvases complete the set. Three of these are industrially woven lining canvases: two typical Italian open-weave paste-glue lining canvases, the “patta” and the “pattina”, from a 2015 lot; the basket weave canvas used in the making of the mockup of a wax lined painting (see chapter 6); the fourth is the manually woven replica of a traditional canvas used by Dutch old masters produced in 2022 within the NICAS project[29] “Canvassing the making”. The complete list can be found in Table 1. This also includes the measures of weight per square meter and pH, that are provided as the mean of the values obtained on the samples from the same specimen. Measurements were performed using the methodology described in the following paragraphs.

		general data			weight measures in grams							
	name	date	fibers	manufacture	sample 1	sample 2	sample 3	sample 4	mean	st. dev.	g/sqm	pH
1	**plain canvas 1**	18th c.	linen	hand	0,076	0,073	0,077	0,079	0,08	0,003	**257**	*6,45*
2	**plain canvas 2**	18th c.	linen	hand	0,130	0,129	0,134	0,125	0,13	0,004	**435**	*6,10*
3	**plain canvas 3**	18th c.	linen	hand	0,068	0,085	0,091	0,086	0,08	0,010	**278**	*6,40*
4	**plain canvas 4**	18th c.	hemp	hand	0,101	0,100	0,092	0,098	0,10	0,004	**329**	*7,35*
5	**plain canvas 5**	19th c.	hemp	hand	0,132	0,132	0,133	0,131	0,13	0,001	**445**	*7,26*
6	**Domenico C. Malinconico**	1728	hemp	hand	0,083	0,076	0,059	-	0,07	0,013	**244**	*6,17*
7	**Bernard d'Agesci**	1817	hemp	hand	0,151	0,126	0,048	0,071	0,10	0,048	**334**	*6,80*
8	**medium paste lining canvas (IT)**	early 19th c.	hemp	machine	0,055	0,047	0,051	0,044	0,05	0,005	**166**	*5,96*
9	**heavy paste lining canvas (IT)**	early 19th c.	linen	machine	0,179	0,189	0,193	-	0,19	0,007	**628**	*5,95*
10	**Fragonard medium paste lining**	mid 19th c.	hemp	machine	0,120	0,118	0,113	0,122	0,12	0,004	**397**	*6,10*
11	**Raffaele Postiglione**	1845	linen	hand	0,083	0,080	0,076	0,075	0,08	0,004	**265**	*5,20*
12	**Alfred Dehodencq**	1870	linen	machine	0,094	0,097	0,102	0,094	0,10	0,004	**326**	*5,55*
13	**Jules Gélibert**	1881	linen	machine	0,073	0,072	0,071	0,068	0,07	0,002	**238**	*5,78*
14	**Louis Augustin Auguin**	1885	linen	machine	0,088	0,091	0,085	0,089	0,09	0,003	**296**	*6,08*
15	**Ludovic Alleaume**	1887	linen	machine	0,072	0,074	0,073	0,076	0,07	0,002	**248**	*5,17*
16	**Hubert Sauzeau 1**	1893	linen	machine	0,058	0,065	0,060	0,060	0,06	0,003	**205**	*6,16*
17	**Hubert Sauzeau 2**	1898	hemp	machine	0,138	0,152	0,150	0,136	0,14	0,008	**485**	*6,62*
18	**Charles Müller**	late 19th c.	linen	machine	0,042	0,047	0,044	0,046	0,04	0,002	**150**	*5,62*
19	**Furcy de Lavault**	late 19th c.	linen	machine	0,067	0,066	0,072	0,066	0,07	0,003	**228**	*6,02*
20	**Louis Alexandre Cabié**	1905	weft hemp; warp cotton	machine	0,085	0,080	0,082	0,081	0,08	0,002	**276**	*5,90*
21	**Louis Lessieux**	early 20th c.	hemp	machine	0,068	0,054	0,052	0,061	0,06	0,007	**197**	*6,39*
22	**Jeannine Gilles-Murique**	mid 20th c.	hemp	machine	0,115	0,122	0,113	0,108	0,11	0,006	**385**	*5,49*
23	**Night Watch mockup canvas**	1975	linen	machine	0,097	0,096	0,101	0,096	0,10	0,002	**380**	*6,24*
24	**"pattina" lining canvas**	2015	linen	machine	0,043	0,043	0,047	0,045	0,04	0,002	**149**	*6,53*
25	**"patta" lining canvas**	2015	linen	machine	0,057	0,051	0,043	0,051	0,05	0,006	**171**	*6,57*
26	**canvassing "03f"**	2022	linen	hand	0,098	0,103	0,103	0,111	0,10	0,005	**349**	*7,78*

Table 1 General data on the samples, with the weight per square meter and pH

[27] The only exception is made for a “basket weave” canvas, a “plain weave” with two parallel yarns. The canvas was added to the group because it was deeply studied in chapter 6.

[28] Among them the canvas used by A.E. Fragonard for his “François 1er armé chevalier par Bayard” to adapt its dimensions when it was first exhibited in the Louvre Museum in 1829

[29] Project directed by Prof. dr. R.G. Erdmann (University of Amsterdam/Rijksmuseum), with S.A.F. Smelt (Rijksmuseum); I. Meijssen (Ingeborg Meijssen Textiles); L. Hassink (Museum Bussemakerhuis); I. Verslype (Rijksmuseum). https://www.nicas-research.nl/projects/canvassing-the-making/

3.1.3 Sample preparation and statistical data collection

Historical textiles require a specific approach to sample selection and preparation. When small samples are available, they are often also difficult to manipulate, so the approach to naturally aged textiles must be as non-destructive as possible. The methods proposed here are based on the observation of a high-resolution scaled image of the samples, rather than a cross section under a microscope as in [Kolcavova Sirkova and Vysanska 2012]. The samples (from both historical and modern textiles) were laser cut according to a common shape to obtain uniform dimensions for the observation area. Furthermore, since samples are intended for mechanical testing, a clear correlation between the characteristics in the samples and their tensile response is established. While the twist measurements proposed here are completely non-destructive, crimp measurements still require the extraction of yarns from the textile in the warp and weft directions. The observation length is typically about 10 mm. The goal of this study is to make the process faster and easier, requiring less specialized equipment, more affordable, and more widely available.

Since they will be subjected to tensile tests, samples are laser cut following a cruciform pattern that allows avoiding any uncertainties about the cutting direction thanks to small indentations in the extremities of the weft clamping area (Figure 10), as described in chapter 4 and in [Iaccarino Idelson et. al., 23]. At least 3 identical samples were cut from each specimen, depending on the quantity of material available. In the cases in which it was possible to cut more (up to 6) the 4 most representative ones were selected for further testing, the remaining being kept as a backup in case of problems during mechanical testing or as possible source of additional information. For the measurements requiring loose yarns, a preference was given to those that could be extracted from the specimen around the boundaries of the laser cut sample, in order to be as close as possible to the sample itself.

Figure 10 The image of one of the laser-cut samples (n. 13), with the indentations in the weft direction (photo credit: Antonio Iaccarino Idelson)

Laser cutting provides a precision measure of the area of the sample, that was used to calculate the weight of the textile in grams/m^2. The sharp 10x10mm testing area, identical for all samples, was photographed at high-resolution[30] with a 2:1 macro lens, and scaled to the real dimensions to take precision measurements of the individual yarns with a CAD[31] software. As a consistent area of observation is defined, a simple statistical treatment of the measures was obtained by dividing the yarns in each direction into subsets for relative dimensions: Small, Medium and Large. One yarn from each subset, chosen as the most representative, was measured at three locations. The mean value of the measures for each subset (Figure 11) was calculated. The process resulted in a matrix of 9 measures of warp and 9 of weft, to describe the value of a specific feature in each 1 cm^2 area of observation (see Figure 12). The method makes it possible to obtain a weighted mean that takes into account the numerosity of each class, thus providing an information that can be considered reliable and meaningful for the observation area.

[30] 5568x3712 pixels, taken with a 2:1 macro lens.

[31] Rhinoceros, Robert McNeel & Associates version 7 was used, but the same tools are found in earlier versions and in other software such as Autocad, and in libreware and non-proprietary applications.

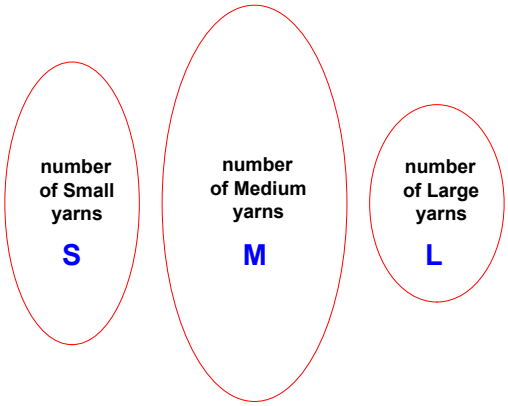

Figure 11 The yarns in warp and weft divided in 3 sets, grouping them for relative dimensions

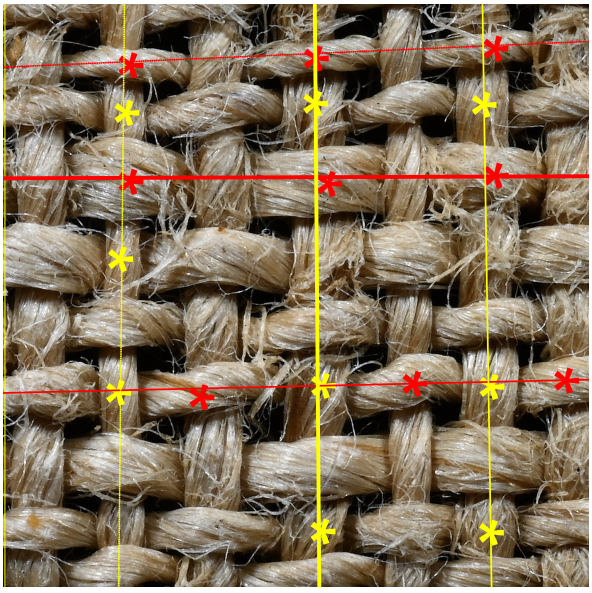

Figure 12 Example of the observations on the subsets. Yarns in warp (red) and weft (yellow) selected as representative of the Small (S), Medium (M) and Large (L) width subsets within the 1cm2 observation area, and the observation points

3.2 Measuring procedures

3.2.1 Weight and thickness of the canvas, thread-count and yarn linear density

The samples[32] were weighed using a certified analytical scale[33] with a resolution of 0.1 mg and a repeatability of +/- 0.05 mg. As the sample surface is a given information thanks to the laser-cutting procedure[34], a simple calculation provided the weight in g/m^2, averaging the weight of 4 samples (though for specimens 6 and 9 only 3 were available). The thickness of the canvas was measured using a 6 mm diameter flat-end micrometer with a resolution of 0.001 mm, that is provided with a constant measuring force mechanism assuring that always the same compression force [35] is applied. Measurements were repeated at 5 points on each of 3 samples, as shown in Figure 13. For thread-count, the number of yarns in both directions was counted at three locations in different samples. The data are correlated with each sample, and the general mean and standard deviation are given.

The thread count of a textile is the subject of many textile engineering studies, and automated methods have been proposed since the second half of the 20th c. [Hosseini and Toriumi, 1995]. Manual counting the yarns is a time-consuming operation that easily incurs in experimental error, but it should also be considered that the thread count is not constant within the same textile. Therefore, in order to obtain values representing the textile, and not only a relatively small area of observation, a valid alternative is counting on large areas (possibly with an automated method) [van der Maaten and Erdmann, 2015] and obtain its average value. Working on small samples, as in all the specimens in this research, the expected variability in the readings on the same textile is about 5-10% (as it can be seen in Table 3 and Figure 17).

Though it was theoretically clear that the linear density of the yarn would not be a reliable information if only very short samples of yarn can be weighted, a few attempts were done with yarns from different specimens. With the length of 20-30 mm, their weight is too close to the lower limit of the analytical scale (0.1 mg), and for this reason the information was excluded from the set of data collected in this research.

---

[32] All tests were carried out at 20°C (+/- 1), and 50% (+/- 5).

[33] Gibertini ETERNITY 100 SMI.

[34] The total area of a cruciform sample, with the indentations in the weft arms, is 297.12 mm^2.

[35] Beslands SXQFC-001eu. The “friction drive” was used, which slips when the set pressure is reached, allowing the spindle to stop moving, even if the user continues to turn the thimble. The compression force is very low, and was measured in approx. 0.02 N/cm^2, which ensures a uniform pressure value during measurements on all samples. Nevertheless, a certain crushing of the sample, depending on its characteristics, must be taken into account, even if it was not noticeable during the tests.

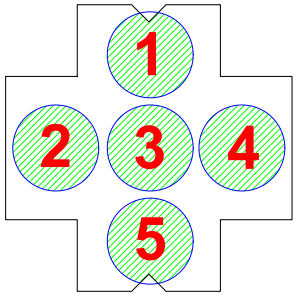

specimen			
sample 1	**sample 2**	**sample 3**	**sample 4**
thickness 1	thickness 1	thickness 1	thickness 1
thickness 2	thickness 2	thickness 2	thickness 2
thickness 3	thickness 3	thickness 3	thickness 3
thickness 4	thickness 4	thickness 4	thickness 4
thickness 5	thickness 5	thickness 5	thickness 5
mean	**mean**	**mean**	**mean**
general mean & standard deviation			

Figure 13 Measuring procedures for the canvas thickness. 5 points in each sample, averaged on 4 samples

3.2.2 Identification of fibers

Individual fibers were extracted[36] from the yarn and mechanically separated using a specillum. A sample was prepared for observation under a mineralogical optical microscope using an object slide, Canada balsam, and object coverslip. The preparations thus obtained were observed under the Zeiss Axioskop polarizing optical microscope with the Zeiss Axio Cam NRc camera attached, and the images were processed using Axio Vision processing software. An analysis of the morphological characteristics of the fibers was performed for comparison with databases in the literature [Markova, 2019] and [Lukesova and Holst, 2024].

3.2.3 pH measures

Measures of pH of an insoluble solid material require bringing free ions into solution in order to read the H^+ concentration. Depending on the type of electrode chosen, it will either be immersed in the liquid phase or measure the pH of a thin liquid film on the surface of the solid. Immersion of the textile sample in the liquid phase is among the standard procedures for textiles[37], and although it involves the destruction of the sample, it was not ruled out as it could be performed after the tensile tests. However, preliminary tests showed that the pH of the liquid phase continued to fluctuate for a long time, probably due to the gradual solubilization of materials in the historical canvas, and even more so when testing a canvas with layers of preparation and paint. The immersion method was therefore not preferred, because the results seemed to be easily influenced by unpredictable factors. A recently developed alternative method is to measure the pH

[36] The identification of the fibers was carried out at the Università della Tuscia, Viterbo, Group of Diagnostics and Materials Science, by Dr. Giorgia Agresti and Prof. Ulderico Santamaria.

[37] An early example is found in [British Standard Handbook n.11, 1963]. Updated versions are ISO-3071-2020 and ISO 6588-1:2021.

of an agarose gel used to extract free ions from the surface [Rota et al., 2021], limiting the diffusion of water into the material. The method is extremely useful for fragile textiles[38] and is also used on paintings[39]. Nevertheless, after careful evaluation of the options, an intermediate approach was chosen, as in [Böhme et al., 2020], based on the use of a contact pH meter with a drop of water placed on the sample[40]. The method used to be the standard approach before the introduction of the agarose gels, and was successfully used on canvas paintings over the past decade[41]. The advantage is that it seems to allow the extraction of more ions from below the surface if compared with the agarose gel, thus providing values with a wider distribution. If compared with the method based on the immersion of the sample, the pH value stabilizes within 3 to 5 minutes, and values appeared to be more repeatable. Of course, the problem is not one offering a single solution, and all methods currently used in conservation practice and conservation science have advantages and limitations.

As we have seen in chapter 2 (*Degree of conservation of the fibers affecting materials properties*), the determination of the DP of the cellulose would be extremely useful to establish a correlation with the mechanical performance of the textiles analyzed in this thesis, as the pH of the textiles appears to be within the critical range for acidic depolymerization only in a small minority of cases (see Table 1) this appears to be a relevant research question but not a very urgent one. The slight correlations between the tensile elastic modulus of the textiles and pH (Figure 79) or their age (Figure 80) appear to be very low. The p-values well above the limit of 0.05 imply that they have no statistical relevance.
Nevertheless, the subject needs to be investigated, and plotting the DP vs tensile modulus would be useful. After attempting a few collaborations with institutions that have longstanding experience in measuring the DP of such a large set of samples, the decision was taken to postpone the tests and wait until results can be made available for the 26 textiles to establish correlations. The samples are well stored and hopefully the dedicated tests will be possible in a close future.

3.2.4 Yarn width assessment

The long axis of the elliptical cross-section of the yarns can be measured using a completely non-destructive observation of the surface of the textile. The large amount

[38] In recent years it has become the standard procedure at the Abegg-Stiftung textile conservation studio (this was learned during a private communication).
[39] https://www.youtube.com/watch?v=bOqZEE7Kb8Y
[40] See the Tappi T 529 standard (1999).
[41] This is a professional statement of the author, who used the method to measure the pH of paintings in conservation practice since 2013.

of potentially available data allows using the above-mentioned statistical method of the weighted mean. Within each 1 cm^2 area of observation, the 3 subsets of relative dimensions in warp and weft were created as in Figure 11 and Figure 12. The representative yarns in each subset were identified and width measurements were taken at 3 different locations along their path. The tangent was traced on the side of the yarn, as shown in Figure 15, and then offset to the opposite side, including its width. The weighted mean and standard deviation were then calculated. The measurement of the short axis of the elliptical cross section of the yarns requires the yarns to be removed from the textile and observed sideways. Related measurements are made along with those of the crimp, as described later.

3.2.5 Twist

Twisting the fibers precedes weaving, being the process by which they are arranged around the axis of the yarn [Neckář and Das, 2018]. Twist is introduced by spinning the fibers in a number of turns that depends on the amount of fibers and their properties, to meet the expected requirements of the yarn. Twist provides the first level of organization of the fibers and determines the appearance, bending stiffness, and tensile strength of the yarn, as well as uniformity, stretch and stiffness of the textile, its durability and even color depth [Usman et al, 2014]. With natural fibers, strength is imparted by increasing the friction between them, and as the twist increases, the lateral force that packs the fibers together also increases, allowing more fibers to contribute to the cohesion and strength of the yarn [Neckář and Das, 2018]. However, the angle that the fibers form with the yarn axis also increases, so the fibers contribute less to yarn strength as the twist exceeds the ideal optimum level [Neckář and Das, 2019; Gorjanc and Sukič, 2020]. Natural fibers are highly variable in length, thickness, and flexural stiffness. As a result, differences in twist along the yarn are very common, especially in traditional spinning processes, and so are differences in the width of the resulting yarns [Kania, 2013]. Fibers can be twisted clockwise or counterclockwise, and the resulting yarn twist is defined as Z or S respectively, as the direction of the fibers visible on the side of the yarn aligns with the transverse element of the letter. The standard reference for measuring twist is the number of turns per unit length, Twist Per Meter (TPM) [Saville, 1999], and twist is typically measured by unwinding a yarn and counting how many turns it takes for the fibers to become parallel to the yarn axis [Gorjanc and Sukič, 2020]. Twist meters or twist testers are machines that mechanically unwind the yarn while counting the revolutions of the axis on which the yarn is clamped. The procedure is described in ASTM D1423, 2022[42], which requires yarn samples of considerable length, at least 20 cm. To reduce error, and to account for the natural variability of twist related to the local

[42] https://www.astm.org/d1423_d1423m-16r22.html

thickness and stiffness of the fiber bundle, often the twist testers allow for longer samples, up to 50 or 100 cm.

The reasons given above have been enough to effectively discourage any attempt to measure twist for conservation purposes, in the yarns of historical textiles or of canvases used for paintings. The closest to a measure of twist has been so far the observation of "twist angle" as defined in the Pierce model [Pierce, 1937], [Seiler-Baldinger, 1996], and in [Flock, 2020 **(a)**]. The twist angle is described by the tangent to the side of the yarn and the direction of a twisted fiber (see Figure 14). It provides a semi-quantitative description of the twist at a given point in the yarn, for comparative uses. A study published in 1973 by two textile engineers studying old canvas paintings [Conti and Tassinari, 1973 **(b)**] proposed an optical method to calculate the number of TPM based on the same geometry used to observe the twist angle (as we will see in Figure 15). A similar procedure is found in [Ozkaya et al. 2010], where it is used as a starting point for a digital image processing method to calculate TPM in textile engineering. An analog computational approach can also be found in [Neckář and Das, 2018].

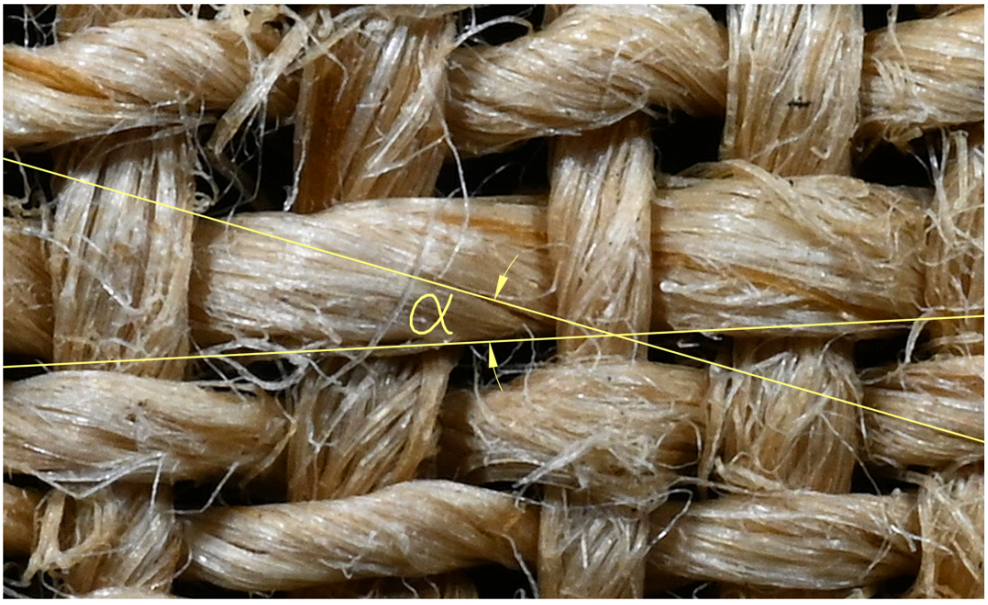

Figure 14 Twist angle traced on the fibers of a yarn

3.2.6 Description of the method for twist measurements in historical textiles

The method is an updated version of the previously mentioned Conti-Tassinari work [Conti and Tassinari, 1973 **(b)**], that used a goniometric eyepiece to construct a simple geometry on the image of the canvas. The method proposed here differs in the use of a

high-resolution digital image[43] scaled to real the size, and of a CAD software used to take measurements on the image file, instead of the goniometric eyepiece they recommended. The geometry is illustrated in Figure 15: the tangent, parallel to one side of the yarn, is drawn (*1*) and then offset to the opposite side (*2*), including its width; a diagonal line is traced along the curvature of the twisted fibers visible on the surface (*3*); the adjacent perpendicular segment provides the local measure of the yarn width (*4*), and forms a right-angle triangle with the second cathetus named "*L"*. The length in mm of *L* is the value of ***L*** in the simple Equation 1 used to calculate the Twists Per Meter (TPM) at a specific location of the yarn:

$$TPM=318/L$$

Equation 1 Calculation of TPM in [Conti and Tassinari, 1973 (b)]

The twist direction (Z or S) is noted, the weighted mean of the TPM and the standard deviation are calculated.

For a complete description and demonstration, please refer to the original paper and to the English translation from the long out of print book [Urbani, 1973] available in the Appendix 3. Conti and Tassinari validated their method by comparing the results it produced for modern canvases, with the values obtained by unwinding the same yarns object of observations, using a twist meter. Their conclusion was that if the observation is made in the straight strands between two crossing points in the woven structure, the expected error is lower than at the crossings where the superimposed yarns are bent. They reported a level of error between 5 and 15%, depending on the curvature of the section of the yarn observed.

[43] Images taken with a 2:1 macro lens. When cropped close to the sample perimeter, as in Figure 2, a square image measuring 21.7mm contains 3230 pixels per side, at a resolution of 6.7 micron/pixel.

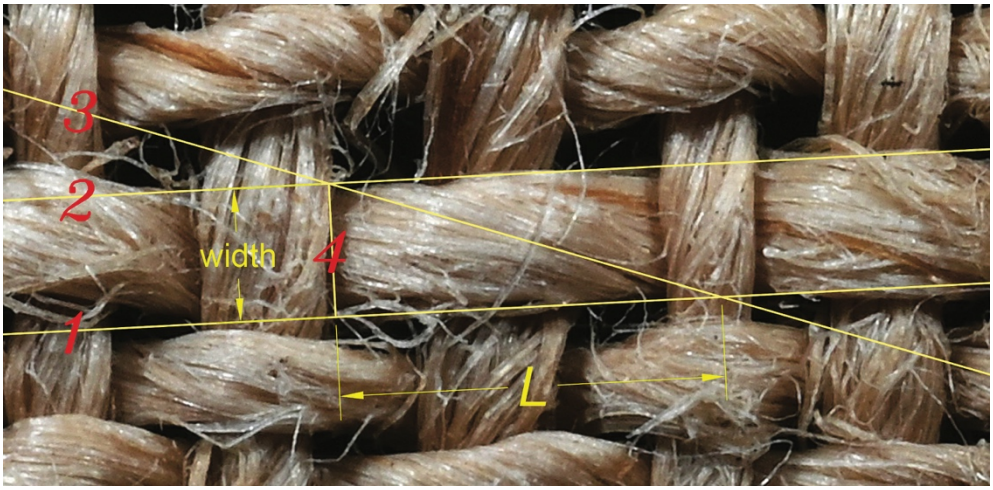

Figure 15 The geometry used for the TPM calculation in the Conti and Tassinari method

3.2.7 Crimp

Crimp is the waviness imparted to the warp and weft yarns of a fabric by their interlacing. The degree of crimp is among the most important parameters in textile engineering and has a huge impact on the properties of a woven structure. It has therefore been the subject of studies that are fundamental references in the field [Pierce, 1937]. Important commodity characteristics of a fabric are related to its crimp, such as its drape and "hand", its flexibility and thermal properties, and even the ballistic performance of special textiles [Wang et al., 2016]. Considering an unrestrained canvas, a higher crimp means greater shrinkage upon wetting [Pierce, 1937, Bilson, 1996]. The amount of crimp also describes the length of yarn needed to weave a textile, as a crimped yarn has a longer path than the sheer amplitude of the fabric[44]. When considering tensile properties, tensile loading reduces the waviness of the yarns, thus de-crimping them as they are stretched. Under uniaxial loading, the effect is to transfer crimp from the yarns in one direction to those in the opposite direction, while under biaxial loading the yarns under tension mutually influence the de-crimping in the opposite direction. The standard reference is the crimp % value [Booth, 1968], measured on a yarn which must be taken out from a textile without changing its shape [Saville, 1999]. The yarn is measured and then stretched, to eliminate its crimp and measure its uncrimped length,

[44] When talking about twist, a textile manufacturer will typically refer to the amount yarn length beyond that required for the final textile product, rather than to the shape the yarns take during weaving. This implies specific “craftsman nomenclature”: in the warp “shortening” or “shrinkage” are used, in Italian “raccorciamento”; in the weft direction, the technical term “take-up”, in Italian “rimborso”, that refers to the shrinkage but also to the methods and mechanical procedures used to control the tension in the weft.

i.e., the length it had before the weaving process. However, pulling on a yarn will eventually cause it to overstretch if the force exceeds that needed to straighten it, and the international standards. ASTM D3883-04, 2020[45] is an often-used example, aim at avoiding this problem[46]. Most commercially available crimp testers mark the operation as complete when a force limit is reached or when the yarn appearance is considered straight enough. Such measurements involve a considerable degree of approximation, which is compensated for by the length of the sample, again in the range of 50 or 100 cm.

Mechanical methods are confronted with the problem that the yarn retains residual deformations when pulled straight, what implies a natural tendency to pulling too far. However, after a certain level of tension, elongation is due to the yarn elastic response, if not to fiber slippage. It is therefore difficult to decide when to end the test. For this reason, the introduction of the analysis of the stress-strain curve of the yarn obtained with a tensile tester was proposed [Postle et al., 1988]. A further improvement [Kovar, 2011] is based on the observation of the tensile plot of the yarn[47], as in Figure 16. The first part of the plot is relatively straight and parallel to the abscissa axis as it describes the decrimping phase when the fibers recover their original straight configuration. As the yarn begins to respond to tension, a deflection point appears in the load curve and, to obtain a repeatable observation, the reading is given by the extension of the next straight part of the curve, corresponding to the elastic behavior of the yarn under tension, at the point of intersection with the x-axis. The plot in Figure 16 was obtained repeating Kovar's procedure with the tensile tester described in chapter 4, and this allowed learning that the results can vary with the initial tension of the yarn, since insufficient tension will produce a longer stretch (indistinguishable from the expected decrimping phase since the force values are also close to zero); too high initial tension will instead partially remove the crimp from the yarn before the test is started. Other researchers have preferred an optical approach based on observing a cross section and taking measurements with a microscope rather than with a tensile tester, also because microscopes are much more common in scientific laboratories. The measure of crimp through the image of a cross section has been proposed in research conducted at the Technical University of Liberec in the Czech Republic [Kolcavová Sirkova and Vysanska 2012], where dedicated software was used to draw a line along the neutral axis of the crimped yarn in the cross section of the textile. The length of the neutral axis was

[45] https://www.astm.org/d3883-04r20.html

[46] The existence of different standards in use, demonstrates the sensitive nature of the problem.

[47] Sample yarns 200 mm long, with a gauge length of 195 mm (as 2.5mm at each end are used for clamping), tested at the speed of 120 mm/min.

therefore measured using the same software and represents the length the yarn would have in a fully uncrimped form, without any mechanical distortion. The method was compared with the mechanical approach in [Mertova et al., 2016] and with different geometrical approximations in [Kolcavová Sirková and Mertová 2020] on industrial textiles, arriving at the general conclusion that its accuracy is equal or higher.

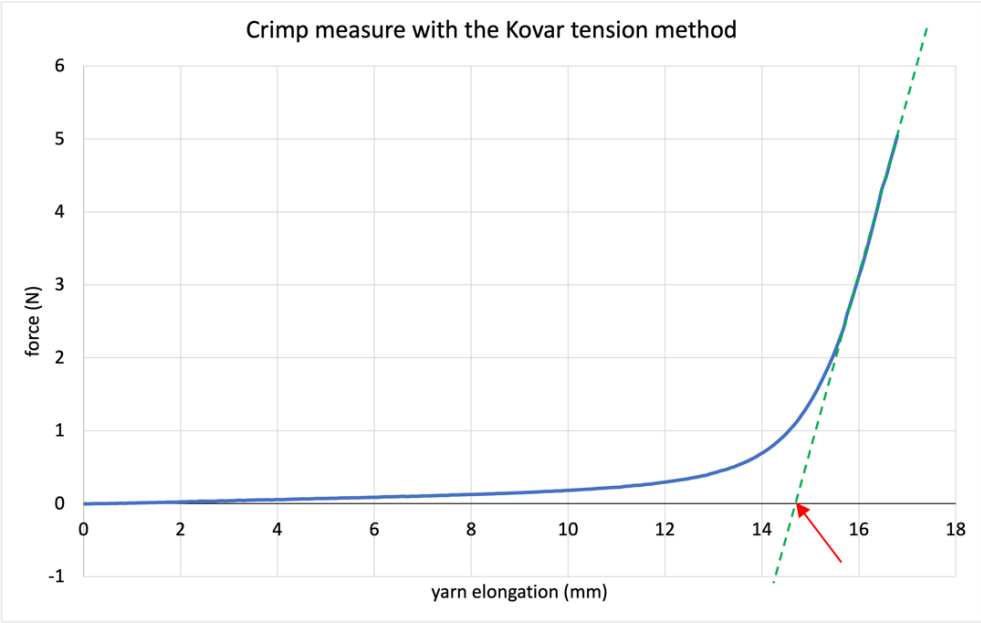

Figure 16 Observation of the yarn tensile plot according to Kovar. The point of intersection on the abscissa marked with the red arrow is the value of the yarn's decrimping elongation

References to crimp measurements in conservation are very rare. In [Young and Jardine, 2012] we see the use of a geometric model derived from the Pierce model [Pierce, 1937] to calculate crimp in modern textiles for use in lining treatments. The method uses the microscope image of a yarn extracted from the textile to measure the wavelength λ and amplitude A of its crimp wave to calculate a crimp factor through a dedicated equation. The choice of using a photographic image of the yarn instead of a resin-embedded cross section is very convenient, and helps reduce the time and costs required for the observation. However, the equation has been tested for this research and has been found to produce inconsistent results for irregular, hand-woven textiles. The reason seems to reside in the fact that the equation describes a waveform consisting of a series of semicircles, which does not correspond to historical textiles. Calculations of crimp based on several geometrical approximations, including those derived from Pierce, have been discussed and analyzed in [Kolcavová Sirková and Mertová 2020] and appears to be

of frequent use for industrial fabrics, in which the waveform of the crimped yarn is homogeneous and more predictable. Methods that use the actual waveform of the crimped yarn to extract the length of the uncrimped yarn, such as in the paper by Kolcavova, Sirkova and Vysanska in 2012 are therefore more compatible with the irregular crimp forms in historical textiles. It should also be noted that the information obtained drawing a line on the image represents the average crimp in the entire sample. With these arguments in mind, a simplified and adapted version of such a method for calculating the crimp % value has been developed in this research [Iaccarino Idelson et al., 2025 **(a)**] and will be described in the following paragraph.

3.2.8 Description of the method for crimp measurements in historical textiles

When measuring yarn crimp in a historical sample, it is critical to obtain data representing the longest portion of the waveform available in the image, considering the error introduced by the unpredictability of the yarn's path. The uneven diameters of the yarns impose different curves at each crossing and, on the other hand, the curve of the crimped yarn may have flattened peaks at yarn crossings due to surface crushing in naturally aged fabrics. Measuring the length of the neutral axis of the yarn by drawing a polyline on it solves such problems, because its length corresponds to that of the actual shape of the entire curve. Therefore, its unevenness becomes irrelevant and, in fact, the measure tolerates all kinds of irregularities. As previously explained, the method proposed here is based on using the image of the yarn to reveal its crimped shape. A section of the yarn is gently extracted from the side of the textile[48], and is placed on double sided adhesive tape to stabilize its position while taking the macro photograph including a dimensional reference. As for the twist measures, the image is scaled to actual size in CAD. The "polyline" tool has been found to be easy and flexible to use, and allows the actual shape of the yarn to be faithfully copied. The length of the polyline, ***P***, providing the full length of the yarn, is used to find the crimp % of the yarn by comparing it to the length ***T*** of the portion of textile, between the start and end points of the same polyline (as in Figure 17), using the standard Equation 2:

$$Crimp\ \% = \frac{P - T}{P}\ x\ 100$$

Equation 2 The standard value of % crimp for a yarn

The procedure is easy, reliable, and less time consuming than the previously described alternatives. A method to deal with the irregular textiles encountered in the field of

[48] Manual extraction of a sample crimped yarn is the common method in the textile industry.

conservation, which does not require the use of microscopes or proprietary software[49], seemed to be useful and necessary.

The procedure requires the extraction of 3 yarn fragments in both warp and weft, which are photographed in high-resolution and scaled to their real dimensions in CAD. In order to observe the same yarns described for width and twist measurements, it would be necessary to completely disassemble the sample. As this would imply the loss of correlation with the mechanical behavior under tensile testing and with all the other data collected, the decision was made to use neighboring yarns from the textile around the laser-cut perimeter. The yarns used measured 6 to 12 mm, thus providing a value that represents the mean of the waveform along their path. For these reasons, only the simple mean and the standard deviation are calculated [Iaccarino Idelson et al., 2025 **(c)**].

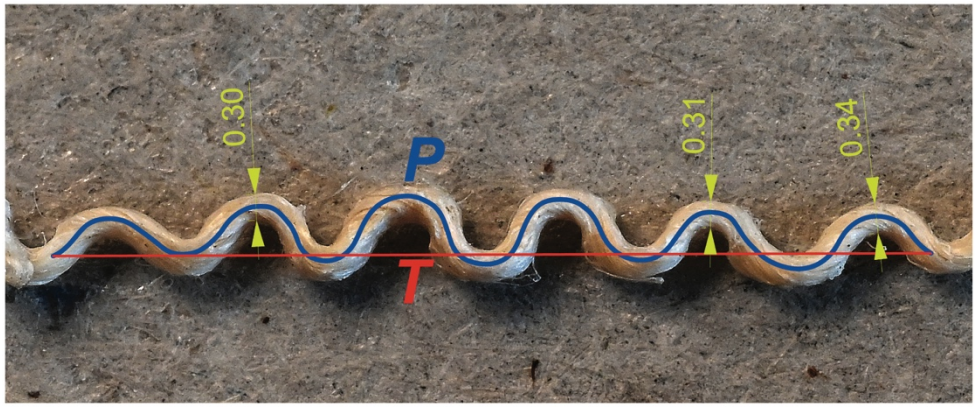

Figure 17 The length of the uncrimped yarn P and of the textile T at the same location to calculate % crimp and of yarn thickness

3.2.9 Yarn thickness measurement

While the image in Figure 15 shows the width of the yarns within the (x-y) plane of the textile, Figure 17represents the yarns along the orthogonal z axis, and was used to measure the, otherwise invisible, thickness of the yarns. The same CAD procedures were used to collect at least 3 measures of thickness from each of the yarns used to calculate the crimp%. For this reason, once again only the simple mean and the standard deviation (of at least 9 measurements) are calculated for the value of the yarn thickness.

[49] The use of dedicated software to draw the neutral axis of the yarn can introduce errors during the automated interpretation of the image, as reported in [Mertova et al. 2016]. Automation of the procedure reduces unpredictable human error and time consumption, but it may be suitable for a significant workload in the textile industry rather than in conservation studies.

3.3 Experimental results

In order to better introduce the results, they will be described starting from the fundamental description of the textile in order to prepare sufficient information to discuss the more complex data derived from the twist and crimp measurements.

3.3.1 Weight and thickness of the canvas, thread-count, fiber identification and pH

The values of the weight of the samples, their mean and standard deviation can be found in Table 1, along with the nature of the fibers and pH measurements. The thickness of the canvas samples, measured according to the described procedures (Figure 13), at 5 points in 4 units, and the general mean values of the 20 readings and their standard deviation are listed in Table 2.

		textile thickness measures					
	name	sample 1	sample 2	sample 3	sample 4	mm	st. dev.
1	plain canvas 1	0,52	0,59	0,52	0,55	**0,54**	0,03
2	plain canvas 2	1,01	0,98	1,00	0,92	**0,98**	0,04
3	plain canvas 3	0,36	0,37	0,32	0,36	**0,35**	0,02
4	plain canvas 4	0,83	0,82	0,84	0,87	**0,84**	0,02
5	plain canvas 5	0,87	0,88	0,86	0,87	**0,87**	0,01
6	Domenico C. Malinconico	0,25	0,27	0,27	0,27	**0,26**	0,01
7	Bernard d'Agesci	0,47	0,38	0,39	0,38	**0,41**	0,04
8	medium paste lining canvas (IT)	0,49	0,49	0,47	0,48	**0,48**	0,01
9	heavy paste lining canvas (IT)	1,32	1,21	1,32	1,28	**1,28**	0,05
10	Fragonard medium paste lining	0,68	0,65	0,72	0,69	**0,68**	0,03
11	Raffaele Postiglione	0,77	0,58	0,62	0,66	**0,66**	0,08
12	Alfred Dehodencq	0,35	0,33	0,29	0,33	**0,32**	0,03
13	Jules Gélibert	0,47	0,45	0,46	0,44	**0,45**	0,01
14	Louis Augustin Auguin	0,22	0,22	0,22	0,21	**0,22**	0,01
15	Ludovic Alleaume	0,44	0,44	0,46	0,44	**0,44**	0,01
16	Hubert Sauzeau 1	0,38	0,38	0,37	0,38	**0,37**	0,00
17	Hubert Sauzeau 2	0,78	0,82	0,85	0,80	**0,81**	0,03
18	Charles Müller	0,25	0,27	0,27	0,27	**0,26**	0,01
19	Furcy de Lavault	0,38	0,38	0,39	0,37	**0,38**	0,01
20	Louis Alexandre Cabié	0,28	0,28	0,27	0,29	**0,28**	0,01
21	Louis Lessieux	0,18	0,18	0,20	0,24	**0,20**	0,03
22	Jeannine Gilles-Murique	0,80	0,85	0,79	0,75	**0,80**	0,04
23	Night Watch mockup canvas	0,72	0,71	0,72	0,72	**0,72**	0,00
24	"pattina" lining canvas	0,45	0,43	0,43	0,44	**0,44**	0,01
25	"patta" lining canvas	0,60	0,56	0,51	0,57	**0,56**	0,04
26	canvassing "03f"	0,78	0,82	0,82	0,81	**0,81**	0,02

Table 2 The thickness of the canvas samples, each sample value is the mean of 5 measurements.

The number of yarns per cm was counted for 3 different samples in each specimen, and the general average values of the readings, and their standard deviation, are listed in Table 3.

		thread count									
	name	warp 1	warp 2	warp 3	weft 1	weft 2	weft 3	warp mean	weft mean	warp st. dev	weft st. dev.
1	plain canvas 1	16,0	17,0	17,0	13,5	14,0	13,0	**16,7**	**13,5**	0,6	0,5
2	plain canvas 2	12,0	11,0	10,0	8,0	8,0	8,0	**11,0**	**8,0**	1,0	0,0
3	plain canvas 3	14,0	13,0	14,0	12,0	12,0	12,0	**13,7**	**12,0**	0,6	0,0
4	plain canvas 4	9,0	9,0	9,0	7,0	7,0	7,0	**9,0**	**7,0**	0,0	0,0
5	plain canvas 5	17,5	16,0	16,0	11,0	10,0	12,0	**16,5**	**11,0**	0,9	1,0
6	Domenico C. Malinconico	13,0	13,0	13,0	13,0	13,0	13,0	**13,0**	**13,0**	0,0	0,0
7	Bernard d'Agesci	19,0	19,0	18,0	15,5	17,5	18,0	**18,7**	**17,0**	0,6	1,3
8	medium paste lining canvas (IT)	8,0	7,0	8,0	8,0	7,0	8,0	**7,7**	**7,7**	0,6	0,6
9	heavy paste lining canvas (IT)	9,0	8,5	8,5	7,0	7,0	7,0	**8,7**	**7,0**	0,3	0,0
10	Fragonard medium paste lining	14,0	14,0	13,0	11,0	12,0	11,0	**13,7**	**11,3**	0,6	0,6
11	Raffaele Postiglione	8,0	8,0	8,0	8,0	8,0	8,0	**8,0**	**8,0**	0,0	0,0
12	Alfred Dehodencq	17,0	17,0	17,0	11,0	11,0	11,0	**17,0**	**11,0**	0,0	0,0
13	Jules Gélibert	24,0	24,0	24,0	19,0	19,0	18,0	**24,0**	**18,7**	0,0	0,6
14	Louis Augustin Auguin	26,0	24,0	26,0	26,0	24,0	25,0	**25,3**	**25,0**	1,2	1,0
15	Ludovic Alleaume	23,0	25,0	24,0	21,0	22,0	22,0	**24,0**	**21,7**	1,0	0,6
16	Hubert Sauzeau 1	22,0	22,0	22,0	19,0	21,0	20,0	**22,0**	**20,0**	0,0	1,0
17	Hubert Sauzeau 2	14,0	14,0	14,0	12,0	12,0	12,0	**14,0**	**12,0**	0,0	0,0
18	Charles Müller	32,0	32,0	30,0	29,0	29,0	29,0	**31,3**	**29,0**	1,2	0,0
19	Furcy de Lavault	23,5	24,0	23,0	23,0	22,0	22,0	**23,5**	**22,3**	0,5	0,6
20	Louis Alexandre Cabié	11,0	12,0	12,0	10,5	11,0	11,0	**11,7**	**10,8**	0,6	0,3
21	Louis Lessieux	21,0	21,0	21,0	21,0	21,0	21,0	**21,0**	**21,0**	0,0	0,0
22	Jeannine Gilles-Murique	8,0	8,0	8,0	8,0	8,0	8,0	**8,0**	**8,0**	0,0	0,0
23	Night Watch mockup canvas	20,0	21,0	19,0	15,0	16,0	17,0	**20,0**	**16,0**	1,0	1,0
24	"pattina" lining canvas	9,0	9,0	9,0	9,0	9,0	9,0	**9,0**	**9,0**	0,0	0,0
25	"patta" lining canvas	7,0	7,0	7,0	5,0	5,0	5,0	**7,0**	**5,0**	0,0	0,0
26	canvassing "03f"	12,0	12,0	12,0	7,0	7,0	7,0	**12,0**	**7,0**	0,0	0,0

Table 3 Thread count analysis

The mean values in warp and weft are compared in Figure 18, and also the difference among the two values is displayed in the histogram. Warp yarns are more numerous than the weft yarns in 20 of the 26 specimens, and the remaining 6 have equal values. This correlation is due to practical and cost related considerations from the manufacturer's point of view[50]: as the main cost in the weaving process is the casting of the wefts in the shed, it is easier and cheaper to use a higher number of warp yarns to achieve a given density. In addition, a high weft density produces more tension in the warp, which will unbalance the fabric and cause it to wear out faster in use. A higher thread count in the warp direction is confirmed by most textile engineering literature, as in [Pan et al., 2015].

[50] Special tanks to Clemente Sironi, from the textile company Sironi in Italy, and to the hand-weaver Ingeborg Meijssen for the useful and interesting conversations on this subject.

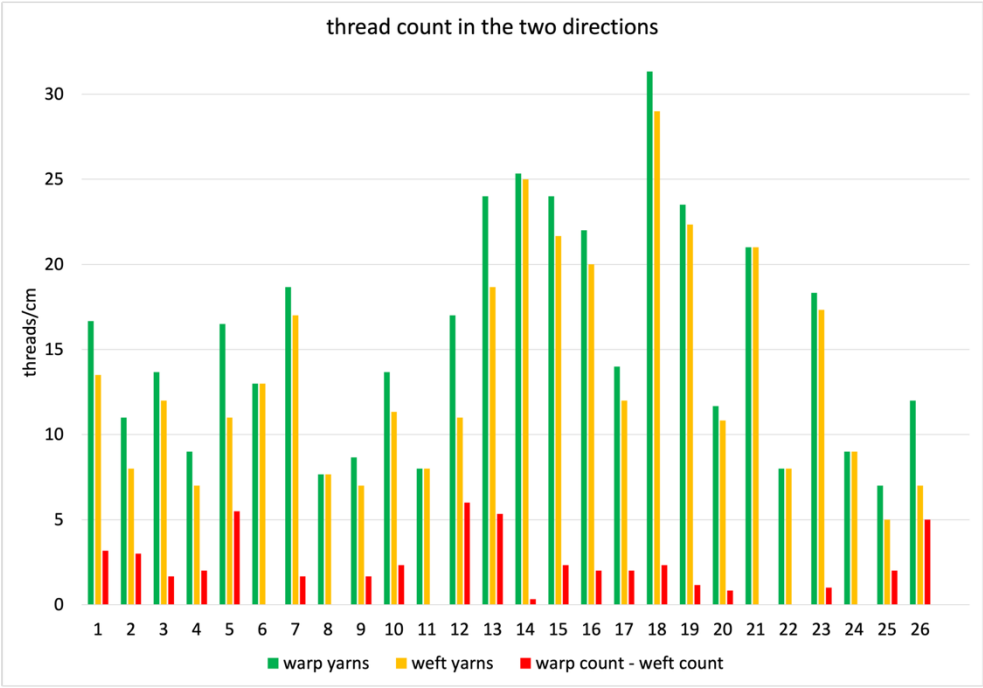

Figure 18 Thread-count in the two directions. Warp yarns are more numerous than weft yarns in 77% of the textiles, or equal

3.3.2 Yarn width, thickness and Z axis compression

The width of the yarns visible in the image of the 1 cm^2 sample (as in Figure 12) was measured using the geometries described in Figure 15, according to the relative dimension sets described in Figure 11. The data in Table 4 describe the variability of the yarns observed in the samples. When the yarns of the intermediate subset (M) prevail on the number of the others (as in ns. 13; 20; 26 in the warp and in ns. 13; 22; 24 in the weft), the textile has a high dimensional homogeneity. If the S and L subsets have a higher share of the population, yarn dimensions are more variable. A further evaluation of the variability can be obtained by comparing the readings in the subsets, using the standard deviation. Specimen n. 10 is a useful example, as the number of yarns in the M subset is prevalent, but in the weft the S value is almost 4 times smaller than the L, and 2 times smaller in the warp yarns.

WARP yarn width		dimensional classes numerosity				yarn width means					yarn thickness				
	sample name	th. count	S	M	L	S mean	M mean	L mean	w. mean	st. dev.	mean 1	mean 2	mean 3	warp	st. dev.
1	plain canvas 1	16,7	4	7,7	5	0,30	0,43	0,67	**0,47**	*0,16*	0,22	0,17	0,22	**0,20**	*0,03*
2	plain canvas 2	11,0	1	7,0	3	0,56	0,79	1,17	**0,87**	*0,28*	0,37	0,24	0,38	**0,33**	*0,08*
3	plain canvas 3	13,7	1	9,7	3	0,53	0,87	1,00	**0,87**	*0,21*	0,31	0,27	0,25	**0,28**	*0,03*
4	plain canvas 4	9,0	2	5,0	2	0,53	0,76	1,16	**0,80**	*0,28*	0,46	0,59	0,41	**0,49**	*0,09*
5	plain canvas 5	16,5	3	8,5	5	0,39	0,59	0,87	**0,64**	*0,21*	0,25	0,24	0,33	**0,27**	*0,05*
6	Domenico C. Malinconico	13,0	2	7,0	4	0,43	0,72	0,80	**0,70**	*0,19*	0,28	0,22	0,23	**0,24**	*0,03*
7	Bernard d'Agesci	18,7	1	13,7	4	0,28	0,34	0,58	**0,39**	*0,15*	0,21	0,28	0,31	**0,27**	*0,05*
8	medium paste lining canvas (IT)	7,0	2	3,0	2	0,62	0,70	1,11	**0,79**	*0,24*	0,39	0,31	0,39	**0,36**	*0,05*
9	heavy paste lining canvas (IT)	8,7	1	5,7	2	0,81	1,18	1,39	**1,19**	*0,25*	0,50	0,52	-	**0,51**	*0,01*
10	Fragonard medium paste lining	13,7	1	10,7	2	0,23	0,74	0,88	**0,72**	*0,30*	0,33	0,23	0,34	**0,30**	*0,06*
11	Raffaele Postiglione	8,0	1	6,0	1	0,41	0,61	0,76	**0,60**	*0,16*	0,34	0,38	0,43	**0,38**	*0,05*
12	Alfred Dehodencq	17,0	2	12,0	3	0,47	0,69	0,94	**0,71**	*0,20*	0,33	0,37	0,44	**0,38**	*0,06*
13	Jules Gélibert	24,0	1	22,0	1	0,40	0,49	0,53	**0,49**	*0,09*	0,21	0,20	0,20	**0,20**	*0,01*
14	Louis Augustin Auguin	25,0	2	21,0	2	0,33	0,38	0,50	**0,39**	*0,10*	0,28	0,23	0,21	**0,24**	*0,04*
15	Ludovic Alleaume	24,0	2	18,0	4	0,30	0,43	0,54	**0,44**	*0,11*	0,15	0,18	0,16	**0,16**	*0,02*
16	Hubert Sauzeau 1	22,0	3	15,0	4	0,38	0,49	0,54	**0,48**	*0,07*	0,21	0,20	0,28	**0,23**	*0,04*
17	Hubert Sauzeau 2	14,0	2	7,0	5	0,58	0,77	0,85	**0,77**	*0,13*	0,29	0,30	0,38	**0,32**	*0,05*
18	Charles Müller	31,3	5	20,3	6	0,27	0,34	0,44	**0,35**	*0,07*	0,15	0,16	0,11	**0,14**	*0,03*
19	Furcy de Lavault	23,5	2	14,5	7	0,32	0,42	0,66	**0,48**	*0,16*	0,18	0,18	0,15	**0,17**	*0,02*
20	Louis Alexandre Cabié	11,7	1	9,7	1	0,62	0,72	0,96	**0,73**	*0,16*	0,40	0,33	0,42	**0,38**	*0,05*
21	Louis Lessieux	21,0	4	12,0	5	0,37	0,46	0,61	**0,48**	*0,11*	0,15	0,15	0,13	**0,14**	*0,01*
22	Jeannine Gilles-Murique	8,0	2	5,0	1	0,95	1,03	1,57	**1,08**	*0,31*	0,33	0,37	0,40	**0,37**	*0,04*
23	Night Watch mockup canvas	20,0	2	14,3	3	0,41	0,72	0,74	**0,69**	*0,16*	0,28	0,27	0,27	**0,27**	*0,01*
24	"pattina" lining canvas	9,0	2	6,0	1	0,37	0,42	0,51	**0,42**	*0,07*	0,37	0,31	0,24	**0,31**	*0,07*
25	"patta" lining canvas	7,0	1	3,0	3	0,54	0,76	0,94	**0,81**	*0,17*	0,33	0,39	0,39	**0,37**	*0,03*
26	canvassing "03f"	12,0	1	9,0	2	0,62	0,71	0,85	**0,73**	*0,13*	0,46	0,54	0,50	**0,50**	*0,04*

WEFT yarn width		dimensional classes numerosity				yarn width means					yarn thickness				
	sample name	th. count	S	M	L	S mean	M mean	L mean	w. mean	st. dev.	mean 1	mean 2	mean 3	weft	st. dev.
1	plain canvas 1	13,5	3	5,5	5	0,38	0,41	0,55	**0,46**	*0,08*	0,23	0,24	0,20	**0,22**	*0,02*
2	plain canvas 2	8,0	1	6,0	1	0,58	0,71	1,13	**0,75**	*0,26*	0,32	0,41	0,50	**0,41**	*0,09*
3	plain canvas 3	12,0	1	9,0	2	0,36	0,59	0,98	**0,64**	*0,28*	0,46	0,45	-	**0,46**	*0,01*
4	plain canvas 4	7,0	1	4,0	2	0,67	0,97	1,11	**0,97**	*0,21*	0,48	0,48	0,36	**0,44**	*0,07*
5	plain canvas 5	11,0	2	7,0	2	0,47	0,59	0,77	**0,60**	*0,13*	0,44	0,43	0,52	**0,46**	*0,05*
6	Domenico C. Malinconico	13,3	3	6,3	4	0,32	0,50	0,57	**0,48**	*0,12*	0,22	0,28	0,29	**0,26**	*0,04*
7	Bernard d'Agesci	17,0	2	10,0	5	0,27	0,48	0,50	**0,46**	*0,11*	0,18	0,18	0,21	**0,19**	*0,02*
8	medium paste lining canvas (IT)	8,0	2	4,0	2	0,53	0,79	0,97	**0,77**	*0,21*	0,30	0,23	0,46	**0,33**	*0,12*
9	heavy paste lining canvas (IT)	7,0	1	5,0	1	0,47	0,81	0,81	**0,76**	*0,17*	0,48	0,56	-	**0,52**	*0,06*
10	Fragonard medium paste lining	11,3	1	7,3	3	0,33	0,73	0,76	**0,70**	*0,21*	0,28	0,33	0,29	**0,30**	*0,03*
11	Raffaele Postiglione	8,0	1	5,0	2	0,54	0,97	1,12	**0,96**	*0,27*	0,40	0,34	0,37	**0,37**	*0,03*
12	Alfred Dehodencq	11,0	2	7,0	2	0,32	0,54	0,62	**0,51**	*0,14*	0,28	0,35	0,33	**0,32**	*0,04*
13	Jules Gélibert	18,7	1	16,7	1	0,34	0,40	0,53	**0,41**	*0,10*	0,22	0,22	0,24	**0,23**	*0,01*
14	Louis Augustin Auguin	25,3	2	21,3	2	0,31	0,32	0,46	**0,33**	*0,07*	0,31	0,28	0,29	**0,29**	*0,02*
15	Ludovic Alleaume	21,7	2	16,7	3	0,28	0,34	0,40	**0,35**	*0,06*	0,16	0,16	0,18	**0,17**	*0,01*
16	Hubert Sauzeau 1	20,0	3	14,0	3	0,37	0,41	0,40	**0,40**	*0,05*	0,23	0,23	0,24	**0,23**	*0,01*
17	Hubert Sauzeau 2	12,0	2	8,0	2	0,50	0,46	0,63	**0,50**	*0,08*	0,32	0,33	0,39	**0,35**	*0,04*
18	Charles Müller	29,0	5	20,0	4	0,19	0,31	0,40	**0,30**	*0,09*	0,11	0,16	0,14	**0,14**	*0,03*
19	Furcy de Lavault	22,3	4	12,3	6	0,24	0,34	0,49	**0,36**	*0,12*	0,18	0,17	0,30	**0,22**	*0,07*
20	Louis Alexandre Cabié	10,8	2	5,8	3	0,61	0,71	1,18	**0,82**	*0,27*	0,43	0,44	0,56	**0,48**	*0,07*
21	Louis Lessieux	21,0	7	12,0	2	0,24	0,29	0,42	**0,29**	*0,09*	0,22	0,17	0,13	**0,17**	*0,05*
22	Jeannine Gilles-Murique	8,0	1	6,0	1	1,11	1,06	1,64	**1,14**	*0,31*	0,47	0,45	0,44	**0,45**	*0,02*
23	Night Watch mockup canvas	16,0	3	11,3	3	0,49	0,45	0,51	**0,46**	*0,03*	0,31	0,32	0,31	**0,31**	*0,01*
24	"pattina" lining canvas	9,0	1	7,0	1	0,27	0,47	0,58	**0,46**	*0,14*	0,38	0,30	0,27	**0,32**	*0,06*
25	"patta" lining canvas	5,0	1	2,0	2	0,60	0,76	0,87	**0,77**	*0,13*	0,41	0,36	0,47	**0,41**	*0,06*
26	canvassing "03f"	7,0	1	5,0	1	0,61	0,66	0,79	**0,67**	*0,08*	0,47	0,42	0,48	**0,46**	*0,03*

Table 4 The relative dimension subsets, the mean values and the weighted mean of the yarn width observations; the mean thickness of the yarns and their standard deviation values.

The weighted mean values in warp and in weft are compared in Figure 19, where the difference between the two values is also shown. In the large majority of cases (20 out of 26, or 77%) the warp yarns are wider than the weft yarns. In the 11 cases under the pale blue band in Figure 19, the differences are very shallow: between 0.08 mm and -0.08 mm. If the subset under the pale blue band is not included in the general evaluation of the correlation between yarn width and weaving direction (i.e. filtering above the

value of +/- 0.07 mm difference), warp yarns are wider in 13 of the 16 remaining textiles, and only in 3 cases is the opposite true, showing a slightly higher prevalence (81%), and they differ by substantial values[51].

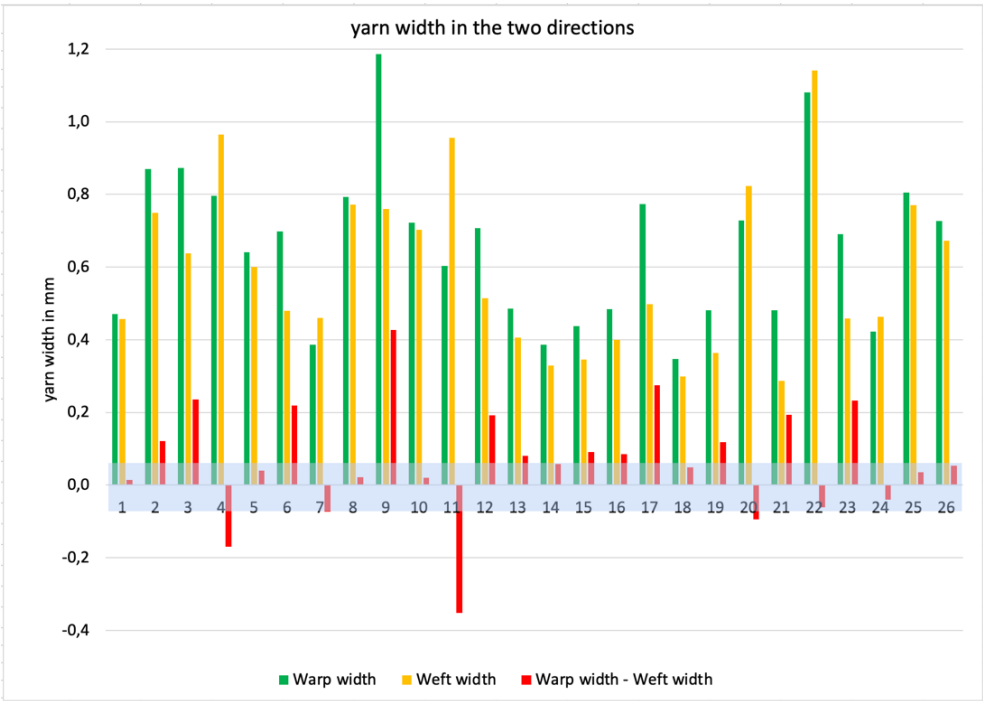

Figure 19 The measures of the yarn's width weighted mean. The warp yarns are wider in 81% of the 26 canvases

In Figure 20, we see the typical cross section of the yarns of a historical textile, showing the elliptical cross section of the yarns. After spinning, the yarns have a circular cross section that becomes elliptical during the weaving process because of the compression forces generated in the crossing areas. The degree of yarn compression (or the width over the thickness of the yarn) appears to be directly correlated with the quantity of twist in the yarns, as we see in Figure 21 where the Z axis compression is compared with the TPM.

[51] With a minimum of 13% and a maximum of 58%.

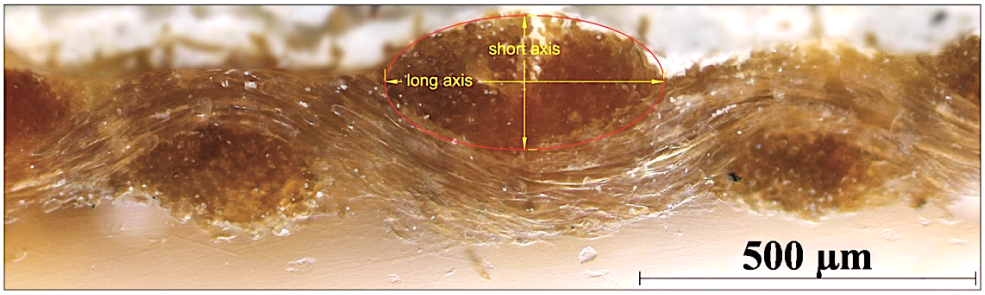

Figure 20 Typical Section of the yarns (credit Giorgia Agresti)

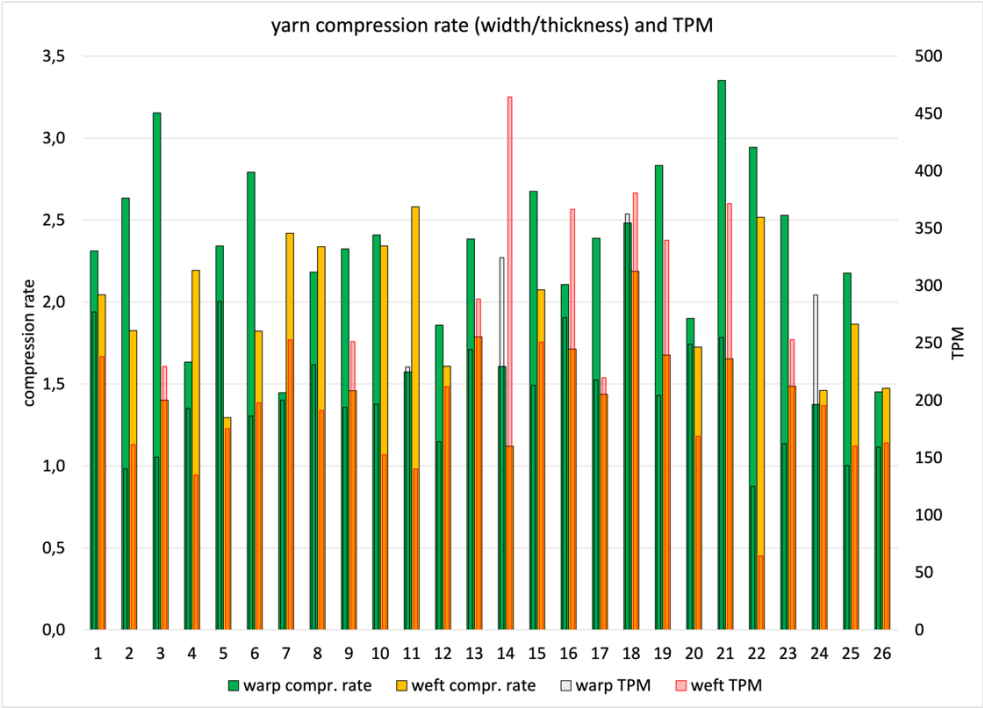

Figure 21 The yarn width over the yarn thickness, indicating the level of yarn compression on the Z axis of the textile, compared with TPM. Higher TPM implies lower yarn compression

Higher twist means better cohesion of the yarn, and higher friction between the fibers, both implying a higher retention of the original circular section, and for this reason the weft yarns generally have lower Z axis compression. In Figure 22 we see the comparison of the yarn compression rate between warp and weft yarns, showing a clear prevalence (77%) for the warp yarns. If the subset under the pale blue band is not included (i.e.

filtering above the value of +/- 0.176 difference), the prevalence becomes 86% (18 over 21 textiles).

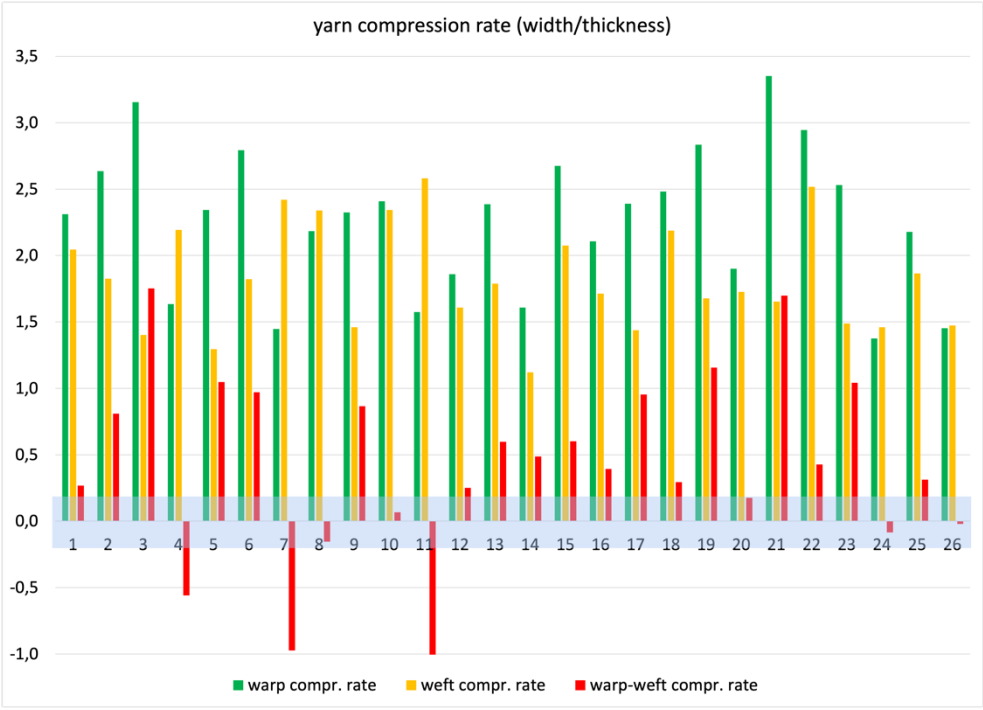

Figure 22 Warp yarns have compression rate between in 86% of the cases

The thickness of the yarns in the two directions is compared in Figure 23, and we see that in 19 cases out of 26 (73%) the weft yarns are thicker than the warp, despite their lower width. If the subset under the pale blue band is not included (i.e. filtering above the value of +/- 0.01 mm difference), the prevalence becomes 70% (14 over 20 textiles). This apparently surprising information further confirms the role of twist in the retention of the original circular form of the yarn. A relation may also be found with the mechanics of the shedding process, that sees the warp yarns physically bent over the weft, thus acquiring more crimp, as we will see in Table 7and Figure 27.

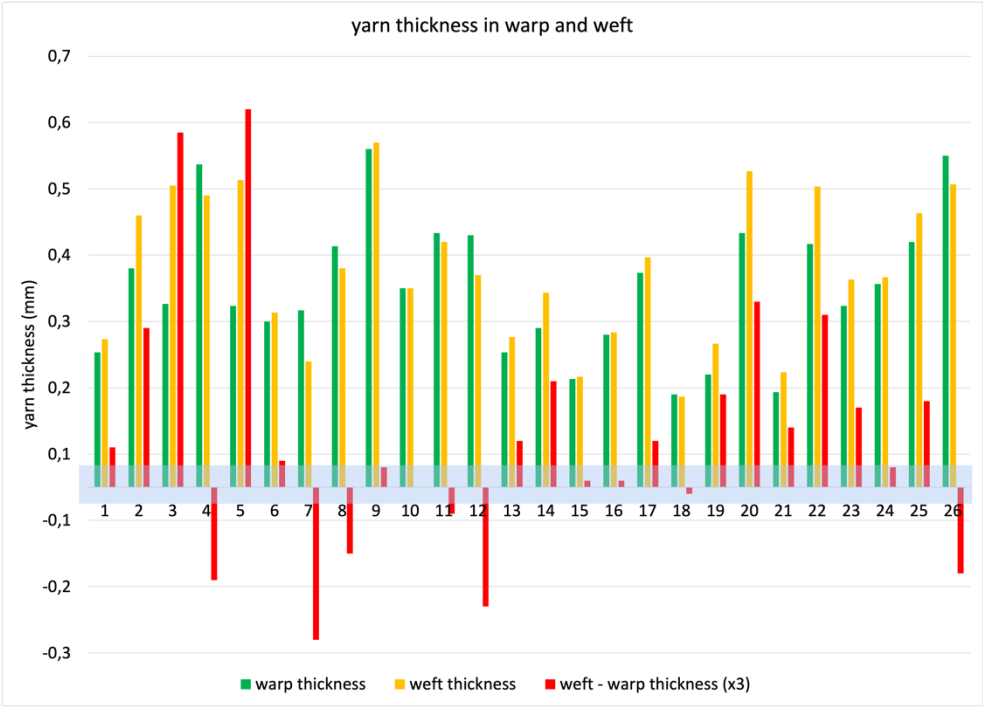

Figure 23 Weft yarns are thicker than the warp yarns in 70% of the cases, because they retain a more circular section during weaving

The elliptical cross section area of the yarns is shown in Figure 24, where we see a prevalence of the warp (15 over 11, or 58%). If the subset under the pale blue band is not included (i.e. filtering above the value of +/- 0.02 mm^2 difference), the prevalence of the warp is reduced to 54% (7 over 13 textiles).

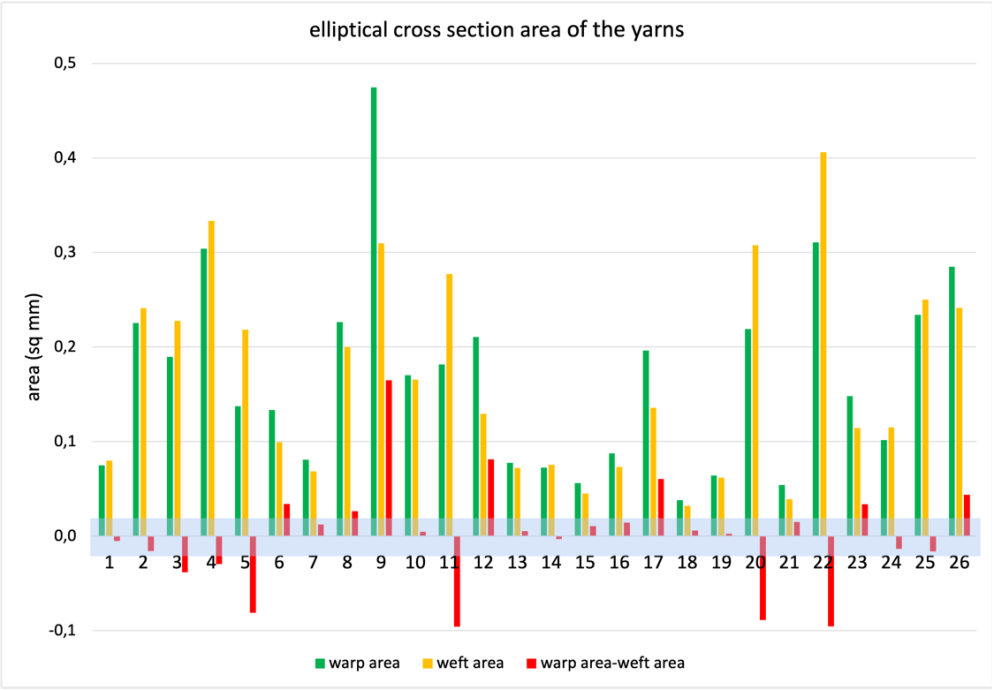

Figure 24 The area of the elliptical cross section in warp and weft yarns is similar in the two directions, with a prevalence of the warp of only 54%

3.3.3 Measures of Twist Per Meter

Before applying the method in the current research, a new validation process was carried out, using the updated procedures on the two industrial canvases [Iaccarino Idelson et al., 2025 **(a)**]. The mean of the values obtained with the optical method on three locations of a single yarn was compared with the twist count on the same yarns after manually unwinding them[52]. The results in (Figure 25) confirm the error predictions in the 1973 paper, as the error is between 3.5% and 10.1%.

[52] Sample yarns were 600 mm long. A certified twist meter was not available but a careful manual and visual process is probably more precise, though it would not be suitable for industrial purposes.

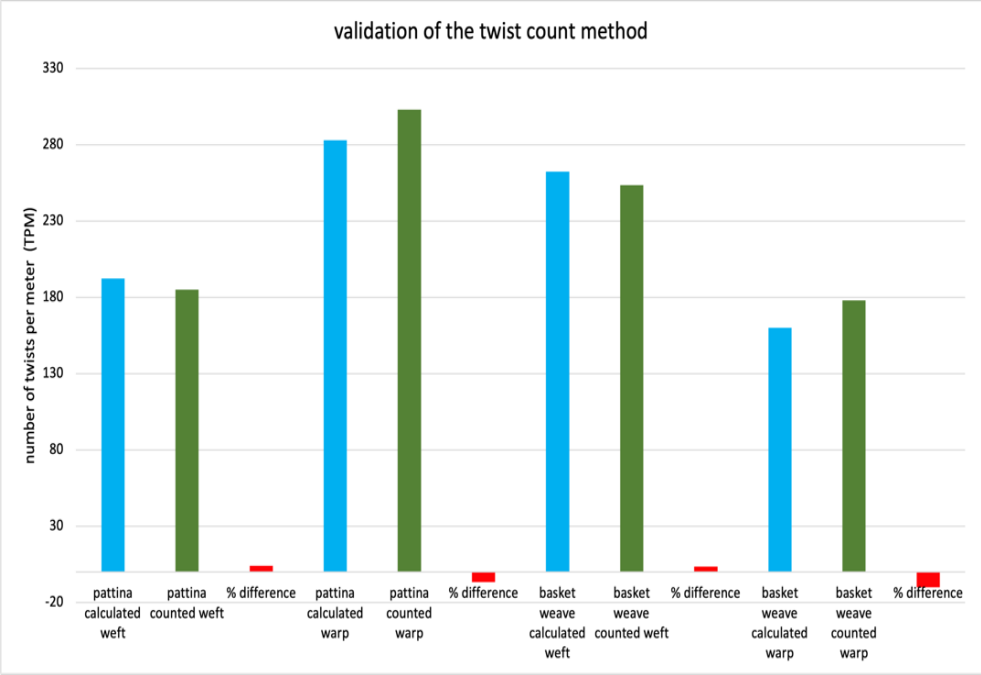

Figure 25 Comparison between the TPM obtained through calculation and unwinding

The amount of twist that natural fibers undergo during the spinning process depends on the characteristics of the fiber strand, which are highly variable [Kania, 2013]. Thinner fiber strands will twist more than a bulkier flock, stiffer sections will twist less, and yarns will have different twist and diameter along their length. "Twist goes where the yarns are thinner", as a traditional spinner would say, and the correlation between TPM and yarn linear density is well known in textile engineering [Saville, 1999]. The data in Table 5 describe the correlation existing between yarn width and TPM, analyzing the difference found between the dimensional subsets of yarns. The yarn width and its TPM value were measured at the same location (as seen in Figure 15), and each of the values in Table 5 is the mean of three measurements on the same yarn. Within the area of observation in the samples, the thinner yarns (class Small) have a higher TPM value, and the wider yarns (class Large) have a lower TPM value. The difference of the TPM values, between the Small and the Large, is always a positive number, and the % difference in TPM is correlated to the % difference measured in the yarn width. This rule explains why the weft yarns have a higher TPM value, as they are normally thinner, as seen in Table 6 where the weighted mean values (based on the 3 dimensional classes) of yarn width and TPM in warp and weft are shown. A correlation similar to that seen for the yarn width in Figure 19 (80%) would be expected, but we find instead a weaker one, since it verifies in 17 cases out of 26 (or 65%). Filtering above the value of +/- 12 TPM difference), the

prevalence of the warp is reduced to 57% (13 over 23 textiles). However, it should be noted that in 5 of the 9 cases where the TPM is higher in the warp yarns, this is actually due to the fact that they happen to be thinner than the weft yarns. In addition, the specimens have other unusual morphological characteristics: n. 8 and n. 24 are very open weave canvases used for lining, with yarns of equal width in both directions; n. 20 and n. 22 are more recent historical textiles (n. 20 has thin cotton warp and thicker hemp weft), both apparently designed for painting, with limited space between the flat yarns (high cover factor). N. 26 is the hand-woven replica of a traditional painter's canvas, produced using the same (industrially spun) linen yarn for both warp and weft, and this is the reason why the TPM values in warp and weft are almost identical. If these were removed from the sample set, we would have a count of 19 among which 16 showing higher twist in the weft, 84% correlation, close to the 80% found for yarn width in Figure 19. For these reasons, we shall keep the intermediate value of 65% corresponding to no data filtering.

WARP		Warp yarn width				Warp TPM			
	sample name	Small	Medium	Large	% Large-Small	Small	Medium	Large	% Small-Large
1	plain canvas 1	0,30	0,43	0,67	55%	374,89	264,12	218,77	42%
2	plain canvas 2	0,56	0,79	1,17	52%	304,32	115,02	145,29	52%
3	plain canvas 3	0,53	0,87	1,00	47%	298,24	143,08	124,82	58%
4	plain canvas 4	0,53	0,76	1,16	54%	291,42	190,29	101,61	65%
5	plain canvas 5	0,39	0,59	0,87	55%	321,07	335,95	180,68	44%
6	Domenico C. Malinconico	0,43	0,72	0,80	46%	438,67	144,33	134,33	69%
7	Bernard d'Agesci	0,28	0,34	0,58	51%	515,59	184,70	173,96	66%
8	medium paste lining canvas (IT)	0,62	0,70	1,11	44%	318,98	235,03	136,80	57%
9	heavy paste lining canvas (IT)	0,81	1,18	1,39	42%	180,63	224,10	115,18	36%
10	Fragonard medium paste lining	0,23	0,74	0,88	74%	394,21	186,25	153,44	61%
11	Raffaele Postiglione	0,41	0,61	0,76	46%	310,29	221,07	196,94	37%
12	Alfred Dehodencq	0,47	0,69	0,94	50%	253,23	150,43	158,78	37%
13	Jules Gélibert	0,40	0,49	0,53	24%	280,13	244,90	193,09	31%
14	Louis Augustin Auguin	0,33	0,38	0,50	35%	357,51	330,46	228,35	36%
15	Ludovic Alleaume	0,30	0,43	0,54	44%	208,60	229,98	140,43	33%
16	Hubert Sauzeau 1	0,38	0,49	0,54	29%	286,27	274,22	253,60	11%
17	Hubert Sauzeau 2	0,58	0,77	0,85	32%	359,85	216,34	162,85	55%
18	Charles Müller	0,27	0,34	0,44	39%	423,32	407,67	158,34	63%
19	Furcy de Lavault	0,32	0,42	0,66	52%	330,62	221,19	133,43	60%
20	Louis Alexandre Cabié	0,62	0,72	0,96	36%	272,36	253,29	186,41	32%
21	Louis Lessieux	0,37	0,46	0,61	40%	312,33	252,49	214,17	31%
22	Jeannine Gilles-Murique	0,95	1,03	1,57	39%	142,19	122,07	104,93	26%
23	Night Watch mockup canvas	0,41	0,72	0,74	44%	183,57	156,32	176,82	4%
24	"pattina" lining canvas	0,37	0,42	0,51	27%	371,56	281,37	196,09	47%
25	"patta" lining canvas	0,54	0,76	0,94	43%	238,53	153,66	101,13	58%
26	canvassing "03f"	0,62	0,71	0,85	28%	191,06	163,57	125,27	34%

WEFT		Weft yarn width				Weft TPM			
	sample name	Small	Medium	Large	% Large-Small	Small	Medium	Large	% Small-Large
1	plain canvas 1	0,38	0,41	0,55	30%	248,47	260,98	207,32	17%
2	plain canvas 2	0,58	0,71	1,13	49%	205,37	161,43	119,35	42%
3	plain canvas 3	0,36	0,59	0,98	64%	296,26	251,11	99,61	66%
4	plain canvas 4	0,67	0,97	1,11	40%	172,27	134,03	117,80	32%
5	plain canvas 5	0,47	0,59	0,77	39%	243,86	170,24	125,13	49%
6	Domenico C. Malinconico	0,32	0,50	0,57	44%	393,67	145,00	134,67	66%
7	Bernard d'Agesci	0,27	0,48	0,50	47%	293,05	289,28	163,69	44%
8	medium paste lining canvas (IT)	0,53	0,79	0,97	45%	185,45	218,86	141,94	23%
9	heavy paste lining canvas (IT)	0,47	0,80	0,81	42%	475,24	222,37	171,52	64%
10	Fragonard medium paste lining	0,33	0,73	0,76	57%	268,46	131,10	166,60	38%
11	Raffaele Postiglione	0,54	0,97	1,12	52%	201,35	150,00	85,68	57%
12	Alfred Dehodencq	0,32	0,54	0,62	49%	403,85	174,84	150,46	63%
13	Jules Gélibert	0,34	0,40	0,53	36%	234,11	297,55	192,11	18%
14	Louis Augustin Auguin	0,31	0,32	0,46	32%	513,44	472,33	333,78	35%
15	Ludovic Alleaume	0,28	0,34	0,40	31%	270,39	251,86	231,90	14%
16	Hubert Sauzeau 1	0,37	0,41	0,40	8%	344,41	392,71	266,18	23%
17	Hubert Sauzeau 2	0,50	0,46	0,63	21%	223,28	239,23	138,78	38%
18	Charles Müller	0,19	0,31	0,40	53%	473,04	385,82	241,81	49%
19	Furcy de Lavault	0,24	0,34	0,49	51%	541,13	354,36	175,30	68%
20	Louis Alexandre Cabié	0,61	0,71	1,18	48%	191,07	198,97	94,84	50%
21	Louis Lessieux	0,24	0,29	0,42	43%	444,86	353,41	224,57	50%
22	Jeannine Gilles-Murique	1,11	1,06	1,64	32%	93,10	56,92	80,82	13%
23	Night Watch mockup canvas	0,49	0,45	0,51	3%	249,46	261,26	229,32	8%
24	"pattina" lining canvas	0,27	0,47	0,58	53%	358,79	174,71	177,12	51%
25	"patta" lining canvas	0,60	0,76	0,87	31%	195,86	168,90	133,92	32%
26	canvassing "03f"	0,61	0,66	0,79	22%	197,55	161,24	136,53	31%

Table 5 Warp and weft TPM in function of the yarn width. TPM is higher for the thinner yarns.

		yarn width w. means		TPM w. means		
	sample name	warp width	weft width	warp TPM	weft TPM	weft-warp
1	plain canvas 1	0,47	0,46	277,10	238,33	-38,77
2	plain canvas 2	0,87	0,75	140,48	161,66	21,18
3	plain canvas 3	0,87	0,64	150,43	229,62	79,20
4	plain canvas 4	0,80	0,97	193,05	134,86	-58,20
5	plain canvas 5	0,64	0,60	286,19	175,42	-110,77
6	Domenico C. Malinconico	0,70	0,48	186,54	197,85	11,31
7	Bernard d'Agesci	0,39	0,46	200,12	252,78	52,66
8	medium paste lining canvas (IT)	0,79	0,77	230,95	191,28	-39,67
9	heavy paste lining canvas (IT)	1,19	0,75	193,95	251,23	57,28
10	Fragonard medium paste lining	0,72	0,70	196,67	152,62	-44,05
11	Raffaele Postiglione	0,60	0,96	229,20	140,34	-88,86
12	Alfred Dehodencq	0,71	0,51	163,99	212,05	48,06
13	Jules Gélibert	0,49	0,41	244,21	288,50	44,29
14	Louis Augustin Auguin	0,39	0,33	324,45	464,63	140,17
15	Ludovic Alleaume	0,44	0,35	213,28	250,80	37,53
16	Hubert Sauzeau 1	0,48	0,40	272,11	366,49	94,38
17	Hubert Sauzeau 2	0,77	0,50	217,74	219,83	2,09
18	Charles Müller	0,35	0,30	362,42	380,99	18,57
19	Furcy de Lavault	0,48	0,36	204,36	339,70	135,34
20	Louis Alexandre Cabié	0,73	0,82	249,19	168,68	-80,51
21	Louis Lessieux	0,48	0,29	254,77	371,62	116,86
22	Jeannine Gilles-Murique	1,08	1,14	124,96	64,43	-60,52
23	Night Watch mockup canvas	0,69	0,46	162,12	253,06	90,94
24	"pattina" lining canvas	0,42	0,46	291,94	195,43	-96,51
25	"patta" lining canvas	0,81	0,77	143,27	160,30	17,03
26	canvassing "03f"	0,73	0,67	159,48	162,90	3,42

Table 6 TPM weighted means in function of the warp and weft, in 17 cases weft has higher TPM. Red values do not follow the general trend.

3.3.4 Measures of crimp %

Crimp measurements are more invasive as they require the observation of yarns carefully extracted from the sample. Extracting the same yarns corresponding to the dimensional classes used for TPM measurements would require complete disassembly of the sample. A similar statistical treatment was therefore excluded, and yarns were extracted from the remaining parts of the specimen, outside the sample but close to the laser cuts. Still, if compared with the twist measurement, the crimp observations involve a much larger section of the yarn (between 6 and 12 mm long, or 4-9 wavelengths depending on the width of the yarn), therefore each of them is an average per se. The method proposed here, based on the direct measure of the crimped yarn on its image, is rather straightforward and, as we have seen, its precision has been validated in [Mertova et al., 2016; Kolcavová Sirková and Mertová 2020]. Nevertheless, a further validation test was carried out also on the crimp measurements, comparing the results with those obtained using the tensile tester to reproduce the operation of a crimp tester on yarns from the “pattina” lining canvas [Iaccarino Idelson et al., 2025 **(a)**]. Yarns were

tensioned[53] and the elongation value was used to calculate the crimp, as shown in Figure 16. The values obtained with the polyline method for this textile are 2.94% in the warp and 1.58% in the weft (see Table 7), and the Kovar method shown in Figure 26 gives values of 3.3% and 2.1%. Another way of extracting a crimp value from the tensile plot is to choose an identical force value for the two sets of yarns, as a visual estimate of when the yarns' response begins to differ from that of de-crimping. With a tension value of 0.7 N, the elongation is 2.66% in the warp and 1.68% in the weft; with a force value of 1 N, the elongation is 2.89% in the warp and 1.81% in the weft. As can be seen, the mechanical crimping tests leave some room for interpretation, also due to the need of an identical initial tension value and to the different scale of the samples. Still, the differences from the method proposed here are in a similar range.

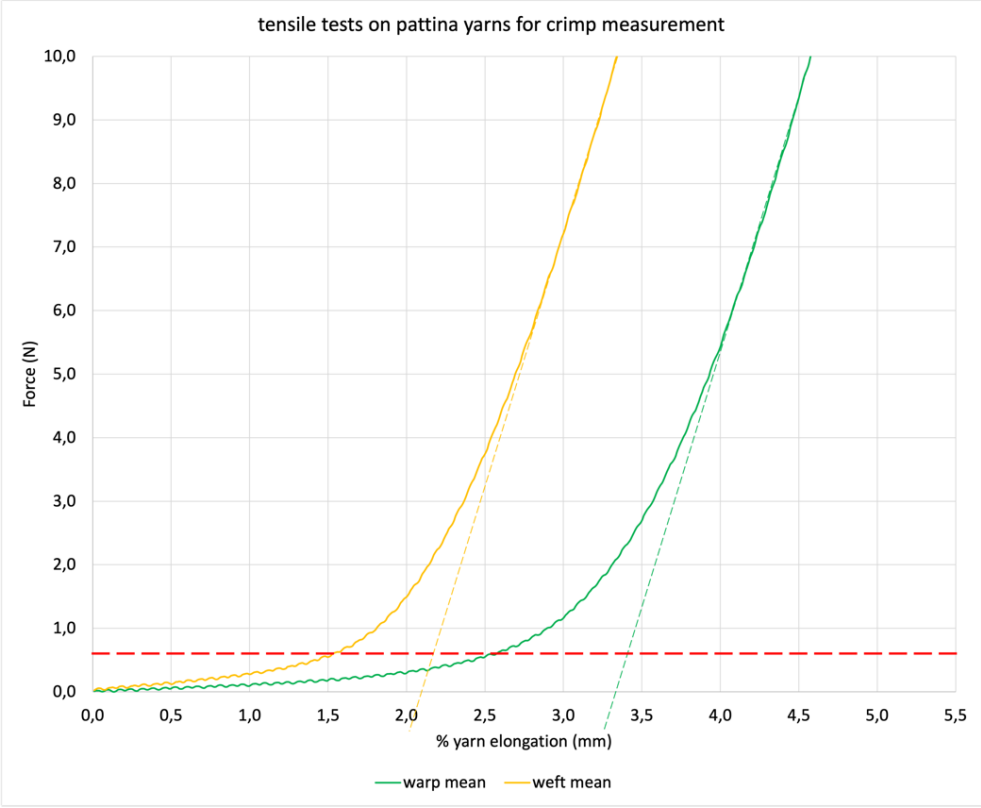

Figure 26 Tensile tests on crimped yarns of the pattina lining canvas (n.24)

[53] 3 yarns in each direction, 140 mm long, tested at the speed of 10 mm/min.

3.3.5 Crimp value

The measures of crimp in warp and weft, as seen in Table 7 and in Figure 27, provide a rather uncontroversial answer about the prevalence of crimp in the warp direction, since it is higher in 24 cases, or 92%. Moreover, the mean difference is very large, about 50% of the value; in 10 cases it is over 64% and in only one case it is less than 23%. If the subset under the pale blue band is not included (i.e. filtering above the value of +/- 0.5 % difference), the prevalence of the warp is increased to 96% (23 over 24 textiles). The reason is to be found in the fact that the weft yarn inserted between the warps causes them to bend over during the shedding process, thus acquiring a crimped shape that becomes permanent in the woven canvas. Such a crimped shape is maintained by the friction and internal tensions between the yarns. As it is usually reduced after wetting and/or stretching of the fabric, we can assume that the crimp values in the historical textiles studied here were probably higher at the origin.

		crimp measures						means		difference
	sample name	warp 1	weft 1	warp 2	weft 2	warp 3	weft 3	warp	weft	warp-weft
1	plain canvas 1	7,69	5,35	8,39	5,78	7,65	5,73	7,91	5,62	2,29
2	plain canvas 2	11,42	3,65	15,38	6,85	9,39	2,44	12,06	4,31	7,75
3	plain canvas 3	8,68	6,45	5,79	5,17	7,46	5,16	7,31	5,59	1,72
4	plain canvas 4	16,3	2,04	8,41	2,05	8,39	2,45	11,03	2,18	8,85
5	plain canvas 5	24,01	1,56	28,11	2,7	12,95	1,77	21,69	2,01	19,68
6	Domenico C. Malinconico	10,35	3,67	9,45	4,18	13,55	5,02	11,12	4,29	6,83
7	Bernard d'Agesci	4,73	10,22	6,82	3,99	7,56	7,65	6,37	7,29	-0,92
8	medium paste lining canvas (IT)	2,28	2,16	0,93	3,59	2,77	1,7	1,99	2,48	-0,49
9	heavy paste lining canvas (IT)	14,09	8,11	14,46	10,95	11,15	9,42	13,23	9,49	3,74
10	Fragonard medium paste lining	8,78	2,66	8,21	3,4	7,81	2,47	8,27	2,84	5,42
11	Raffaele Postiglione	8,09	2,49	2,93	4,25	4,45	3,06	5,16	3,27	1,89
12	Alfred Dehodencq	15,51	2,78	14,87	2,45	15,5	1,78	15,29	2,34	12,96
13	Jules Gélibert	12,3	3,4	11,36	3,58	12,1	3,71	11,92	3,56	8,36
14	Louis Augustin Auguin	17,67	5,8	13,78	3,87	7,44	4,28	12,96	4,65	8,31
15	Ludovic Alleaume	9,71	6,54	11,82	8,62	12,56	5,11	11,36	6,76	4,61
16	Hubert Sauzeau 1	13,28	6,38	9,54	5,63	18,14	5,18	13,65	5,73	7,92
17	Hubert Sauzeau 2	19,08	5,12	20,47	5,84	19,45	7,05	19,67	6,00	13,66
18	Charles Müller	11,82	4,96	8,49	6,47	10,48	5,66	10,26	5,70	4,57
19	Furcy de Lavault	13,68	3	14,28	3,63	14,66	2,45	14,21	3,03	11,18
20	Louis Alexandre Cabié	11,25	3,3	9,62	3,11	-	-	10,44	3,21	7,23
21	Louis Lessieux	11,9	5,09	13,27	7,38	15,94	6,44	13,70	6,30	7,40
22	Jeannine Gilles-Murique	7,72	3,92	5,07	3,81	-	-	6,40	3,87	2,53
23	Night Watch mockup canvas	7,03	1,04	7,63	2,63	6,83	1,06	7,16	1,58	5,59
24	"pattina" lining canvas	2,93	0,72	2,45	1,42	3,44	2,59	2,94	1,58	1,36
25	"patta" lining canvas	3	1,65	1,94	2,17	1,85	2,18	2,26	2,00	0,26
26	canvassing "03f"	5,69	2,59	5,86	2,59	4,91	2,34	5,48	2,51	2,98

Table 7 Crimp measures, means and difference between warp and weft

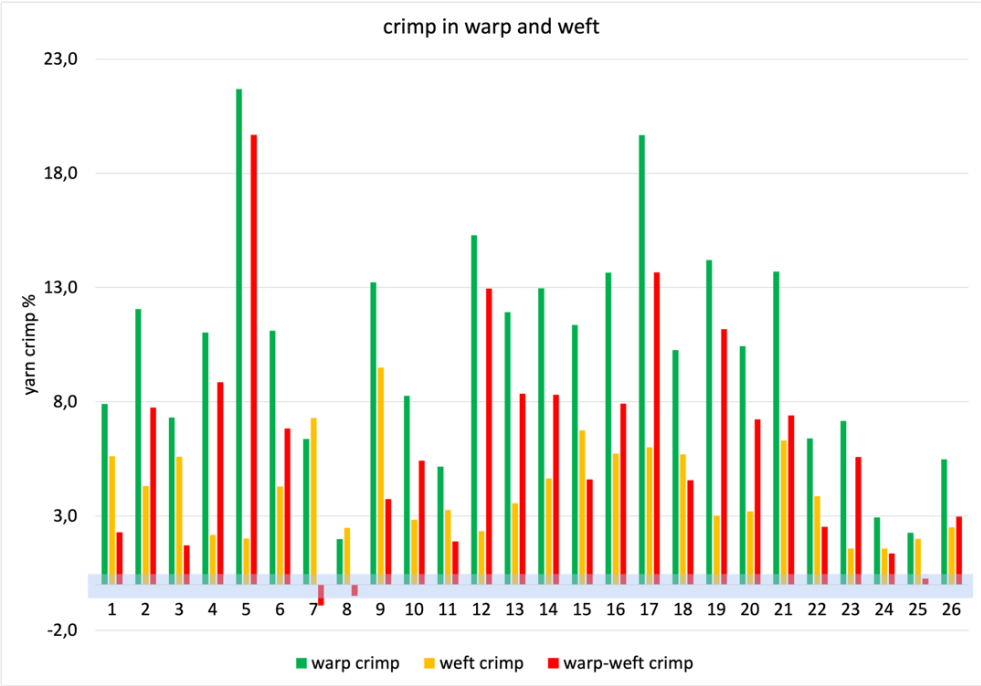

Figure 27 Crimp values in the warp are higher than in the weft in 96% of the cases

3.4 Discussion

3.4.1 Characteristics allowing the identification of warp and weft without a selvedge

Some of the values obtained from the study of the 26 samples show recurring characteristics in traditional plain canvas woven structures, as shown in Table 8. This information may be useful for distinguishing warp from weft yarns in the absence of a selvedge.

The higher crimp in the warp provides the most robust correlation (96%), and is also found in the literature, both in conservation [Young and Jardine, 2012; Flock, 2020 **(a)**] and in textile engineering [Mertova et al., 2016]. The higher thread-count (77%) and yarn width (81%) in the warp are also useful indicators, and they seem to be a general feature directly related to convenience in weaving practice. As we have seen, it is easier and cheaper to produce a textile with more warp yarns than with more weft yarns. The reason why warp yarns are wider is most likely due to the need for a thicker and stronger yarn, as its failure during the weaving process is more problematic, while weft yarns are easily reconnected, as when the shuttle needs to be refilled. Still, another reason is found

in the fact that the warp yarns acquire a more elliptical cross section, as we have seen in figures 20 and 21, and therefore appear wider in the x-y plane of the textile. This opens up for the hypothesis that the yarn diameter was not as different between warp and weft before weaving as the yarn width in the textile would suggest. This assumption seems to be supported by the results in Figure 24, where the prevalence of the warp cross sectional area (54%) appears lower than that in the yarn width (80%). This seems intuitively understandable as the warp yarns bend over the weft yarns, which by their position provide a fulcrum for a very favorable leverage, causing their higher crimp and compression along the Z axis.

Nevertheless, clear evidence is derived from the examination of our group of textiles that higher twist is associated with lower yarn width. This confirms the observation of the width of the woven yarn to be a reliable indicator even though it is actually related to the original diameter of the unwoven yarn, an information that is not available for historical textiles. Moreover, the differences found in the TPM values are not in agreement with the hypothesis of a similar yarn being used for warp and weft during weaving of pre-industrial or traditional textiles, and the statement that the warp yarns are stronger and of better quality than those in the weft is quite common in the literature. The subject would benefit from the production and analysis of more specimens woven from yarns with a well-defined initial diameter and twist. This is the case of n. 26, which is woven with the same yarn and has very similar values for yarn width and TPM in warp and weft. Yet these characteristics make n. 26 an outlier in the data set. As the subject is promising an interesting insight, but it does not appear to be relevant for the identification of warp and weft in a woven historical textile in the absence of a selvedge, no definitive answer is proposed here.

Experience gained during this research shows that the difference in crimp is sometimes clear enough at the naked eye observation to make predictions about the weft and warp directions. All other features require the more detailed observation made possible by the use of a macrophotograph. As the sample set is wide and heterogeneous, including both hand-woven and industrial textiles, the correlations found with this research appear particularly relevant.

higher value	**crimp**	**z compress.**	**yarn width**	**thread count**	**yarn thickn.**	**twist**
warp	96%	86%	80%	77%	30%	35%
weft	4%	14%	20%	0%	70%	65%

Table 8 General correlations with warp and weft directions found in the 26 specimens

3.4.2 Warp and weft correlations in literature

Rouba proposed experience-based methods for identifying warp and weft by visually examining the reverse of the painting [Rouba, 1992]. The first and most interesting result is that the warp yarns run parallel, while the weft may be curved and show irregularities created during the weft casting and beating with the comb. She noted that the warp yarns are usually of better quality, woven regularly and without defects, and may outnumber the weft yarns in thread count, both statements consistent with our results. She also suggested, which contradicts our observations, that warp yarns have more twist and less crimp.

Van de Wetering and Bosshard observed the structure of the canvas using X-ray images of the paintings to investigate the origin of the textiles and to identify warp from weft [van de Wetering, 1997]. The method allowed them to measure yarn orientation and density, local thickening, and deviations from straightness, but not yarn width, twist, or crimp. They found that the warp count was more consistent and often higher, while the weft was spun with coarser material and showed frequent thickenings. Some irregularities in the weave were associated with the weft, such as stripes of uneven density caused by the beating of the comb or the rolling of the fabric. They noted occasional thickenings caused by the friction of the comb along the warp, accumulations of loose fibers that cause the weft to bend over. They also suggested that the warp yarns had more twist and less crimp, but like Rouba, they could not measure these characteristics and they openly formulated a hypothesis about these two aspects.

A direct evolution of van der Wetering's studies is based on the use of algorithms ad artificial intelligence to describe the weaving density and angle maps in warp and weft [van der Maaten and Erdmann, 2015]. This allowed correlations between pieces of textiles belonging to different paintings to be determined and provided a much deeper understanding[54]. Weaving density and angle maps are innovative and important pieces of information and, as the research was extended to 400 van Gogh paintings [Johnson et al., 2013], it also allowed for statistical studies. For what concerns the specific subject of this thesis, the correlations with warp and weft directions they offer are similar to those deriving from van der Wetering's work, as twist and crimp of the yarns, and their width, are not visible.

Automated methods to measure thread densities from simple images of the fabric are being developed in the textile industry [Pan et al, 2015; Aldemir et al., 2019], but they unfortunately only provide a single aspect of the woven structure and would not be useful to reduce the amount of work required by the protocols described in this chapter.

[54] https://countingvermeer.rkdstudies.nl/6-exploiting-weave-maps/

3.5 Conclusions and future work

Effective and relatively simple methods to measure the usually inaccessible characteristics of historical textiles have been developed and organized in this chapter. The protocols were tested on a heterogeneous group of samples, confirming their effectiveness. The quantity of data provided allowed drawing a first set of general conclusions that will be verified widening the set of textiles. Correlations have been found for warp and weft yarns that allow a certain degree of reliability in their identification in the absence of a selvedge. The data collected in this chapter to describe the morphology of the specimens will be linked to the biaxial tensile response of the samples extracted from them, as we will see in chapter 5.

The first direction of the future work, in perspective after this thesis, as related to the morphological description of historical textiles will be to conduct statistical tests to determine the probability that the observation of one of the "characterizing features" (see Table 8) on a sample will allow identifying the warp from the weft, and how the probability is increased by the simultaneous observation of more than one characterizing features.

A second open subject is more exquisitely morphological and is based on the above-mentioned questions about the distortions acquired by the yarn during weaving. The null hypothesis could be that the yarn traditionally used to weave warp and weft was derived from identical productions. In order to test the hypothesis, mockups woven from yarns with a well-defined initial diameter and twist would be analyzed. The expected outcome is an insight in the amount of increase of yarn width and reduction of yarn thickness, or z axis compression, in correlation with yarn twist, a characteristic for which no alteration is anticipated due to weaving.

An interesting perspective for future research emerged from tests carried out on a single linen yarn provided by Helena Loermans, Dutch weaver in Portugal, in June 2025. The yarn is the raw material for samples of hand-woven textiles she provided as a continuation of the present research. The original idea was to analyze the effect of winding onto a bobbin to prepare the weft threads, as this could have an effect on the TPM because of the accidental twisting this operation could imply. The yarn was therefore provided as on the industrial cone, and also wound on weft bobbins: clockwise or counterclockwise winding, using a standard tension or more than the usual force. Unexpectedly, the TPM measures on the different sets of yarn revealed that a relevant, measurable untwisting of the yarn is connected to winding under additional testing, more than to the direction used.

In order to verify if this information could be applied to the warp yarns to explain why, as we have seen in Table 8, they show a lower TPM in 65% of the cases. In order to

simulate the tension of a warp yarn on the loom during weaving, a 15 cm long piece of the yarn was submitted to 6 repetitions of the load of 4N. Such value was selected because it was experimentally found that the yarn exhibits noticeable crimp above the tension of 3.5 N, and was therefore considered to be a realistic guess of the loads on a loom. As it can be seen in Figure 28, the simulation reproduced the same reduction of TPM. From 241 TPM in the untreated state, to values of about 190 TPM after clockwise and counterclockwise winding on the bobbin with additional tension, and after the 4N tension cycles. This therefore hints at the possibility that the weft yarns were not intentionally having more twist, but that rather the warp yarns lost some of their original twist because of the tension on the loom.

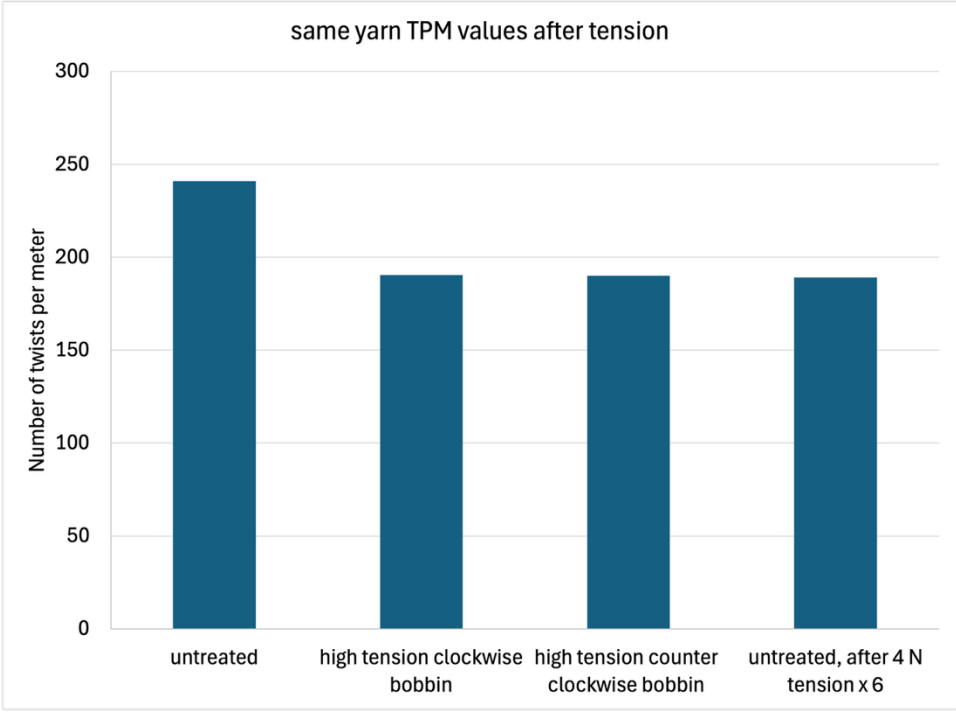

Figure 28 Reduction of TPM due to tension of the free yarn

Chapter 4 Design and construction of testing devices

Outline of the chapter

4.1 The construction of a biaxial tester
- 4.1.1 The need for a custom designed biaxial tensile tester
- 4.1.2 The biaxial tensile tester in context
- 4.1.3 General requirements for tensile testing of canvas paintings samples
- 4.1.4 Samples dimensions
- 4.1.5 Testing loads, speeds and run limitations
- 4.1.6 Testing procedures

4.2 Mechanical design
- 4.2.1 Concept
- 4.2.2 Mechanical construction
- 4.2.3 Description of the motion actuators
- 4.2.4 The load cells and clamping devices
- 4.2.5 The end stops

4.3 Electronic design
- 4.3.1 The electronics
- 4.3.2 Software development
- 4.3.3 Machine controller firmware
- 4.3.4 Pre-tensioning algorithm
- 4.3.5 PC software development
- 4.3.6 File format

4.4 Build instructions
- 4.4.1 Construction of the steel cross
- 4.4.2 Perforation of the structure for fixing the actuators
- 4.4.3 Test the assembly of the actuators and powder coat the structure
- 4.4.4 Installation of the cables and of the actuators
- 4.4.5 Construction of the sample clamps
- 4.4.6 Construction of the box for the electronics
- 4.4.7 The box for the switches

4.5 Operating instructions
- 4.5.1 Clamping the sample
- 4.5.2 Test procedures tips

4.6 Validation and characterization
- 4.6.1 Displacement of the carriages
- 4.6.2 Load cells data

4.7 Results
- 4.7.1 Pre-tensioning
- 4.7.2 Biaxial and uniaxial tensile tests
- 4.7.3 Peel tests

4.8 The open-source format

4.9 Design and construction of a portable uniaxial tester

4.10 Design and construction of a Displacement Tester and hand-held probe

4.11 Conclusions

This chapter is mainly devoted to the reasons why a new biaxial tester was needed in the field, to a related literature review devoted to the subject and finally to its design, construction and use. Two minor sections are also present, devoted to the construction of two other devices: a portable version of the tester, working with only one axis, mostly used for peel tests; a displacement testing device, used to apply a force on a painting to measure its resistance to displacement. All devices were built between 2021 and 2023 as part of the work of this thesis.

4.1 The construction of a biaxial tester

4.1.1 The need for a custom designed biaxial tensile tester

The mechanical aspects of canvas painting conservation and the study of the effects of conservation treatments benefit greatly from quantifying the mechanical characteristics of the materials. However, this is seldom possible as only few labs have the necessary equipment. The development of a biaxial tester is described here, designed to be used for samples of naturally aged canvas paintings. An effort was made to create a system that is easy to assemble, with parts that are easy to source and with an overall cost well below the commercial units available. The control software includes the function of automated pre-tensioning to improve the accuracy of the measurement. The broader purpose here is to make an easy-to-replicate machine available to help conservators and conservation scientists perform tensile tests to make informed choices in materials science, and to make the design and software open source. The main part of this chapter has been published in [Iaccarino Idelson et al., 2023].

4.1.2 The biaxial tensile tester in context

A typical painter's canvas consists of yarns woven together at a 90-degree angle, the warp and weft, and it exhibits different mechanical properties depending on the direction being stressed. If the two are stressed simultaneously, the resulting force will be different from a uniaxial loading because the yarns in each direction influence the behavior of the other. Researchers have been studying this relationship for decades, first in the textile industry [Clulow and Taylor, 1963], then in the conservation of paintings on canvas [Russell and Berger, 1982]. In standard conditions, a painting on its stretcher is subjected to tensions simultaneously acting in two orthogonal directions in the painting's plane [Iaccarino Idelson, 2004 **(a)**; dePolo et al., 2021]. Current research is mainly based on uniaxial tests performed on each of the main directions of the canvas, but uniaxial data can, in some cases, become misleading. The role of biaxial testing is that of reading the interaction between the orthogonal forces. Only in recent years have biaxial testing machines been built by leading industries for specific engineering

purposes[55], and some low-cost machines have been designed with the use of Arduino boards [Pereira et al., 2020; Shiwarski et al. 2020]. Biaxial testing machines need to be designed to meet the needs of a specific field of investigation regarding loads, sample dimensions and clamping. Currently available machines are typically targeted for architectural tension structures based on coated textiles [Junhao et al. 2022; Van Craenenbroeck et al., 2019] or for biomedical purposes [Jiang et al., 2021] and are out of scale for painting conservation, being either too large and powerful or too miniaturized. An assessment of the history of the machines used for testing the mechanical behavior of paintings on canvas up to the end of the 20th century was carried out extensively by C. Young [Young, 1996 **(a)**]. Among the historical biaxial testing machines, we only refer here to that built in 1963 by Clulow and Taylor for the textile industry [Clulow and Taylor, 1963]. It was designed to apply forces simultaneously on the four ends of the two axes, thus allowing the center of the sample to remain in a stable position. Force values were read through springs located at one end of each axis. The machine could test cruciform samples of 10x10 cm, but 10 cm uniaxial arms of the same material at each end were needed to redistribute the non-orthogonal stresses. Therefore, the actual sample size was 30x30 cm.

The first biaxial testing machine for canvas painting conservation was built in 1982 by Russel and Berger [Russell and Berger, 1982] and implemented in 1986 [Russell and Berger, 1990]. It was designed for testing relatively large samples (25x25 cm), monitoring tensions over long-duration tests, and it also intended to simulate environmental changes. Force was actuated at one end of each axis with manual adjustment bolts, and a micrometer screw allowed fine adjustment at the opposite end. The motion was not symmetric, and the sample was not kept centered in the setup during testing. Samples were connected with fiberglass threads glued with epoxy resin dot joints to the moving bars of the machine for a better alignment. Such a fixture method allowed lateral movements, favoring tension redistribution within the sample. Tension was applied by turning the nuts and reading with two load cells placed in the moving ends. In the first version [Russell and Berger, 1982], tension was applied with dead weights and pulleys. The device was active over a short time span in the mid-1980s [Russell and Berger, 1982; Russell and Berger, 1990].

The second biaxial tester in conservation was built at the Tate Gallery for C. Young's Ph.D. in 1996 [Young, 1996 **(a)**]. Data was presented in 1996 [Young, 1996 **(b)**] and in 1999 [Young and Hibberd, 1999]. The typical sample dimension was 26x20 cm. At one end of each axis, a stepper motor and a load cell were placed on coaxial rail guides; at the opposite end was a manual adjustment stage. Like in the Russell-Berger setup, motion

[55] Among others, Instron and Zwick Roell have planar biaxial testing machines displayed on their websites, for applications in general mechanics, elastomer industry, biomechanics.

was asymmetric from the center; still, displacements and strains were measured using optical Electronic Speckle Pattern Interferometry (ESPI) [Young, 1999], a technique gathering information on the entire sample. Stepper motors were used for fine adjustment of position and force and to operate and measure displacement when performing "load-extension" (stress-strain) tests. The tester has been active since 1996 [Young, 1996 **(a)**; Young, 1996 **(b)**] and was still in use at the Courtauld Institute in London in 2006[56].

Machines built after 1999 in the field are few. One was built for Chiriboga's Ph.D. [Chiriboga, 2013] at the Delft University of Technology, Faculty of Aerospace Engineering, in 2013. Chiriboga's, like the previously described machines, was intended to study large samples (40x40 cm or 30x40 cm). A very simple structure, with hand-operated screws actuators and a load cell on each axis, it was used to set a known value of tension before exciting the sample with a sound wave for reading vibration and deformation patterns with a laser vibrometer. A similar stretching device was used by Leila Sauvage to study vibrations in pastels on paper [Sauvage et al., 2017]. The latest use of a biaxial testing machine in conservation, appears to have been for the evaluation of the mechanical performances of adhesives used for butt joining individual threads in canvas paintings tear mending [Flock, 2020 **(b)**]. The machine works with four motors, thus with a symmetric motion from the center, and its most interesting feature seems to be that it allows a finely adjustable pre-tension [Flock et al., 2020 **(a)**], though this is not thoroughly described. A similar machine was presented in 2019 by the same working group at Saarland University [Morris et al., 2019].

The aim here was to create a new biaxial tensile test machine that is as inexpensive and easy to build as possible, in order to make it available to the largest number of researchers, obtaining high-quality results. The machine presented in this paper is the fruit of the interdisciplinary work and collaboration between a painting conservator, a computer scientist and an expert in materials characterization. Biaxial tensile tests procedures for canvas using a cruciform sample are currently being developed by ISO[57], under the name: ISO/AWI 13118:2024 "Textile- Biaxial tensile properties of a woven fabric- Determination of elasticity properties using a cruciform test piece". The standard specifies a CRE (Constant Rate of Extension) biaxial tensile testing machine, with the pretensioning procedure referenced in ISO 20932-1:2018, 3.9. However, this clause does not provide a defined value for the initial tension, while it establishes a minimum sampling rate of 8 Hz. The cruciform sample dimensions described in the standard—300 mm × 300 mm (see Figure 29)—are designed for industrial textiles and are far

[56] When I was kindly invited by Christina Young to see the machine.
[57] https://www.iso.org/standard/84281.html.

beyond what is feasible for historical specimens. Moreover, the sampling distribution proposed to avoid reusing the same yarns in different specimens is inapplicable in the context of historical materials due to their limited size and availability. The corner radius is defined in order to limit the corner effect during high stress conditions and during load cycles.

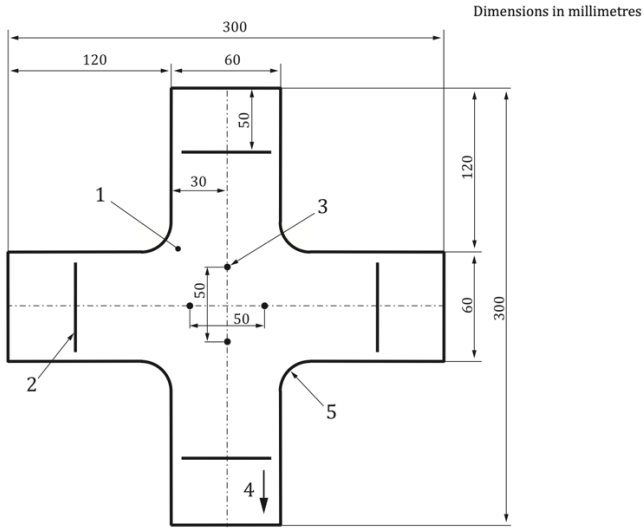

Key

1 specimen
2 line for mounting
3 gauge mark
4 direction of warp
5 internal corner (radius: 15 mm)

Figure 29 The cruciform textile sample for biaxial tensile tests as defined in ISO 20932-1:2018

In the following paragraphs, the test conditions and requirements for the machine design will be defined. Hardware will be described, along with the firmware and the operating software. A step-by-step assembling guide and operating instructions will follow, concluding with a description of the results of some of the tests possible with the machine.

4.1.3 General requirements for tensile testing of canvas paintings samples

The structure of a canvas painting is generally described by the canvas support, woven with natural or synthetic fibers; a " size" layer, with animal glue or a synthetic emulsion, making the canvas surface less absorbent and more suitable to receive subsequent layers; a thicker "preparation" layer, with binders and charges, filling the spaces between the threads and building the surface that will receive the paint [Stols-Witlox, 2017]; finally,

the paint layers. The painting is thus a composite material, and a tensile testing procedure aimed at the elastic modulus of the entire stratigraphy, i.e., before reaching the failure of individual layers, has been privileged in the present study because it allows the behavior of the painting under normal conditions to be described, and not only the critical situations that are to be avoided for conservation purposes. The elastic modulus of the whole stratigraphy can be used in predictive finite element simulations and to compare different materials. Such low strains and loads occupy only a small part of the plot when testing to the ultimate load and are easily blurred in the initial reorganization of the sample when the test is started. Tensions ranging between 1 and 3 N/cm are generally considered to be typical and not harmful for most paintings on canvas [Iaccarino Idelson, 2004 (b); Roche, 2003; Iaccarino Idelson, 2009]. Under such test conditions strains are typically below 5%, with very small lateral dimensional changes in the clamped sample, therefore the long compensation arms of the cruciform samples described in the literature become unnecessary in a symmetrical testing system. Therefore, only the material required for clamping is needed, in addition to the area designated for testing.

4.1.4 Samples dimensions

For research in conservation, the possibility of testing small samples is crucial, because naturally aged materials (e.g., an old painting) are unique, variable according to local characteristics, and very scarce. Sample size is connected to both the dimensions of the machine and the forces involved. International standard procedures exist on uniaxial tests (ASTM, UNI, DIN) and are generally based on a common value of 1" or 25mm for the width of the sample. If a 25mm square sample can be easily cut in new canvases, this is often unrealistic for naturally aged samples, also because the number of replicas implies statistical relevance. A sample width of 1 cm for naturally aged materials was chosen as a reasonable balance[58] between their morphological heterogeneity and their inherent rarity.

4.1.5 Testing loads, speeds and run limitations

Testing up to 30 N/cm (10 times more than the paintings' normal working conditions) provides a wide enough range of data, implying a very small force build-up on the machine's structure[59]. Nevertheless, the structure was designed to withstand forces up to approx. 1000 N without undergoing relevant deformations. Testing speed influences the response of viscoelastic materials, as fast loading increases reaction force. Test speed must be adjusted to specific test conditions within a relatively wide range of velocities.

[58] All biaxial tests performed with the machine on different sample sizes produced, so far, comparable or superposable stress-strain plots.

[59] The force reaches 75 N on each axis for the 25 mm samples.

In the case of a 5% strain for a 10 mm sample at the speed of 0.2 mm/min, the 0.5 mm run will be covered in 2.5 min. Assuming a theoretical sampling rate of 8 samples per second for force values, such a duration would detail the force path with 1200 readings, which is a more than adequate number. Peel tests are at the opposite end of the range, as previous research [Iaccarino Idelson and Garofalo, 2019] has set the reference speed to 100 mm/min. Elongation is to be measured with a precision of about 5 microns, in order to provide data for low-strain tests. Aiming at higher resolution would be impractical as it would require a very accurate environmental control for the machine's dimensional stability. The run of the clamps is limited by the length of the linear rails, and the choice was made to use 300 mm rails ensuring an overall run of approx. 400 mm in each direction.

4.1.6 Testing procedures

The main tests that prove useful for conservation purposes[60] are the following.

1. **Low-stress tensile test**. The test is designed to analyze the mechanical behavior of a painting facing stresses that are as similar as possible to those it would undergo in a typical conservation environment and conditions. The reference standard will probably become ISO/AWI 13118, once it will be published[61]. The sample is pulled at a constant speed until reaching a given target force. The test will finish when the force is reached or, as a safety feature, if a maximum distance of 250 mm is covered during the test. The target force and maximum distance are the values that can trigger the termination of the test procedure.
2. **Yield and failure test**. The test is designed to analyze the mechanical behavior of a painting under extreme conditions. The reference standard will also be ISO/AWI 13118. The sample is pulled at a constant speed while the force is recorded. The test is terminated when the measured force falls -70% from the recorded maximum value (due to fiber breakage of the specimen). As a safety feature, a maximum distance of 250 mm is covered during the test. The maximum distance and target force are also variables that can trigger the termination of the test procedure.
3. **Constant load test**. The test is designed to measure creep and similar behaviors under a specified load[62]. The sample is pulled at a constant speed

[60] Among others in the literature of this paper, see [dePolo et al., 2021].

[61] https://www.iso.org/standard/84281.html

[62] Long duration tests (constant elongation or constant load) in the field of paintings conservation have often been adapted to specific needs [Young, 1996 a; Berger and Russell, 1990; Chiriboga, 2013; Sauvage et al, 2017]. Standards are not mentioned in research publications and do not appear to be available.

until reaching a given target tension. The machine keeps the tension constant by moving the clamps if needed. The elongation and force are recorded. This test can last a long time (hours) and may be performed in an environmental chamber so the sample response to changing environmental conditions can be analyzed.

4. **Constant elongation test**. The test is designed to measure changes in the tension produced within the sample over time after an initial load[63]. The sample is pulled at a constant speed until reaching a given target force. The machine does not move the clamps but records tension as it evolves. Changes of the environmental conditions, or the simulation of conservation treatments, can be associated with the test.
5. **Uniaxial tensile tests**. Tests designed to analyze the mechanical behavior of paintings material samples, as done with a uniaxial testing device. All the previously described tests can also be performed uniaxially, using only one pair of opposing actuators. Standards for uniaxial tensile tests for canvas are in ISO 13934[64].
6. **Peel test**. Peel tests are used for the characterization of the adhesive bond and are considered a reference for studies on lining techniques for canvas paintings. The test is a special case for uniaxial testing, intended to determine the bond strength of the adhesive used to bind together two textiles (in treatments such as lining) and is, by definition, a uniaxial test. Two opposing clamps will tear apart the two adherends at a set speed while the force is recorded. The test will end when the set distance is reached. The Peel test is described in the ASTM D 903 – 98[65], and a maximum travel distance of 350 mm[66] is sufficient.

4.2 Mechanical design

4.2.1 Concept

The reference structure of the machine is a stiff metal cross to which four identical actuators are connected, allowing the sample to remain centered during the test. Using a ball screw and ball nut for traction allows it to work in a condition that makes backlash less relevant than with other methods and allows to indirectly measure the elongation of the sample by counting the number of revolutions of the shaft. Stepper motors allow an accurate knowledge of position, provided that the forces involved do not exceed their

[63] Ibid.
[64] https://www.iso.org/standard/60676.html
[65] https://www.astm.org/d0903-98r17.html
[66] Distance is to be divided between the two opposing actuators, thus 175 mm each. ASTM D903-98 prescribes a total run of 304,8 mm.

torque, as this would make them lose steps. For the force measurement, load cells were seen as the most convenient sensor type because they are reliable and offer a robust mounting structure for the clamps. The mechanical design process was iterative: first, a proof of concept was implemented using components readily available in the workshop in Rome. An M12 threaded rod and a sliding door guide were used, all coupled to a stepper motor. That was the foundation of a one-axis actuator prototype that allowed us to start with a physical model for which it was possible to write code[67] and obtain the first test results. It should be noted that the entire process of designing and building the prototype and the final machine was done by working remotely in Spain and Italy. Most of the work was carried out during the COVID-19 lockdown in Europe. Sourcing the parts and obtaining semi-finished parts, laser cutting or machining from contractors was more challenging than usual. In the final design, each of the four arms of the cross houses an identical actuator consisting of a stepper motor[68] and a recirculating ball screw[69], which moves a carriage on two parallel linear guides[70]. Connected to each carriage is a load cell[71] for force measurement and a clamp to hold each sample edge. The symmetrical design increases accuracy, as displacement is determined by two motors on each axis, and forces are read by four load cells[72]. Such a design also allows high flexibility of use. A CAD drawing of one of the four actuators of the biaxial tester is shown in Figure 30. A ball screw and ball nut have been used to drive the motion instead of a threaded rod because of their greater smoothness, lower friction, and almost complete absence of play due to the preload of the ball bearings the ball nut rides on. These are definitely a more expensive choice but they were chosen because of their superior performance. Besides, the efficient elimination of the backlash means that sample elongation can be measured precisely through the angle of motion of the ball screw. Such a feature avoids the need for additional methods for measuring sample elongation. The pulling action of the machine is divided between pairs of actuators cooperating with simultaneous action on the same axis, so each produces only half the required speed and displacement.

---

[67] All coding (firmware and software) was written by Miguel Sanchez, and the mechanical design was the fruit of his collaboration with the author. The mechanical construction, wiring and the assembly of the electronics was done by the author.

[68] NEMA 23, with the remarkably high torque value of 4Nm.

[69] RM1605 Ballscrew, with Anti-Backlash Ballnut, with C7 class ball bearings.

[70] SBR16 supported round rail (16 mm diam shaft, h6 tolerance, induction hardened), 300 mm long, with SBR16 long open linear bearings.

[71] S type load cells, class C3.

[72] The presence of two opposing load cells on each axis improves the management of sensor-related errors, as readings from two cells are averaged.

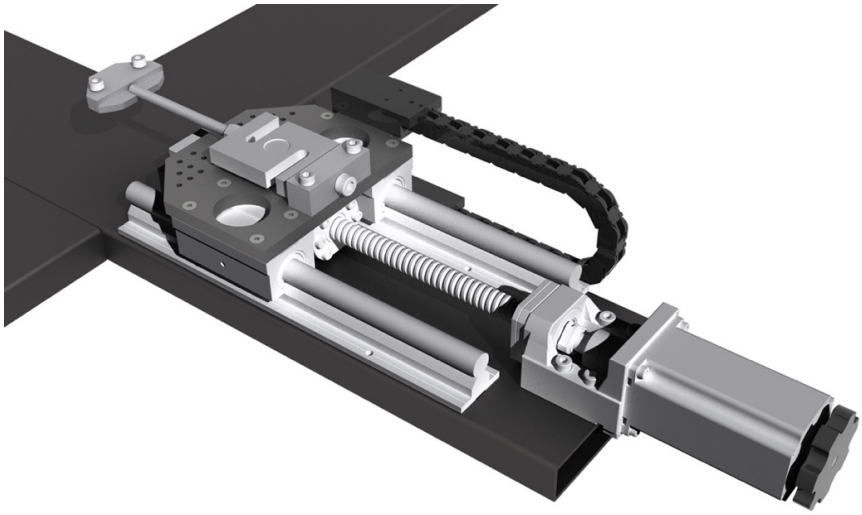

Figure 30 CAD drawing of one of the four actuators. From left to right: the sample clamp connected to the S-shaped load cell fixed to the carriage moving on the linear rails thanks to the ball nut (under the carriage) and ball screw turned by the stepper motor, with an additional knob for the manual motion

4.2.2 Mechanical construction

The cross was built by welding 150x30 mm, 3 mm thick standard carbon steel profiles. In order to compensate heat-related tensions, welding[73] was performed by gradually adding weld spots on opposite sides, a careful procedure that allowed for obtaining a perfectly planar structure. Before welding, holes were drilled on the two sides of the main element of the cross, under the connection with the short arms, in order to allow cables to pass through the structure (see Figure 31).

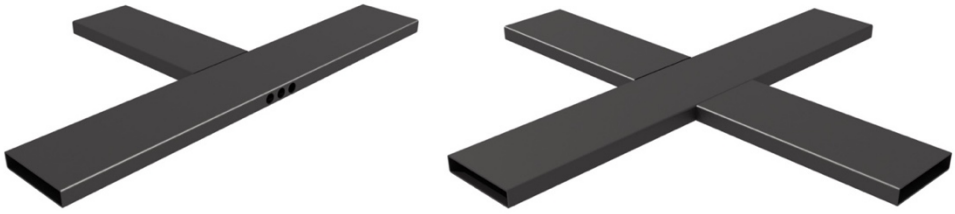

Figure 31 CAD drawing of the parts of the steel cross, made by welding two short elements to a long one, with holes on the side for the passage of the cables

[73] In this case, TIG welding was used, as it is very controllable and accurate.

The overall dimensions of the cross, 91.9 cm, were determined by the length of the actuators, leaving a free 17.5 cm square area in the center for positioning and clamping the samples. All parts were mounted on the welded structure using stainless steel screws and bolts in threaded holes in the cruciform structure. After a complete cycle of testing the mechanics and alignment of the moving parts, all elements were disassembled to powder coat the cruciform structure with a Polyester – TGIC Free varnish[74] to prevent corrosion, and then the machine was finally reassembled (see Figure 32). Steel parts for the main cross, carriage plates, and clamps were sourced directly from suppliers, as were industrial laser cutting and powder coating services. Welding, precision mechanical assemblies and 3D printing of parts were carried out in the workshop of Equilibrarte ltd[75], in Rome. The linear guides, all parts needed for motion actuation, the motors and most of the electronics were purchased through online stores. The total weight is approximately 45 kg.

[74] AkzoNobel Powder Coatings, Interpon 610 NW300M INT 610 HR IRONANTHRACITE.

[75] Equilibrarte is a conservation company, with Antonio Iaccarino Idelson as CEO and Technical Director.

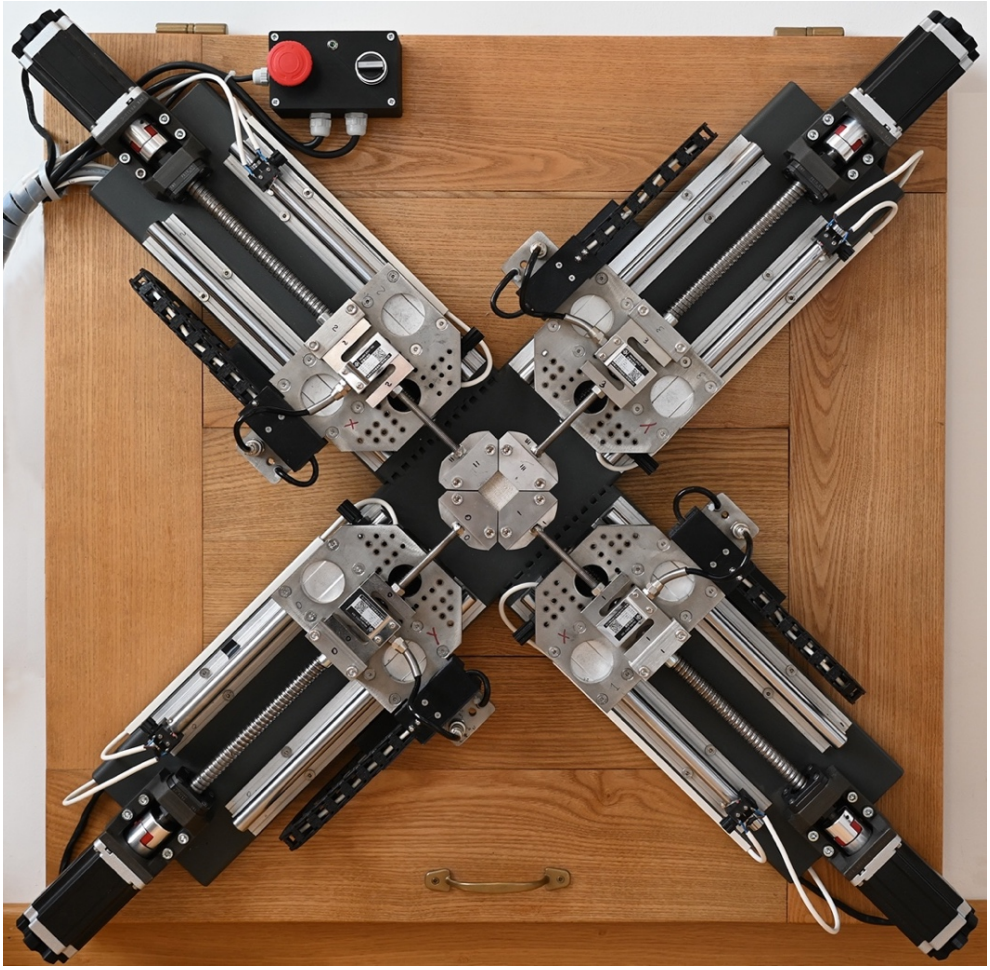

Figure 32 The biaxial tester assembled on a wooden table, with the control box for the security switches

4.2.3 Description of the motion actuators

Stepper motors can lose steps, thus making the measurement of the carriage position unreliable when the force opposing their motion exceeds their value of maximum admitted torque. The NEMA 23 4Nm stepper motors were chosen because they display a remarkably high torque[76] for their compact size at an affordable price. Each motor was

[76] The high torque value of the motors protects the system with a large margin of safety from the risk that they might lose steps with the loads predicted by the design. In any case, should this ever happen,

mounted on a cast steel support, which also holds the ball screw support bearing. The motor shaft is connected with a flexible aluminum coupler to the anti-backlash ball screw and ball nut, which is supported at the opposite end by a ball screw support floating bearing.

The ball nut is fixed with six bolts into an aluminum mount, providing a solid connection with the carriage plate on top of it. The carriage plates were laser cut from 10 mm AISI 304 stainless steel. Plates are connected to the 85 mm long open linear bearings running on the 16 mm diameter supported round rails in steel, as seen in Figure 30, and holes were drawn for their connection to the linear bearings and the load cell supports. To reduce their mass by 20%, additional large holes were designed where they would not affect the rigidity (see Figure 33). Protruding lateral support was designed to house the load cell amplifier board[77] protected with a 3D printed box that also allows connecting the cable chain carrying the digitized load cell signal wires to the Arduino, as described in the next section.

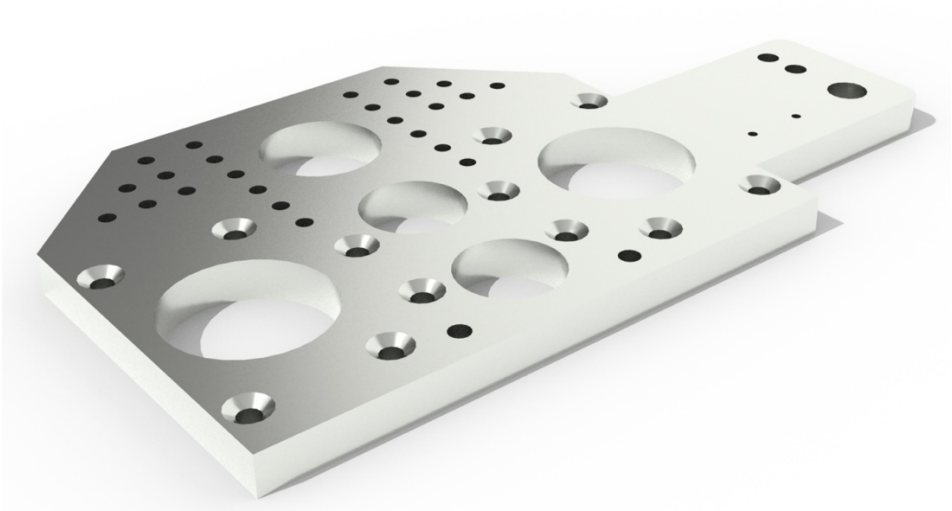

Figure 33 CAD drawing of the plate of the moving carriage, cut in 10 mm AISI 304 stainless-steel

it would manifest an anomalous behavior in the force/displacement graph, allowing the part of the test following the anomaly to be discarded.

[77] HX711 board.

4.2.4 The load cells and clamping devices

The load cells are mounted on supports manufactured from a 20x20 mm bar of AISI 304 stainless steel (see Figure 34). Two vertical holes connect them to the moving plate with M6 bolts, while a transverse hole connects the load cell with an M8 bolt. Load cell bolts are tightened with a dynamometric wrench at 5 Nm in order to reduce possible sources of different behavior.

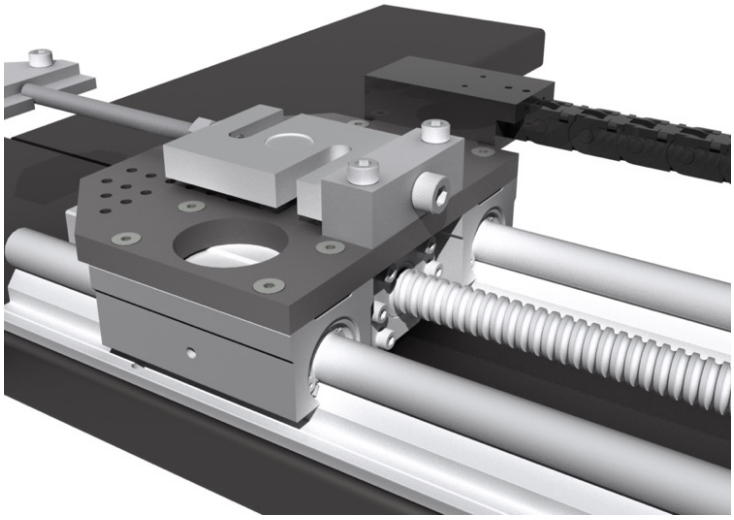

Figure 34 CAD drawing detail of the moving carriage showing the load cell on its support and the transverse bolt holding it

Three series of load cells[78] can be mounted on the machine with different load ranges. Load cells are in class C3, and manufacturer's specifications are as follows. Sensitivity: 2.0+/- 0.05 mV/V; Linearity: +/- 0.03% FS; Repeatability: +/- 0.03% FS. The load cell signal is digitized and amplified with an HX711 board, which is placed on the side of the moving carriage in order to reduce the analog cable to a minimum length. Since multiple load cells can be used, a 4-pin aviation screw connector is used in order to ensure stable contact and replacement ease. The digitized signal runs in a cable chain to protect the wires, then it is sent to the main control board through the machine structure, along with all the other cables, as will be described in the electronic design section.

The sample clamps (see Figure 35 and Figure 36) are connected to the M8 ending of the load cell and are designed in order to keep the sample centered on each axis. Two AISI

[78] All produced in China by XNQJALYCY

304 plates are used, one welded to the M8 bar and the other serving as a sample holder, connected to the former with M6 bolts. The shape of the plates is designed in order to reduce the space between the clamps without reducing their rigidity. Therefore, 45° cuts allow the edges to come close together, reducing the gage length to a minimum value very close to that of the sample area[79].

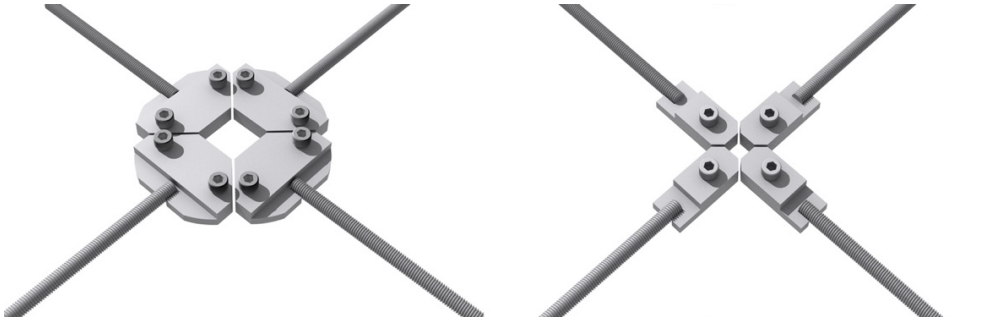

Figure 35 CAD drawing of the 25 mm and 10 mm sample clamps. The M8 rod is welded to the base plate, and the sample holder is fastened with M6 bolts

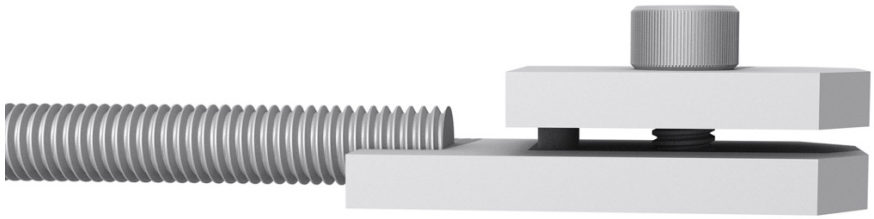

Figure 36 CAD drawing detail of the 10 mm sample clamp. The sample holder is guided with a 3 mm pin and fastened with a single M6 bolt

Samples are laser-cut to achieve a clean, linear perimeter and to avoid the mechanical stresses in the samples that may occur when cutting them with blades or scissors. As the directions of warp and weft are crucial information that may be lost once the sample is extracted from the material it was cut from, a triangular indentation in the perimeter of the clamping area allows the weft to be identified (see Figure 37). Samples are designed

[79] Minimum gage length is typically 10.6 mm for the 10 mm sample clamps and 25.8 for the 25 mm clamps.

so as to minimize the use of specimen material. The clamping areas are as small as possible, according to the clamps performance to avoid sample slippage. The internal corners are not rounded (as in Figure 29) because this allows stacking samples together in the same file, leaving no unused material. As the rounded corner is related to high loads and cycles, and the historical samples are tested to characterize the initial loading conditions in the awareness that they will undergo irreversible plastic deformation after the first event, their elimination from the sample design seemed to be coherent and not problematic.

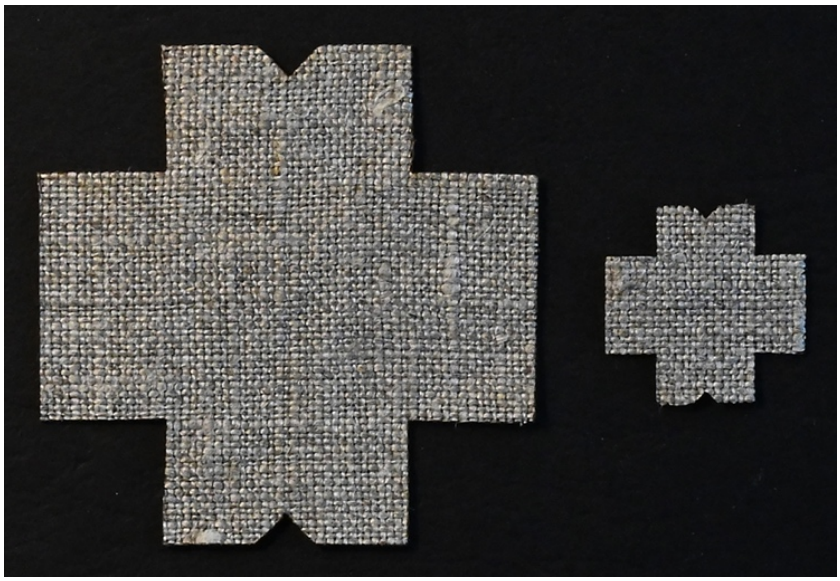

Figure 37 Laser-cut canvas samples, for the 25mm and 10mm clamps. The triangular indentation identifies the weft direction

4.2.5 The end stops

To avoid collision of the carriages with the physical limits of the machine (i.e., motor mounts at one end of the linear rails and other carriages or clamps at the other end), limit switches are used to delimitate their run by sending an electrical impulse to the main control board. The limit switches are fixed on 3D-printed supports mounted on linear rails (see Figure 38). As such supports can be easily unlocked and moved, the delimitation is also used for the homing process, a procedure allowing a temporary reference position for the carriages to be created. Such an additional tool proves extremely useful to replicate the starting point when a series of identical tests is to be repeated.

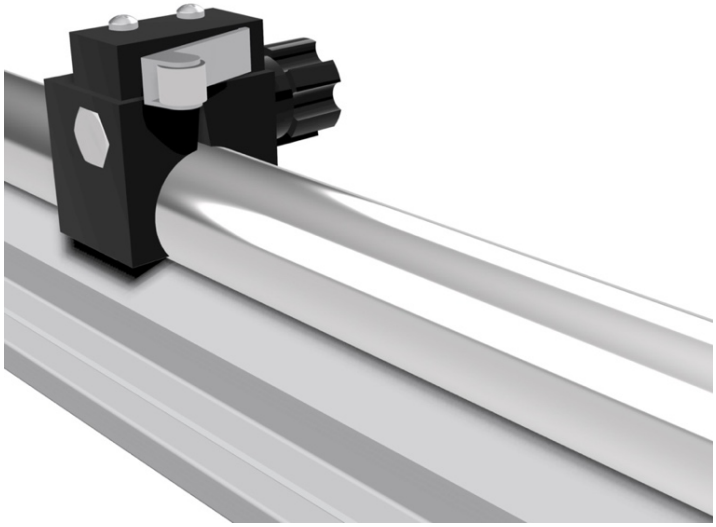

Figure 38 CAD drawing detail of a limit switch clamped on the linear rail

4.3 Electronic design

4.3.1 The electronics

In Figure 39 is a schematic of the electronics. A personal computer controls the whole testing process with the help of an Arduino microcontroller board that acts as a machine controller. The Arduino offloads some tasks from the PC, deals with time-critical signals and performs some data filtering too. It provides all the necessary inputs and outputs to interact with stepper motor drivers, the load cell amplifiers, which include a 24-bit analog to digital converter (HX711 chip), and the limit switches for the moving carriages. The four stepper motors used are numbered from 0 to 3, where motors 1 and 2 will pull from both sides along the X axis, while motors 3 and 0 will do the same along the Y axis. Each motor moves a carriage with an associated load cell and two end stops, each one at one end of the carriage travel. The personal computer is connected to the Arduino using a USB cable. Stepper motor drivers are powered by a 36V power supply, while the other components are powered by a 5V supply. Load cells and their amplifiers are powered with a separate 5V power supply unit[80], providing very low ripple/noise (2mV RMS).

[80] PS2125 produced by Oxford Electrical Products ltd, Oxon UK.

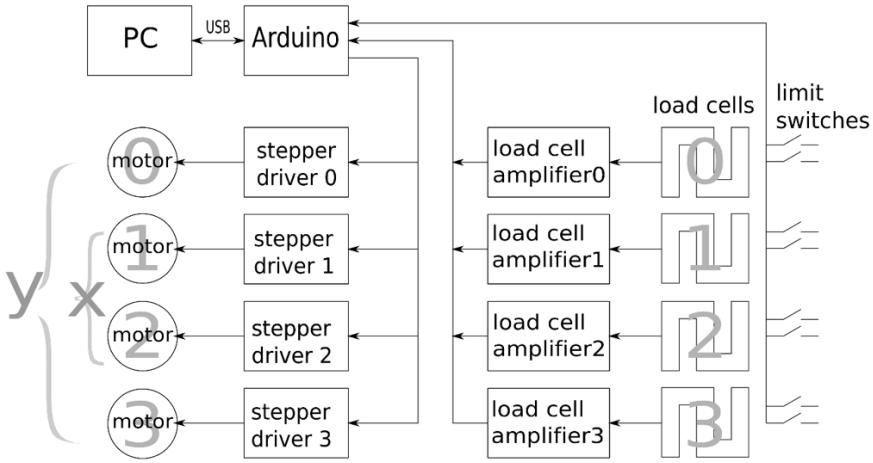

Figure 39 Schematic of the electronics

4.3.2 Software development

Stepper motors allow an open-loop control of the motion of the carriages. In a nutshell, a stepper motor moves in small-angle increments called steps. These steps can happen clockwise or counterclockwise depending on a digital signal called direction. The controller sets the direction input and supplies the number and frequency of step pulses so the motion will happen in the desired direction at the set speed. For a constant speed, the step pulse frequency will be constant too. Once the choice of using stepper motors and their drivers is made, a machine controller is needed to provide all the signals to move each motor while it can read all the sensors to precisely control the biaxial tester operation. Different approaches are possible, like creating a stand-alone controller that would include the required user interface to operate the machine or a split approach where a personal computer would run the user interface that will interact with a simpler machine controller. It was this latter approach the one that was selected as it seemed easier to replicate by others. Software development involves the creation of two different elements. On the one hand, the machine controller and firmware, built and developed around a microcontroller that will interface directly with motor drivers, load cells, and limit switches. On the other side, the biaxial tester will be operated from a personal computer with a second piece of software that will communicate with the machine controller and display data as real-time graphs on the display within the graphical user interface.

4.3.3 Machine controller firmware

As soon as we had the first mechanical one-axis prototype, the next development step was to create a machine controller that could handle all the electronics and create the proper signals for it to work as desired[81]. Generating the stepper motor signals was one of the tasks, but reading the force of the different load cells would be another. A third task of the controller is to accept commands from a computer and to send all the measurements performed to it, so the data of an experiment can be stored, graphed, and interpreted. Given these basic requirements, using an Arduino board was the first choice for such a controller and an 8-bit Arduino UNO proved to be sufficient for the task.

The regular operation of our biaxial test machine is to perform a battery of tests on several samples. Each test consists of an initial setup where the sample is clamped to the machine and centered in the cross. This requires some motion of the carriages that can be done by hand if the stepper motors are disabled, or by using a collection of pushbuttons on a Graphical User Interface (GUI) in the PC program that controls the biaxial tester. Once the sample is appropriately positioned, an initial tension is applied to it to produce a standard starting condition ("pre-tensioning"); the test will begin whenever the user commands it. While the test takes place, the computer will receive the measurements performed and transmitted by the controller. Depending on the test, that information is just stored in a file, or it can also be displayed as a graph on the computer screen. Real-time graphs and video recordings of the sample can give the researchers a clear view of what is happening.

The controller software will continuously be connected and operated via a computer. The controller software will always be commanded from the computer it is connected to. The typical connection from the computer to the controller is a USB connection that emulates a serial port connection in the case of the Arduino boards. Therefore, the controller software will be a basic command interpreter that waits for a new command to be received over the serial port. Commands are all a single line of text ended by a carriage return (see Appendix 4). Once a command is received, it is parsed, and the command is executed. Depending on the command, the response is immediate or takes a long time. Depending on the command, there might be some data transmitted to the computer by the controller while a command is being performed (i.e., a peeling test will move the motors while it transmits back the measured forces on the load cells). Every time a new serial connection is opened from the PC, the Arduino board is reset, and the controller program starts with the default values for variables like home speed, test speed, elongation, maximum force, etc. These values can be changed from the PC

[81] The firmware was written by Miguel Sanchez, co-author of the design and construction of the devices presented in this chapter.

software with the suitable command from the list above. Currently, the firmware default values are hardcoded, and any changes will vanish once the controller is reset. For each type of test, a sequence of the existing commands is all that is needed, and the concatenation of several commands to make a test will be done by the PC software.

4.3.4 Pre-tensioning algorithm

Biaxial tests describe the mechanical behavior of a sample and the interaction between warp and weft. It is therefore crucial that the initial conditions are as close as possible to a desired balance of forces before starting a test. The ideal condition is that tension is equal in the two axes, which is difficult to achieve because the sample reacts in both directions when an action is performed on one. An algorithm has been developed (see below) so the controller firmware can perform this initial adjustment much quicker and more accurately than a human. In cases where the test is uniaxial, the algorithm applies only to the actuators of the chosen axis.

The algorithm can be described as follows:

1. For each actuator, probed in a clockwise direction, a load cell measurement will be taken. Depending on the measured force, an additional pull (that is, moving the carriage one impulse outward) will happen if that carriage force sensor does not experience a pulling force higher than the pre-tension value set for that axis. However, if that force were exceeded by more than 10%, the carriage would move one step inward to compensate for that.
2. The process in 1 is repeated until either the desired pre-tensioning time has been exhausted or both axes have reached the desired pre-tension.

4.3.5 PC software development

One of the first requirements for PC software was to make it multiplatform so that it could run on different operating systems[82]. Real-time graphics of a test in progress were implemented using Python3 and the PySimpleGUI library that, combined with Matplotlib, offered a simple way to deliver a GUI with excellent graphics for Windows, Linux, or OSX users, see Figure 40. The general instructions are on the top line, the tests description and launching commands are on the bottom; in the middle of the screen is the plot of the readings of the four load cells, which are also shown as numbers in the four white spaces with colored text, above the graph.

[82] The software was written by Miguel Sanchez, co-author of the design and construction of the devices presented in this chapter

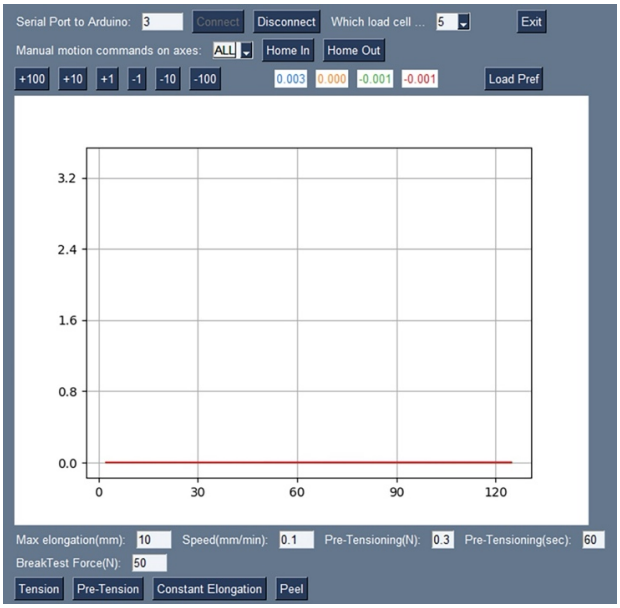

Figure 40 Screenshot of the user interface

The task of this program is to allow the user to prepare a test, load the sample on the biaxial tester, and perform a test. While the test is running, the machine controller will be streaming data to the PC software that will be used for the real-time graph shown in the program's GUI and later stored in a file for future uses. The biaxial tester may perform single-axis tests as well as biaxial ones. The user can perform manual moves of the carriages either individually, two carriages along the same axis, or four carriages at once for any configuration required for a test.

Let us see, as an example, how a low-strain biaxial tensile test (including pre-tensioning) is performed:

1. The user will start the PC software by clicking the program icon.
2. The proper serial port name will be selected on the program GUI and communication with the machine controller will start when the user presses the "Connect" button.
3. As soon as the connection is made, the real-time graph on the GUI will start to be updated as samples are collected from the four load cells (by means of the "?" command sent to the Arduino board).
4. Using the home button ("O" command) and perhaps the manual motion buttons ("X" command), the user will locate the clamps to the initial position, and then a new sample will be placed in the clamps that will be properly tightened.

5. The user will pre-tension the sample using a specifically developed procedure assuring that the sample will be subject to a defined tension value, by operating independently on each axis. Pressing the "Pre-Tension" button will trigger the setting of the pre-tension forces (commands "K" and "J"), and then the pre-tension algorithm is started (command "W") for a specified amount of time. The test will finish when the desired tension is reached on all axes or if the maximum time is reached. The user can see on the real-time graph whether the case was the former or the latter and act accordingly.
6. The user will place the desired values for the test speed (command "V") and maximum elongation (command "L"), and next, will press the "Tension" button. This will set the maximum stopping force (command "C") and the motors involved (command "M") that will be the four of them for a biaxial test. Next the speed of the motors is set (command "V") and the elongation is reset (command "R"). Finally, the test motion is started (command "X") until either the maximum force or the maximum elongation is reached. The graph in the GUI will show the real-time evolution of the test.
7. Once the test is over, all received data is stored in a file in a given folder for future use.

4.3.6 File format

Data obtained from any test is stored in text format as comma-separated values (CSV file). Using CSV format makes it easy to process data later using other programs such as Microsoft Excel or Gnuplot.

Each line on the CSV file contains six different values:

1. Timestamp in milliseconds: this is the number of milliseconds since the PC was connected to the Arduino, and it changes for each line, increasing monotonically.
2. Elongation in millimeters: This is the total distance the sample has been pulled at this moment. For very low-speed tests, it is possible to get several lines with the same elongation, meaning several measurements are taken for the same elongation.
3. Load cell 0 force in Newtons: This number is positive for a pulling force (that will be the case for most tests).
4. Load cell 1 force in Newtons.
5. Load cell 2 force in Newtons.
6. Load cell 3 force in Newtons.

For the sake of simplicity, the file format does not change whether a uniaxial or biaxial test is performed. For any uniaxial test, only two load cells will show useful values.

In the current iteration of the tester, the elongation value is an inferred one. Elongation is based on the theoretical distance between the two opposing clamps as a result of the number of steps the stepper motors have moved from the beginning of the test. Validation tests show us that absolute error is of the order of a few microns.

4.4 Build instructions

4.4.1 Construction of the steel cross

The steel cross design is the result of a negotiation between weight and rigidity which proved easy to source and build and efficient for the model and the uses described. Before welding, it is necessary to perforate the hidden faces of the central element so as to allow the passage of all the cables. It is important to clean the inside of the hole with a file so as to remove sharp edges. A set of 3-20 mm- holes proved sufficient, but up to 6 holes could be drilled. The distortion-free welding process is not within reach of a beginner, but a professional could accomplish it for an affordable cost, as indicated in the Bill of Materials. Alternative solutions can be pursued for the main structure, such as using lighter metals or even carbon-epoxy composites, keeping as the only constraint the width of the face on which the linear guides rest, whose overall footprint is 150 mm.

4.4.2 Perforation of the structure for fixing the actuators

The walls of the steel tubes with which the structure is constructed are 3 mm thick also to enable the holes to be threaded, for easy attachment of the superposed elements. The position of the holes must be transferred with great precision, so the use of the supplied CAD drawing is recommended. The transfer can be done through a paper print or a cardboard model made with a laser cutting machine. Linear guides require M5 screws, while the cast iron motor mount and the ball screw support require M6. It is recommended to use the CAD model to make small guide holes (2.5 or 3 mm) and then enlarge to the required diameter for the necessary threading (4.2 and 5 mm, respectively).

4.4.3 Test the assembly of the actuators and powder coat the structure

Before having the structure powder coated, it is recommended to test the assembly and motion of the four actuators and make any connection holes with external secondary structures, such as a tabletop. As the final preparation for powder coating, it is recommended that all roughness and surface defects on the steel be removed and the steel is thoroughly cleaned with degreasing substances.

4.4.4 Installation of the cables and of the actuators

The load cell cables will not be subjected to intense bending stresses, not only because they run in the cable chains but also because the movements of the machine are much slower than in industrial automation. Cable quality does not need to meet very high standards but needs to ensure a reliable connection. The cables need to be grouped within a spiral cable wrap. The carriage plates are designed with holes matching those on moving parts of the linear rails, plus two M6 placed to hold the load cell support, which shall be corrected according to the load cell model chosen for any future construction. The design is laser cut, and will require some extra work for manual tapping or countersinking a few of the holes.

4.4.5 Construction of the sample clamps

Two series of sample clamp designs are provided for the 25x25 mm and the 10x10 mm samples. Both are made from laser cut 5 mm thick AISI 304 stainless steel, with a M8 threaded bar welded in a dedicated housing so as the axis of the sample plane corresponds to that of the load cell (which also has an M8 connection). Two threaded M6 holes are used for tightening the top plate and the sample.

4.4.6 Construction of the box for the electronics

To hold the electronic components (stepper drivers, Arduino board, and power supply units) a dedicated box was designed, in veneered plywood with a thick aluminum bottom plate to help dissipate heat. On one side a grid is cut to favor air exchange from the PSU, on the other a hole is cut to house a Plexiglas plate designed to hold the pin connectors. The construction requires the availability of a suitable laser cutter for plywood and Plexiglas and simple hardware tools for the bottom plate and the assembly. But such a feature is not necessary as the electronics can be housed in any container or even simply fixed on a support or rail. The cables reach the box through pin connectors on a Plexiglas plate in order to make disassembly and transportation easier (see Figure 41).

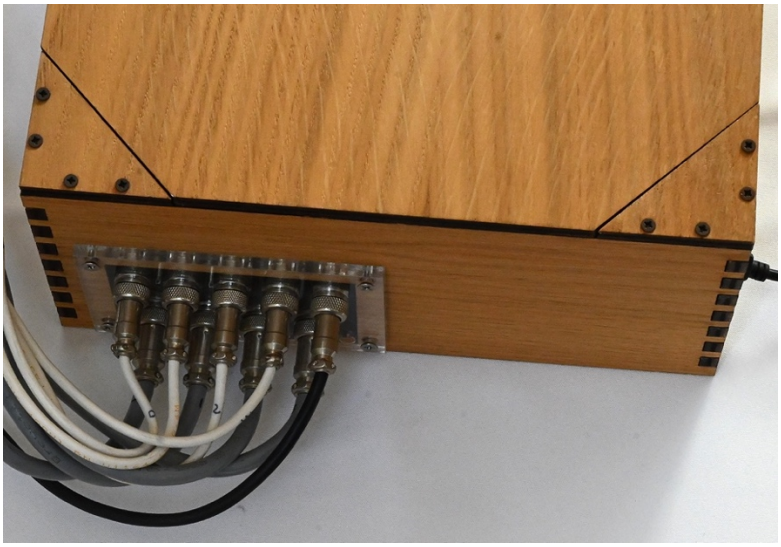

Figure 41 The pin connectors on the box for the electronics. On the right the USB cable connection to the laptop

4.4.7 The box for the switches

The red emergency button needs to be placed in an easily accessible location in the work space. It was decided to add an – optional – switch in the same spot to provide power to the stepper motor drivers, to simplify manual motions of the carriages with unpowered steppers, if any were necessary. A box to hold the two switches and for a green LED light was made in 3D printing and is visible in Figure 32.

4.5 Operating instructions

4.5.1 Clamping the sample

When clamping a sample, two aspects are very important: keeping track of the orientation of the textile and avoiding any kind of distortion, which would end up affecting the test result. Regarding the first aspect, it was decided as a convention to always place the warp between actuators No. 1 and 3. In order to avoid any distortion of very light and flexible fabrics, adjustable supports were 3D printed to set up a continuous support plane connecting the lower surfaces of the clamps, as in Figure 42, where for clarity only the sample holding part of two of the four clamps is shown. This allows the specimen to be held in position, even with light finger pressure, while tightening the clamps. To prevent slippage of the fabric inside the clamps, which have a flat surface, it was found sufficient to make that surface somewhat rough by machining or to glue a layer of sandpaper.

Figure 42 The adjustable temporary support for the samples to be used during clamping

4.5.2 Test procedures tips

The previous description of the software has already provided enough information about the different test procedures. A few tips are listed here, for the best use of software which is fully operational but can still be improved. After clamping the sample, the pre-tensioning procedure can be launched: a relatively long pre-tensioning time is recommended (at least 200 seconds), as the procedure will stop as soon as the result is obtained and it can be difficult to make a reliable prediction of the time it will require[83]. The chosen test procedure can be launched directly upon completion of the pre-tensioning (which produces a "pre-tensioning.csv" file keeping track of the entire operation). When the "homing" procedure is needed (either "home in" or "home out") to reach a predefined position to repeat a test, restarting the software becomes necessary. It only takes seconds to reboot, but doing so offers the advantage of safely starting the new test, and it is recommended to reboot the software frequently. A video showing the screen interface during the pre-tensioning to 0.3 N/cm (as in Figure 43) and of the and biaxial tension of the sample (as in Figure 44) is available at: https://www.youtube.com/watch?v=p3qZJt3natk. Another video, showing the same procedures on the machine side, is available at: https://youtu.be/sCjQdkxGuNs .

[83] Pre-tensioning time depends on the material's stiffness and on the accuracy of the clamping procedure.

4.6 Validation and characterization

4.6.1 Displacement of the carriages

The expected accuracy of carriage positioning is related to the angular rotation of the motor shaft due to a single pulse emitted by the driver and the pitch of the ball screw drive system. Each pulse at the chosen microstepping rate (16 microsteps) produces a rotation of 1.8/16 degrees, that is 0.1125 degrees. The pitch of the ball screw is 5 mm for a complete turn; therefore, the expected motion for 0.1125 degrees is 0,00156 mm. I decided to use a digital dial indicator[84] with 0.001 mm resolution to measure the accuracy and repeatability of the motion of the carriages under the control of the software. Such a test would also verify the statements of the manufacturer of the parts. A 3D printed part was designed to keep the dial indicator fixed on the linear rail while the carriage moves towards and away from it. The motion was performed under the control of the user interface.

Two sets of commands were tested: the first was a 5-mm forward and 5-mm backward movement (each corresponding to 5760 microstepping commands); the second was a 10-mm movement obtained by repetition of two single 5-mm commands (to accumulate any errors in the procedure), followed by the same backward path. Both groups of movements were recorded in three series of 6 repetitions in each direction. Only the outward movements were analyzed, as these are involved in the actual testing motion during the machine's use. Therefore 18 outward measurements for each carriage for each group were used, and a statistical treatment of motion data (a total of 144 recordings) yielded an average error with respect to the required displacement of 0.004 mm, with a standard deviation of 0.003 mm.

The homing process, which uses end stops as an additional tool for positioning the carriages in the same location, was tested for repeatability with a series of 12 consecutive homing movements for each limit switch. The typical average value of the 12 measures provides a positioning error of 0.005 mm, with a standard deviation of 0.001 mm.

4.6.2 Load cells data

Load cell calibration and subsequent readings were done with a set of F1 precision weights: 100g; 500g; 1000g and 5000g[85]. The load cell readings were performed through the machine's electronics: the HX711 digitizing board, cables, connectors, and finally, the

[84] Neoteck, model NTKTL287-FBA

[85] Reference masses were rented from Gibertini Ltd and tests were performed in the presence of qualified technicians from the same company. https://www.gibertini.com/

Arduino board and the PC software interface. After an initial calibration with the 1000g mass, the load cells provided readings that correspond to the C3 class manufacturer's specifications, thus indicating that the electronics does not introduce significant error (see Table 9).

Test mass (g)	Reading on screen (N)	Reading (g)	Difference (g)	Error (%)
100	0.973	99.218	-0.782	0.782
500	4.494	499.080	-0.920	0.184
1000	9.797	999.016	-0.984	0.098
5000	49.045	5001.198	1.198	0.02

Table 9 Measurements with the load cells

4.7 Results

4.7.1 Pre-tensioning

The pre-tensioning procedure is based on continuous cycling attempts to bring the load cell reading on each actuator to a value that is close to the average of the four, and the average to the target value. The procedure is influenced by the stiffness of the material since the amount of force transmitted from one motor to the load cells on the others depends on the elastic modulus of the sample. An oscillatory behavior is intrinsic to the procedure itself and is broader when the sample modulus is higher. When the target value is reached as the average of the four, or the target pre-tensioning time has elapsed, the procedure is automatically ended. The sample plotted in Figure 43 is an industrial cotton duck canvas: 0,72 mm thick, 350 g/m^2.

Achieving an automated and relatively accurate pre-tensioning procedure is considered a major advance in materials testing for the specific field and a so-far unique feature of this machine. Manual pre-tensioning is easy for uniaxial samples, but experience says it would never achieve comparable levels of accuracy for biaxial samples. A finely adjustable procedure is extremely important when dealing with low stress and strain values since the quality of any test performed subsequently is affected by the initial tensile conditions of the specimen. In our preliminary work we found significant differences in biaxial tensile test results using identical specimens with different pre-tensioning conditions.

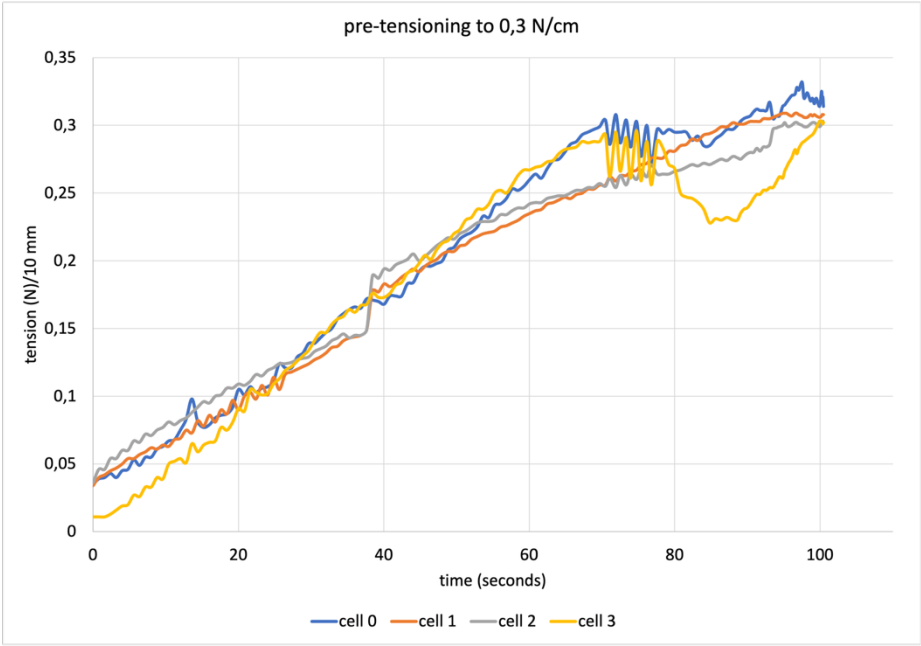

Figure 43 A typical plot for a pre-tensioning procedure with the target force of 0.3 N/cm

4.7.2 Biaxial and uniaxial tensile tests

The biaxial and uniaxial tensile tests are based on readings from the two load cells working at opposite ends of each axis. The availability of the four force values makes it possible to investigate any internal misalignment of the sample's behavior, but the basic way to use them is to average the values of the load cells at opposite ends of each axis. In Figure 44 we see the plot of 5 identical samples (10x10 mm) of the same cotton duck for which pre-tensioning is shown in Figure 43. The pre-tensioning procedure is mostly depending on the manual clamping procedure it aims to even out; biaxial test plots are instead connected with the sample response to the symmetric action of the tensile tester. One of the sample directions will require a greater force for the same elongation, and some transfer of stiffness will occur, which will increase the tensile strength of the more yielding direction. Nevertheless, the more yielding direction can prove less constant in its characteristics, as is the case of the warp in Figure 44. The plot in Figure 45 is the value obtained by averaging the results of the 5 samples shown in Figure 44.

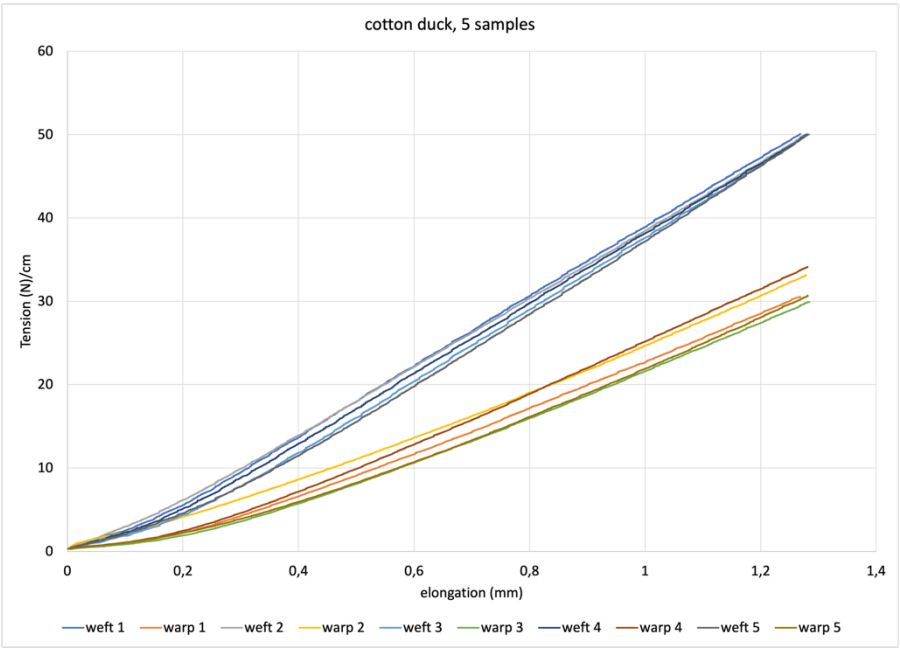

Figure 44 Plot for biaxial tensile test of 5 samples measuring 10x10 mm of the same cotton duck, starting from 0.3 N/cm as obtained in Figure 43, with the target force of 50 N

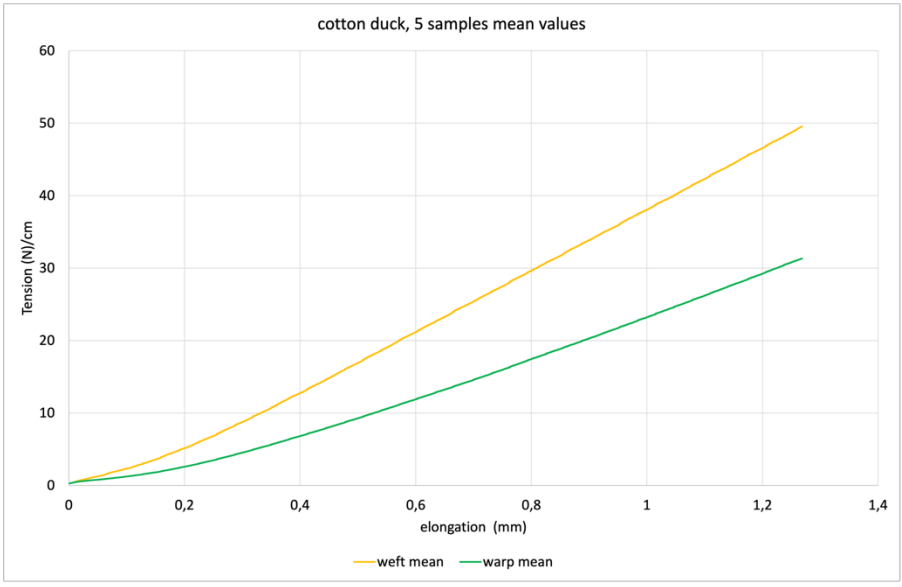

Figure 45 Plot of the average values of the 5 tests shown in Figure 43

4.7.3 Peel tests

Peel tests are long-stroke uniaxial tensile tests that measure the force required for the mechanical separation of two adherents. The result obtained allows one to evaluate the bond strength obtained by a specific bonding procedure and compare it with that derived from other techniques or their variations. A typical peel test plot is characterized by oscillating values because the curve moves upward until the force buildup is sufficient to cause the bond to fail, which causes a reduction in the reaction force until the movement of the carriages allows new force buildup. Uniaxial testing machines move a single carriage away from a fixed point, but the existing setup allowed splitting the long displacement between two opposing actuators, allowing us to make better use of machine space. The sample in Figure 46 is a lined mockup painting.

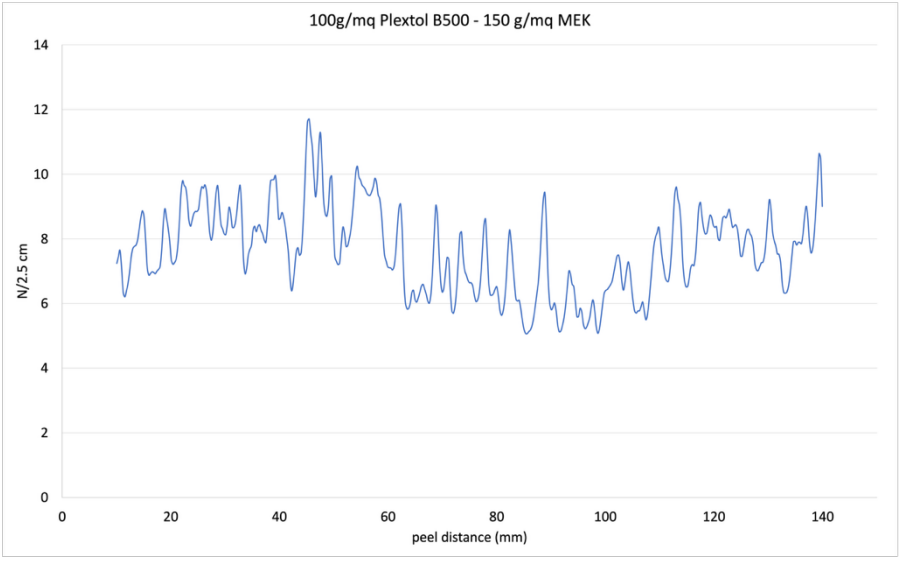

Figure 46 A typical plot for a peel test of a lined canvas sample

4.8 The open-source format

Publishing the design and detailed instructions for the biaxial tester in a high-impact, open-access journal with an open-source license was a deliberate choice, dictated by the desire to see as many similar devices as possible develop in the field of cultural heritage conservation. Indeed, the lack of comparable data seems to be a rather serious problem for research, and the goal of reducing this gap seems to be a priority.

The low-cost biaxial tester has been custom-designed and built without the support of a manufacturing company specialized in automation. Easily available components were

chosen, and the overall cost is very low (in the range of € 2.5 K at 2022 prices), if compared with commercial machines (€ 50 K - € 100 K +) or with other self-built machines. The cost of a recent comparable example [Corti et al., 2022] is six times higher. The system was tested to verify error and repeatability, and the machine demonstrated high-performance standards.

The goal of keeping construction not too complex nor expensive was considered crucial because research in painting conservation would benefit from the availability of biaxial tensile testing, and from that of the different mechanical tests the machine can perform. For the same reason, we chose the open-source format to promote the construction and dissemination of similar machines, and to learn from the feedback of potential future users. Software development was challenging as it happened remotely during the pandemic, with the machine's hardware in Italy and the software and firmware being developed in Spain. But if we could do it remotely during COVID, the information provided in this chapter would make building a duplicate or a better machine a relatively easy task.

4.9 Design and construction of a portable uniaxial tester

In order to perform peel tests during the “Comparative Lining Workshop” held by Antonio Iaccarino Idelson at the National Gallery of Ireland in Dublin in May 2023, a simplified version of the testing machine was designed and built in dimensions that could fit into a normal size airplane luggage. The new device is simply one of the four actuators working on the sample, reorganized in a more compact and lightweight structure. In order to optimize the use of the space, as peel tests require up to 305 mm motion, the loadcell was placed in a static position opposite to the moving carriage. Further optimization was obtained with the position of the moving clamp. This includes the alignment plate for the sample necessary during the delamination process (Figure 47 a), according to the previously mentioned ASTM D 903 – 98 (Figure 47 b). This is located on the carriage, at the end close to the motor instead of stepping out of it as in the biaxial version, thus using that space for the sample during the peel test. Turning the sample holder by 180° in the plane, it is fixed on threaded holes at the opposite end on the carriage, closer to the loadcell. In this position it offers the opposite end for simple tensile testing, requiring much shorter run, and the alignment plate is located outside of the testing area.

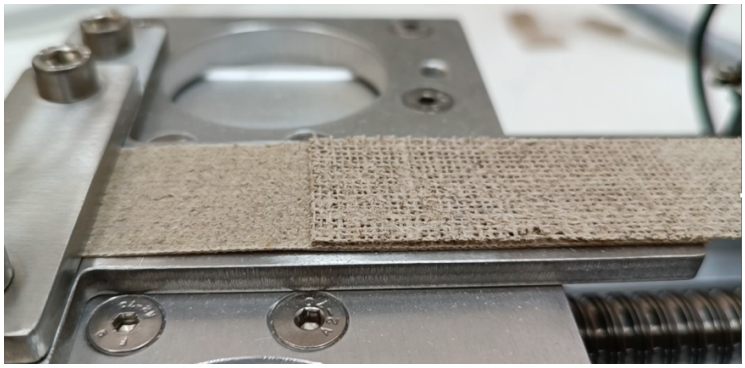

a

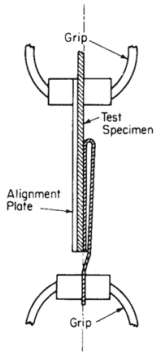

b

Figure 47 The alignment plate for the sample during the delamination (a), as prescribed by the ASTM D 903 – 98 (b)

The device is designed for traveling, therefore the most of parts are made in aluminum (alloy 6082, with the relatively high elastic modulus of 68,9 GPa) and laser cut from a slightly thinner plate (8 mm instead of the 10mm used for the AISI 304 steel). The base plate is also made in aluminum, thus considerably reducing the overall weight (Figure 48). The support for the loadcell is instead in made in welded AISI 304 steel, as it is the part that bears most of the concentrated loads, and so are the sample clamps. A plastic box was designed to protect all the cables under the base plate, and house the amplifier for the loadcell reading. This part was 3D printed in PLA, just like the external box housing the power supplies, the driver for the stepper motor, the control board and the safety switches (Figure 49). The linear rails, the stepper motor, and all the electronic components are the same as for the biaxial tester. The firmware is also the same, though the screen interface is simplified for the use of a single actuator.

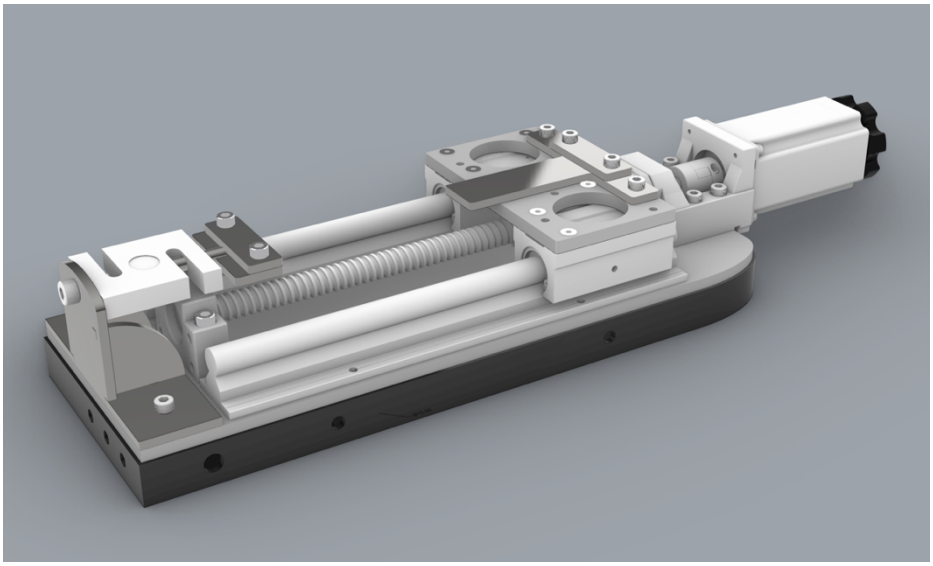

Figure 48 Render of the design of the portable uniaxial testing machine

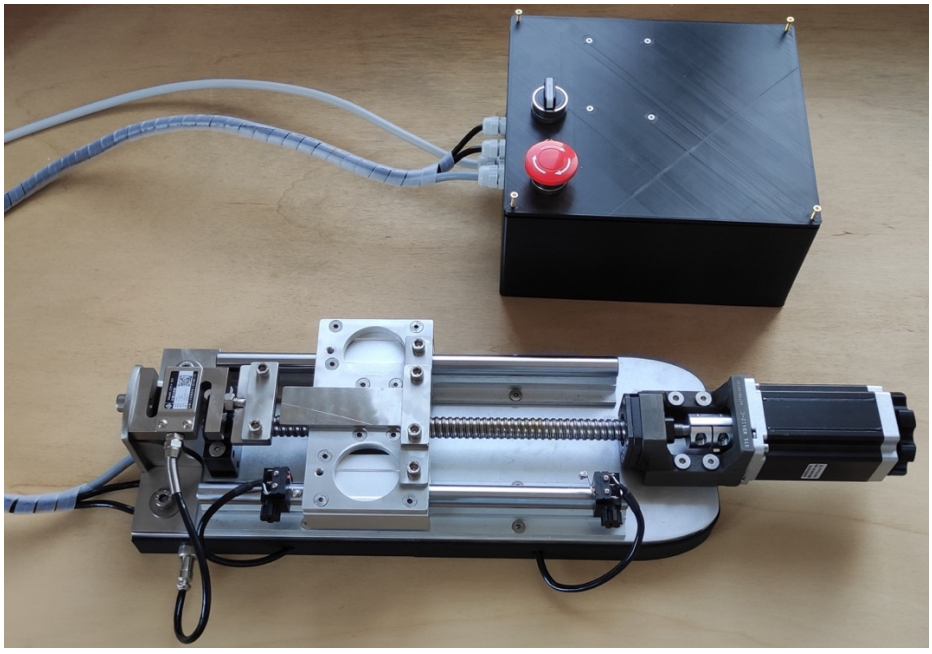

Figure 49 Overall view of the portable uniaxial testing machine

4.10 Design and construction of a Displacement Tester and hand-held probe

In order to test the mechanical response of a painting when a force is applied orthogonal to its surface, a digitally controlled device[86] was designed and built as an updated and improved version the 2002 force/displacement test method described in [Iaccarino Idelson, 2004 **(b)**]. The Displacement Tester is made using a C-Beam® Linear Actuator with a smaller Nema 23 stepper motor (with a 1.23 N/m holding torque). A 5 kg loadcell was mounted on the moving element, with an M8 threaded bar bearing a spherical contact point, 8 cm in diameter, 3D printed in PLA (Figure 50). The connection to the stretcher of the painting is made using V-slot linear rails and custom-made clamps in aluminum that are thin enough to be inserted between the painting and the stretcher (Figure 51).

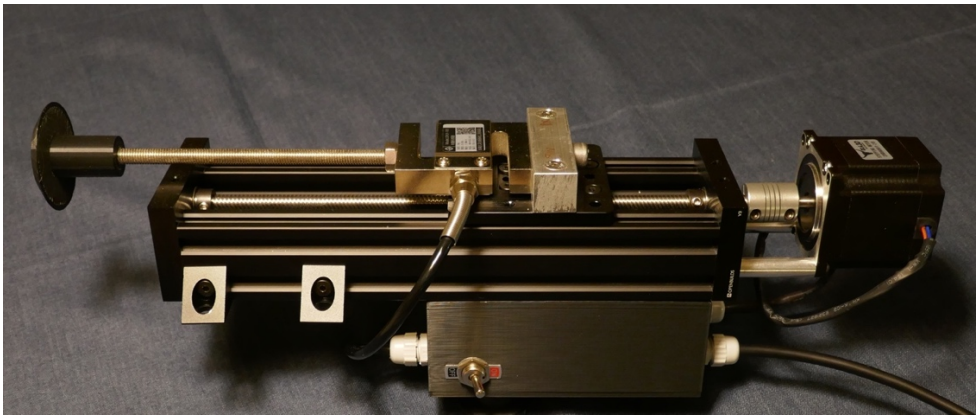

Figure 50 The body of the Displacement Tester, with the C-beam linear actuator, the loadcell and the rounded contact point. The box of the electronics with the manual switch is on the bottom

The device is controlled by an Arduino board connected to a CNC shield V3 (AZ-Delivery). The load cell moves at the speed of 0.5 mm/sec, chosen because very gentle and progressive for the painting but not exceedingly slow. The homing speed is faster, to reduce the overall duration of the test before the next repetition can be started. The stepper motor is also used to measure the displacement by counting the microsteps. The load cell readings are used to control the motion of the actuator, as a limit value is set that ends the procedure. This limit value depends on the dimensions and characteristics

[86] The device was designed and built in December 2021 by Antonio Iaccarino Idelson with the support of Miguel Sanchez, Ph.D. computer scientist at the Polytechnic University of Valencia, Spain, who also wrote the firmware and software for its operation.

of the painting and is the force considered safe for the test. When the target value is reached, the device stops and a fast-homing process is started. The threshold value of 12 N was chosen by the conservators of the Rijksmuseum conservation department[87] using a hand-held force sensor device, also custom built[88], that allows reading the force on a display while manually applying pressure on the reverse of the painting (Figure 52).

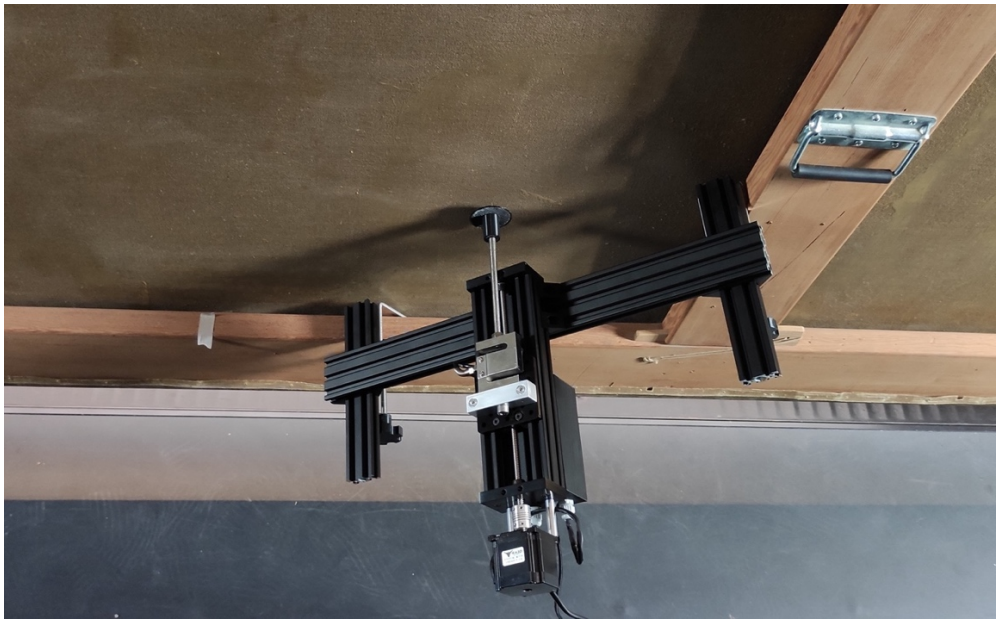

Figure 51 Overall view of the Displacement Tester mounted on the stretcher of The Night Watch

[87] In this case Petria Noble, Lisette Vos and Anna Krekeler were present.

[88] The hand-held pressure measuring device was designed and built by Antonio Iaccarino Idelson, by reassembling the elements of a kitchen scale.

Figure 52 The hand-held force probe rendering (a), and in use on The Night Watch (b)

4.11 Conclusions

The design of the biaxial tester proved to be modular enough to allow the reuse of the same firmware and software, with minor adaptations, for the construction of another device using only one of the four actuators.

A full range of examples of the use of the biaxial tester will be found in Chapter 5, which is entirely devoted to the tensile testing of the 26 specimens that are the subject of this thesis. The biaxial tester will also play a key role in Chapter 6, for the mechanical characterization of the materials used for the mock-up of a wax-resin lined painting. An other example of the use of the uniaxial tester can be found in Chapter 8, where the device was used to measure the adhesion of the new lining applied to the detached Tiepolo fresco at the Louvre Museum. For this same project, the biaxial tester proved useful to characterize the mechanical response of the lining canvas in combination with a mock-up replicating the structure of the painting.

The Displacement Tester, on the other hand, was necessary for the research on The Night Watch, which is described in Chapter 7.

Chapter 5 Biaxial tensile testing of the historical textiles and correlations with morphology

5.1 Introduction and general parameters

Outline of the chapter

5.1 Introduction and general parameters
- 5.1.1 Preliminary considerations about samples dimensions
- 5.1.2 Comparing test results obtained using two sample dimensions
- 5.1.3 Considerations about testing speed

5.2 Calculating the E modulus of the set of samples
- 5.2.1 The tensile modulus of a canvas
- 5.2.2 A review of the approaches to the loading area for stress in textiles
- 5.2.3 The method developed to calculate the loading section area of the samples
- 5.2.4 The "object related" and the material E modulus values for the set of samples

5.3 The E modulus values in the conservation science literature
- 5.3.1 Early studies
- 5.3.2 More recent studies

5.4 Analysis of the biaxial testing data of the set of specimens
- 5.4.1 Correlation with the warp and weft directions
- 5.4.2 E modulus and crimp
- 5.4.3 E modulus and twist
- 5.4.4 E modulus decreasing after A
- 5.4.5 Very low warp modulus
- 5.4.6 High modulus textiles
- 5.4.7 General correlations between tensile modulus and morphological characteristics
- 5.4.8 Uniaxial or biaxial testing and ratio between weft and warp E moduli
- 5.4.9 Tensile modulus and fiber, pH and age of the textile
- 5.4.10 Additional biaxial tests performed on four naturally aged paintings

5.5 Conclusions and future work

Destructive tensile tests on naturally aged, historical textiles, is rarely carried out because of the limited availability of sampling materials. The use of the biaxial tensile testing device described in chapter 4, designed to work on the relatively small samples size of 1 cm^2, allowed working with 3 to 5 repetitions notwithstanding the small dimensions of the specimens. The group of specimens tested in this thesis is described in Table 1, chapter 3, and specimens are all plain canvas without paint or preparation layers. They

all have a selvedge to identify warp from weft, and are part of a larger collection. The group consists of samples from 14 historical paintings with known provenance and date (from the 18th to the 20th century), 8 less documented historical textiles (from the 18th and 19th century), 3 modern textiles used as lining supports, and finally a hand-woven replica of a historical Dutch painting support textile. All were morphologically described using the methods seen in chapter 3, in order to quantify the crimp and twist of the yarns, and the dimensions of their elliptical cross section, in warp and weft. The set of data collected for the textiles also includes their thickness, weight per m^2, thread count, fiber identification, pH.

Biaxial tensile tests were performed using a set of four 250 N loadcells (sensitivity: 2.0 ± 0.05 mV/V; linearity: ±0.03% FS; repeatability: ±0.03% FS) moving simultaneously on each axis at a speed of 2 mm/min. The maximum force of 200 N was set for the 1 cm wide samples, aiming at recording the ultimate load for most of the samples. It should nevertheless not be forgotten that for conservation purposes the typical tension values are usually between 0.5 and 3 N/cm. Tension values beyond 4 N/cm are mostly useful to describe the behavior of a textile in critical conditions, to obtain an overall characterization of the material and increase the data set for comparation purposes. The relatively slow test speed used allowed detailed information to be obtained on the biaxial tensile response of the specimens at the different ranges of tension. According to the dimensions and condition of each specimen 3 to 6 samples were tested, and the plots generally correspond to their mean values. The data from samples showing inconsistent response due to their different state of conservation was not used to produce the mean value and the plots reported in this chapter and in Appendix 1.

5.1.1 Preliminary considerations about samples dimensions

Sample size is a crucial factor when testing materials from historical artifacts. The specimens available in the collection used in the present research would rarely provide 25 mm wide cruciform samples (50 x 50 mm including the clamping area). Moreover, their number would not allow to repeat the test to obtain statistical relevance. The 10 x 10 mm sample size (20 x 20 mm including the clamping area) is instead a good compromise between specimen availability and the requirements for statistical analysis, and it allowed the extraction of at least three “identical” samples from each historical piece. Nevertheless, the question whether a sample size 2.5 smaller than the standard 25 mm width could be used without significative alterations of the mechanical response is relevant.

A general consideration is that, the smaller the samples size, the higher its sensitivity to local features of the specimen. A sample averages the behavior of the different local characteristics found within the area of the textile it represents, and of each of the yarns it contains. Larger samples have the advantage of more accurately representing the

overall behavior of the textile. However, from a mechanical testing standpoint, larger samples require higher forces to be tested, which in turn demands stronger and stiffer testing equipment. This becomes an issue considering that the sensitivity of load cells is inversely related to their maximum capacity, and sensors designed to handle higher loads are typically less precise in detecting small force variations.

The focus of the present research is that of characterizing historical textiles within the range of the forces a textile typically undergoes during its conservation. As we have seen (Figure 8 and Figure 9), the typical value of tension is about 2 N/cm, and an unlined painting is not likely to withstand more than 2.5 N/cm without undergoing creep (see chapter 1). The low range of tensions was therefore privileged in this study, in the awareness that the initial tensile response is extremely sensitive to experimental conditions, such as initial loads resulting from the sample clamping procedures. For this reason, each test was started from the same, accurately defined, biaxial pre-tension value of 0.3 N/cm to provide the same initial conditions and a clear interpretation of the data. Standard tensile testing procedures have a very different perspective, as they aim instead at the definition of the ultimate load and at the description of the slope of the straight-line area of the plot indicating its elastic response, to calculate the Elastic tensile modulus.

In the negotiation between accuracy of the measurement and relevance for the conservation load ranges, the 10 mm cruciform sample size offer the advantage of allowing the use of high precision load cells. As their maximum load is 250 newtons, the threshold value of 200 newtons was set for all tests. The ultimate load values are not as relevant for conservation studies, and were only reached accidentally during testing.

5.1.2 Comparing test results obtained using two sample dimensions

To address the above research question, the three modern textiles in the present study—specifically, samples 23, 24, and 25—which were available in sufficient quantities, were subjected to comparative tests using the two sample sizes. In order to reduce the error caused by their variability, 10 samples were tested for each specimen. For a meaningful comparison between the two sample sizes, the force values were scaled to N/cm, corresponding to that of the 10 mm-wide samples. As a first, straightforward approach, the data from the 25 mm-wide samples were normalized to match those of the 10 mm ones. Specifically, the force values were divided by 2.5, and the elongation values were adjusted by the ratio of the gauge lengths (26.2 / 10.9 ≈ 2.4).

For a clearer assessment of the differences between the results, tests were plotted using the reference normalized elongation of 0.35 mm. The normalized elongation of 0.1 mm was instead used to represent the conservation range. In Figure 53 we see the comparison of the test results for the textile n. 23. While the behavior in the warp

direction is almost completely superposable, we notice a certain difference in the response in the weft direction. Differences are much smaller when the comparison is focused to the conservation range, in Figure 54.

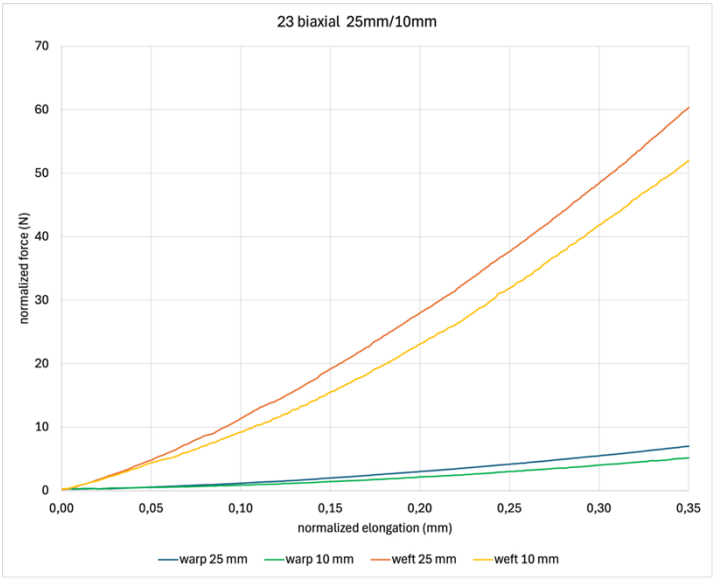

Figure 53 Textile 23. 25 mm vs 10 mm samples biaxial tensile test, mean of 10 samples

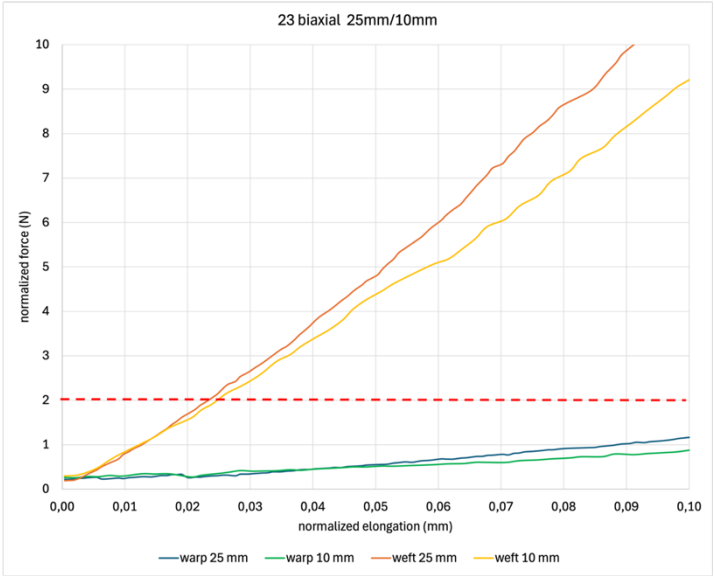

Figure 54 Textile 23. 25 mm vs 10 mm samples biaxial tensile test. Detail of the forces in the conservation range

Textile 24 shows a similar comparison (Figure 55 and Figure 56), the wefts diverging more than the warps, which appear to be almost completely superposable in the conservation range.

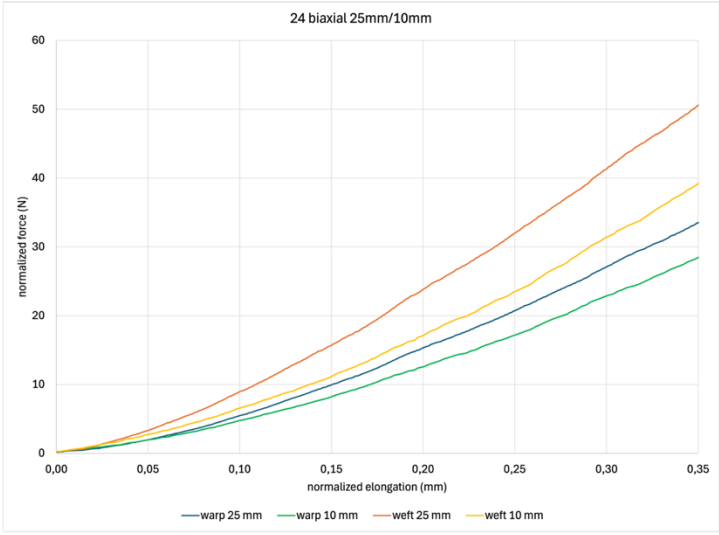

Figure 55 Textile 24. 25 mm vs 10 mm samples biaxial tensile test, mean of 10 samples

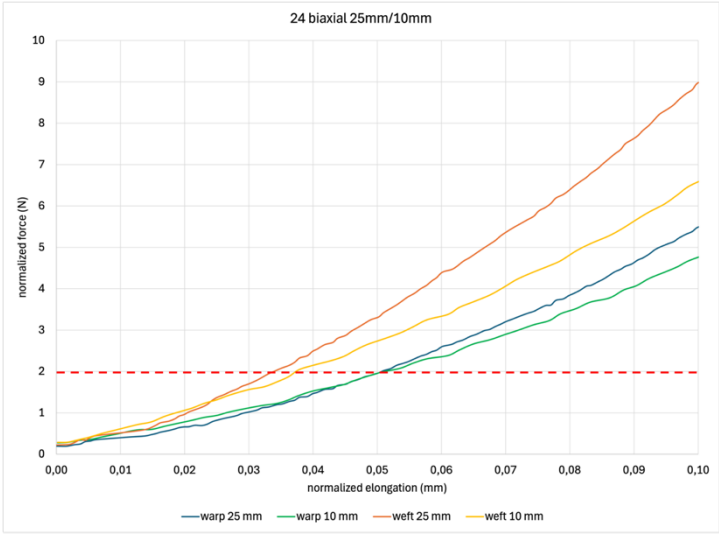

Figure 56 Textile 24. 25 mm vs 10 mm samples biaxial tensile test, mean of 10. Detail of the forces in the conservation range

Textile 25 shows a different pattern (Figure 57 and Figure 58), the wefts and the warps in the two sample sizes running parallel after the initial pre-tensioning. They appear to be a very close offset when observed in the conservation range.

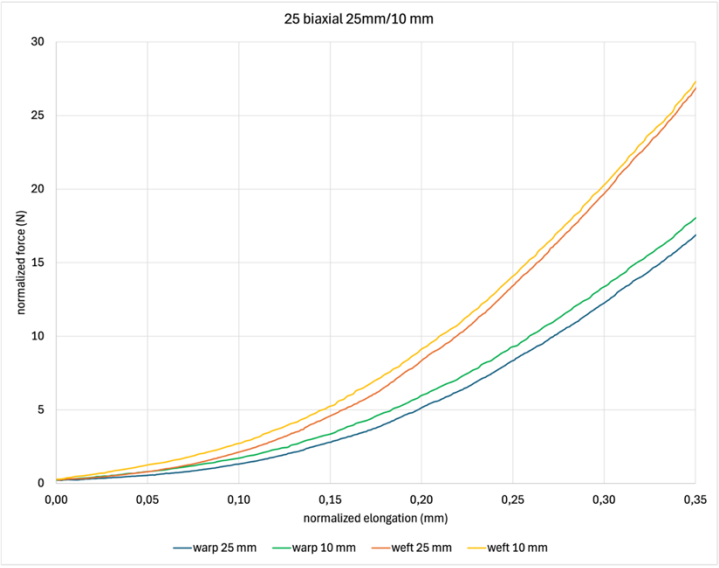

Figure 57 Textile 25. 25 mm vs 10 mm samples biaxial tensile test, mean of 10 samples

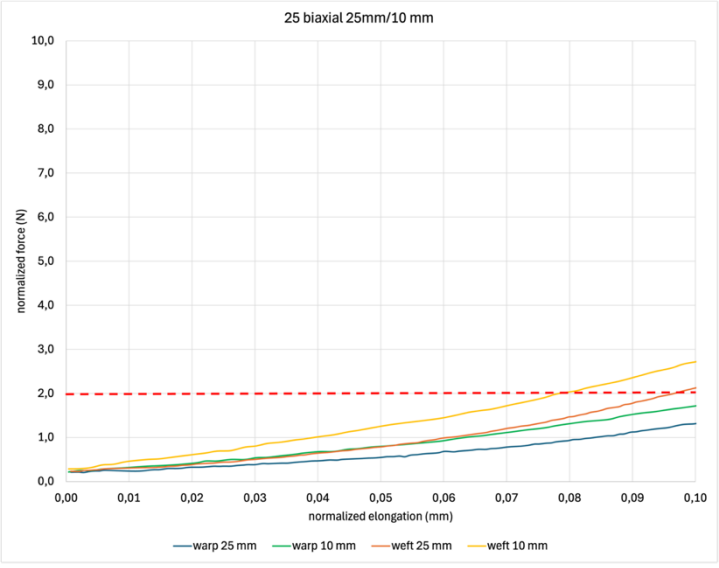

Figure 58 Textile 25. 25 mm vs 10 mm samples biaxial tensile test, mean of 10. Detail of the forces in the conservation range

It can be safely stated that the two testing conditions produce very similar results. Notable differences only emerge after the conservation range of forces, and the phenomenon is very likely related to the interactions between yarns. However, with current knowledge, it remains difficult to identify a clear cause for this behavior. The number of yarns in the samples was counted, obtaining a more detailed and purpose dedicated definition of the thread count shown in Table 3. The results confirmed the expected ratio of approximately 2.5, with values ranging from 2.48 to 2.75.

For textile n. 23, with 18,3 warps and 14,3 wefts per cm, the plots are almost identical for the warp direction and slightly diverging in the weft direction. Textile n. 24, with the much lower thread count of 9 warps and 9 wefts per cm, shows a similar pattern. Textile n. 25, with the lowest thread count (7 warps and 5 wefts per cm), also shows quite similar plots in the two directions, possibly because of the much fewer points of contact between yarns. It seems therefore reasonable to assume that the lower friction between the yarns implies a lower influence on the response of the fabric. The weft yarns have a much lower decrimping phase (see chapter 3, Table 7 and Figure 27, and Appendix 2), and their mechanical is more influenced by the physical presence of the warps causing a stiffness transfer (as it will be seen later in this chapter, and in chapter 6). Some kind of non-linearity can be expected when considering the interactions between yarns, especially as their number is increased. The mechanical response of the 10 mm samples from the three textiles in both uniaxial and biaxial tests, and results of the tests performed on the individual yarns, can all be found in Appendix 2.

In conclusion, future studies will be needed to gain a deeper understanding of these phenomena, and relevant preliminary data are already provided in Appendix 2, laying the groundwork for further investigation. Combining Digital Image Correlation (DIC) [Malowany et al., 2014], [Lennard et al., 2022] with mechanical testing would likely yield a clearer insight into the dynamics and underlying causes of the differences observed between the two sample sizes. Among the most probable factors are the non-linear interactions between yarns and a potential corner effect in the cruciform samples, which become appreciable once a certain strain threshold is reached (and apparently not within the conservation range of tensions).

Nevertheless, within the boundaries of this research—where sample availability is undoubtedly a major constraint—the differences observed between the standard 25 mm sample size and the chosen 10 mm size appear to have a negligible impact on the overall mechanical response. Future testing campaigns should validate these findings by employing larger sample sets, enhanced statistical analysis, and complementary full-field strain measurement techniques (like DIC).

5.1.3 Considerations about testing speed

International standards for mechanical testing, such as ISO 6892 1 and ASTM E8, specify that testing speed and data acquisition rates must ensure accurate stress–strain curves. ISO 6892 1 recommends that "at least 500 data points be recorded throughout the test", while ASTM E8 states that "data shall be recorded at intervals sufficient to permit plotting of the complete stress–strain diagram." [89]

Testing speed determines the duration of the test, as the target condition (e.g., crosshead displacement or force buildup) is reached over a time defined by the movement speed. The sampling rate, governed by the machine's electronics and firmware, remains largely fixed. For this biaxial tester, a sampling frequency of 18 Hz (18 samples/second) was chosen as a practical balance. Consequently, faster tests yield fewer data points per displacement unit, producing less detailed curves.
Figure 59 illustrates this effect: the same textile (sample 24) tested at four speeds produces curves of similar shape, but with very different data densities for 1 mm elongation:

- 0.4 mm/min ≈2016 data points/mm
- 2 mm/min ≈405 data points/mm
- 10 mm/min ≈89 data points/mm
- 50 mm/min ≈18 data points/mm

The 2 mm/min speed was selected as the optimal compromise between test duration and curve resolution. Although higher-resolution data (> 400 points/mm) could be obtained with faster electronics, the current biaxial tester, operating at 18 Hz, complies with both ISO 6892 1 and ASTM E8 at this speed.

The influence of speed is also tied to the viscoelastic behavior of many materials, which display time-dependent deformation. At higher speeds, materials often appear stiffer due to limited molecular relaxation, while at lower speeds they may show increased creep or stress relaxation. This behavior, observed in peel tests, see [Iaccarino Idelson and Garofalo, 2019], is also visible in Figure 59: at 0.4 mm/min, greater elongation is required to reach the same ultimate load, and the curve slope decreases. By contrast, tests at 2, 10, and 50 mm/min produce nearly identical responses. Hence, a single test speed of 2 mm/min was used all over the thesis to minimize creep while ensuring

[89] ISO 6892-1:2019, Annex A, §A.3.4; ASTM E8/E8M-24, §11.4.

accurate characterization. Full data on the two textiles tested using the 4 speeds is available in Appendix 2.

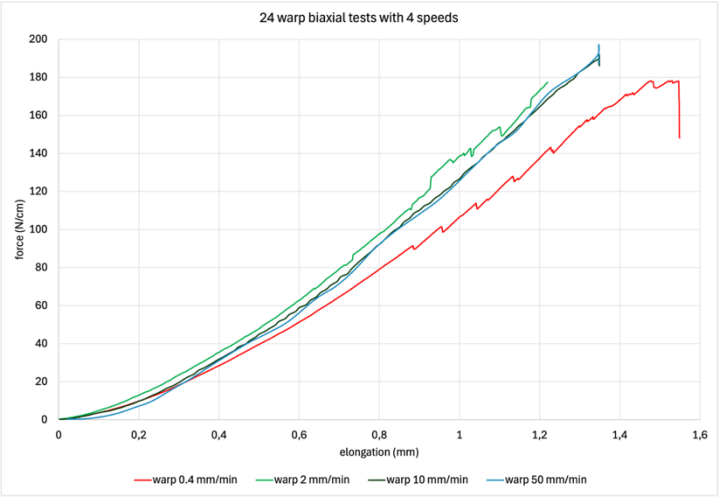

Figure 59 Textile 24, biaxial tensile test - warp direction - comparison between 4 test speeds

5.2 Calculating the E modulus of the set of samples

5.2.1 The tensile modulus of a canvas

The elastic modulus, or E modulus, is the ratio between stress and strain (*E=stress/strain*) where *stress=force/area* (the tensile force acting on the area of the cross section of the sample) and *strain=elongation/length* (the difference in length due to the test, divided by the initial length). E is a key factor in materials engineering because it allows comparing the behavior of different materials and allows predictions to be made. A high value of E describes a material with a high resistance to deformation, with a low value of strain indicating that a given force has little effect on the material being tested. The standard equation for E is

Equation 3, where *F* is the force, *w* is the sample width, *h* is its thickness, L_0 the initial length and L_f the elongated length of the sample:

$$E = \frac{\frac{F}{wh}}{\frac{(Lf - L0)}{L0}}$$

Equation 3 The standard calculation for Elastic modulus

The elastic modulus is a value that allows a comparison with the stiffness of different materials, thus providing a simple and straightforward mechanical characterization. Still, general engineering studies deal with the modulus of homogeneous materials like steel,

or of materials that have been statistically studied, like concrete or wood. Calculations based on such data are useful because they are predictive, and are made with this purpose.

In order to obtain predictive calculations, the data must conform to engineering parameters, which is often not easy when dealing with the complex structure of a canvas painting. The uncertainty in the exact definition and distribution of materials within a painted canvas is much higher than for a steel structure such as the Eiffel Tower or a bridge. Mechanical testing of complex historical materials therefore produces descriptive data about their overall mechanical response, and their transformation into standard information is not straightforward. Descriptions are extremely valuable for general understanding of their structural behavior and for qualitative or semi-quantitative predictions. For quantitative engineering predictions to be possible, their structure must be described in a simplified manner. Simplifications imply approximations, that are justified if the resulting predictions are close enough to the described behavior of the complex material.

In general engineering studies, the E modulus is the slope of the elastic region of the tensile plot, the main straight-line part of the curve. Materials such as plastics, elastomers, and composites, exhibit significant nonlinearity, and do not show a clear linear elastic region but a varying behavior described by a series of straighter zones in the curve, each with a different slope. The “secant elastic modulus” is then preferred, which describes a single location along a specific part of the curve, calculated as the slope of a secant line drawn from the origin to a specific point. The secant modulus considers the slope of a line drawn from the origin (or a specified reference point) to a chosen point. This provides an average stiffness of the material over the specified strain range to define, and compare, its performance under specific loading conditions rather than on the entire plot.

The secant tensile modulus was calculated at 4 locations along the test plots, corresponding to the different tensile response of the sample during the test. In Figure 60 we see the plot of one of our samples in weft (under biaxial loading), showing a typical behavior. The secant modulus was calculated for all samples at the same strain locations, named A, B, C and D. The first value (A) is the most relevant for conservation studies, as it is located at the very beginning of the plot, where the loads are about the standard values of tension for a painting on stretcher. The elongation of 0.05 mm was chosen for A (corresponding to a strain of 0.47% - or 0.0047- as the gauge length is 10.6 mm), where the loads are generally below 2.7 N/cm. This value also corresponds to the initial reorganization of the yarns and has been described [Roche, 2003] as the phase in which the response due to the friction between fibers is read. The second secant modulus value extracted from the plots (B) is at the elongation of 0.2 mm (1.89% strain). This

corresponds to the de-crimping phase, in which the tensile response is lowered by the reduction of crimp causing a straightening of the yarns. The third (C) is at 0.5 mm (4.72% strain), and is about the passage between the de-crimping phase and the start of the straight-line response of the yarns. The fourth (D) is at 0.9 mm (8.49% strain), and in most of the plots it is located in the straight-line plot of the elastic response. In some cases, the ultimate load corresponds to a lower strain and therefore the 0.9 mm elongation is outside of the meaningful area of the plot. It should be noted that in general engineering studies the E modulus of a material would be chosen in an area of the plot corresponding to C or D. For this reason, the secant modulus at C will be used to compare- with a single value- the tensile response of our textiles with those found in literature studies.

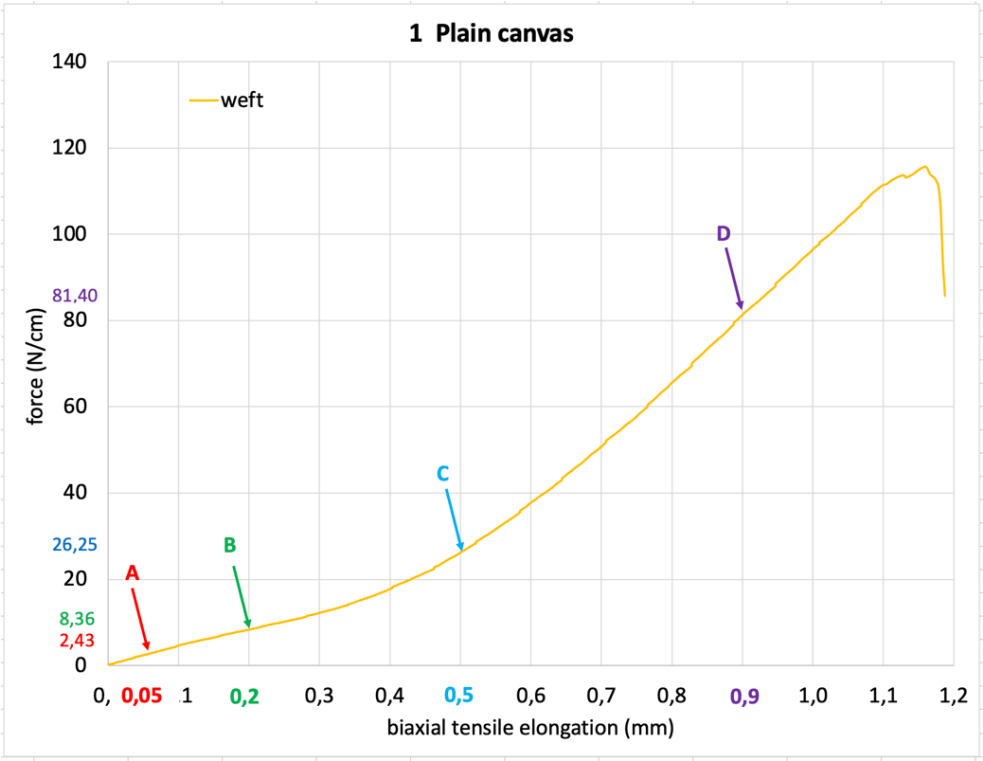

Figure 60 A typical tensile plot with the indication of the 4 secant modulus values measured. A: initial response; B: decrimping; C: start of the elastic response; D: final elastic response

5.2.2 A review of the approaches to the loading area for stress in textiles

In Art in Transit [Mecklenburg, 1991], the area of the loading cross section was estimated by a volumetric analysis. "*Using a large sample from the test fabric, the warp yarns were separated from the weft yarns and their separate volumes were measured* [by immersion] *using a nonpolar solvent. This volume was divided by the yarn length resulting in a total fiber bundle cross-section area. In turn, this total area was divided by the number of yarns resulting in a mean fiber cross-sectional area per yarn. By counting the yarns in a tensile test specimen, a mean fiber area could be obtained and enabling calculation of the main fiber stress and modulus.* […] *The average cross-sectional area of the yarns was only about 22% of the nominal textile area if the area was taken to be the linen "thickness" times the specimen width*"[90], as in Figure 61. Therefore, the volume of the fibers was divided by yarn length, presumably referring to the dimensions of the piece of textile[91], and the cross-sectional area was obtained by counting the yarns in its width, in warp and weft.

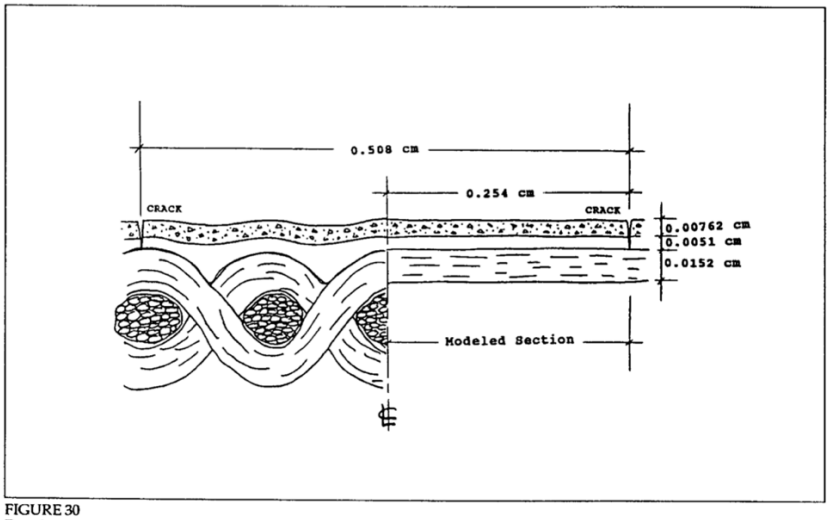

FIGURE 30
Detail section view of a painting from crack to crack, illustrating the difference between the actual structure and the computer model of the same structure. The reduction in thickness of the fabric is necessary to account for the voids in fabric and hence correct for the fact that the in-plain stiffness of a canvas is considerably higher than the bending striffness, though both are low. Details of the correction factors are in reference 3.

Figure 61 The reduction of the sample thickness used to model the canvas, from [Mecklenburg, 1991]

Young [Young, 1996 **(a)**] measured the yarn thickness (along the Z axis) under the microscope as part of the observations used to calculate the crimp value. Thickness was

[90] Art in Transit studies, page 143.
[91] Thus unrelated to the yarns crimp.

approximated to the diameter of a circular yarn cross-section, then multiplied by thread count per meter. The resulting Equation 4 is:

$$A = \pi \; x \; (thickness/2)^2 \; x \; thread \; count$$

Equation 4 Cross sectional area of the textile in [Young, 1996(a)]

The error was estimated to be ±11%, as the area of the ellipse was calculated from the minor axis alone. The resulting loading area is then correlated to the 260 mm of the sample side, although also in this case the procedure is not explained in full detail.

Chiriboga [Chiriboga, 2013], set a procedure based on a detailed description of the textile structure to calculate the loading area section. The goal being that of eliminating the voids in the textile, in order to model the fibers as a continuous plate in the FEM, the main question was to determine the thickness of such plate. A Representative Unit Cell (RUC) of the textile is described, containing two yarns in X and two in Y (or warp and weft). Its dimensions are, in X and Y, the distance between the neutral axis of the yarns; in Z the nominal thickness of the textile. The cross section of the yarn is described as "lentil shaped" and the area is approximated to that of a circle with a diameter calculated as the mean of the long and the short axes (which is another way of describing the area of an ellipse). The empty spaces between the fibers in the twisted yarn are extracted introducing a "packing factor" of $\pi\sqrt{3}/6$ (or 0.907), that is the maximum hexagonal packing of circles. The area of the cross section (*A*) is therefore Equation 5:

$$A = \pi (mean \; of \; the \; short \; and \; long \; axes/2)^2 x \; \pi\sqrt{3}/6$$

Equation 5 Cross sectional area of the textile in [Chiriboga, 2013]

The value of crimp is introduced by simply adding the uncrimped length to that of the side of the RUC (representing the crimped length of the yarn). The volume fraction of the fibers corresponds to that of the yarns alone within the volume of the RUC, that is the volume of the two yarns in each direction, divided by the volume of the RUC. The space between the yarns is considered as the inverse of the thread count, and the

Equation *6* to obtain the volume *fraction (Vf) of the fibers in X and Y is correlated with the nominal thickness of the textile and the crimp of the yarns:*

$$Vf = \frac{Area * thread \; count \; * (1 + crimp)}{nominal \; thickness}$$

Equation 6 Fiber volume fraction in [Chiriboga, 2013]

The volume fraction of the fibers in the yarn (*Vf*) in the equivalent plate is the ratio between the volume of the plate (obtained by removing the empty spaces from within and between the straightened yarns) and the volume of the RUC. The thickness of the equivalent plate in X and Y is calculated applying this same ratio to the nominal thickness of the textile. The thickness of the equivalent plate in X and Y is used to calculate the area of the effective section for the E modulus.

5.2.3 The method developed to calculate the loading section area of the samples

Based on the literature described above, a method was developed to calculate the loading area of the textiles using the quantitative morphological information obtained during the observation of the samples. The approach is similar to [Chiriboga, 2013], and the first step is the calculation of the yarns cross-section area and volume. These are then correlated to the volume of a RUC of the plain weave textile and transformed in the equivalent volume of parallel fibers in each direction. The elliptical cross-section area of the yarn is calculated by using the measure of the semi-minor axis and the semi-major axis, obtained from the values of yarn width (w) and thickness (t) derived from the measures in the Table 4 of chapter 3, with the
Equation 7 for the area of the ellipse:

$$A = \frac{\pi w t}{4}$$

Equation 7 Calculation of the area of the elliptical yarn cross section

The packing factor of 0.907 proposed by Chiriboga was used to subtract the empty spaces between the fibers as it seemed to be a reasonable estimation, also in consideration of the fact that the [Lubachevsky and Graham, 1997] calculated a very similar packing factor[92] of 0.88. The % crimp (*c*), obtained from Table 7 (chapter 3), allows the length of the yarn within the textile to be calculated, as *c* is the % length that needs to be added to the textile's dimension. The volume of a yarn is therefore an elliptical cylinder, for which the section area, *A*, is multiplied with the decrimped length of the yarn in the Equation 8, describing the Yarn volume *Yv*:

$$Yv = A * \pi\sqrt{3}/6 * l\,(1 + c\,/\,100\,)$$

Equation 8 Calculation of the fiber volume in the yarns

[92] This is used by Maraghechi in a paper currently under review: information derived from his 2024 06 20 NICAS presentation and from a private communication.

A Representative Unit Cell (RUC) of the textile structure is a volume described by X and Y axes in warp and weft, and the textile thickness (T_t) for the Z axis. In this case, the decision was made to attribute the same value of 10 mm to the length (l) of the X and Y sides of the textile RUC, and to use the value of the thread count (Yc) obtained from the Table 3 of chapter 3 to define the yarn density. The volume of the textile RUC (Tv) is obtained multiplying the length of the two sides (l) by its thickness (T_t):

$$Tv = l * l * Tt$$

Equation 9 Volume of the textile RUC

The yarn volumes (in warp and weft) within the RUC are the simple product of the single yarn volume (Yv) and the thread count (Yc), a value that is already referred per 10 mm of textile (as in a 10 mm wide sample). The fiber volume fraction (F_f) of each direction is calculated by dividing the yarn volumes by the volume of the RUC using Equation 8 and Equation 9, according to Equation 10:

$$Ff = Yv * Yc/Tv$$

Equation 10 Fiber fraction in the sample

The thickness of the equivalent fiber plate (P_t) is obtained in warp and weft by applying the same ratio existing between the volume of the yarns and that of the textile, or the fiber fraction (F_f) in Equation 10, to the thickness of the textile (T_t) (Equation 11):

$$Pt = Ff * Tt$$

Equation 11 Equivalent fiber plate thickness of the sample

The values of P_t are needed to calculate the E modulus of the specimens when it has to be used to compare the materials tensile response, as for a FEM simulation. The general Equation 12 was calculated (based on the above Equation 8 to Equation 11) in which the data collected with the observation protocol in chapter 3 (Table 3, Table 4 and Table 7) may be directly substituted.

$$Pt = \pi wt/4 * \pi\sqrt{3}/6 * Yc * (l + lc/100)/l^2 \qquad \text{or}$$

$$Pt = \pi^2 * \sqrt{3}/24 * w * t * Yc * (1 + c/100)/l$$

Equation 12 Calculation of the Equivalent fiber thickness in the samples using yarn morphology

All the samples were cut in a cruciform pattern for testing, in which l is 10 mm, and the values of yarn width (w), thickness (t), thread count (Yc) and crimp (c) are directly obtained from the observation of the samples in chapter 3, allowing the equivalent thickness (Pt) in warp and weft to be easily calculated.

5.2.4 The "object related" and the material E modulus values for the set of samples

The values of the secant tensile moduli derived from the biaxial tests on the set of samples using their dimensions without using Equation 12 can be described as pertaining to the textiles as real-life objects. The area of the cross-section of the sample is at the denominator in the calculation of the stress (
Equation 3) and its value has a significative influence on the final result.

In Table 10 the values of the secant moduli in the chosen 4 strain conditions for the 26 specimens are listed under biaxial testing, calculated for both the Textile thickness (T_t) and the Fiber Equivalent Thickness (E_t). As we will see in the next paragraph, comparing the values obtained in the weft direction at C and D for the new textiles (n. 23-26) they appear consistent with the literature references not including mathematical adjustments of the fiber equivalent section [Roche, 2005, Janas, 2022; Larcroa website[93]] (object related, using T_T). They are also consisted with those adapted for FEM uses [Mecklenburg, 1991; Young, 1996 **(a)**; Young, 1996 **(b)**] (E_T). The values for "Amazone linen" and "Waal linen" proposed by Chiriboga (table 19) are instead about 3 times higher. In Table 11, the values of the ultimate load and ultimate elongation of the textiles in biaxial testing.

[93] https://www.larcroa.fr/informations-techniques/

	A (strain 0,00472) secant modulus (Mpa)				B (strain 0,01887) secant modulus (Mpa)				C (strain 0,04717) secant modulus (Mpa)				D (strain 0,08491) secant modulus (Mpa)			
	A warp tt	A warp et	A weft tt	A weft et	B warp tt	B warp et	B weft tt	B weft et	C warp tt	C warp et	C weft tt	C weft et	D warp tt	D warp et	D weft tt	D weft et
1	55,2	246,9	95,3	501,0	42,0	188,0	82,0	431,2	57,0	255,4	103,1	541,8	105,4	471,8	177,5	933,3
2	13,7	52,2	32,9	176,7	11,4	44,3	43,6	233,7	28,4	110,2	86,9	466,1	47,4	184,1	120,6	646,7
3	11,4	15,6	41,0	54,2	4,9	6,7	39,9	52,8	4,9	6,7	52,8	74,0	-	-	-	-
4	14,1	42,6	22,9	88,6	9,4	28,3	20,5	79,1	21,2	63,9	35,8	138,1	49,9	150,3	80,8	312,4
5	12,3	43,3	66,5	262,5	5,2	18,2	80,4	317,1	4,2	14,8	117,6	464,0	5,7	20,1	168,1	663,2
6	53,7	82,2	70,7	151,7	50,5	77,3	77,1	165,5	105,9	162,1	143,5	307,9	-	-	-	-
7	90,0	249,9	32,5	117,6	95,5	265,4	36,4	131,5	128,8	357,8	71,7	258,9	-	-	-	-
8	42,3	140,3	42,3	136,9	53,6	177,8	56,9	184,2	78,8	261,7	96,3	311,7	-	-	-	-
9	32,8	98,6	69,6	413,2	29,1	87,7	82,7	491,8	36,0	108,3	106,5	632,0	44,1	132,7	126,3	749,7
10	38,2	113,7	130,4	510,7	71,2	212,3	204,9	802,3	121,0	360,7	266,8	1044,5	-	-	-	-
11	11,4	55,0	14,6	46,1	15,8	76,4	25,9	81,7	25,8	124,5	39,7	125,3	-	-	-	-
12	17,9	15,4	155,8	385,9	12,9	11,1	284,6	704,8	-	-	-	-	-	-	-	-
13	26,3	63,1	28,0	96,9	18,7	45,0	23,6	81,6	27,7	66,4	36,8	127,3	67,6	162,3	92,6	320,6
14	30,8	35,0	252,3	306,3	29,8	33,8	281,8	342,0	72,9	82,8	444,4	539,4	118,1	134,2	587,8	713,6
15	27,1	89,6	23,9	108,1	18,6	61,7	19,9	90,1	24,1	79,7	31,1	140,6	57,1	189,3	82,6	373,4
16	25,1	47,3	41,8	111,6	18,3	34,4	39,1	104,6	41,5	78,1	76,3	203,8	87,0	163,8	158,3	423,0
17	17,9	49,3	38,5	196,7	11,9	32,9	36,8	188,1	21,5	59,3	63,1	322,5	40,5	111,6	118,4	610,1
18	20,9	45,1	26,5	75,3	29,8	44,9	27,5	78,1	38,2	82,4	51,1	144,9	96,5	208,3	118,2	335,3
19	30,1	73,4	41,0	120,2	28,9	70,3	41,7	122,3	43,6	106,3	77,5	227,5	71,5	174,3	159,5	467,9
20	24,7	27,2	95,1	85,3	35,3	38,7	209,6	187,9	90,1	98,9	431,8	387,1	-	-	-	-
21	112,2	196,5	468,0	1194,7	96,3	168,5	551,9	1408,6	125,9	220,4	569,5	1456,6	-	-	-	-
22	33,5	110,5	31,8	83,7	25,6	84,4	23,9	62,9	49,9	164,7	45,2	119,1	97,2	320,9	93,2	245,6
23	13,5	34,2	117,1	511,0	20,1	50,8	189,1	825,2	39,2	99,5	262,1	1143,7	58,9	149,2	314,6	1372,9
24	42,6	218,1	36,6	167,9	99,0	507,3	96,1	441,1	198,1	1015,2	210,7	967,5	274,9	1408,7	303,3	1392,7
25	31,1	113,9	45,7	223,2	62,4	228,7	98,3	480,3	139,2	510,3	192,1	938,3	209,0	765,9	238,5	1164,9
26	11,2	27,5	67,5	347,1	17,1	42,2	109,8	564,6	36,3	89,3	158,6	816,0	68,8	169,4	212,0	1090,6

Table 10 The secant tensile moduli (biaxial testing) calculated using Textile thickness (T_t) and the Fiber Equivalent thickness (E_t).

	name	warp ult load (N/cm)	warp ult elong (mm)	weft ult load (N/cm)	weft ult elong (mm)
1	plain canvas 1	71,85	1,17	114,14	1,17
2	plain canvas 2	62,61	1,23	142,33	1,23
3	plain canvas 3	7,17	2,14	9,83	0,53
4	plain canvas 4	98,48	1,53	140,21	1,48
5	plain canvas 5	-	-	-	-
6	Domenico C. Malinconico	14,18	0,53	31,76	0,77
7	Bernard d'Agesci	49,84	0,86	28,17	0,85
8	medium paste lining canvas (IT)	29,58	0,80	32,74	0,70
9	heavy paste lining canvas (IT)	50,67	1,03	144,85	0,98
10	Fragonard medium paste lining	48,20	0,70	105,58	0,64
11	Raffaele Postiglione	13,71	0,75	21,40	0,75
12	Alfred Dehodencq	20,00	1,10	23,85	0,30
13	Jules Gélibert	41,00	1,13	54,85	1,13
14	Louis Augustin Auguin	27,40	1,10	129,29	1,08
15	Ludovic Alleaume	23,59	0,95	32,66	0,95
16	Hubert Sauzeau 1	33,67	1,06	60,77	1,06
17	Hubert Sauzeau 2	38,58	1,11	120,39	1,11
18	Charles Müller	22,25	0,96	27,25	0,96
19	Furcy de Lavault	27,50	1,02	60,75	1,03
20	Louis Alexandre Cabié	-	-	-	-
21	Louis Lessieux	56,06	0,55	11,26	0,51
22	Jeannine Gilles-Murique	78,04	1,07	82,54	1,06
23	Night Watch mockup canvas	-	-	132,00	0,72
24	"pattina" lining canvas	165,72	1,23	157,96	1,24
25	"patta" lining canvas	111,26	0,91	117,71	1,06
26	canvassing "03f"	-	-	-	-

Table 11 Ultimate load and ultimate elongation in warp and weft (biaxial testing)

5.3 The E modulus values in the conservation science literature

If tensile tests on canvas paintings and textiles used in conservation are quite rare in conservation literature, the value of their elastic modulus is even more rare. A chronological survey of the data available in the literature is following, providing an overview of the expected values with no pretention of exhaustivity. As a general remark, the E modulus is only mentioned when engineering predictive studies are involved in the research or foreseen. In many cases, the E modulus is "object related" as no analysis of the internal structure is used to calculate the equivalent loading section. When tests aim to compare different materials the values of force are mentioned, but often the data needed to calculate the E modulus is not included in the text. [Hedley and Villers, 1982] and [Berger and Russell, 1988] are interesting early examples.

5.3.1 Early studies

In 1973, Sorta proposed a non-destructive method to calculate the elastic modulus of paintings by measuring the velocity of an elastic wave in the material [Sorta, 1973]. The method has never been used after, and therefore the values provided cannot be directly compared with those obtained with more conventional destructive methods. Nevertheless, it has two potential advantages, that of being nondestructive and therefore replicable in a potentially infinite number of locations on the painting, and that of describing the material's characteristics as a whole, not requiring simplifications. This is of course also a limitation, as the information provided cannot be referred to a defined layer or material, but to the painting's complex structure. Though there is a possible ambiguity in the interpretation of the raw data from the paper, the values obtained (Table 12) appear to range from 490 MPa to 5886 MPa for the sample set including a raw canvas, 4 paintings with a hemp canvas support, and 7 paintings with a linen canvas support, most of which naturally aged. Such values seem to be compatible with the those obtained with different methods, but cannot be used before further investigations are made.

Linen canvases	approx. age	E module (MPa)	Hemp canvases	approx. age	E module (MPa)
raw canvas	0	**4708**	painting n.1	0	**2943**
painting n.1	100	**1157**	painting n.2	0	**3041**
painting n.2	200	**687**	painting n.3	0	**3139**
painting n.3	150	**490**	painting n.4 (paste lined)	75	**490**
painting n.4 (paste lined)	50	**2943**	painting n.5	100	**1177**
			painting n.6	10	**5886**
			painting n.7	120	**1177**

Table 12 The elastic modulus obtained with the elastic wave propagation, from [Sorta, 1973].

Hedley published the data about a series of tensile tests at the ICOM CC 1981 meeting [Hedley, 1981]. A series of synthetic textiles are tested under the loads of 2, 4, 10 kg on 25 mm wide and 150 mm long samples, and their thickness and the % elongation are

also provided, what allows us to calculate the E modulus (as reported in Table 13). Russel and Berger provided stress and strain values for biaxial tests on 6 textiles, but not the area of the section of the samples, therefore the E modulus cannot be calculated, in [Russel and Berger, 1982] and also in [Russel and Berger, 1990]. Colville, Kilpatrick and Mecklenburg [Colville et al., 1982] elaborated on a Finite Element Model of a canvas painting on stretcher using a list of data derived from [Mecklenburg, 1982] including the E modulus: originally in psi, it is transformed here in MPa (Table 14). The model was used to provide a description of the forces and not a prediction of the behavior of a specific painting, and the results were validated through the comparison with the typical patterns of cracks appearing in canvas paintings.

The Elastic module of leather artifacts, which may be considered a useful reference for fragile materials, can be found in [Nimmo et al., 1996], where approximated values between 30 and 60 MPa are reported for direction A and between 45 and 180 MPa for direction B, of three different specimens of painted and gilded leather.

	thickness (mm)	direction	% elong	force (N)	E (MPa)		thickness (mm)	direction	% elong	force (N)	E (MPa)
fibre glass A	0,09	warp	0,66	19,60	1319,87	Polyester C	0,27	warp	2,00	19,60	145,19
	0,09	weft	0,59	19,60	1476,46		0,27	weft	5,90	19,60	49,22
	0,09	warp	0,92	39,20	1893,72		0,27	warp	3,00	39,20	193,58
	0,09	weft	0,72	39,20	2419,75		0,27	weft	7,70	39,20	75,42
	0,09	warp	1,25	98,00	3484,44		0,27	warp	5,10	98,00	284,68
	0,09	weft	1,00	98,00	4355,56		0,27	weft	11,00	98,00	131,99
	thickness (mm)	direction	% elong	force (N)	E (MPa)		thickness (mm)	direction	% elong	force (N)	E (MPa)
fibre glass D	0,24	warp	1,31	19,60	249,36	Acrylic primed linen	0,75	warp	2,60	19,60	40,21
	0,24	weft	0,66	19,60	494,95		0,75	weft	1,60	19,60	65,33
	0,24	warp	1,84	39,20	355,07		0,75	warp	7,20	39,20	29,04
	0,24	weft	0,95	39,20	687,72		0,75	weft	3,60	39,20	58,07
	0,24	warp	2,30	98,00	710,14		0,75	warp	13,50	98,00	38,72
	0,24	weft	1,21	98,00	1349,86		0,75	weft	5,30	98,00	98,62

Table 13The elastic modulus calculated from [Hedley, 1981]

RH	material	E (MPa)	RH	material	E (MPa)	RH	material	E (MPa)
90% RH	ulster linen 8800 warp	244,76	50% RH	ulster linen 8800 warp	38,61	20% RH	ulster linen 8800 warp	31,03
	ulster linen 8800 weft	861,85		ulster linen 8800 weft	655,00		ulster linen 8800 weft	465,40
	glue size	120,66		glue size	1965,01		glue size	3275,01
	white lead ground	41,37		white lead ground	165,47		white lead ground	255,11
	titanium dioxide paint	82,74		titanium dioxide paint	193,05		titanium dioxide paint	272,34

Table 14 The elastic modulus from [Colville et al., 1982], derived from [Mecklenburg, 1982].

In Art in Transit [Mecklenburg, 1991] the elastic modulus of 13 years old paint layers was tested at different temperatures and relative humidity values, providing values between 689 MPa and 1172 MPa for Naples Yellow in linseed oil (reaching up to 1440 MPa at 5%RH, and up to 4019 MPa at -3°C); between 737 MPa and 1241 MPa for Vermillion in safflower oil; and between 137 MPa and 173 MPa for Burnt Sienna in linseed oil (reaching up to 561 MPa at 5%RH, and up to 2757 MPa at -3°C). The values for rabbit skin glue are higher than in [Mecklenburg, 1982], as 4481 MPa are reported at 23°C and 50% RH, rising to 5515 MPa at 5% RH. Gesso grounds are reported to have E modulus (at 23°C and 63% RH) ranging from 1709 MPa and 4136 MPa depending on the gesso to glue ratio.

Regarding the modulus of the canvas support, in Art in Transit the area of the loading cross section was estimated using the above-mentioned volumetric analysis, introducing a standardized factor of 0.22 to obtain the thickness of the fiber section of the sample. This was the first time that the "object related" approach was not used, and the reason is found in the destination of the values for a FEM use. The E modulus values are presented in Table 15, and were used to describe a "typical linen textile" (not a specific textile) within a comprehensive model destined to simulate the stresses occurring to a painting during transportation and environmental changes.

mean fiber modulus in typical linen textile	E module (MPa)
RH 18% warp	**24**
RH 18% weft	**289**
RH 40% weft	**675**
RH 48% warp	**24**
RH 59% weft	**758**
RH 70% warp	**69**
RH 75% weft	**2275**
RH 91% warp	**213**
RH 93% weft	**1585**
RH 95% warp	**606**
Saturated warp	**510**

Table 15 The elastic modulus calculated on the "average cross-sectional area", in Art in transit 1991.

Accardo, Santucci and Torre used the FEM model to describe the distribution of stresses in the painting by Caravaggio "S. Jerome reading" [Accardo et al., 1992]. The lining canvases used for the paste lining of the painting were tested uniaxially in warp and weft, first as individual textiles and then as a sandwich of the two, including the paste glue adhesive. Two different sandwiches were prepared, with the wefts running parallel or orthogonal to each other. The E Modulus (Table 16) was calculated from the thickness of the textiles from a manual compression with the caliper aiming to reduce the voids between the fibers, as no better alternative could be found for a lined sample. The aim was to compare the distribution of tensions in the painting on a key expandable stretcher and on a strainer with rounded profiles and springs providing tension in different configurations (see Figure 7, chapter 2). Aside from showing the better distribution within the elastic system, the paper provides values of E modulus that is useful for comparation here, as the same commercial textiles were tested, biaxially, in the present research, numbers 24 and 25 in the sample set in this thesis[94]. It should be noted that the material with the highest tensile modulus is the "pattina linen canvas", a stiff and

[94] Comparing the thickness of the textiles in [Accardo et al., 1992], and those found in table 10, we find that the values are not identical but still compatible: for n. 24 we have 0.35 mm and 0.44 mm; for n. 25 we have 0.56 mm and 0.57 mm.

thin material. This is also present in the two lining sandwiches, that have a lower tensile modulus because of the higher cross-sectional area.

Material	*direction*	E module (MPa)
pattina linen canvas	*warp*	**339**
	weft	**706**
patta linen canvas	*warp*	**260**
	weft	**211**
lining sandwich with parallel wefts	*warp*	**130**
	weft	**196**
lining sandwich with orthogonal wefts	*warp*	**242**
	weft	**295**

Table 16 The elastic modulus of unaged lining canvases from Accardo et. al, 1992

5.3.2 More recent studies

Mecklenburg, Tumosa and Erhardt, published [Mecklenburg et al., 2005] the E Modulus of paint films obtained from cold pressed linseed oil and different pigments, that had naturally aged at the Smithsonian Institution for 12-14 years (see Table 17). The results describe how the interaction between binder and pigment produces paint films with extremely different mechanical behavior, with basic lead white showing an intermediate stiffness, raw umber a very low stiffness and zinc oxide producing very stiff, and brittle, films.

cold pressed linseed oil	*age (years)*	E module (MPa)
raw umber	*12,25*	**5**
red iron oxide	*12,25*	**5**
malachite	*12,25*	**89**
titanium dioxide	*14,4*	**140**
basic lead carbonate	*14,75*	**300**
zinc oxide	*14,5*	**1667**

Table 17 The elastic modulus of naturally aged paints from Mecklenburg, Tumosa and Erhardt 2005

In Young's Ph.D. thesis [Young, 1996 **(a)**] the loading section area is calculated through the above-mentioned method, based on measurements derived from microscope observations of the yarns. The E modulus calculated for the two industrial textiles is in Table 18.

raw material	*direction*	E module (MPa)
12 oz Cotton Duck Uniaxial	*warp*	**330**
	weft	**570**
12 oz Cotton Duck biaxial	*warp*	**330**
	weft	**960**
Superfine Belgian Linen Uniaxial	*warp*	**480**
	weft	**1970**
Superfine Belgian Linen Biaxial	*warp*	**820**
	weft	**5550**

Table 18 The elastic modulus of textiles from [Young, 1996 a]

In [Young, 1996 (b)] the E modulus of 260x260 mm cruciform samples, extended to 360x360 mm to reach the clamps, of a cotton duck canvas under biaxial and uniaxial tension. The modulus (Table 19) was measured under the same load of 50N in different conditions, raw, wetted and sized. The loading area was calculated from measurements of the number of yarns/m and average yarn diameter, using a Shadowgraph [Settles, 2001]. The data reported in Table 18 and Table 19 provides a useful estimation of the difference in the measured behavior of the material under uniaxial and biaxial testing conditions. As seen in the values from the two test conditions for the raw textile, the E modulus is higher in biaxial testing because of the interaction between the two sets of yarns that mutually reduce the possibility of de-crimping to happen. In [Young and Hagan, 2008] the E modulus of modern paints used for priming flexible supports at different temperatures is listed.

cotton duck at 50N/260mm	*direction*	E module (MPa)
raw uniaxial	*warp*	**375**
	weft	**680**
raw biaxial	*warp*	**603**
	weft	**1315**
wetted uniaxial	*warp*	**282**
	weft	**504**
wetted biaxial	*warp*	**362**
	weft	**777**
1st sized biaxial	*warp*	**688**
	weft	**973**
2nd sized uniaxial	*warp*	**612**
	weft	**915**
2nd sized biaxial	*warp*	**812**
	weft	**1138**

Table 19 The elastic modulus of cotton duck in different test conditions from [Young, 1996 b].

Chiriboga modeled the canvas as a homogeneous plate, whose thickness is obtained from the fiber volume fraction occupied in the volume of the woven structure, as previously described. The E modulus of the textiles elaborated on the fiber volume fraction are in Table 20. Because the mechanical tests on the samples of the modeled

textiles were uniaxial, the introduction of the Poisson's ratio and of the shear modulus was needed to complete the simulation of their actual behavior in a biaxial tensile state on the stretcher. Still, the high ratios (129; 19; 23) between the warp and weft moduli of the linen textiles seem to be disproportioned if compared to the results obtained from actual biaxial tensile testing, as we will see in the following pages.

Material	nominal thickness	*direction*	model thickness	E module (MPa)
Rijn linen	0,562	*warp*	0,215	**6**
		weft	0,094	**774**
Waal linen	0,396	*warp*	0,132	**207**
		weft	0,082	**3937**
Amazone linen	0,369	*warp*	0,182	**158**
		weft	0,116	**3670**
Cotton	0,453	*warp*	0,148	**632**
		weft	0,169	**939**

Table 20 The elastic modulus of the textiles from Chiriboga, based on the fiber volume

The research group that saw the collaboration between the Polish Academy of Sciences of Kraków, Poland, the Polytechnic University of Valencia, Spain and The Royal Danish Academy of Copenhagen, Denmark, published the mechanical properties of canvas paintings textile supports and glue sizing [Janas et al., 2022]. The mean fiber cross-section was calculated using the 0.22 coefficient derived from Art in Transit [Mecklenburg, 1991], and the samples were tested at different relative humidity values after being glue-sized with different quantities and methods. The average E modulus values recorded were 550 MPa (+/- 240 MPa) in the weft and 160 MPa (+/- 86 MPa) in the warp direction at 50%RH, that abruptly decreased at 90% RH, to 120 MPa (+/- 30 MPa) in the weft and 30 MPa (+/- 19 MPa) in the warp.

An unconventional and interesting research project saw uniaxial tests performed on 50 mm wide canvas samples cut with a variety of angles from the weft direction (angles of 0°, 15°, 30°, 45°, 60°, 75°, 90°) to explore the response of the textile in combination with mathematical predictions [Penava et al., 2015]. The canvas was progressively coated with up to 3 preparation layers and testes in the different conditions. The values of the E modulus in warp and weft are collected in Table 21, and appear to become surprisingly high when the preparation layers are added. Still, there is a possible source of misunderstanding in this paper, as the unit mentioned in the paper is KPa and not MPa, and we assume that they were actually mentioning MPa as the opposite would make the data surprisingly low[95]. It shall be noted that no mathematical treatment of the

[95] The same assumption was made in [Dings, 2022]. I wrote to Penava, to ask for more information on the subject, but had no reply.

loading section area was introduced in this paper, thus obtaining the “object related” E modulus value.

Material	nominal thickness	*direction*	E module (MPa)
linen textile	0,51	*warp*	**171**
		weft	**324**
with one layer	0,76	*warp*	**4058**
		weft	**5098**
with two layers	0,83	*warp*	**4911**
		weft	**6116**
with three layers	0,89	*warp*	**6001**
		weft	**7279**

Table 21 The elastic modulus of a painter canvas with layers of preparation, from Penava, with a doubt about the interpretation of the data, as the unit in the paper is KPa and not the expected MPa

Dings [Dings, 2022], based on the literature data, and mostly on Chiriboga and Penava, used as reference values for the E modulus 1000 MPa in the weft direction and 400 MPa in the warp. The values considered possible in the study were ranging from 300 to 7000 MPa in the weft, with ratios between warp and weft ranging from 10 to 80, assuming as theoretical reference the ratio of 40.

Roche [Roche, 2005] reported the value of E module for canvas paintings materials: 218,75 MPa for the canvas support and 1450 MPa for the paint layers. In a document available on the website of Larcroa[96] the E modulus for 8 commercial painters' canvases that are very popular among French artists (see Table 22) is reported. In both cases, the E modulus was “object related”, being calculated for the thickness of the actual material with no elaboration on the loading section of the yarns.

	thread count							E module (MPa)	
toiles Marin	**warp**	**weft**	**weave**	**sizing**	**charges in the ground**	**g/sqm**	**thickness**	**warp**	**weft**
1- coton moyen Ref: 202	11	15	plain	acrylic	titanium white, silica	512	0,7	**168**	**294**
2- coton fort Ref: 405	28	20	lousiana	acrylic	calcium carbonate, silica	627	1,06	**222**	**225**
3- coton fin Ref: 456	23	15	plain	animal glue	none	300	0,47	**170**	**290**
4- coton extra fort Ref: 481	42	31	lousiana	animal glue	none	450	0,67	**150**	**220**
5- coton mixte Ref: n/a	10	10	plain	vinylic	tit. white, calcium carbonate	825	1,2	**206**	**324**
6- lin-chanvre moyen Ref: 503	11	10	plain	animal glue	tit. white, calcium carbonate	572	0,83	**789**	**1278**
7- lin-chanvre moyen Ref: 264	14	14	plain	vinylic	tit. white, calcium carbonate	370	0,75	**672**	**2247**
8- polyester moyen Ref: 435	32	26	plain	vinylic	tit. white, calcium carbonate	582	0,5	**317**	**369**

Table 22 The elastic modulus of commercial painter’s canvases from Roche, Larcroa website

[96] https://www.larcroa.fr/informations-techniques/

If the object related elastic modulus cannot be directly used for predictive simulations, it provides nevertheless a tool for comparisons, with similar materials under the same testing conditions, or of the same material under different testing conditions.

5.4 Analysis of the biaxial testing data of the set of specimens

5.4.1 Correlation with the warp and weft directions

The elastic modulus is higher in the weft direction in 24 over the 26 specimens (92%), as seen in Figure 62. Still, a significant group of 7 specimens has a difference of less than +/- 15MPa, meaning that the modulus is very close to being equal. Not considering those, we can say that for our 26 specimens the modulus in C is higher in weft in 18 out of 19 (95%), or equal. As we will see later, a higher modulus in the weft direction is common to most textiles.

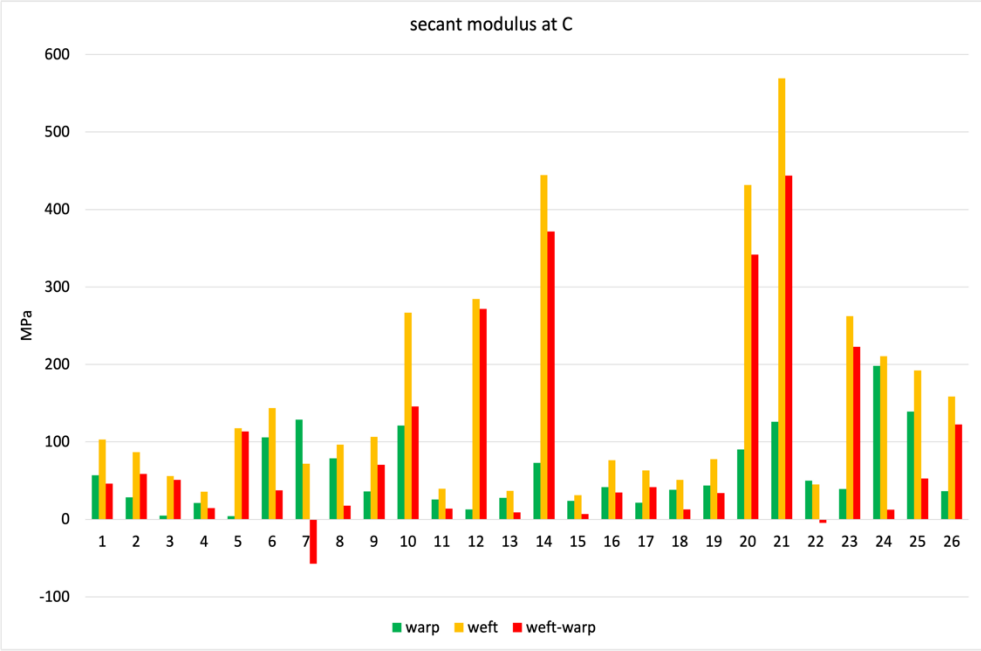

Figure 62 Weft secant modulus at C is higher than warp for most of the specimens

The specimens n. 3 and n. 5 show an extremely low value in the warp direction, the weft being 11.5 and 28 times higher than the warp. These are outliers, since for the remaining 24 the minimum ratio is 1.1 (n. 24); the maximum ratio is 6.1 (n. 14); the mean of the remaining is 2.6. (21 specimens, excluding the outliers, and the above-mentioned n. 7

and 22 that have a higher warp module). It should be noted that the ratio between the elastic modulus value in the two directions increases when the samples are tested uniaxially, because of the stiffness transfer in biaxial testing. This will be seen in the next chapter, where the uniaxial tests are confronted with the biaxial ones for the specimen 23 and for a 17th c. painting, and in chapter 8.

5.4.2 E modulus and crimp

The higher crimp in the warp direction implies that the E modulus of the textiles is lower than in the weft, as we see in Table 23. Nevertheless, a clearer correlation between crimp and the mechanical response of the textile is seen in uniaxial loading conditions because they do not generate the stiffness transfer that takes place in the textile between the orthogonal yarn sets under biaxial loading. Uniaxial tests are not the main objective of the present study and were performed only on a limited number of textiles, therefore this specific correlation will be investigated in future research.

	sample name	warp E at C	weft E at C	weft - warp E at C	warp crimp	weft crimp	warp -weft crimp
1	plain canvas 1	57,0	103,1	46,0	7,9	5,6	2,3
2	plain canvas 2	31,4	56,8	25,4	12,1	4,3	7,8
3	plain canvas 3	4,9	56,0	51,1	7,3	5,6	1,7
4	plain canvas 4	21,2	35,8	14,5	11,0	2,2	8,9
5	plain canvas 5	4,2	117,6	113,4	21,7	2,0	19,7
6	Domenico C. Malinconico	105,9	143,5	37,6	11,1	4,3	6,8
7	Bernard d'Agesci	128,8	71,7	-57,1	6,4	7,3	-0,9
8	medium paste lining canvas (IT)	78,8	96,3	17,5	2,0	2,5	-0,5
9	heavy paste lining canvas (IT)	36,0	106,5	70,5	13,2	9,5	3,7
10	Fragonard medium paste lining	121,0	266,8	145,8	8,3	2,8	5,4
11	Raffaele Postiglione	25,8	36,1	10,3	5,2	3,3	1,9
12	Alfred Dehodencq	22,5	52,2	29,7	15,3	2,3	13,0
13	Jules Gélibert	27,7	36,8	9,1	11,9	3,6	8,4
14	Louis Augustin Auguin	72,9	444,4	371,5	13,0	4,7	8,3
15	Ludovic Alleaume	24,1	31,1	7,0	11,4	6,8	4,6
16	Hubert Sauzeau 1	41,5	76,3	34,8	13,7	5,7	7,9
17	Hubert Sauzeau 2	21,5	63,1	41,6	19,7	6,0	13,7
18	Charles Müller	38,2	51,1	12,9	10,3	5,7	4,6
19	Furcy de Lavault	43,6	77,5	33,9	14,2	3,0	11,2
20	Louis Alexandre Cabié	90,1	431,8	341,6	10,4	3,2	7,2
21	Louis Lessieux	125,9	569,5	443,6	13,7	6,3	7,4
22	Jeannine Gilles-Murique	49,9	45,2	-4,6	6,4	3,9	2,5
23	Night Watch mockup canvas	33,8	189,2	155,5	7,2	1,6	5,6
24	"pattina" lining canvas	90,6	82,2	-8,4	2,9	1,6	1,4
25	"patta" lining canvas	139,2	192,1	52,8	2,3	2,0	0,3
26	canvassing "03f"	36,3	158,6	122,4	5,5	2,5	3,0

Table 23 The secant tensile modulus (at C) is higher in the weft, where crimp is lower

5.4.3 E modulus and twist

The effect of yarn twist on the E modulus of the textile is due to the intrinsic characteristics of the yarn. In Table 24we see a correlation between the textiles showing a higher modulus, either in warp or in west, and the value of TPM. It is not a general one, as we have seen for other characteristics of the textiles, but when a high modulus is

recorded the TPM value is always also high, or at least not low, and the lowest twist values are associated with low tensile response. This appears to be correlated to the higher cohesion the yarn acquires with twist. Nevertheless, tensile response is first of all due to the quality and state of conservation of the fibers, which are highly variable in naturally aged, historical textiles. As we have seen for crimp, it seems very probable that uniaxial tests would me more appropriate to isolate this characteristic. In Table 24 also the yarn width value is displayed, as an additional indicator. In the following paragraphs more detailed observation of individual specimens can be found.

	sample name	warp E at C	warp TPM	warp yarn width	weft E at C	weft TPM	weft yarn width
1	plain canvas 1	**57,0**	277,1	0,47	**103,1**	238,3	0,46
2	plain canvas 2	**31,4**	140,5	0,87	**56,8**	161,7	0,75
3	plain canvas 3	**4,9**	150,4	0,87	**56,0**	229,6	0,64
4	plain canvas 4	**21,2**	193,1	0,80	**35,8**	134,9	0,97
5	plain canvas 5	**4,2**	286,2	0,64	**117,6**	175,4	0,60
6	Domenico C. Malinconico	**105,9**	186,5	0,70	**143,5**	197,9	0,48
7	Bernard d'Agesci	**128,8**	200,1	0,39	**71,7**	252,8	0,46
8	medium paste lining canvas (IT)	**78,8**	231,0	0,79	**96,3**	191,3	0,77
9	heavy paste lining canvas (IT)	**36,0**	194,0	1,19	**106,5**	251,2	0,76
10	Fragonard medium paste lining	**121,0**	196,7	0,72	**266,8**	152,6	0,70
11	Raffaele Postiglione	**25,8**	229,2	0,60	**36,1**	140,3	0,96
12	Alfred Dehodencq	**22,5**	164,0	0,71	**52,2**	212,0	0,51
13	Jules Gélibert	**27,7**	244,2	0,49	**36,8**	288,5	0,41
14	Louis Augustin Auguin	**72,9**	324,5	0,39	**444,4**	464,6	0,33
15	Ludovic Alleaume	**24,1**	213,3	0,44	**31,1**	250,8	0,35
16	Hubert Sauzeau 1	**41,5**	272,1	0,48	**76,3**	366,5	0,40
17	Hubert Sauzeau 2	**21,5**	217,7	0,77	**63,1**	219,8	0,50
18	Charles Müller	**38,2**	362,4	0,35	**51,1**	381,0	0,30
19	Furcy de Lavault	**43,6**	204,4	0,48	**77,5**	339,7	0,36
20	Louis Alexandre Cabié	**90,1**	249,2	0,73	**431,8**	168,7	0,82
21	Louis Lessieux	**125,9**	254,8	0,48	**569,5**	371,6	0,29
22	Jeannine Gilles-Murique	**49,9**	125,0	1,08	**45,2**	64,4	1,14
23	Night Watch mockup canvas	**33,8**	162,1	0,69	**189,2**	253,1	0,46
24	"pattina" lining canvas	**90,6**	291,9	0,42	**82,2**	195,4	0,46
25	"patta" lining canvas	**139,2**	143,3	0,81	**192,1**	160,3	0,77
26	canvassing "03f"	**36,3**	159,5	0,73	**158,6**	162,9	0,67

Table 24 The secant tensile modulus (at C) shows higher values correlated with high TPM

5.4.4 E modulus decreasing after A

N. 1 was chosen as typical example (Figure 63), for a large group of specimens (10 out of 26) showing a temporary decrease in the modulus in B. In Figure 64 the difference between the modulus in B and A is shown for all samples. The phenomenon shows that in the B zone the textile elongates offering a lower mechanical response than that seen in A, describing the influence of the decrimping in reducing the mechanical performance of the textile. Figure 64 also shows that in about a third of the specimens (n. 5 and n. 12 are clear examples) the reduction in the B module is true only for the warp, where the crimp value is higher.

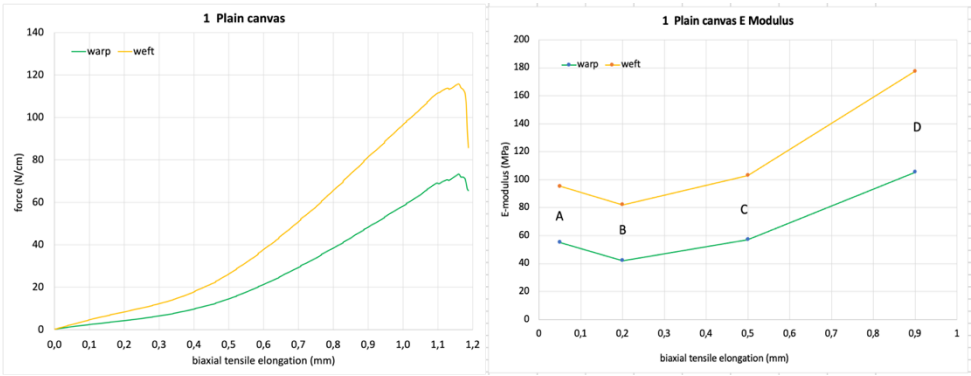

Figure 63 The correlation between high modulus and high twist is 65% (17 in 26)

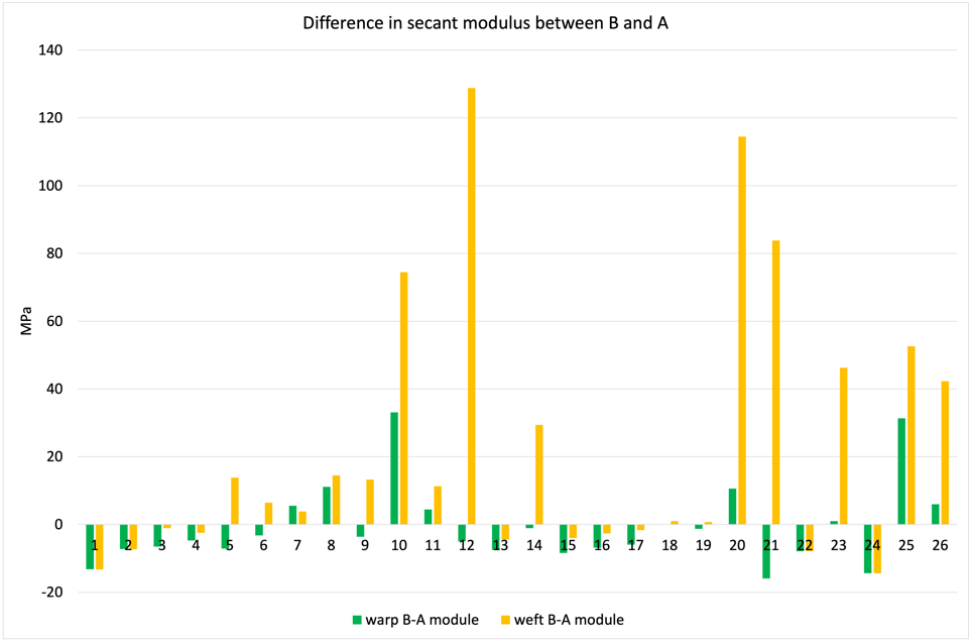

Figure 64 The difference between the B and the A modulus values

5.4.5 Very low warp modulus

As seen in Figure 64, a group of samples shows an extremely low value of E Modulus in the warp direction, with n. 5 as a typical example (Figure 65).

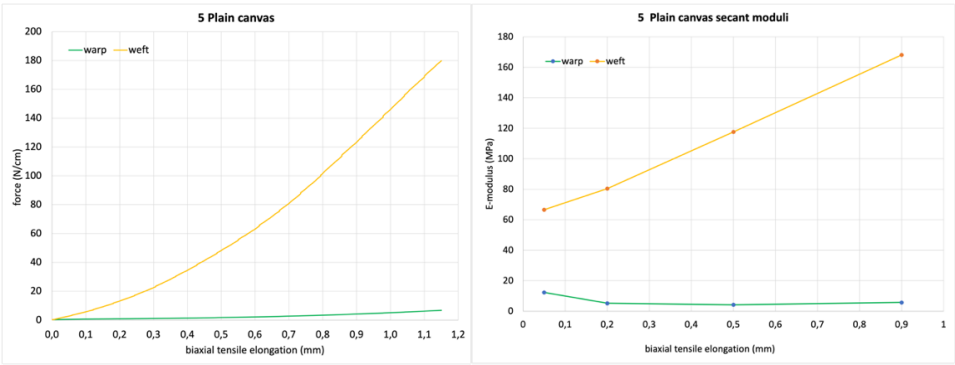

Figure 65 A group of specimens shows an extremely low modulus in the warp, with n. 5 as a typical example

In Figure 66, the % ratio of the warp vs weft C secant moduli in shown. For n. 5 and n. 12 the warp modulus is less than 5% of that in weft, with a clear correlation with the crimp value as these are the specimens showing the highest crimp in the warp (21.7% for n. 5 and 15.3% for n. 12). The warp modulus is much lower than that in weft (between 8.7% and 22.9% of the value) for n. 3, 14, 20, 21, 23 and 26. Though the high crimp in the warp seems to be the main cause (and particularly for n. 14, 20 and 21), it seems not to be the only one. For n.3 in particular, the crimp values are not distant between warp and weft (7.3% in warp and 5.6% in weft), and so are twist (150 TPM vs 229 TPM) and yarn width (0,87 mm vs 0,64 mm) values. Such low modulus in warp may therefore be due to other characteristics that did not make the object of our observations, such as the quality and length of the fibers used for the warp yarns, or their degree of polymerization (though an acidic depolymerization does not seem probable as the pH is 6.4). The n. 23 and n. 26 also show a similar modulus ratio with relatively low values of warp crimp. In particular, in the recent manufacture of n.26 the same yarn was used for both warp and weft, which therefore have the same twist (Table 6, chapter 3) and very similar width and thickness (Table 4, chapter 3). The difference may therefore be connected with the tension used during the weaving, that may have been stored because of the friction between the yarns.

Another exception is found in the fact that the specimens n. 2, 6, 9, 13, 15, 16, 17, 18 and 19 all have a warp crimp higher than 10% but do not show as high a difference in the modulus in the two directions (% values between 32.6 and 77.4). The reason is probably connected with the presence of adhesives (n. 2, 6 and 9) and the high yarn density (n. 13 to 19) promoting the stiffness transfer.

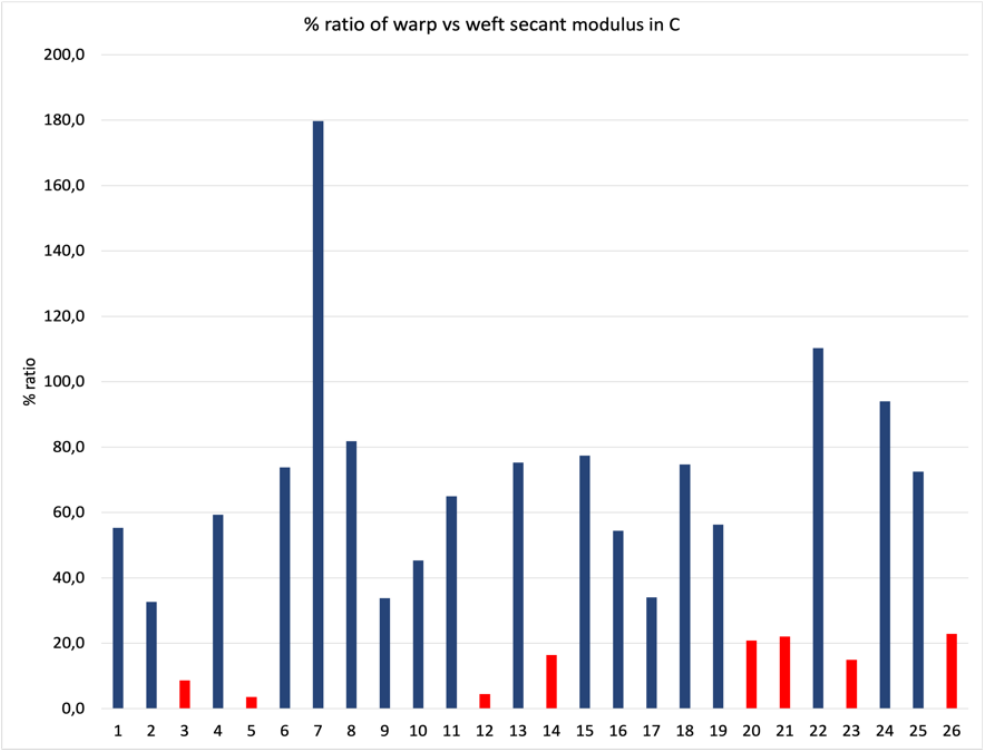

Figure 66 The % ratio of the warp vs weft modulus in C, in red the lowest ratios

5.4.6 High modulus textiles

The area of the transverse section of the samples plays a key role in the calculation of the E modulus, as the stress is the force over the area of the section, and this explains why the thinnest specimens (n. 14, 20, 21) show the highest modulus values (Figure 67). Still, this appears surprising if we consider that the highest modulus in the set of samples (468 MPa in C, 569 MPa in D) is for n. 21, that also has among the highest crimp (13,7% in warp and 6,3% in weft, as seen in Table 23). Looking at the tensile plots in Figure 68, we see that the weft shows a straight-line response and that the slight reduction at B is only seen in the warp. We would expect the de-crimping phase to be directly correlated with the value of crimp, but still, n. 21 and n. 14 seem to compensate with a high thread count (25x25 and 21x21 yarns/cm). This implies a strong mechanical interaction between the yarns, reducing the possibility for them to change their crimped shape, thus justifying the absence of the de-crimping knee. Moreover, their relatively thin yarns also have a very high TPM (Table 5, chapter 3) to provide an efficient fiber cohesion, preventing or reducing fiber slippage. We may therefore say that the high modulus of these specimens is related to the absence of empty spaces between the yarns and to

the fact that also the fibers are tightly packed in the yarn itself. Such characteristics imply that the yarns are not allowed to change their angle nor the fibers their relative position, thus the plot in the weft direction is describing a mechanical response that is very close to that of the fibers that constitute the textile. As previously stated, this would have a lower influence on the overall behavior of the textiles under uniaxial testing conditions.

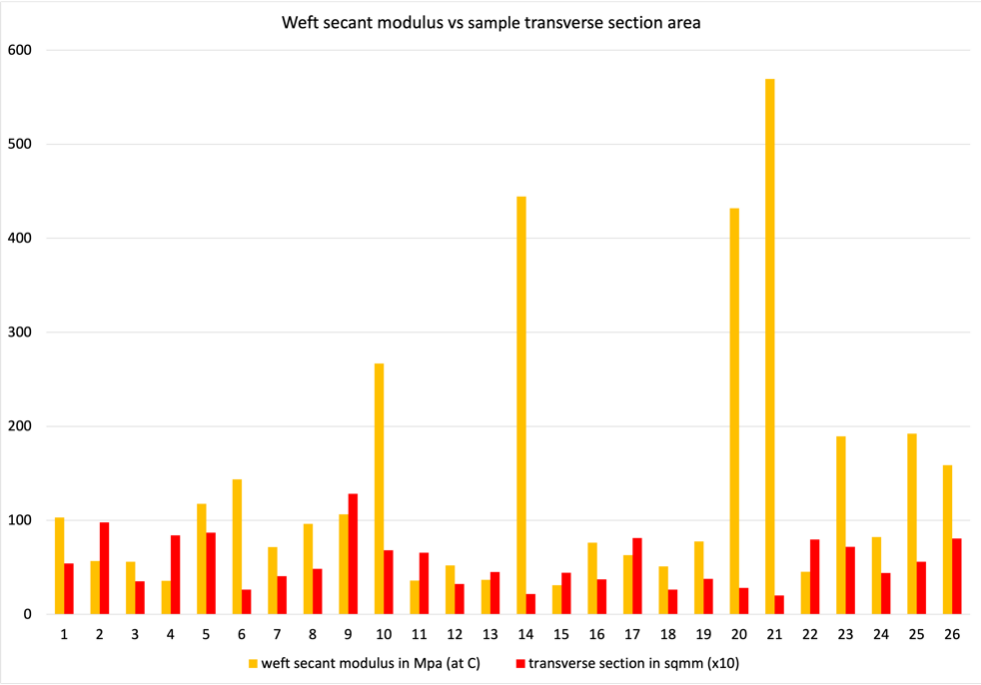

Figure 67 The secant modulus as function of sample transverse section

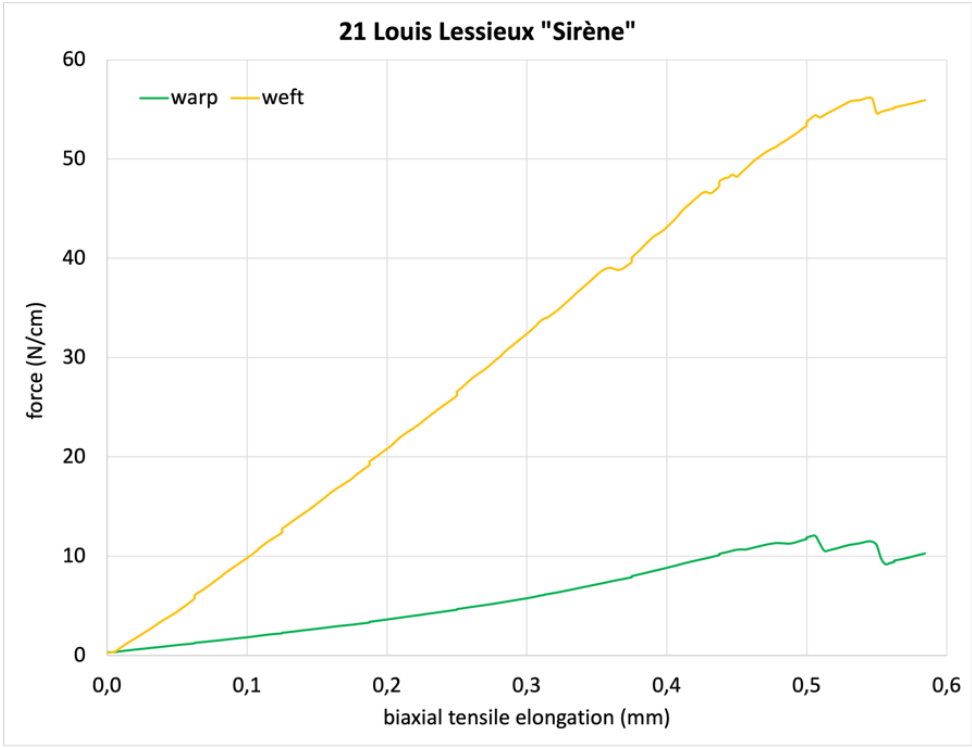

Figure 68 N. 21 shows high modulus despite a high crimp (13,7% in warp and 6,3% in weft), likely because of high yarn density (21/cm in warp and weft) and twist (255 in warp and 372 in weft)

5.4.7 The tensile modulus correlated to textile morphology

The following plots describe the correlation existing between individual morphological characteristics and the tensile modulus under biaxial testing. Some general tendencies are highlighted, despite the number of specimens is still relatively low. The first general information obtained from testing the specimens, is that the tensile modulus is higher in the weft direction, as in Figure 69 (and in Figure 62).

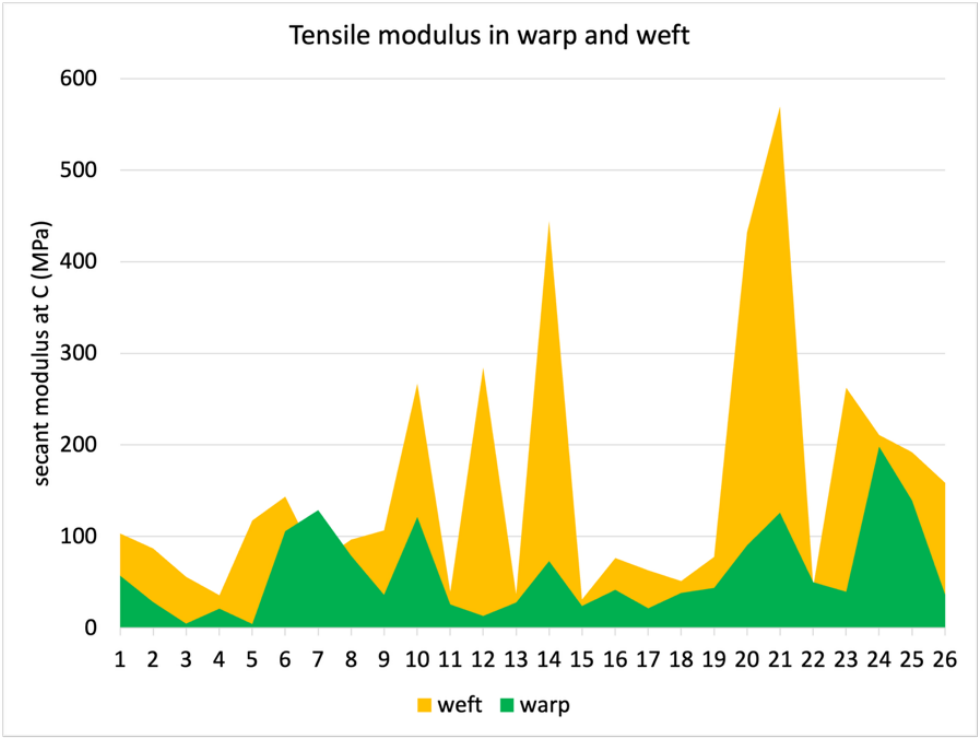

Figure 69 Tensile modulus is generally higher in the weft than in the warp direction

In the warp direction, a decreasing crimp value is clearly correlated to higher tensile modulus, as seen Figure 70, where the data from Table 23 is plotted unrelated from the other characteristics of the specimens.

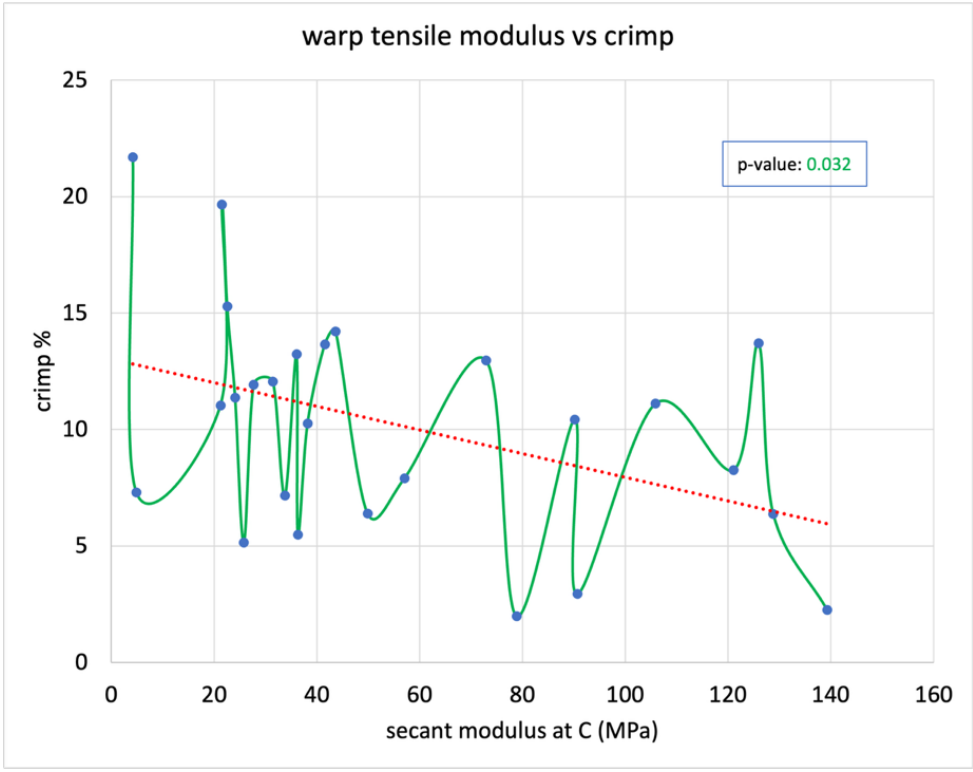

Figure 70 Crimp is negatively correlated with tensile modulus in the warp direction. The p-value below 0.05 confirms full statistical relevance.

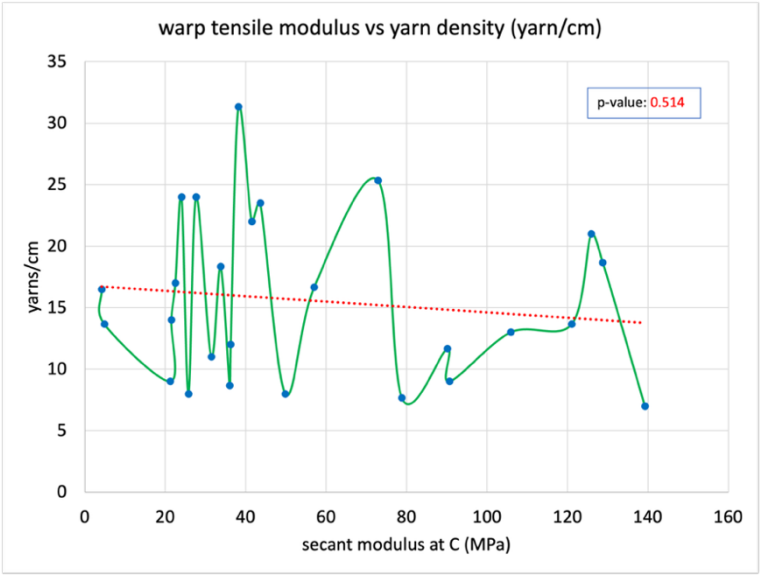

Figure 71 The low negative correlation between thread count and modulus in warp. The p-value above 0.05 implies low statistical relevance.

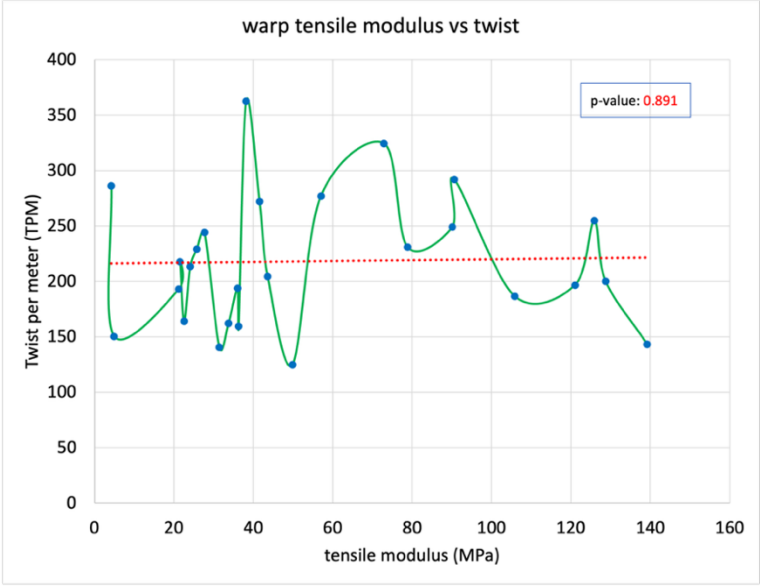

Figure 72 The very low correlation between TPM and modulus in warp. The p-value well above 0.05 implies no statistical relevance.

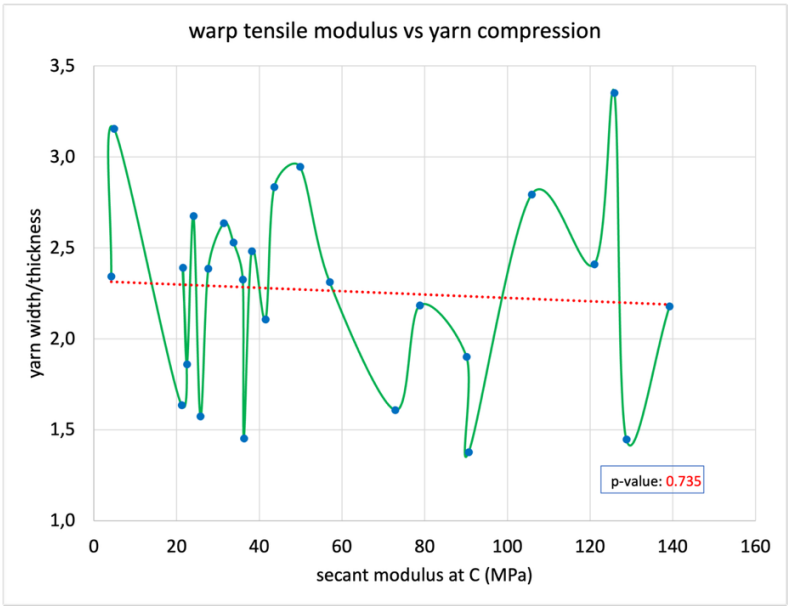

Figure 73 The moderate correlation between yarn compression (more circular cross section) and modulus in warp. The p-value well above 0.05 implies no statistical relevance.

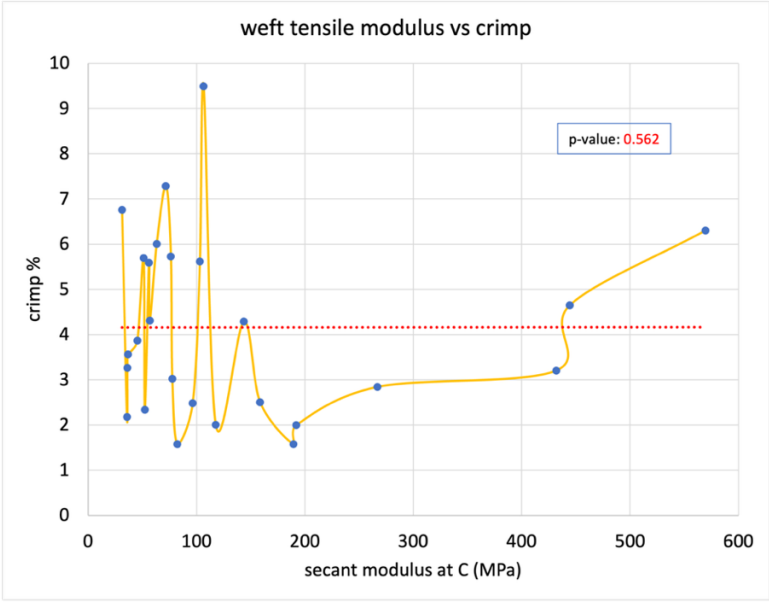

Figure 74 The low correlation between crimp and modulus in the weft direction. The p-value well above 0.05 implies no statistical relevance.

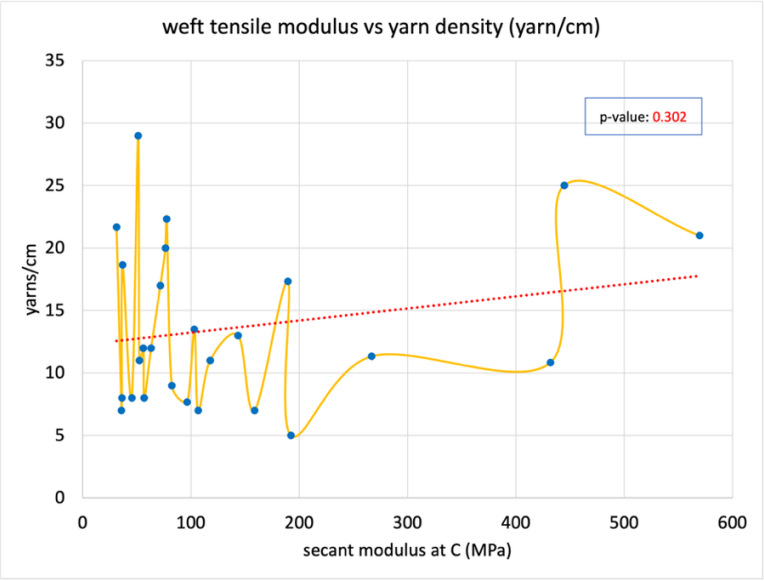

Figure 75 Increasing thread count correlates with modulus in weft. The p-value above 0.05 implies low statistical relevance.

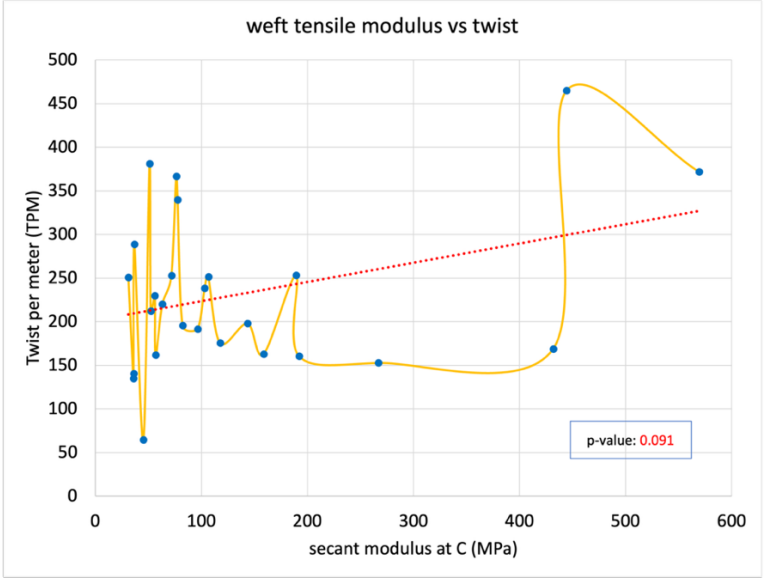

Figure 76 Increasing twist correlates with modulus in weft. The p-value above 0.05 implies low statistical relevance.

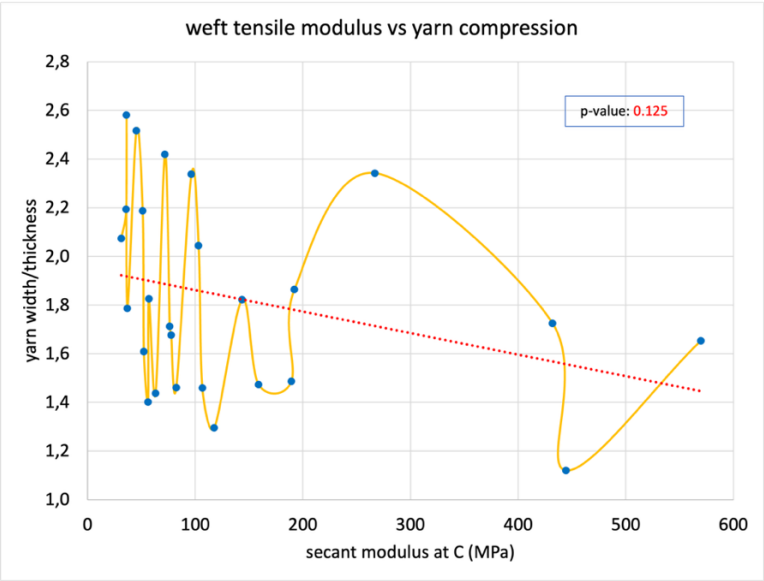

Figure 77 Decreasing yarn compression (more circular cross section) correlates with modulus in weft. The p-value above 0.05 implies low statistical relevance.

In conclusion, the only statistical correlation validated by a p-test is that occurring between the tensile modulus in the warp direction and its crimp (Figure 70). Though the other scatter plots, and their linear fit combined with the p-values, suggest that other correlations are completely absent or showing low statistical relevance, the mechanical response of the textiles under biaxial tensile loads seems to be controlled by different parameters in the warp and weft directions.

The inverse correlation with the thread count in the warp (higher thread count showing lower tensile modulus, Figure 71) is unexpected, but the amplitude of the phenomenon (p-value 10 times higher than the limit of 0.05) is such that it is possible to consider it almost neutral. This appears to be definitely the case for twist and yarn compression (Figure 72 and Figure 73).

In the weft, we see that none of the correlations is supported by a p-value close to 0.05. The generally lower crimp values (Table 7, Figure 27) appears to have an almost neutral effect on the tensile modulus, Figure 74. It shall be noted that crimp is consistently lower in the weft direction (Table 23) and its lower amplitude produces a much smaller decrimping area. This appears with increased evidence in biaxial testing, as the examples in Appendix 2 show quite clearly (see Figure 106 and Figure 107). The thread count

shows a tendency but no statistical relevance in the determination of the tensile modulus, Figure 75. The TPM, Figure 76, also shows a tendency but a slightly higher statistical relevance. The yarn compression, Figure 77, which is dependent on TPM, is a secondary feature showing a similarly low correlation with the tensile modulus.

5.4.8 Uniaxial or biaxial testing and ratio between weft and warp E moduli

Most of the literature data is based on uniaxial testing, and in Table 18 and Table 19 biaxial and uniaxial test results are compared [Young, 1996 **(a)** and **(b)**]. In wider samples the influence of the uniaxial conditions is reduced, making them closer to the biaxial testing. For this reason, those values are not easy to extrapolate because the sample width was not standard. (about 10 times wider than the common sample width of 25 mm).

As previously stated, the use of uniaxial testing imposes a limitation to the reliability of the data when it is needed to characterize biaxial loading conditions, what is normally the case for canvas paintings. In order to mathematically transform uniaxial testing data into something closer to biaxial loading conditions, Chiriboga introduced corrections based on the use of the Poisson's ratio and the shear modulus of the materials. Tests aiming at the determination of the correspondence between the theoretical formulae used to calculate the different behavior of a textile depending on the uniaxial testing direction (samples were tested being cut at angles of 0°, 15°, 30°, 45°, 60°, 75°, 90°) where are performed by Penava in 2015 [Penava et al., 2015]. The results showed that predictability increased significantly by adding layers of preparation to the canvas surface, thus simplifying its behavior because they reduce the anisotropy of the composite.

The ratio between the E modulus in the two directions measured with the biaxial tensile tests on the 26 specimens in this thesis is ranging between a minimum value of 0.36 and a max of 62.47. Such a broad variability is influenced by the presence of four outliers (n. 5, 12, 14, 23), and is reduced to the smaller interval of 0.36 to 13.33 when the outliers are not included. The overall mean of the ratios is 4.41, reduced to a mean value of only 2.63 not counting the 4 outliers (the complete data set is in Table 25).

	A weft/warp ratio		**B** weft/warp ratio		**C** weft/warp ratio		**D** weft/warp ratio			
	textile t	fiber t	textile t	fiber t	textile t	fiber t	textile t	fiber t		
	all data ratios								gen mean	st dev
mean	2,91	3,67	4,42	7,04	3,79	4,90	3,74	4,84	**4,41**	1,25
st. dev.	2,53	3,85	5,08	12,19	5,50	6,21	6,53	7,37		
	ratios not including the outliers								gen mean	st dev
mean	2,02	2,42	2,66	3,58	2,52	3,30	1,84	2,70	**2,63**	0,59
st. dev.	1,37	1,95	2,10	3,16	2,34	2,78	0,72	1,80		

Table 25 Ratios between weft and warp secant moduli obtained in the 26 specimens biaxial tests

The ratios appearing in the literature are in the same range when looking at the fiberglass textiles in [Hedley, 1981], the painter canvases in Larcroa website[97], the textiles in [Young, 1996 a], the cotton in [Chiriboga, 2013], and the glued textiles in [Janas, 2022]. The ratios between the warp and weft E moduli in [Colville et al., 1982; Mecklenburg, 1991; and Chiriboga, 2013] show unexpectedly high reference values, higher than the 22 naturally aged (thus less predictable) specimens tested here (Table 25). Chiriboga provided more insight in the analysis and treatment of the uniaxial tensile response data to elaborate the biaxial response of the modeled textiles. The Poisson's ratio and the shear modulus were introduced to simulate the behavior under a biaxial loading condition on the stretcher. Still, the high ratios (129; 19; 23) between the warp and weft moduli of the linen textiles seems to be disproportioned if compared to the results obtained from actual biaxial tensile testing. It seems possible that such extreme values were conditioned by the uniaxial testing technique and not adequately compensated by the introduction of the Poisson ratio and the shear modulus, as no stiffness transfer is possible in such conditions and the samples elongate much more freely, in particular the warp ones when they have a high crimp.

5.4.9 Tensile modulus and fiber, pH and age of the textile

The effect of the remaining parameters (fiber, pH and age of the textile) was investigated vs the secant tensile modulus at C. As the modulus in weft is generally higher, and more differentiated between the specimens, it was preferred for the analysis.

The nature of the fibers, Figure 78, seems to have a minor impact on the tensile modulus. Nevertheless, considering the last 4 linen textiles as outliers (as 23-26 are not historical specimens), we see that hemp fibers are associated with 3 of the 4 specimens with E > 150MPa (textiles 10; 14; 20; 21). In [Lewin, 2006], we find slightly higher mechanical characteristics for hemp compared to flax.

[97] https://www.larcroa.fr/informations-techniques/

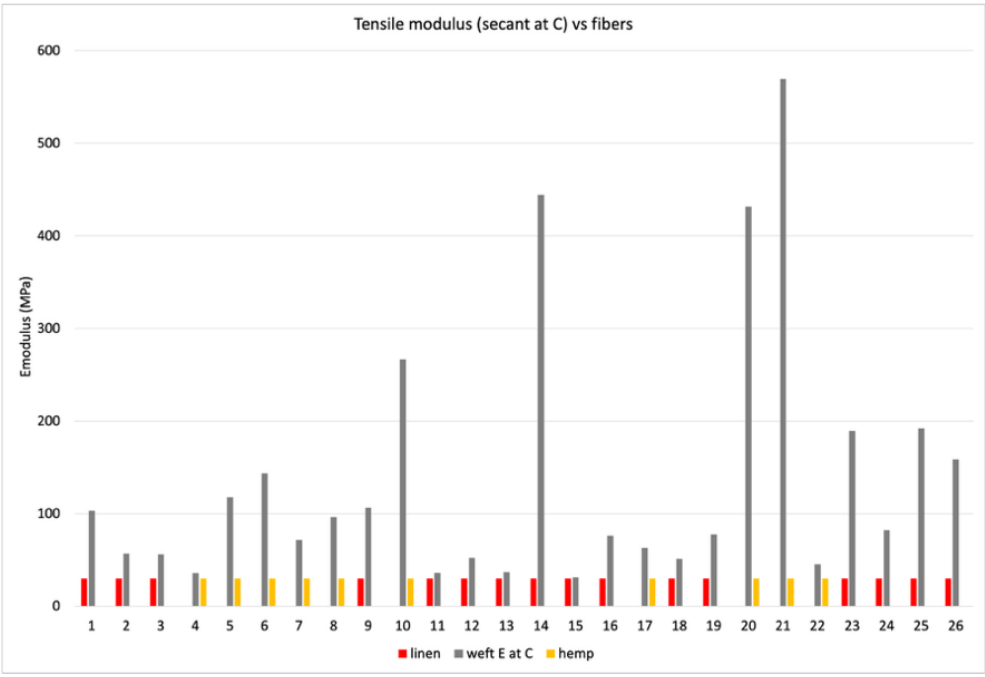

Figure 78 Influence of the fiber nature on the tensile modulus (biaxial load, weft direction)

The pH of the textiles has very little variability, with a mean value of 6.2, a maximum of 7.8, a minimum of 5.2 and the relatively low standard deviation of 0.6. In paintings conservation, such values are considered to be safe, as the limit value for acidic depolymerization is generally considered 5.5 and in only 2 cases the pH has the slightly lower value of 5.2 (textiles 11 and 15). Figure 79 shows the tensile modulus plotted vs the pH values, and a very low tendency to showing modulus increasing with pH. The p-value of the dataset appears to be extremely high, ruling out any statistical correlation. The analytical values are found in Table 1. Not considering the modern textiles (23-26), we do not spot a recurring correlation between the high pH and E values. N. 11 and n. 15 (with the lowest pH value of 5.2) also have a low tensile modulus, but this is not very different from that of textile 4 (pH 7.4) and of textile 13 (pH 5.8).

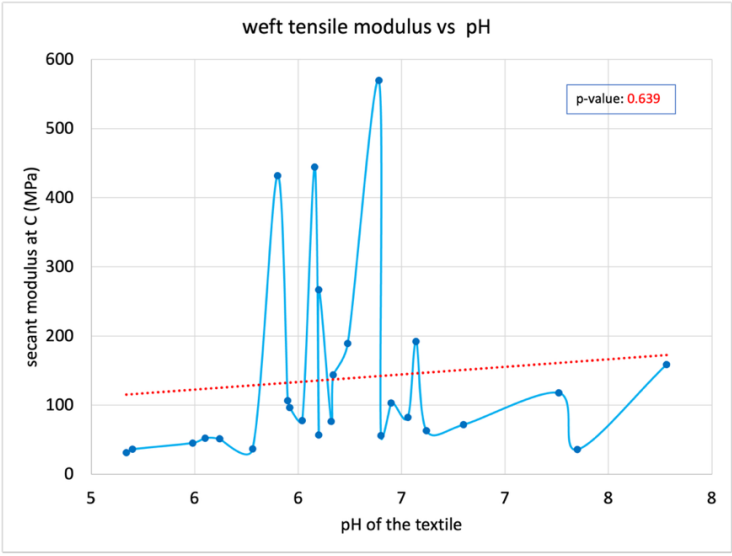

Figure 79 Influence of the pH of the textile on the tensile modulus (biaxial load, weft direction). The p-value well above 0.05 implies very low statistical relevance.

The age of the textile is plotted vs the tensile modulus in Figure 80, showing a feeble negative correlation, at least with textiles that are -at most- about 300 years old. The p-value of the dataset being very high, no statistical correlation appears to be established.

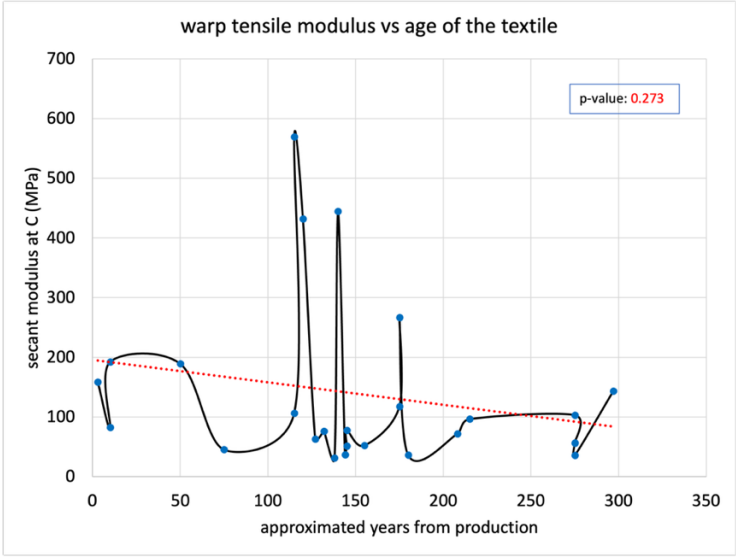

Figure 80 Influence of age (years from production) on the tensile modulus (biaxial load, weft direction). The p-value above 0.05 implies low statistical relevance.

The analytical values are found in Table 1, where we can see that the highest E values among the historical textiles are found in numbers 20 and 21, relatively young hemp textiles. Number 10 has a modulus that could possibly have been influenced by age, as it is almost 100 years older than the other 2 high modulus hemp textiles. N. 14 (only a few decades older than 20 and 21) has a similarly high modulus but it appears to be an outlier if compared with the other linen textiles.
Figure 79

5.4.10 Additional biaxial tests performed on four naturally aged paintings

In order to further contextualize the data provided so far, the tensile response of 4 paintings have been tested and are listed in Table 26. One is an 18th century painting, never restored nor lined; the second is a 19th century painting, but previously restored and impregnated with a wax-resin mixture; the third is an 18th century painting with a 20th c. wax-resin lining; the fourth is a paste lined 19th century painting. All paint layers are oil-bound, the canvas support of the 4 paintings is relatively thin, with a high thread count, and n. 16 is a representative example to describe them all. The lining canvases are also thin and have a similar or slightly higher thread count. The four specimens are part of another ongoing research and the results are used here as an example of a different kind of materials from the 26 specimens and the literature data of mostly single canvases without paint layers or lining adhesives. The transformation of the tensile data into FEM adapted values, only including the fiber fraction and related working section, is more complex due to the presence of stratifications and lining adhesives.

18th c. unlined painting			**19th c. painting wax-resin impreganted**			**wax-resin lined 18th c. painting**			**19th c. paste lined painting**		
thickness 0,50 mm			thickness 0,88 mm			thickness 1,38 mm			thickness 1,37 mm		
E module at 0,05 mm elongation			E module at 0,05 mm elongation			E module at 0,05 mm elongation			E module at 0,05 mm elongation		
warp	**256** MPa	ratio	warp	**289** MPa	ratio	warp	**151** MPa	ratio	warp	**215** MPa	ratio
weft	**368** MPa	*1,44*	weft	**334** MPa	1,16	weft	**207** MPa	1,37	weft	**240** MPa	1,12
E module at 0,2 mm elongation			E module at 0,2 mm elongation			E module at 0,2 mm elongation			E module at 0,2 mm elongation		
warp	**193** MPa	*ratio*	warp	**236** MPa	ratio	warp	**95** MPa	ratio	warp	**219** MPa	ratio
weft	**357** MPa	*1,85*	weft	**262** MPa	1,11	weft	**150** MPa	1,58	weft	**200** MPa	0,92
E module at 0,4 mm elongation			E module at 0,4 mm elongation			E module at 0,4 mm elongation			E module at 0,4 mm elongation		
warp	**190** MPa	*ratio*	warp	**185** MPa	ratio	warp	**75** MPa	ratio	warp	**180** MPa	ratio
weft	**346** MPa	*1,83*	weft	**219** MPa	1,18	weft	**125** MPa	1,66	weft	**211** MPa	1,17

Table 26 The elastic modulus of four naturally aged paintings (biaxial tensile tests)

5.5 Conclusions and future work

All the mechanical tests presented here are biaxial, in the awareness that biaxial loading provides a much more realistic information about the tensile response of a stretched textile. Nevertheless, all choices imply a limitation, as we have seen in the previous paragraphs. Tensile modulus is indeed higher in the weft, where crimp is lower, in a large majority of the 26 specimens (about 92%), but uniaxial loading conditions would have helped in obtaining more detailed insight, as they do not imply stiffness transfer between the orthogonal directions and would have allowed isolating the single direction. Similar considerations could possibly apply for the correlation with twist. In the next chapter we will see the characterization of the specimen n. 23, a basket weave canvas like that used for the lining of Rembrandt's *The Night Watch*, in which uniaxial and biaxial tests will be

used and compared. In chapter 8 we will see the same uniaxial/biaxial characterization of the textiles involved in the conservation treatment of Tiepolo's *Juno in the clouds*.

Another direction of the future research is performing uniaxial and biaxial tensile tests on specimens of paintings including the preparation and paint layers, in order to build a correlation database. As we will see in chapters 6 and 7, this will be extremely useful to obtain reference data for the tensile modulus of paintings as a layered structure.

The experience acquired with tensile testing of historical textiles suggests a general question about the current use of the value of the elastic modulus for similar artifacts in conservation science. The definition of "elastic modulus" is based on the concept that the strains involved, and described by the modulus, are fully reversible. However, this does not appear to be the case, as permanent deformations are clearly visible in the textile even after testing well below its supposed yield point. This is clearly due to a reorganization of the textile, where the first step is some slippage between the yarns. The next step is slippage between the fibers, which is clearly a more permanent deformation and should be defined as damage.

The next step is therefore that of organizing an automated test set up dividing the displacement in very small traits, so as to isolate the permanent deformation. After the initial pretension, required to obtain homogeneous distribution of tensions in the sample, a small increase in tension will be done and the clamps reverted to the initial position. As the machine is able to memorize and reproduce a specific location, cycles divided in small, incremental steps will provide useful insight. A similar approach may be devoted to stress related creep, though only within a relatively narrow the time frame.

Chapter 6 Construction and testing of a mockup to investigate the mechanical behavior of a wax-resin lined painting

Outline of the chapter

6.1 The use of mockups
- 6.1.1 Definition of the elastic moduli and characterization of the materials

6.2 Materials and methods
- 6.2.1 The naturally aged painting
- 6.2.2 The wax-resin lining of the mockup painting
- 6.2.3 The tensile tests
- 6.2.4 The new flexural testing tower and the flexural tests
- 6.2.5 The tensile and flexural moduli

6.3 Results and discussion
- 6.3.1 Morphological data on the textiles
- 6.3.2 Tensile response of the materials under biaxial and uniaxial testing
- 6.3.3 The lining canvas
- 6.3.4 The effect of wax-resin on the lining canvas
- 6.3.5 The naturally aged painting
- 6.3.6 The mechanical behavior of the lined mockup and the calculation of the elastic moduli
- 6.3.7 Calculation of the loaded section area of the mockup

6.4 Conclusions and future work

6.1 The use of mockups

Paintings on canvas are complex, multi-layered structures composed of canvas, size, ground and paint layers, varnishes and the materials from past conservation treatments, such as consolidation and lining adhesives, and additional lining supports. Research into the mechanics of canvas paintings is limited by such complexity, but perhaps even more so by the fact that most mechanical tests require meaningful samples of suitable dimensions to be taken from the painting. This is easy to understand, since in order to know how much force is needed to stretch, bend, or break a material, it is necessary to test a physical object. The values of the Elastic Modulus and of the Ultimate Strength are the cornerstones of materials engineering, and the procedures to obtain them require cutting a sample with a defined shape, and submitting it to destructive testing[98]. Attempts have been made in engineering and conservation science to reduce sample

[98] Ennio Sorta, in "Problemi di Conservazione" [Sorta, 73], proposed to use a Dynamic modulus tester, DMT PPM-5R produced by Lawson Hemphill (Swansea, MA) to measure of E Modulus of paintings. The non-destructive method, based on the use of an elastic wave, has never been used. The original paper can be found here: https://doi.org/10.5281/zenodo.14834185

dimensions to the nano scale [Tiennot et al., 2020], and the micro scale [Maraghechi et al., 2023 **(a)**], which are very promising but need to be correlated with the macroscopic, or real size, scale of the artifact. Understanding the mechanical properties of a painting is crucial for conservators in evaluating the effects of stretcher tension on their structural integrity. As we saw in chapter 5, the conservation and conservation science literature offer very little data on the tensile response of canvas paintings, and practically nothing is available for the evaluation or quantification of its bending properties through its flexural elastic modulus.

This chapter presents the design, construction, and use of a physical mockup of a wax-resin-lined painting that draws inspiration from the structure of Rembrandt's 1642 wax-resin lined oil painting known as *The Night Watch* because of the great wealth of knowledge available about the precious painting. Moreover, the 1975 lining procedures are described in [Kuiper and Hesterman, 1976], and a similar lining canvas was available. To create the mockup, a large fragment of a 17th century Italian canvas painting was used, in the purpose of obtaining otherwise inaccessible information on the mechanical behavior of the complex structure of a wax-resin lined paintings. This chapter addresses the challenges and benefits for conservation science and practice. In particular, the possibility of obtaining quantitative data to implement predictive FE models of such complex structures is discussed. Mechanical tests were conducted on the mock-up using the custom-built equipment described in Chapter 4, to evaluate its tensile and flexural responses.

The mockup is used to describe the mechanical behavior of the individual constituent layers and of the assembled structure. It was built as a research object for destructive mechanical testing. The debate about the use of mockups and models in science has always been very lively, also on a general epistemological level [Cassini and Redmond, 2022]. The topic is often discussed in conservation science, and the value and limitations of the use of models have been analyzed, as in [Stoveland et al. 2021; dePolo et al. 2021]. Physical simulations are sometimes considered unreliable with respect to the materials used, their aging[99], and the variability of the original structures. This leads to a kind of prejudice that favors digital simulations because they appear to be more anodyne and because they produce quantitative results that can be adjusted to real data by simply working on the numerical parameters of the model rather than with the complex and time-consuming production of a new physical model. However, if validation is relatively easy when dealing with new or reproducible artifacts, as in standard engineering, it

[99] As seen in the Introduction, a lively public debate about the use of aging protocols of materials used in [Carr et al., 2003], to mimic the mechanical behavior of a "typical 19th c. English painting", can be found in Studies in Conservation, vol 49 (2004), in the Letters to the Editors at p. 70-72.

becomes very difficult with heritage materials that cannot be sacrificed for destructive testing.

An interesting by-product of constructing a handmade artifact to simulate the painting's build-up is that it allows the behavior of each element in the layered structure to be studied in detail. The mere checking of the model's adherence and differences from the original is an opportunity to test the assumptions on which the interpretation of the structures is based. This process is thus an advanced expression of all the investigation modes, both morphological and mechanical, developed in this thesis research. It also required the adaptation of the mechanical testing machine to carry out flexural tests according to ASTM D 790-07 (see Figure 82b and Figure 83), what is, per se, a further improvement in material testing of canvas paintings materials because no precedent was found in the literature.

6.1.1 Definition of the elastic moduli and characterization of the materials

Stretched canvas paintings are made of canvas, preparation layers, paint and varnish layers, their complexity can be further increased by the presence of a lining canvas and lining adhesive (as discussed in chapter 2). Test results describing the tensile response of a painting are crucial in the evaluation of the effects of stretcher tension on the structural integrity of paintings, and could therefore be helpful also for conservation practice.

As discussed in chapter 5, the cross-sectional area of the sample is a key factor to calculate the tensile modulus, a value allowing comparing the response of different materials. Young's modulus is necessary for predictive models (FEM), that can also be useful to investigate a painting's structural behavior. A common approach to determining the tensile modulus of a material composed of layers with different stiffness, is to test them individually and calculate the weighted average of their moduli based on their thickness. The other side of the problem is that the definition of Young's modulus is based on the assumption that the materials have a homogeneous structure, but canvas paintings are complex composite structures, and contain voids at the macro as well as the micro scale. The methods used for reducing the cross section of a painting to a homogeneous material as required in the definition of the Young's modulus are an open research question, as seen in chapter 5. When dealing with an untreated textile, precedents in the literature are available involving the calculation of the cross-section of the fibers reacting to the tensile load. The procedure is based on subtracting the empty spaces between the fibers and between the yarns, and the area is often approximated to about 25% of the textile's cross-section. Equation 12 was developed here to quantify the fiber equivalent cross-section in each textile with increased accuracy. When a stiff material is superimposed and well bonded to another of lesser stiffness, the tensile

modulus is often calculated as deriving from the stiffest material alone instead of using the weighted of the two layers.

Determining the flexural (bending) modulus of a layered material depends on the stiffness and thickness of each layer as well as their contribution to the flexural stiffness, with materials farther from the neutral axis contributing more to the flexural rigidity.

The morphology of the textiles involved in the construction of the mockup was analyzed using the protocol described in chapter 3, and tensile tests were performed on each layer of the mockup. Data on the lining canvas, specimen n. 23, was already available, as it was morphologically described in chapter 3 and mechanically characterized in chapter 5, and in the Appendices 1 and 2. To gain a more detailed understanding of the material behavior, aside with the biaxial tests, additional uniaxial tests were performed on the lining canvas and on the 17th century painting fragment.

6.2 Materials and methods

6.2.1 The naturally aged painting

The naturally aged painting used for the mockup used to be a 19th century extension of a 17th century painting. The cross section (Figure 81) shows that an earlier painting had been used, containing smalt blue, a pigment which was commonly used in the 16th and 17th centuries, on an oil-based ground above the pure linen canvas. Ground and paint layers are relatively thin (about 60 µm), and a discolored varnish is visible at the interface with a thick oil-based 19th century overpaint (about 350 µm) containing lamp black, earth colors, lead white, and Prussian blue. The presence of the overpaint increases the overall thickness with additional naturally aged paint materials. The specimen bears a thick layer of paste glue, as it had been lined in the 19th century, most of which was removed using an agarose gel to soften it. At the end of the process, the average thickness of our specimen was 0.727 mm and its weight 693 g/m^2.

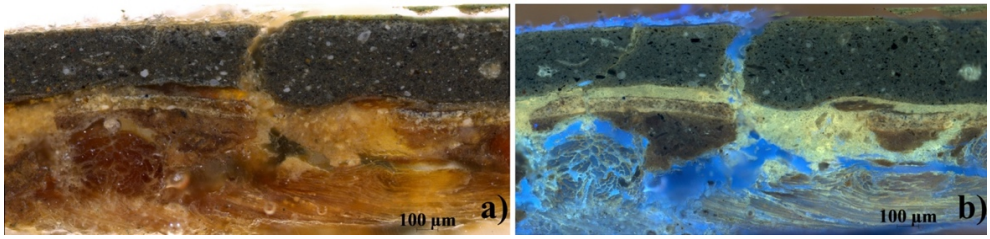

Figure 81 Cross section of the naturally aged painting used for the mockup. 10x magnification, a) visible light, b) ultraviolet light (credit: Giorgia Agresti)

The Rijksmuseum's Paintings Conservation Department still holds pieces of lining canvas that have a comparable weave and thread density to the canvas used to line The Night Watch. Wax-resin lining is no longer used in the Rijksmuseum since the end of the 1980s and the canvas was supplied before that time. This canvas, specimen n. 23 in Table 1, was used to line the mock-up. The same textile, supplied by Claessens in Belgium, is still available for sale with the code 026[100].

6.2.2 The wax-resin lining of the mockup painting

The lining for the mockup was done by Justine Sionneau[101], with the participation of the author, following the wax-resin method used in [Kuiper and Hesterman, 1976]. The mixture of 5 parts of beeswax and 2 parts of colophony was melted and applied by brush on the lining canvas, then ironed to make it penetrate the painting and create an evenly distributed layer, connecting the two canvases upon cooling. The completed mockup is 1.83 mm thick and weighs 1701 g/m^2, meaning that the lining canvas and adhesive have added about 1 mm in thickness and almost exactly 1 kg/m^2 of weight (to a painting weighing about 0.7 kg/m^2). The variability in the thickness of the impasto and the different material properties that would influence the local behavior in a larger painting, could not be replicated in a mock-up. Nevertheless, as the lining canvas and the lining method strongly characterize the mechanics of a lined painting, this mockup is considered to be an acceptable approximation for an average 17th c. wax-resin lined painting.

Tensile tests on the individual layers were performed to evaluate and quantify their influence on the tensile response of the complete mockup. As the wax-resin adhesive is permeating all layers, in order to prepare the samples, it was necessary to decide how much of it should be applied to each layer for the individual tests. The decision was made to use an indirect approach to determine the quantities present in the different layers with reasonable approximation. Part of the impregnated lining canvas, extracted from the mockup as a standard reference, was treated so as to extract the adhesive mixture with heat, ironing samples between layers of absorbent paper until no visible residues were left on the paper. The difference in weight, about 120 g/m^2, is the quantification of the material exceeding the closest interaction with the fibers. To describe the quantity of wax-resin adhesive in the canvas, a useful similarity can be established with the possible quantities of water in wood. Saturated wood dries in two distinct phases: during the first, water defined as “free water” empties the hollow lumen of the cells and

[100] https://www.claessenscanvas.com/en/products/canvas/detail/026

[101] French conservator from the Atelier Buti, Le Poiré sur Vie, 85170 France. She has established wax-resin lining practicing experience.

channels; during the second, the water within the fibers, defined as “bound water”, evaporates, leaving the wood completely anhydrous. In our parallel, the untreated lining canvas is in the anhydrous state, and the impregnated textile is in the saturated condition. The wax-resin that remained after the heat extraction process is considered like the “bound water”, dependent on the characteristics of the specific textile, while the extracted quantity is the “free water”, and the quantity of adhesive that can be measured. In our case, the “bound adhesive” was replicated on the clean lining canvas and on the mockup painting by impregnating them and then removing the excess using the same procedure, until reaching the “bound” configuration. This process allowed quantifying the bound adhesive, that is, approx. 90 g/m^2. The “free water” configuration was replicated by adding the wax-resin mixture to the “bound” configuration until the quantity of approx. 120 g/m^2 found in the impregnated textile was reached, by gradually repeating the procedures used for lining. This configuration was therefore defined as “emulated”. This time-consuming procedure was necessary in order to have enough material for mechanical testing, with homogeneous characteristics (Table 27).

material weight (g/sqm)	***clean***	***bound***	***emulated***
mockup lining canvas	380	466	589
sample painting	693	801	

Table 27 Weight of the textiles with the different quantities of the wax resin mixture

6.2.3 The tensile tests

As described in chapter 5, all specimens were laser cut to the sample shape required for the tensile tester. Biaxial samples were cut into a cruciform shape providing a sharp 10x10 mm test area, which extends into 5x10 mm arms on each side to be used for clamping. A small V-shaped indentation is cut in the clamping areas corresponding to the weft in order to keep the information in the otherwise symmetrical sample (as seen in Figure 10, chapter 3). The uniaxial samples are simple 20x10 mm strips, with the same V-shaped indentation if aligned with the weft, or with a semicircular one if prepared along the warp.

As seen in chapter 4, the tensile tester is equipped with two pairs of actuators, motors that move a load cell and a sample clamp for each axis (Figure 82a). Their simultaneous motion ensures that the center of the cruciform sample always remains in the same position throughout the test, while the four ends are moving. Homogeneous distribution of the tension in the sample at the beginning of each test is granted thanks to the pre-tensioning procedure. This is based on micrometric displacements of the four actuators, in laps, until the four load cells read the same target value (Figure 43). The use of four load cells also allows anomalies to be read during the tensile test, and the mean value

of the pair of opposing load cells provides the value for each axis. Uniaxial tests performed with the device are instead equal to the standard tensile procedures, with the only difference that the overall motion and speed are divided between the two opposing motors. Measuring the tensile response of the two axes simultaneously makes testing conditions closer to those of a painting on stretcher. This is because biaxial testing also measures the interaction of the yarns in the two directions, an information that is lost in uniaxial tests (as discussed in chapters 2, 4 and 5). Tests were performed at the speed of 2 mm/min, or 1 mm/min for each actuator.

6.2.4 The new flexural testing tower and the flexural tests

The flexural experimental setup is based on the use of only one of the four actuators, applying orthogonal force at the center of the sample while it is resting on a support allowing it to bend from two fixed points in a "three-point bending" procedure. A flexural testing tower was designed and built, that holds the sample in front of the two supports, while standing free of constraints on the sample rest, and a steel plate moves perpendicular to its center at the speed of 0.5 mm/min, reaching it with a rounded contact blade parallel to its surface (Figure 82b and Figure 83). In order to meet the testing standard requirements for the ratios between length, width and thickness of the material (ASTM D 790 – 07), slightly bigger samples were needed, measuring 26x55 mm[102]. The thickness of 1,83 mm proved to be enough to meet the requirements of the standard procedure. The ASTM standard is designed for use with Universal Testing Machines, in which the load is applied vertically against a horizontal beam. The flexural testing tower keeps the sample vertical against the supports as the actuators of the biaxial tensile tester, that move horizontally. The influence of gravity appears nevertheless neglectable, what allows considering the procedure equivalent to the ASTM standard for this particular application.

[102] According to ASTM D 790 – 07, for plastic materials at least 1.6 mm thick, a minimum ratio of 16 between the length (including the overhangs after the supports) and the thickness of the sample is required, while the width needs to be at least twice the thickness. Samples for the flexural tests were 55 mm long, 1.83 mm thick and 26 mm wide; the distance between the supports on the flexural tower (fixed in the center of the device) is 47.4 mm. Therefore, the sample dimensions fully comply with the geometric requirements set by ASTM D790 – 07, ensuring that the specimen is primarily under bending stress rather than shear.

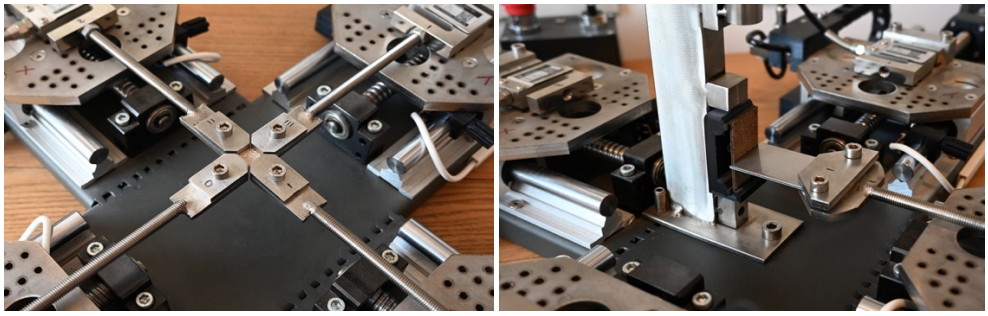

a *b*

Figure 82 The biaxial tester clamps (a); the flexural tower holding the sample vertical against one of the actuators (b)

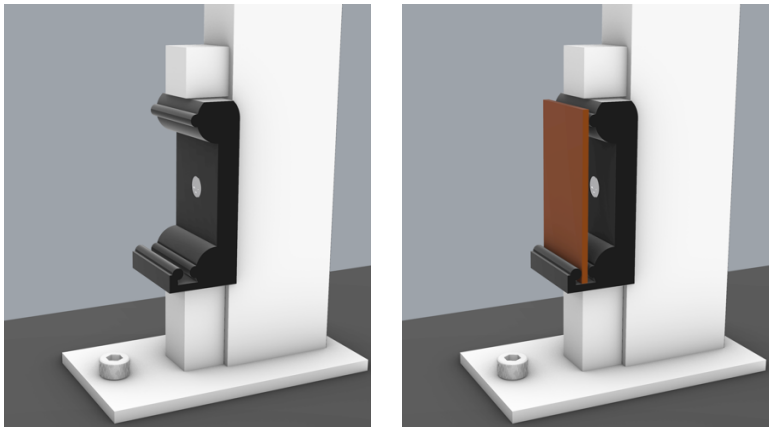

Figure 83 CAD design of the flexural tower holding the sample vertical in front of the two supports

6.2.5 The tensile and flexural moduli

The definition and use of the tensile modulus (*E*) was already introduced in chapters 4 and 5, as the ratio between stress and strain (*E=stress/strain*) where *stress=force/area* (the tensile force acting on the area of the cross section of the sample) and *strain=elongation/length* (the difference in length due to the test, divided by the initial length). So, if stress is a description of the force acting on the sample, strain provides an indication of the response of the sample to that force and this makes *E* a key factor in materials engineering. A high value of *E* describes a material with a high resistance to deformation, and a low value of strain indicates that a given force has little effect on the material being tested. The standard equation for *E* modulus is recalled here, where *F* is the force, *w* is the sample width, *h* is its thickness, L_0 the initial length and L_f the elongated length of the sample, in Equation 13:

$$E = \frac{\frac{F}{wh}}{\frac{(Lf - L0)}{L0}}$$

Equation 13 The standard calculation for Elastic modulus

The flexural modulus (E_f) is a special case for *E*, describing the resistance the material offers to bending. The resistance to bending depends on the distance between the two supports (correlated to length of the sample) and the point of application of the force at the center, but also on the thickness of the sample and its width. The standard Equation 14 must therefore include all variables, and *L* is the distance between the supports, *F* is the force, *w* is the width of the sample, *h* is its thickness, *d* is the deflection.

$$E_{flex} = \frac{L^3 F}{4wh^3 d}$$

Equation 14 The standard equation for the Flexural modulus

The two Elastic moduli were calculated according to

Equation 3 and Equation 14 and, considering the complexity of the layered structure, the decision was made to keep it in the form of "object related" *E* modulus described in chapter 5. The structural description of an unlined painting has been treated in previous literature, and the subject analyzed in chapter 5 with several examples, but that of a lined painting is a subject needing further investigation, as no precedent was found in the literature.

6.3 Results and discussion

6.3.1 Morphological data on the textiles

The morphological analysis of the textiles is a useful example to describe the insights and possibilities offered by the new protocols introduced in chapter 3. The lining canvas for the mockup (n. 23) has a thread count of 20 warps and 16 wefts/cm. The data sheet from Claessens website shows that the textile sold today has the slightly different thread-count of 20.5 warps and 14.5 wefts, what still falls within the expected variability (see chapter 3, specifically Table 3 and Figure 18). A general consideration is that the warp count is the backbone of a textile organized on the loom at the beginning of the weaving process, while the number of weft yarns cast during the production can be changed by reducing the frequency of the spool in the shed. As we have seen in chapter 3, a slight reduction of the weft count ensures a cheaper production while not introducing substantial changes in the quality and performance of the canvas.

The observation protocols provided a quantitative insight on their structures. For the naturally aged painting, the thread count sees 10 warps and 9 wefts/cm, crimp, width and thickness of the textile are also very similar in the warp and weft directions, while the twist count (TPM) is 60% higher in the weft direction (see Table 28).

Morphological data on the textiles used to build the mockup						
Yarns described		*Thread count/cm*	*Crimp (%)*	*Twist (TPM)*	*Thickness (mm)*	*Width (mm)*
Mockup lining canvas	***Warp***	20	7,16	181	0,27	0,69
	Weft	16	1,58	262	0,31	0,46
Naturally aged painting	***Warp***	10	3,09	151	0,35	0,77
	Weft	9	2,93	252	0,39	0,63

Table 28 Numerical data on the yarns of the textiles

6.3.2 Tensile response of the materials under biaxial and uniaxial testing

Tensile tests on the materials allow the structure and mechanical behavior of the mockup to be described. All tests were carried out at 20°C (+/- 0.5)[103], and 50% (+/- 5) relative humidity, at the same speed of 2 mm/min on at least 3 samples for each specimen[104]. Samples have the same dimensions (10 mm wide) and gauge length (10,6 mm). Tensile data in Table 29 are taken for the same 1,89% strain, corresponding to the location B of the data in chapter 5 (Figure 62 and Table 10). The choice of a relatively low value of elongation is due to the fact that the overall goal here is to study the tensile response of the mockup in a range of forces not too far from those a painting experiences during treatment, handling and environmental changes. When compared to the secant modulus of the other textiles (Table 10, chapter 5) all values appear to be within the expected range.

In the existing literature, as seen in the section *"The E modulus values in the conservation science literature"* of chapter 5, the values also appear to be within the same range. The comparison must nevertheless take into account that the *E*-modulus value in the literature is the general *E*-modulus, referring to strains closer to C or D rather than to the B (1,89 %) strain chosen here (Figure 84, Figure 60), and are likely to take higher values. Still, in biaxial testing the tensile modulus is generally higher (Table 29) and this is probably compensating for such difference because most of the literature values refer to uniaxial loading. In any case, if the modulus of textiles has very few literature references to compare with, that of painting materials is even more rare, and the value of *E* for naturally aged paintings is not currently available for comparison (two lined and two unlined paintings were tested here, data in Table 26). The data in Table 29 is a clear

[103] Special care was given to the control of temperature, seen the presence of the wax.
[104] With the exception of the "1975 bound wax", for which only one sample was available.

example of the different test results obtained with uniaxial and biaxial loading, and the role of crimp in developing tensile response. Uniaxial tensile tests show 89 times lower response in the warp (because of the high crimp and low twist), and the warp/weft ratio is only 12 in the biaxial tests due to the stiffness transfer between the yarns during simultaneous loading. The phenomenon of crimp transfer, or "crimp interchange" [Behera and Hari, 2010] is clearly seen in Figure 84, where the biaxial testing mitigates the difference in tensile response between warp and weft. The weft yarns complete the decrimping phase well before the warp yarns, reducing the latter's decrimping by creating a rigid constraint in the woven structure. The warp yarns begin to respond to tension earlier, and experience a "stiffness transfer" from the weft yarns, which in turn experience a reduction in tensile response.

test values at B (1,89% strain)	test	direction	**force (N)**	**E (MPa)**	ratio
mockup lining canvas	uniaxial	warp	0,3	2,4	88,67
		weft	29,3	215,4	
mockup lining canvas, bound wax-resin	uniaxial	warp	0,6	4,5	36,80
		weft	23,6	166,4	
mockup lining canvas, emulated wax-resin	uniaxial	warp	2,5	16,1	4,43
		weft	10,9	71,4	
mockup lining canvas	biaxial	warp	2,5	18,0	11,77
		weft	28,8	212,3	
mockup lining canvas, bound wax-resin	biaxial	warp	2,4	17,2	7,82
		weft	19,1	134,9	
mockup lining canvas, emulated wax-resin	biaxial	warp	4,2	27,7	3,24
		weft	13,7	89,8	
painting	uniaxial	warp	26,9	195,2	1,22
		weft	32,9	238,8	
painting	biaxial	warp	16,9	122,9	1,98
		weft	33,6	243,6	
painting, bound wax-resin	biaxial	warp	23,6	166,7	1,54
		weft	36,4	257,5	
complete mockup	biaxial	warp	**35,5**	**102,8**	0,98
		weft	**34,8**	**100,6**	

Table 29 The tensile response and secant tensile modulus at the same 1,89% strain (location B)

6.3.3 The lining canvas

Looking into the behavior of the lining canvas, it is of no surprise that it exhibits very different values in the warp and weft directions. In Figure 84, the plots show the evolution of the tensile response during the elongation of the samples for more detailed information on the mechanical response of the textile, in both uniaxial and biaxial testing,

please refer to Appendix 2. We know that crimp in the warp is much higher than in the weft (7.16 % vs. 1.58 %, Table 28), and in Figure 85 we see the full plot of the uniaxial response in the warp direction. This shows a “pure decrimping behavior” [Kovar, 2011] (as seen in Figure 16, chapter 3) up to the elongation of 0.2 mm, during which almost no response from the textile is measured. A straight-line progression is seen up to about 1.2 mm, with a change in the slope around 1.5 mm suggesting a stiffening due to permanent deformation, and a new straight segment up to about 2.6 mm, when the material starts failing. The total elongation of the weft yarns is much shorter, with a similar slight change in slope at about 0.15 mm instead of 1.5 mm. The decrimping in the weft is also very short, and the tension build up is much steeper also because of higher cohesion provided by the higher twist (262 TPM vs. 181 TPM, Table 28). Such differences in the morphology of warp and weft are relatively common in textiles, as seen in chapters 3 and 5, but still, their rather exceptional value seems to be a special characteristic for this basket weave canvas.

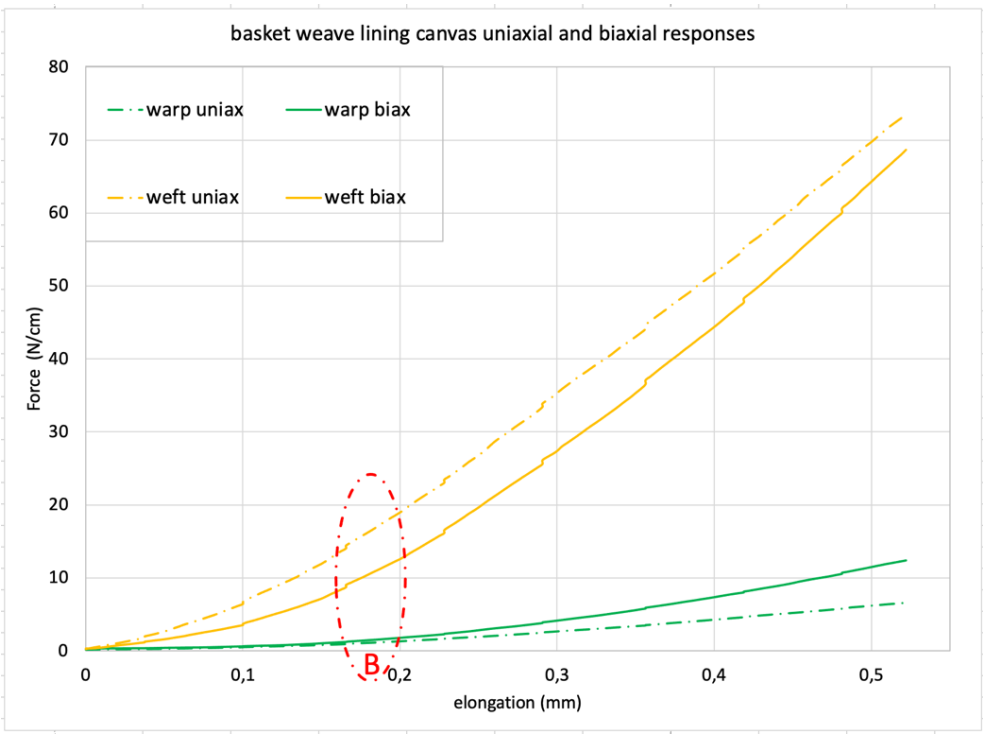

Figure 84 The tensile response of the lining canvas in uniaxial and biaxial tests (specimen 23).

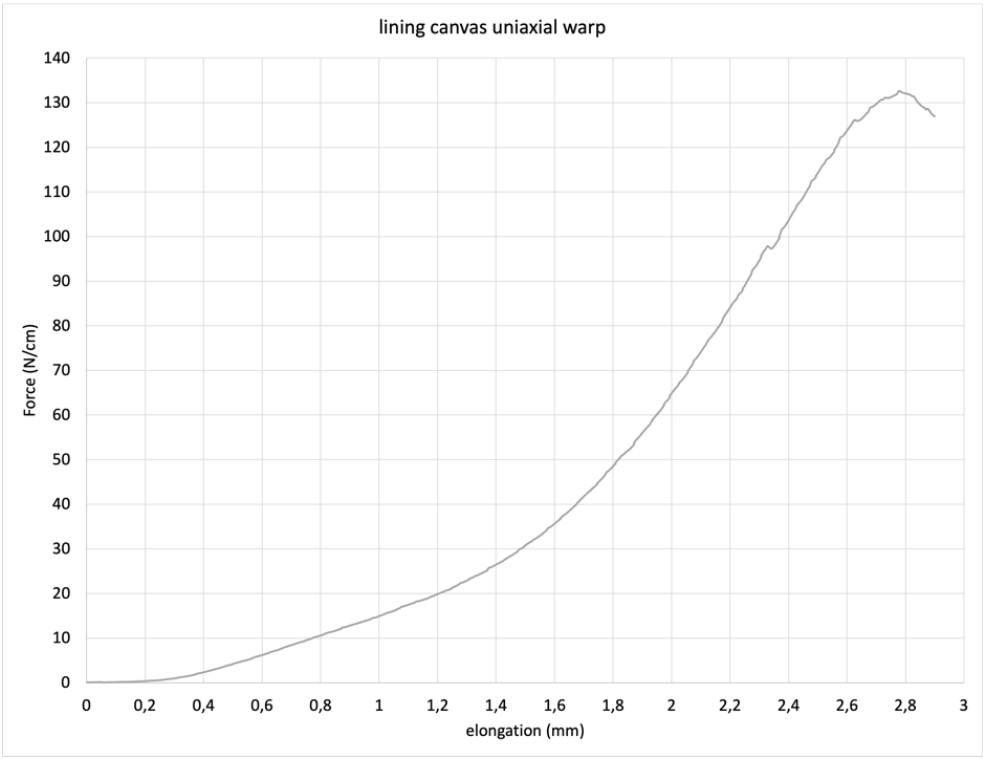

Figure 85 Complete uniaxial plot of the warp tensile response (specimen 23)

6.3.4 The effect of wax-resin on the lining canvas

The ratios between warp and weft in Table 29 show that the presence of the lining adhesive introduces a stiffness transfer also in the uniaxial tests. In the first three lines we see the dramatic reduction of the ratio in uniaxial testing increasing the quantity of adhesive. Looking in more detail, we see that the ratio is reduced because the modulus increases in the warp and decreases in the weft. This also implies that the increase of wax-resin reduces the tensile response of the textile, as the weft reaches a force of 10.9 N (3 times less than of the initial value of 29.3 N) and the warp stays on very low values (though increasing 8 times). The reduction of the tensile modulus is also seen in the biaxial tests (the following three lines in Table 29). It should be noted that the *E* modulus is reduced in the "emulated" configuration also because the thickness of the sample is slightly increased by the addition of wax-resin, and so is that of the cross section.

The information available in the literature on this subject can be summarized in the following three contributions. In [Berger, 1972] we see that impregnation causes chemical degradation of the fibers and a reduction of the mechanical performance of

the textile after artificial aging (what does not apply to the present study). In [Hedley, 1975 **(b)**] five textiles were tested in three conditions: samples uniaxially tested in warp, in weft and at 45°. Tests were repeated after impregnation, and the stiffness was found to be increased in the initial region (strain about 2%, as in our B secant modulus). Another relevant result of that research is that the difference of the tensile response between the three tensile conditions was reduced after impregnation, witnessing a more isotropic behavior of the textile. In [Tassinari, 1973 **(a)**] we see that the impregnation produces an increase of the stiffness and the ultimate load of the four textiles tested, in both the warp and weft directions. The results in Table 29 seem therefore to be proposing a relatively unexpected behavior, possibly due to the uncommonly high difference in crimp between the warp and weft direction of the textile.

6.3.5 The naturally aged painting

In Table 28 we see that the 17th century canvas of the painting fragment has relatively low crimp, and the warp and weft yarns share similar values for most of the measured characteristics. It is therefore no surprise that the tensile response of the naturally aged painting shows less difference between warp and weft, in both uniaxial and biaxial tests, if compared with the two lining canvases. The preparation and paint layers seem to have relevant influence on its mechanical behavior, since the values of force and of the *E* modulus do not show significative variations due to the wax-resin impregnation. It seems interesting to note that the presence of the "bound" wax-resin acts in this case as a consolidant, slightly improving the mechanical performance in the warp direction.

6.3.6 Mechanical response of the mockup and calculation of its elastic moduli

The plots in Figure 86 describe the tensile behavior of the mockup, which is almost identical in warp and weft up to a tension of 45 N/cm (in the area identified as strain C), where they start diverging slightly. The orthotropic tensile response of the lining canvas is mitigated by the presence of the lining adhesive and is stabilized by the superpositions in the layered structure, as the ratio becomes close to 1 (Table 29).

If, as stated in chapter 5, a straight-line tensile plot for such a complex composite structure does not guarantee a reversible elastic response, as if it were a homogeneous elastic material, a reversible elastic behavior seems to be extremely likely for the initial part of the plot. The tension values typically used for canvas paintings is located at the very beginning of the straight-line behavior of the mockup, if we consider that the Maximum Useful Tension (about 2.5 N/cm, chapter 2, Figure 8). For the mockup, MUT

corresponds to the very low strain value of 0.13%, approx. 3 times smaller[105] than the strain at the location A for the tests listed in chapter 5, Table 10.

Analyzing Table 29 more in detail, we see that the biaxial tensile response of the mockup (35.5 N and 34.8 N) is higher than that of the lining canvas alone (2.5 N and 28.8 N)[106]. This may imply that the 17th c. painting contributes to the stabilization of the sandwich, since the wax resin impregnation is found to reduce the tensile response of the lining canvas. But the increased isotropy, tensile response and overall tensile modulus may also be due to the stratification and superposition of the materials.

In conclusion, as the warp and weft values are very similar, the mockup can be considered as isotropic in the plane, with the "object related" secant tensile modulus in B of 102,8 MPa in warp and 100,6 MPa in weft (and a mean value of 101.7 MPa).

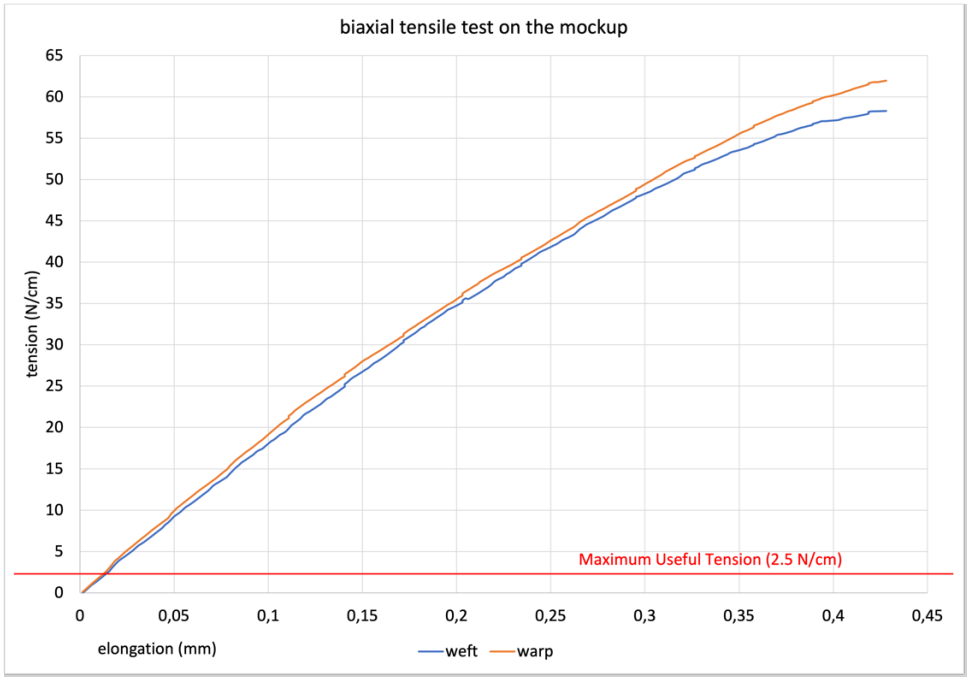

Figure 86 The biaxial tensile results: load-elongation curve of warp and weft shows a very similar behavior: curves follow a straight line until 45 N/cm.

[105] The strain of 0.13%, is the elongation of 0.014 mm of the 10.6 mm sample.
[106] As previously discussed, and analyzed in chapter 5, the values of stress (and therefore of the tensile modulus) are less straightforward, though in this case they would allow for very similar conclusions.

The flexural, or bending, tests (Figure 87) allow the value of the flexural modulus of the mockup to be calculated in about 1600 MPa, using Equation 14. The only reference for the flexural modulus of a canvas painting was found in [Chiriboga, 2013], where much lower bending stiffness values were found, because the mockup of an unlined painting was tested, built with a thin and flexible canvas and thin preparation and paint layers.

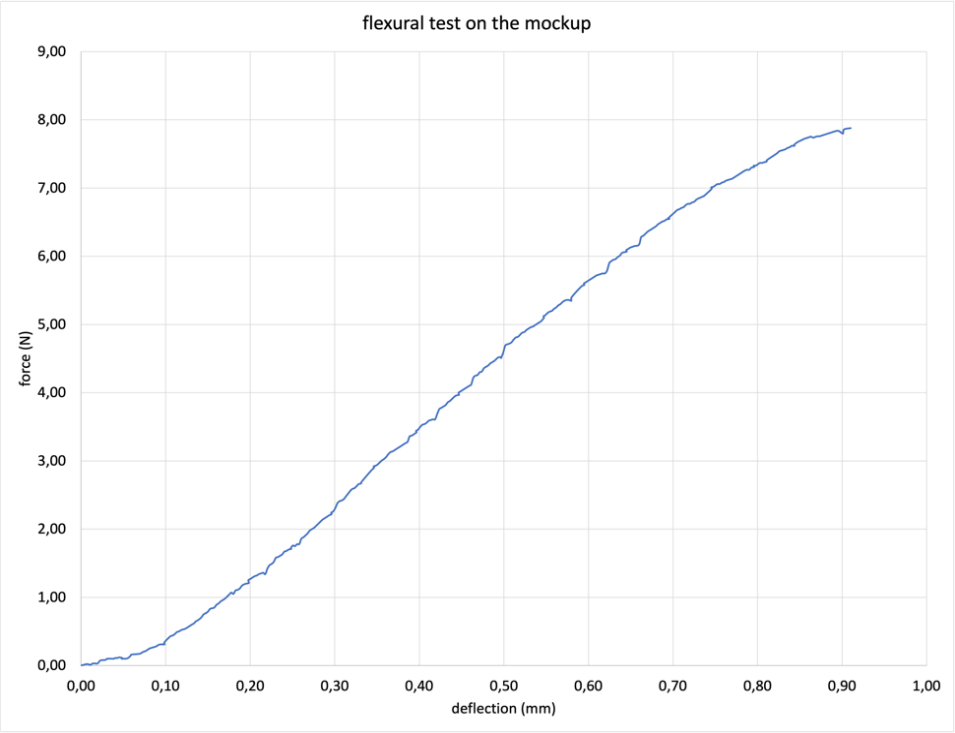

Figure 87 The flexural tests plot showing a wide linear response area

6.3.7 Calculation of the loaded section area of the mockup

In the flexural tests, the force was applied to the verso of the painting, on the side of the lining canvas[107]. The lining canvas is therefore subjected to compression, while the paint layers undergo tensile loading. The lining canvas alone would have very low resistance to compression, but the presence of the lining adhesive stabilizes the yarns and fibers, and a relatively high stiffness can be expected from the wax-resin mixture in the initial phases

[107] This was done to replicate the Displacement Tests that we will see in chapter 7, and those described in [Iaccarino Idelson, 2004 **(b)**].

of compression loading. On the other side of the sandwich, the tensile response of the oil-based preparation and paint layers depends on the pigments they contain, and the tensile modulus can be relatively high in the presence of metal ions [Mecklenburg, 2007]. The flexural test plot Figure 87, after a very short initial stiffening until 0.1 mm deflection, shows a substantially straight-line behavior until about 0.7 mm, progressing rapidly towards a drastic reduction of the resistance to bending, to the point that around the value of 0.9 mm it stops increasing.

To calculate the flexural modulus, we have used Equation 14, obtaining the value of 1600 MPa. No precedent is found in the literature, with the exception of [Chiriboga, 2013] who was dealing with completely different materials and testing methods. But looking into the flexural modulus of other classes of materials this value appears to be in the expected range. The decision was made to keep the flexural modulus as "object related", because reducing the theoretical thickness as done for the tensile modulus, the values become too high. This is due to the highly sensitivity of Equation 14 to the thickness of the material, as it appears at the denominator with a power of 3 ($/h^3$): all possible criteria for the reduction of the thickness lead to unjustifiably high values. To give an example, solving Equation 14 for the equivalent thickness of the lining canvas alone (obtained with Equation 12) we obtain the value of 991 GPa for the flexural modulus, what is clearly out of range, since it would be about 5 times than that of steel (E_f 200 GPa). Using an intermediate value, equivalent to the thickness of the two canvases and that of the paint layers, we obtain the E_f of good quality oak wood (20 GPa), still far too high if compared to that of any lined canvas painting. The value of 1600 MPa for the flexural modulus of the mockup seems therefore to be sufficiently backed up and ready to be used for digital engineering simulations and modeling (FEM).

Coming to the tensile modulus, the common approach in engineering and conservation science, is that of using the tensile modulus of the stiffest material in the layered structure, assuming that this will be the one facing the loads [Mecklenburg, 1991]. The lining canvas alone, using Equation 12 as in Table 10 (chapter 5), displays a value of 825 MPa in weft for the secant modulus in B, though in general, the modulus is calculated for strains corresponding to C or D, where the values are higher: 1.14 GPa in C and 1.37 GPa in D. Still, as our tensile tests are conservation related, we can only discuss about the values in B, where the stiffest element is the paint layer of the 17th c. painting, as the original canvas is highly degraded, and the tensile modulus calculated for its thickness is 1271,9 MPa in warp and of 883,2 MPa in weft. If the "object related" tensile modulus of the mockup were instead to be considered (101.7 MPa), the difference from the flexural modulus (1600 MPa) would be unnaturally high. Such a wide difference is typical of materials like sandwich composites, with high modulus outer layers kept at a distance by a softer core material, where a high bending stiffness is obtained thanks to the overall thickness, and the case does not apply to a lined canvas.

The problem finds a simpler solution when considering the previous research described in chapter 5, though literature data about the tensile modulus of paintings is extremely rare (in chapter 5 we find scattered data in Table 21, Table 22 and Table 26). In [Dings, 2022] the range of tensile modulus used for *The Night Watch* is between 0.3 and 7 GPa, obtaining a match with the painting's deformations in the FEM. The tensile modulus of textiles alone often exceeds 1 GPa [Young, 1996 **(a)** and **(b)**; Chiriboga, 2013]. Defining the tensile modulus of about 1.5 GPa for a painting similar to the mockup, including the contribution of the paint layers, seems therefore very reasonable and would solve the problem of the exceeding difference from the flexural modulus. The data in Table 29 show a very isotropic biaxial tensile response of the lined paintings, and both the paste glue and the wax-resin lined ratios are close to 1. The complete mockup (see Table 29) shows a 0.98 ratio, what seems to be related to the lining adhesive (the clean lining textile has a biaxial ratio of 11.77 that becomes 3.24 after impregnation), and even more so to the stratification including the painting. It therefore seems very reasonable to expect an isotropic tensile response from a lined painting in general.

6.4 Conclusions and future work

The tensile and flexural modulus values are key factors in the implementation and use of digital simulations to predict the behavior of a painting. We have seen that such values can only be obtained using destructive mechanical testing as it was done for all the samples in this research. Similar values can be obtained for historical artifacts using nanoindentation (for the paint layers) [Tiennot et al., 2020], or microtensile testing (for individual fibers or yarns) [Maraghechi et al., 2023 **(a)**], methods that provide information about a small detail of the artwork that needs to be scaled up to the real-life size.

An alternative approach for future work will be to use a finite element model (FEM) of a painting to reverse-validate the values of the elastic moduli. The FEM must incorporate all relevant forces and boundary conditions and be capable of reproducing the painting's mechanical response under varying loading conditions. In this way, a non-destructive mechanical test can be performed on the actual painting to quantify its response, and the same conditions can be replicated within the FEM. If the elastic modulus values used in the model are accurate, the simulated response will match the behavior observed in the physical object—thus validating the assigned material properties.

Chapter 7 Investigating the mechanical behavior of *The Night Watch*

Outline of the chapter

7.1 Introduction
7.2 The choice of an elastic system for the structural conservation of The Night Watch
7.3 The elastic strainer for The Night Watch
7.4 Displacement testing of The Night Watch
7.5 Conclusions

7.1 Introduction

This chapter presents the mechanical testing and treatment performed on Rembrandt van Rijn's 1642 large-format canvas painting known as *The Night Watch*[108], as part the "Operation Night Watch", a large research and conservation project started by the Rijksmuseum Amsterdam in 2019, dealing with the study and conservation of the painting. As part of this project structural treatment of the painting took place between January and March 2022. In March 2022, a new elastic strainer replaced the existing wooden stretcher, and this is briefly described here to provide context.

The main scientific objective of the research presented in this chapter is the acquisition of quantitative data describing the mechanical behavior of *The Night Watch.* This will provide structural information that may be used to determine the painting's tensile and flexural moduli, as well as its tension on stretcher prior to treatment. The research employs a non-destructive testing method that measures the painting's mechanical response to an out-of-plane force applied to its surface. These measurements not only support the assessment of the required force on the strainer, but also lay the groundwork for future investigations, as outlined in the "Conclusions and Future Work" section at the end of the chapter.

7.2 The choice of an elastic system for the structural conservation of The Night Watch

The Night Watch is Rembrandt's largest existing canvas painting measuring 379 x 453 cm[109]. Its conservation history is complex, starting from the transfer of the painting to

[108] The full name of the painting is: "Officers and other civic guardsmen of District II in Amsterdam, under the command of Captain Frans Banninck Cocq and Lieutenant Willem van Ruytenburch". The large oil painting (before the start of the structural treatment measured: 379.5 x 453.5 cm) is on loan to the Rijksmuseum from the City of Amsterdam since 1808, with the inv. no SK-C-5.

[109] The original canvas, which now measures 362 x 428 cm, was originally was originally larger, approx. 4 x 5 m.

the Amsterdam Town Hall in 1715, that involved trimming the perimeter to a slightly smaller size. The painting was lined at least four times, first with paste glue and, in 1851, 1945 and 1975, with wax-resin. This was done with a well-documented wax-resin treatment [Kuiper and Hesterman, 1976] using a seamless "basket weave" (two warp over two weft yarns) pure linen canvas. The painting was mounted with a double row of steel nails on a wooden stretcher weighing approx. 103 kg[110]. For reasons most probably related to environmental changes and handling, the tension of the painting on the stretcher became insufficient and deformations appeared. When the picture was on display in the Philips Wing of the Rijksmuseum during the renovation of the museum (2003-2013), deformations were noticed in the painting: sagging of the lower part of the painting and pronounced diagonal undulations in the upper left corner were clearly visible (Figure 88). The exact reasons causing the appearance of the distortions are still unclear, but studies like [Krarup et al, 2014; Gregers-Høegh et al, 2019], show that wax-resin impregnation favors creep and does not hinder the moisture take-up of the textile, what may become a problem in situations of high environmental humidity[111], though it has not been the case for the Rijksmuseum in recent times.

[110] This information, as well as the measures of the painting, was supplied by the Rijksmuseum conservation team, in particular by Lisette Vos, Anna Krekeler and Petria Noble, on November 3, 2021.
[111] L. Dings [Dings, 2022] describes the deformations as correlated to the differential expansion and contraction of the stretcher and canvas from environmental changes in the galleries. Master Thesis, Technical University of Eindhoven, 2022, under the supervision of Suiker, A. S. J., Bosco, E. Noble, P., Keune, K.

Figure 88 The diagonal undulations in the upper left corner before the structural treatment. (credit: Rijksmuseum Amsterdam)

During the research phase of Operation Night Watch (2019-2021), the Rijksmuseum investigated the material aspects of the painting and explored possible treatment options. To make an informed decision regarding the structural treatment it was crucial for the conservators to assess the condition of the lining canvas. The wax-resin mixture showed no sign of deterioration and the adhesion of the lining canvas appeared good, under visual and manual inspection. This was further confirmed by shearography measurements conducted in key areas in 2021, which demonstrated proper adhesion between the lining canvas and the painting [Tao et al., 2023], thus supporting the decision to rule out another relining of *The Night Watch*. The knowledge that no local treatment could address the sagging in the lower part of the painting, and that the wooden stretcher was contributing to the deformations locking it in an unbalanced

distribution of tensions [112], favored the decision to proceed with a new tensioning system. As seen in chapter 2, Pieneman's "The Battle of Waterloo", a painting almost three times as large [113], was a successful precedent of an oversize wax-resin lined paintings [Sozzani et al., 2013]. The new elastic tensioning system, designed by Anna Krekeler, Lisette Vos, Petria Noble and Antonio Iaccarino Idelson, like that used for the "The Battle of Waterloo" allows measuring the forces acting between the painting and the springs, and therefore the tension value can be precisely quantified. The choice of the value of tension was based on previous research and experience (see chapter 2).

7.3 The elastic strainer for The Night Watch

The new strainer for *The Night Watch* is made in aluminum, for its stability and light weight, and is designed with a lattice structure with reinforced screw connections in order to maximize torsional and flexural rigidity. Strainer design was assisted with a FEM simulation[114], so that predictions could be made about its deformation under the loads resulting from the elastic tension and the weight of the painting, initially estimated at 35 kg. The crossbars need to be removable to allow complete inspection of the reverse of the painting, therefore the 484 cm long top horizontal element, bearing most of the weight of the painting, is not supported and its inflection was quantified using the FEM. The perimeter of the lining canvas was flattened, a narrow pocket was sewn along its outer edges to house a stainless-steel rod. The diameter of the rod (5 mm) provides enough bending stiffness to evenly distribute the loads between the points of connection to the springs, spaced about 20 cm. These are connected using thin steel wires, at 90° angles on grooved ball bearings, in order have them parallel to the rod and therefore reduce the space needed to house them on the strainer. The tensioning system is therefor built on the same plane as the paint layers[115], and the lining canvas is not bent over the stretcher profile, as the painting is on the front of the strainer. Such solution is normally used for the elastic tension of double-sided paintings or banners [Iaccarino Idelson and Serino, 2021], it implies that the strainer is larger than the painting, what also allows the display or inspection of the reverse. The solution allows the virtual

---

[112] After the removal of the stretcher, strong tensions were found to be existing within the wooden elements.

[113] *The Battle of Waterloo* was stretched in August 2012 and measures 46.7 m^2, *The Night Watch* is 17.5 m^2. The project is described in more detail in chapter 2, and the choice of tension is in the paragraph "boundaries for the choice of tension" again in chapter 2.

[114] The strainer was designed by Antonio Iaccarino Idelson for Equilibrarte srl, with crucial contributions from Anna Krekeler, Lisette Vos and Petria Noble, and the simulation was done by Luca Fattore for Exemplar srl, using Abaqus Simulia, general-purpose Finite Element Analysis software designed to assist engineers to simulate complex real-world problems. By Dassault Systèmes.

[115] The treatment carried out between January and March 2022, and the details of the construction of the new strainer will be described in more detail in a future paper.

elimination of any constraint to the movement of the painting as no friction is involved, and the canvas does not need to bend over the perimeter. The springs being on the front of the strainer, access to the perimeter for monitoring the value of tension and for any future adjustment does not require moving the painting from the wall (see Figure 89).

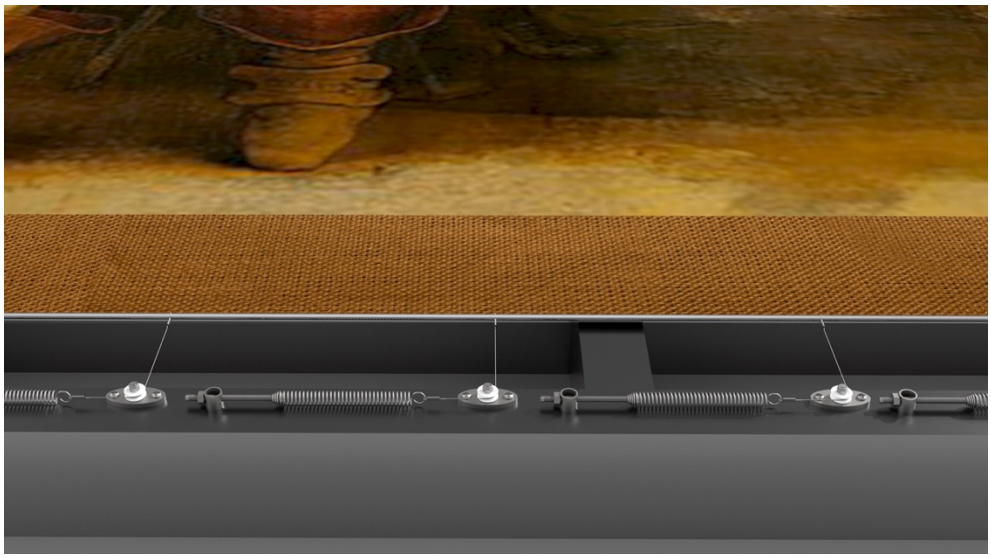

Figure 89 The new strainer with the springs, the wires deflected on grooved ball bearings connected to the rod in the sewn pocket in the lining canvas (rendering by the author)

The custom-made springs[116] have a relatively low elastic constant (1.02 N/mm), allowing stability of tension over time. To give a practical example, let us assume the common case of a 2 mm contraction in the horizontal direction of the painting, for which the tension of 2.4 N/cm has been chosen. Such dimensional variation[117], affects the two identical sets of springs on the vertical sides, 1 mm per side. The average distance between the springs on the vertical sides is 18.5 cm; the 1 mm elongation increases the spring force by 1.02 N, which is distributed over the 18.5 cm producing an almost negligible change of tension, from 2.4 to 2.455 N/cm. The own weight of *The Night Watch* plays a significant role in the distribution of tension, as the gravity loads are concentrated on the upper part and margin of the painting. To compensate for the weight of the painting, it was necessary to apply 0.7 N/cm more tension to the springs on the top (2.7 N/cm) than on the bottom side (2.0 N/cm). The difference in force was

[116] Springs are custom made for Equilibrarte, in stainless steel AISI 302, by Mollificio Ciullo s.r.l., Roma Italy. https://www.mollificiociullo.com.

[117] An average painting can experience a maximum dimensional variation of about 0.5% (about 22 mm for the horizontal direction) in response to significant environmental variations.

calculated using the spring elongation and the value was obtained by successive approximations, until the painting was stabilized in the expected position on the strainer. The process also provided an additional estimation of the painting's weight[118] in 29.84 kg (or 1705 g/m^2). As we have seen, the force applied to the vertical sides is the average of the two horizontal loads, or 2.4 N/cm. As shown in the previous chapters (see Figure 8 and Figure 9), such values of tension are consistent with previous experience and research.

7.4 Displacement testing of The Night Watch

The amount of tension *The Night Watch* had on the 1975 wooden stretcher could be described as insufficient, and caused evident localized distortions, but no information was available on the actual value of tension. A series of mechanical tests were performed by Iaccarino Idelson and the conservators to establish a correlation between the unknown value of tension and the painting's response to an out of plane force causing its displacement. The procedure is based on the measurement of the amplitude of the displacement caused by a force perpendicular to the plane of the painting using the Displacement Tester – DT – (see Figure 51). The digitally controlled device[119] is used to perform an updated and improved version of the 2002 testing method described in [Iaccarino Idelson, 2004 **(b)**] (see chapter 2). It applies a gentle pressure orthogonal to the lining canvas, providing a quantification of its mechanical response. The force is applied to the reverse of the painting through a spherical contact point, 8 cm in diameter. The DT uses a linear rail to move a load cell towards the painting, at the speed of 0.5 mm/sec, under the impulse of a stepper motor, which is also used to measure the displacement by counting the microsteps (figures 45-46, chapter 4). When the load cell reads a target value in the reaction force from the painting, the device stops and rapidly recovers the initial position away from the painting. The entire process takes a relatively short time (about 5 minutes including the positioning of the machine), and therefore tests were repeated 6 times at each location to achieve a higher statistical significance.

The use of a stepper motor allows very smooth motion, a pre-requisite for low noise force recording, but it also requires a safe target force value to be chosen for the painting.

---

[118] To stabilize the painting's position in the center of the strainer, the springs on the top side need to provide 0.7 N more than the ones on the bottom, for each of the 452 cm of the horizontal rod. The overall force needed to compensate gravity is therefore: 0.7 N/cm * 452cm = 316.4 N corresponding to 32.3 kg including the stainless-steel rods (weigh 154 g/m, for approx. 16m, or 2,46 kg) for a weight of 29,84 kg, or 1705 g/m^2. The alternative estimation of the weight of the lined painting, obtained by the Rijksmuseum conservation team by weighing the different parts, is between 32 and 38 kg.

[119] The device was designed and built in December 2021 by Antonio Iaccarino Idelson and Miguel Sanchez, Ph.D. computer scientist at the Polytechnic University of Valencia, Spain, who also wrote the firmware and software for its operation.

The threshold value was chosen using a second custom-built device[120], a hand-held force sensor device that allows applying a pressure on the reverse of the painting while a display shows the value of force being used at each moment (Figure 52, chapter 4). The DT is clamped to the crossbars and/or to the perimeter of the stretcher with the painting standing upright, supported by the holder so as to reduce vibrations. The force involved in the test is low enough that any deformation in the stretcher (and in the strainer) due to the interaction with the DT action can be considered neglectable with regard to the precision of the displacement measurements. The output of the DT operating software is a series of data pairs, aligned with a time clock, representing the force acting on the load cell and the distance of the probe from the initial position. The system is sensitive enough to detect fluctuations in force caused by airflow from the air conditioning system, which causes imperceptible movement of the painting[121].

The first series of DT tests was performed in January 2022, when the painting was still on 1975 wooden stretcher. Measurements were carried out at 48 measurement points, 8 in each of the 6 rectangular spaces defined by the crossbars of the stretcher (Figure 90). Locations were divided in four groups: group A, 6 points around the center of the horizontal crossbar; group B, 16 points distributed in a ring zone around group A; group C, 12 points clamping the DT at 45° between the cross bar and the perimeter; group D, 14 points clamping the DT along the perimeter. The progression from group A to group D is about an increasing mechanical limitation due to the proximity of the stretcher. The displacement is mostly a function of the distance from the perimeter and of the value of tension, because the mechanical characteristics of the painting can be assumed as relatively constant, with few exceptions. Differences may be expected due to the different thickness of the impasto, to local accumulations of the wax-resin during the 1975 lining, and of course to the deformations existing in the painting.

[120] The hand-held pressure measuring device was designed and built by Antonio Iaccarino Idelson.
[121] Plots waviness accounts for the sensitivity of the load cell to minimal variations of the force opposed by the painting during the travel of the probe's end, due to the almost imperceptible air currents in the exhibition room. Tests performed in the perimeter of the painting are straighter than the ones in the center because of the stabilization offered by the proximity of the strainer.

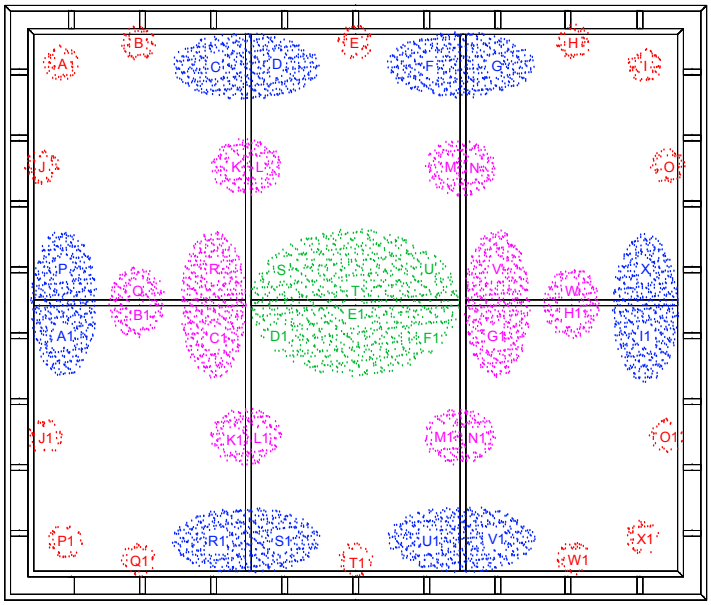

Figure 90 The 48 measurement points on The Night Watch divided in groups identified with a color: A in green, B in magenta, C in blue, D in red. The crossbars have the same pattern on the wooden stretcher and on the new elastic strainer.

The plots in Figure 91 show the response of the painting in selected locations. The “top mid” point (E in Figure 91) is the one exhibiting the steepest slope and an almost straight-line response, because the proximity of a physical boundary (the wooden stretcher or the elastic strainer, as we will see in Figure 92) implies an unfavorable leverage in the action of the DT, and this is confirmed by the similar plot in the symmetric “bottom mid” (T1 in Figure 91). The difference in slope between the two points of application of the DT (E and T1) shows effect of the gravity along the upper edge, where the slope is steeper because of such additional tension. The “undistorted right side” (J in Figure 91) point shows a curved section indicating lower tension on the stretcher and a tension build-up until, around 3 N, the behavior becomes similar to the previous two points since the curve is almost parallel. The symmetric point, “distorted left side” (O in Figure 91) has a very different behavior because the spherical contact end of the DT is reaching the distorted area in a location where a convex bend was present in the painting. Therefore, the curve is initially steeper than in J until the bend in the painting is reverted, between 3 and 4 N, and the slope of the curve becomes parallel to that of the symmetric point J. The last curve, corresponding to the center of the painting, shows a very low slope at the beginning, and a very wide displacement (23 mm) at the maximum force. The other interesting characteristic of this curve is that it shows very visible random undulations,

due to the airflow in the exhibition room. These are the very small variations of the force read by the load cell due to the air flowing on the painting, and become less visible as the force applied by the DT increases tension in *The Night Watch*, thus reducing its mobility.

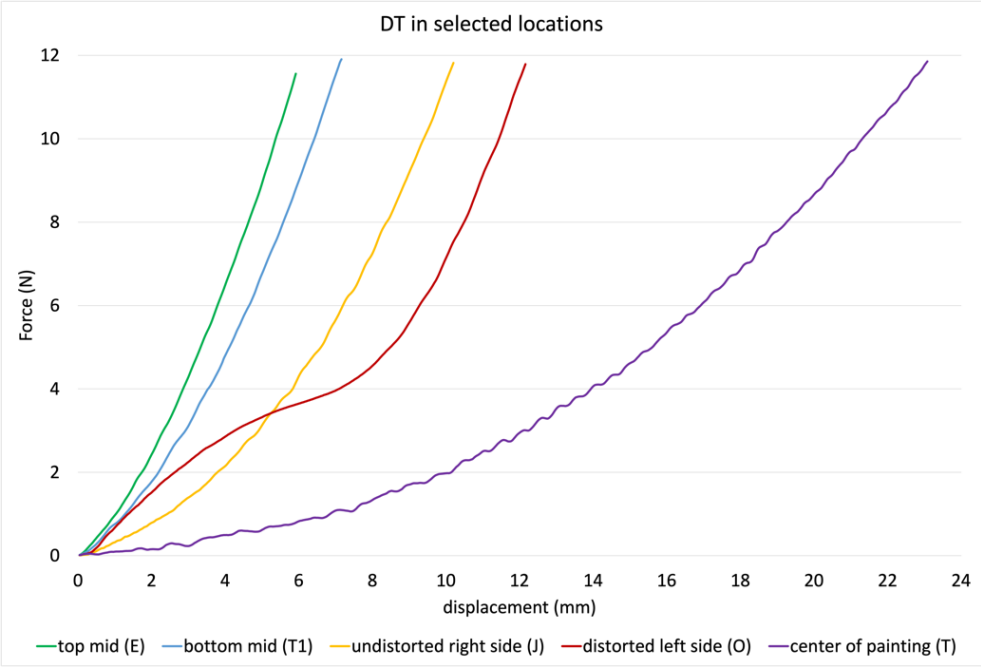

Figure 91 Force readings on The Night Watch on the 1975 stretcher in 5 selected locations

The tests were repeated in April 2022 when the painting was on new strainer, with the aim of obtaining the same information under known tension conditions. In Figure 92 we see the comparison of the plots at the same point T in the center of *The Night Watch* (seen in Figure 91), obtained during the two campaigns. Under elastic tension, the displacement of 18.5 mm is measured for the target response of 12 N, against the 23 mm on the wooden stretcher. A first level of interpretation of this difference is that it describes the quantified value of tension on the elastic strainer as slightly higher than that on the rigid stretcher, what appears to be an interesting information, even without delving into the underlying reasons for selecting this specific tension value (seen chapter 2, Figure 8 and Figure 9). The difference in the two plots until the force of 4 N, and the fact that after this value they become parallel, provides useful insight about the difference between the two tensioning systems. As we have seen analyzing the plots in Figure 91, the DT is causing a buildup of tension during the first part of the test on the wooden stretcher, but this appears to be almost neglectable in the tests on the elastic strainer, where the plot appears much straighter, since the very beginning. The different

behavior of the painting until 4 N is the consequence of the difference in tension, since the material properties of the painting are unchanged, and so is the museum environment.

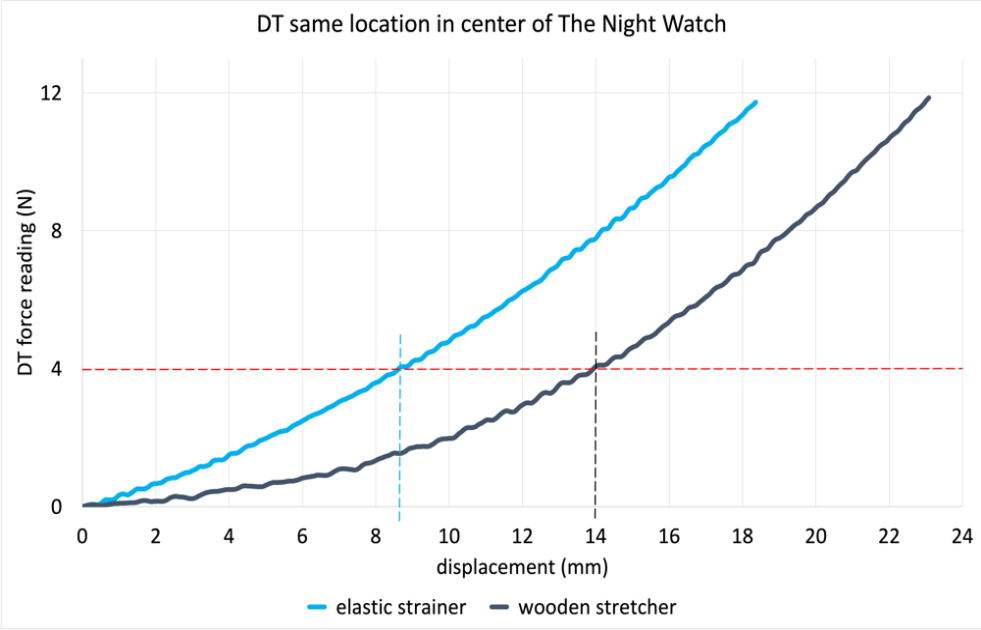

Figure 92 Comparison of the force readings in the displacement tests on the wooden stretcher and on the elastic strainer in the center of The Night Watch

In Figure 93 we see the 48 DT plots obtained during the second campaign, on the elastic strainer. From right to left, we see the tests in group A (around the center of the painting, plotted in green), then those in the groups B, C and D, progressing towards the perimeter and showing the painting's increasing resistance to displacement. As seen in Figure 90, the measurement points are chosen as a function of repeatable locations on the stretcher bars and crossbars, rather than of rigorously homogeneous distances from the perimeter or from the center, and the groups were created to simplify the description of the different responses. The dispersion in the plots in each group depends on the actual distance from the perimeter. The very low dispersion showed by group A seems to be due to the fact that the change of location happens mostly along a horizontal direction about the center, and the distance from the perimeter is compensated by the rectangular shape of the painting. The points in group C, also showing low dispersion, are located at a homogeneous distance, and are far from the corners, where slight differences in the behavior can be expected. Group B has a less homogeneous distance causing higher dispersion. The response of the painting in Group D seems to be influenced by less predictable factors, as the local variability in the structure of the

painting or thickness of the wax-resin layer, since they are located right along the edge. As we have seen in Figure 91, the proximity of the physical boundary implies an unfavorable leverage and a steeper slope in the test plot, but also an amplification of the sensitivity of the test to minor local differences, and this remains true notwithstanding the different tensioning conditions.

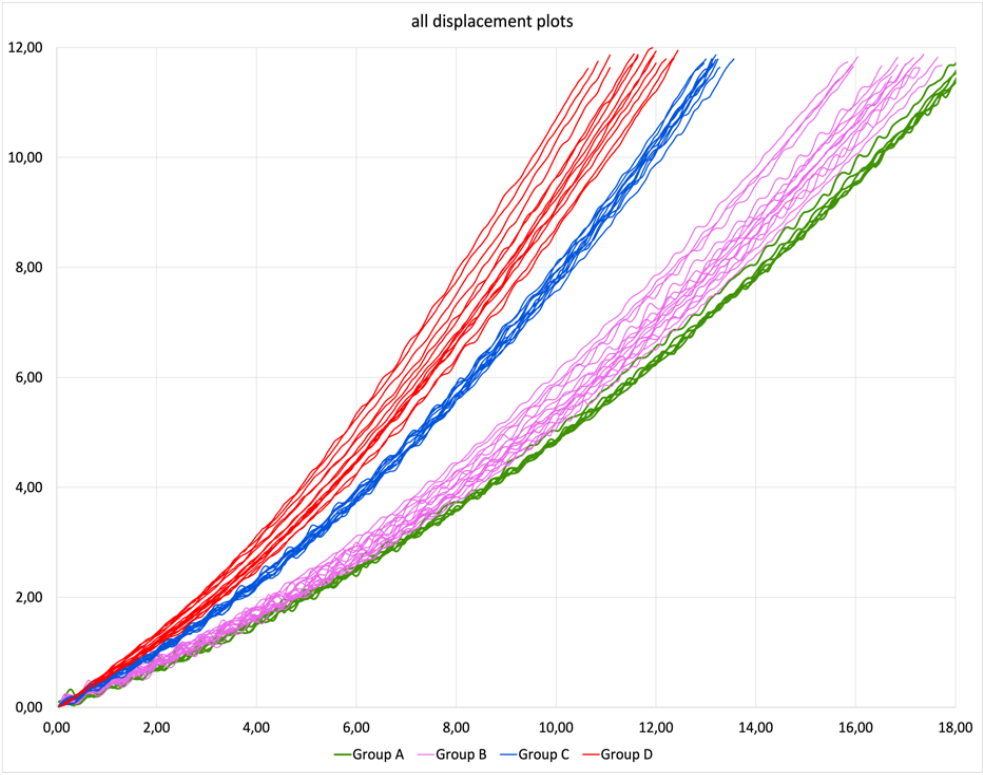

Figure 93 The force/displacement plots of the of The Night Watch on its elastic strainer. Groups identified with a color: A in green, B in magenta, C in blue, D in red

7.5 Conclusions

The DT test data (two series of 48 plots resulting from the mean of 6 DT tests each) describe the mechanical behavior of the painting as a function of its material properties and tension on stretcher. Their differences allow analyzing the effect of the tension and boundary conditions on the wooden stretcher and on the elastic strainer. As the elastic tensioning system provides quantified and precisely described boundary conditions, an FE model of the painting on the elastic strainer can be implemented, to reproduce the DT tests at the same locations. The model will allow analyzing the correspondence with

the experimental data[122], providing an innovative, non-destructive approach to the quantification of the material properties of a canvas painting.

A first level of approximation for the tensile and flexural moduli of the painting is provided by the work done with the mockup of a wax-resin lined painting (about 1.5 GPa for the tensile modulus, and 1.6 GPa for the flexural modulus). Nevertheless, as we have seen in chapters 5 and 6, determining the elastic moduli for a painting, be it lined or unlined, still represents an open problem in conservation science. As we know by now, the very definition of elastic modulus relies on the assumption that a material is homogeneous and responds to specific loads in a fully elastic and reversible manner, and such assumption is difficult to apply to complex composite structures such as canvas paintings. This clearly represents one of the main obstacles to developing reliable predictive models of their mechanical behavior. Chapter 5 and Appendix 1 are entirely dedicated to exploring different approaches to define the loading area used in stress calculations for textiles. The resulting tensile modulus values for the simple textile are highly dependent on the method employed and this is clearly described there. As structural complexity increases, through the addition of ground and paint layers, and especially with the presence of a lining canvas and adhesive, current methods become increasingly approximate. To date, no reference data have been found in the literature for the tensile modulus of similarly complex structures, see Chapter 5. A tentative overall approach to the problem is delineated in Chapter 6.

The displacement tests introduced in this chapter offer a non-destructive alternative for quantifying the response of a painting to external forces, and interpreting the resulting quantitative data requires a dedicated theoretical and experimental framework, typically supported by finite element method (FEM) software. The use of an elastic strainer provides detailed data on the geometry, tension, and boundary conditions, while the remaining characteristics of the painting (weight and thickness) can be estimated with reasonable accuracy. With all this information available, it becomes possible to solve the multivariable equation required to determine the painting's elastic moduli through the results of the DT tests.

A quantitative correlation between the value of tension of *The Night Watch* and its measurable effects is therefore established, providing information relevant to conservation practice and conservation science.

---

[122] A test version of the FE model has been developed by Luca Fattore with the collaboration of Antonio Iaccarino Idelson.

Chapter 8 Conservation treatment of Tiepolo's "Juno in the clouds", assisted by structural testing, at the Louvre Museum Paris.

Outline of the chapter

8.1 Introduction
8.2 The painting and its conservation needs
- 8.2.1 The possibility of using a rigid panel
- 8.2.2 The need for a new lining

8.3 Introduction to the lining method and to treatment reproducibility
- 8.3.1 The first phase of the structural intervention
- 8.3.2 The support fabric

8.4 Mechanical tests on the materials
- 8.4.1 tensile tests
- 8.4.2 The cold and dry lining method, characterized by peel tests

8.5 The elastic system
8.6 Conclusions

8.1 Introduction

In this chapter I will introduce the conservation treatment of a detached wall painting transferred to canvas in 1901. This is part of the mechanical and material characterization of canvas paintings, and extends the process to the aspects more directly connected to interventive conservation, and has recently been published [Iaccarino Idelson, 2025 **(b)**]. Among the main goals of this process is that of proving the simple fact that a precise quantification of the materials and processes used in conservation practice is an unreplaceable and necessary prerequisite to learn from experience and make it repeatable, and to draw conclusions for future choices. In this case, the quantification also included the materials used for the intervention and the effect produced by specific operating techniques. The biaxial tester was used to measure the mechanical tensile response of the materials under uniaxial and biaxial loads. The lining fabric was tested and compare them with those of the mockup, which is designed to mimic the structure and adhesion surface of the painting at the interface with the lining. The portable uniaxial tester was used to measure the bond strength achieved in the lining with peel tests. Both devices are described in chapter 4.

8.2 The painting and its conservation needs

Gianbattista Tiepolo (Venice, 1696- Madrid, 1770) painted "Juno in the clouds", in a ceiling of the Sagredo Palace in Venice in 1735, a wall painting in the best “fresco” technique. In 1901, the painting was removed from the wall and placed on canvas with a wooden strainer by the Steffanoni, a family and a team of restorers who specialized in detachment of wall paintings and operated in the whole Europe. The painting was

acquired in 2020 by the Louvre Museum, and the “Cercle des mécènes de la Société des Amis du Louvre” financed its conservation in view of its permanent exhibition in the museum premises.

The strainer on which the painting has come down to us is a wooden[123] grid on which the canvases used to support the painting are placed. As canvases are quite flexible, and most of the materials involved are sensitive to thermo-hygrometric variations in the environment, the problem of paint stability and flatness has always been considered critical. The tendency of the laminated textile system to creep, and the fragility of the paint layers, make it impossible to pull the canvas in tension on a stretcher, but for the same reason tensioning would not have offered a lasting solution in any case. The wooden structure consists of an elliptic perimeter with numerous crossbars (15 on the long axis of the ellipses, 9 on the short) at a distance of about 15 cm, to provide distributed support over the entire surface. To ensure connection across the entire surface, small pieces of fabric are glued in all the spaces between the crosspieces, between the canvas and the wooden structure (in this case, about 280 glued strips were used). It is therefore an artifact of considerable historical importance.

8.2.1 The possibility of using a rigid panel

For similar cases it has become normal, since the 1970s [Mora et al., 1984], to replace the wooden structure with a panel in composite material. Such a choice would certainly have restored the painting to a structural configuration closer to that of the mural still in situ, because it proposes a continuous rigid reference similar to a wall. But the painting's considerable dimensions would have led to flexibility concerns, as any flexing of the support would have been directly reflected on the paint layers, attached to a skin of the composite material. To obtain the necessary rigidity, the panel would have had to be reinforced with an additional aluminum structure fixed to the back, influencing its weight and thickness. In addition, the adhesion of the painting to a continuous rigid support makes it more difficult to separate it for replacement, hence the need to add a "reversibility" layer that can be acted upon to facilitate its removal during the future treatments. Among the main disadvantages of using a rigid panel was in any case that of the loss of the historical support on which the painting came to us.

The method to conserve the wooden strainer as the rigid reference structure for a new elastic system, as seen in chapter 2, is described here. The very flexible springs[124], absorbing the dimensional variations of the painting and its supporting layers, and those of the wooden structure.

---

[123] Morphological macroscopic identification of the wood describes it as spruce (picea alba).
[124] The same used for The Night Watch, described in chapter 7.

8.2.2 The need for a new lining

The support of the painting was made of a superposition of fabrics: a cotton gauze and a denser canvas laid with calcium caseate, and then a more open-weave lining canvas in linen, glued with paste glue and polyvinyl acetate. The adhesion between such fabrics was compromised, and they were severely distorted following the shape of the wooden grid[125]. Once the canvases were removed from the strainer, it was clear that attempting to restore the flatness of the support while ensuring reliable adhesion to the paint layers appeared to be an approach with little chance of success, and a rather complex one at that. It was therefore decided to replace the backing fabrics with a new lining support.

8.3 Introduction to the lining method and to treatment reproducibility

A cold dry lining method was chosen, a direct evolution of Mehra's methods [Mehra, 1972], involving an interpretation of the "Mist lining" [Seymour and van Och, 2012]. The most innovative practice introduced in the conservation practice by the Mist lining developed at the SRAL in Maastricht is the method used for the reactivation of the adhesive with solvent vapors. The Mist lining procedure is based on two acrylic emulsion adhesives, Plextol K360, whose glass transition temperature of only-9°C makes it tacky on contact when dry, and Plextol D540, more stable and rigid thanks to a Tg of 29°C. This blend of 7 parts K360 and 3 parts D540 was replaced in 2020 by a 50% mixture of K360 and D512 (Tg: 26°C) [Arvind, 2021]. The adhesive mixture is spray applied on the lining textile and let dry. Reactivation is achieved by means of solvent vapors transported inside a low-pressure envelope by a solvent-impregnated fabric, placed in contact with the lining fabric carrying the dry adhesive. This system makes it possible to manage adhesive reactivation over large surfaces, which was not possible with the first declinations of the methods introduced by W. Mehra, even with the use of large quantities of solvent [Mehra, 1975; Phenix and Hedley, 1984].

The system used for Tiepolo is derived from the mist lining with a series of changes, the most important of which is in the substitution of the adhesive blend with a single acrylic dispersion, Plextol B500, characterized by an intermediate Tg of 9°C. The reason for this choice is that the use of K360, is risky in hot climates, as its melting temperature of 40°C results in loss of the adhesive bond and the possibility of migration in the painting if the temperature is higher than the values recommended by Museum Standards. The second change is in the use of a sealed vacuum bag instead of the low-pressure envelope, because a sealed environment allows the user to know the exact quantity of solvent interacting with the lining adhesive and the paint layers, while the low-pressure envelopes are open systems, originally developed to favor evaporation and drying. The

[125] It is at present (August 2024) unfortunately not possible to show images of the painting because they are still unpublished from the Louvre side.

method was developed in 2012 for the restoration of Titian's "David and Goliath" in the sacristy ceiling of the Basilica della Salute in Venice, where temperatures regularly exceed 40°C during the summer months. In this case, a carbon-fiber lining fabric was used on account of its high tensile modulus of elasticity [Iaccarino Idelson et al., 2018]. The third change is that, since then, the various parameters involved in the lining process were recorded in order to construct a reference database. Some of the most significant examples are listed in Table 30.

painting	date	location	dimensions	adhesive	solvent	lining year
Tiziano Vecellio "Davide e Golia"	1544	Venice, Basilica della Salute	8,6 m^2	**110 g/m^2**	**180 g/m^2**	2012
C. Saraceni "Ostensione del sacro chiodo"	1618	Rome, S. Lorenzo in Lucina	5,4 m^2	**100 g/m^2**	**144 g/m^2**	2013
M. Stanzione "Immacolata Concezione"	1643	Pescocostanzo, AQ, Chiesa di Gesù e Maria	1,7 m^2	**90 g/m^2**	**64 g/m^2**	2014
G. Strazza "Trittico verde"	1964	Termoli, MACTE	0,35 m^2	**70 g/m^2**	**65 g/m^2**	2014
Anonymous "Arcangelo e Demoni"	17th c.	Bari, private collection	5,2 m^2	**100 /m^2**	**135 g/m^2**	2015
Mattia Preti "Martirio di S. Lorenzo"	1689	Birgu, Basilica di S. Lorenzo, Malta	24,3 m^2	**120 g/m^2**	**180 g/m^2**	2018
G.B. Tiepolo "Santa Tecla praying"	1758	Este, Duomo di S. Tecla	26,4 m^2	**120 g/m^2**	**180 g/m^2**	2019
A. Capalti "Circoncisione di Cristo"	1841	Rome, Chiesa del Gesù	19,2 m^2	**100 g/m^2**	**180 g/m^2**	2019

Table 30 Lining parameters for selected paintings over the last decade

The influence of the parameters used for this lining method on adhesive bond strength has been studied using peel tests since 2015 [Iaccarino Idelson and Garofalo, 2019]. The aim was to create a database and assign theoretical reference values to the bond strength obtained with the quantities of adhesive and solvent on the same reference substrate (an identical mockup painting). The availability of the new test machines described in chapter 4 has enabled the case study to be extended to other adhesive/solvent couples. The research is continuing, also with a perspective of sharing in teaching[126], and is currently being extended to different adhesives and solvent mixtures to make the method adaptable to a wider variety of paintings and conservation contexts. This approach also offers the possibility of carrying out preliminary tests to make predictions that can guide operational choices on a specific painting conservation treatment. In the case of the Tiepolo, tests were carried out with the materials to be used for the lining, validating the general choices and accurately assessing the balance of forces within the stratified composite structure formed by the painting with its new support canvases, working on a mock-up.

8.3.1 The first phase of the structural intervention

Only the first cotton gauze, in direct contact with the paint layers and completely embedded in the calcium caseate adhesive, shows the necessary adhesion, and is thin

[126] Like the comparative study of 25 different types of lining carried out on the same painting mock-up during a workshop conducted by the author in May 2023 as part of the Getty Conserving Canvas initiative at the National Gallery of Ireland, Dublin, thanks to the use of the new portable uniaxial testing machine seen in chapter 4.

enough to consolidate it and hold in place after all the others have been removed. An acrylic microemulsion[127] was chosen as the consolidant, due to its good penetration in the limited porosity of calcium caseate. As an additional support for the cotton gauze kept in contact with the rear of the paint layers, a thin, lightweight polyester fabric was added[128]. This is also an additional protection in view of the next structural treatment, that will hopefully become necessary in a distant future.

8.3.2 The support fabric

The choice of the support textile influences the transfer of forces, and the stresses to which the paint layers are subjected. The lining fabric needs to be flexible, so that it can bend and slide over the edge of the strainer, but its needs to have a small strain under tension compared to the detached wall painting, which is hard and brittle. For this reason, a fabric with a high tensile modulus was chosen, a triaxial-weave fabric[129] with a 1 mm hexagonal mesh. The fabric consists of three groups of yarns, crossing each other at 60° angles. The warp yarns are aligned with the loom, and the two wefts, more properly defined as “transverse yarns”, are angled. A very thin and light in weight (0.234 mm thick for a weight of 98.6 g/m^2), that was impregnated with epoxy resin[130], using only as much resin as was needed to saturate the fibers[131], while leaving the hexagonal meshes free and empty (Figure 94 and Figure 98). The layering of materials in vacuum lamination is based on the alternation of porous and absorbent materials, to promote the transport of excess resin to the peripheral temporary layers, so that it can be removed with them (Figure 94). In direct contact with the two sides of the polyester fabric is a very fine nylon fabric, called "peel-ply" precisely because of its characteristic of being able to be peeled off, removing the excess resin from the surface[132]. The next layer is a micro-perforated polyethylene release film [133], whose calibrated holes have sufficient diameter and frequency to allow excess resin to pass through, while retaining a sufficient quantity in the triaxial textile fibers. The outer part of the system consists of a highly absorbent polyester non-woven[134] called "breather fabric", in which the excess resin is deposited and which also has the function of distributing the pressure evenly inside the vacuum

---

[127] Acril ME, CTS.

[128] Polyester Delay, thread count: 31 warp and 28 weft/ cm; weight 50 g/sqm, CTS. The textile was adhered with Plextol B500.

[129] Polyester TWF SK-507, Sakase Adteck, Japan. For the Titian painting the carbon fiber TWF SK-802 was chosen, with the same triaxial structure. www.sakase.co.jp/home

[130] Raku-tool EI-2500/EH2970, Rampf tooling GmbH &Co. www.raku-tool.com

[131] The quantity of epoxy resin impregnating the fibers was measured in 67 g/m^2.

[132] Peel ply nylon, 80 g/m^2. Richmond Aerovac. www.aerovac.com

[133] Orange release film A2200, 25µm. Richmond Aerovac. www.aerovac.com

[134] Breather fabric AB100, 150 g/m^2. Richmond Aerovac. www.aerovac.com

bag[135]. This treatment was necessary to join the strips (148 cm wide) and achieve the considerable size of the picture, but also to make the textile more isotropic, as we'll see in the next paragraph, and in particular in Figure 95.

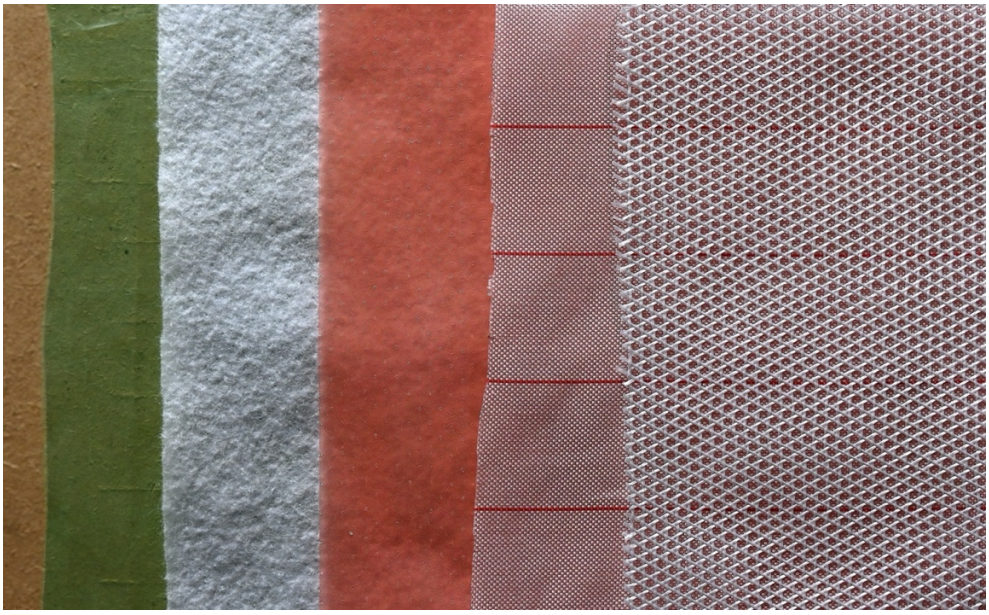

Figure 94 Materials used in the vacuum epoxy resin impregnation process of the triaxial fabric: from left to right: vacuum bag; breather fabric; release film; peel ply; triaxial fabric (warp is vertical)

8.4 Mechanical tests on the materials

8.4.1 tensile tests

The mechanical properties of the lining fabric were measured with uniaxial (plotted as line and dot curves) and biaxial tests (solid curves), before and after epoxy resin impregnation, Figure 95. The tensile tester (chapter 4) was used on 25 mm cruciform samples, for both uniaxial and biaxial tests, with the speed of 2 mm/min. The unimpregnated fabric shows a different response between the warp and the transverse yarns in uniaxial tests, due to the hexagonal mesh allowing perfect alignment with the testing direction only for the warp yarns. In the biaxial tests, where the material is subjected to simultaneous tension in both axes, the behavior becomes balanced, because the textile is designed for biaxial loading conditions. After impregnation the fabric anisotropy is almost completely eliminated, as the uniaxial tests converge on the biaxial test plots. The behavior of the lining fabric remains in the linear phase (elastic

[135] Vacuum bag FLM 120, 75 µm. Angeloni srl. www.g-angeloni.com

curve) until the end of the test, at 50 N/2.5cm. This tension value corresponds to a force of 20 N/cm, i.e., 8 times greater than the tension chosen for the lined painting (as we'll see in the last paragraph, the tension of 2.4 N/cm was chosen for the painting).

The impregnated fabric is therefore isotropic and has a relatively high modulus of elasticity (279 MPa), despite being very flexible, and still very light (165.89 g/m^2) and thin (0.353 mm) [136]. The hexagonal meshes are completely free, allowing equilibrium with environmental conditions and the passage of solvent vapors used for the lining and for its reversibility.

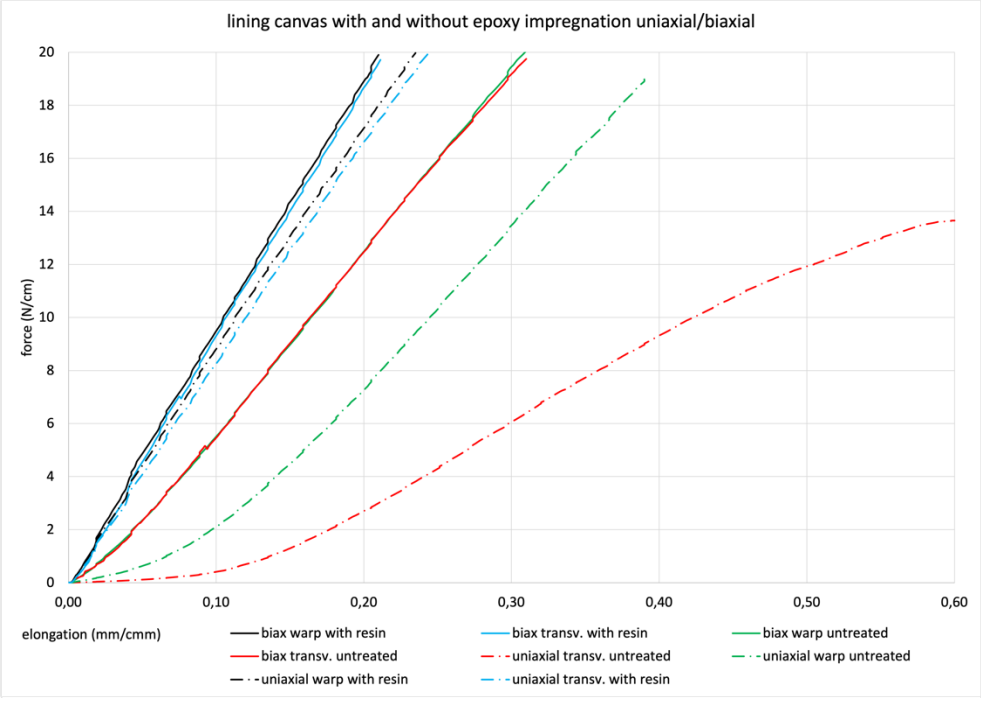

Figure 95 Uniaxial and biaxial tests on lining fabric before and after epoxy resin impregnation, showing the high stiffness and isotropy achieved with the treatment

[136] The weight of the fabric before resin impregnation is 98.6 g/m^2, and its thickness 0.234 mm. The treatment therefore adds 67 g/m^2 of the epoxy resin to the initial weight, and the thickness of the fabric increases by 0.12 mm. As the cross-section of the triaxial fabric contains approximately 50% empty space, the modulus of elasticity would have to be calculated on a lower resistant cross-section, which would bring the value to 560 MPa, but in the composite industries the thickness is calculated excluding the contribution of the epoxy resin (normally less stiff than the fibers), thus bringing the value of the tensile modulus to about 1GPa.

In order to assess the mechanical characteristics of the Tiepolo in relation to its lining, a physical model was created using a linen canvas[137] with a layer of calcium caseinate to represent the transferred pictorial layers and adhesives. This was consolidated, and reinforced with the polyester voile, repeating the methods and materials used on the Tiepolo to complete the stratigraphy of the "in vitro" mockup [Stoveland et al. 2021]. In this case, the purpose of the mockup was not to obtain a representation of the materials composing the stratigraphy of the painting after treatment. The linen canvas used to make the mockup most likely has a much higher tensile modulus than the painting before the lining. Its modulus of elasticity has been calculated only to evaluate its expected orthotropy and the difference with that of the lining canvas and the lined sandwich. The primary function of the mockup was to serve as a surface for the adhesion of the lining textile, with the objective of emulating the adhesion force of the Tiepolo and investigating its reversibility.

Biaxial tensile tests show the difference in mechanical behavior between the weft and the warp direction, which is more extensible, and make it possible to measure the “object related” tensile modulus of the mockup, in 47 MPa in warp and 66 MPa in weft. This is much lower than that of its new lining support, 279 MPa in both warp and transverse directions[138]. The superposition of the curves of the lined mockup on those of the lining fabric alone (Figure 96) demonstrate that stress transfer on the stiffer material is complete. The value of tension chosen for the painting is located at the very beginning of the tensile plot, and the technological polyester textile used for the lining is expected to have a completely reversible elastic tensile behavior (no creep foreseen).

[137] A linen canvas with a weight of 193 g/ m^2, thickness 0.477 mm, 12 weft threads and 14 warp threads. The thickness of the completed model is 0.85 mm.
[138] About 1GPa if calculated using only the fiber section area.

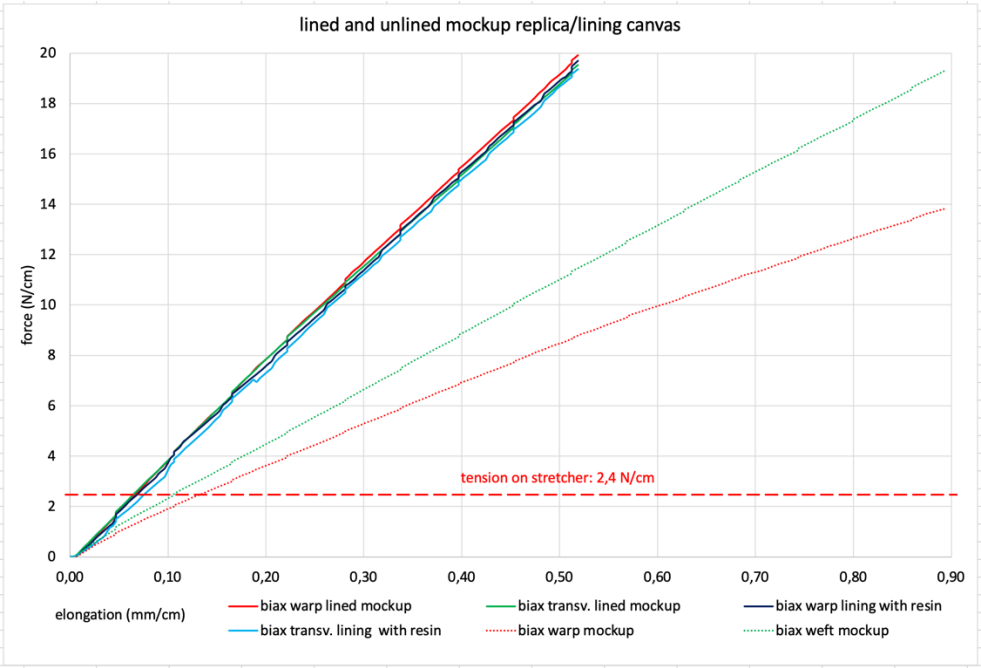

Figure 96 Biaxial tests on the mockup before and after lining. The curves of the lined mockup are overlapping those of the lining fabric alone

8.4.2 The cold and dry lining method, characterized by peel tests

The weight of Plextol B500 applied on the lining canvas is 100 g/m^2, reactivated with 120 g/m^2 of MEK for 45 minutes of permanence in the vacuum bag at 650 mbar, during which part of the solvent is extracted through the vacuum pump. After this initial period, the pressure was reduced to 250 mbar for 30 minutes, establishing a controlled air passage to better evacuate the remaining solvent vapors, and the bag was opened when the adhesive was dry. Such parameters were chosen on the basis of previous experience (Table 30), allowing to predict a bond strength appropriate to the painting's conditions and conservation requirements. Figure 97 shows the preparation of the lining canvas for adhesive spraying; Figure 98 shows two macro details of the canvas, after epoxy impregnation and with the adhesive particles covering its surface in the form of small droplets; Figure 99 shows the preparation of the vacuum bag for lining.

Figure 97 The support fabric prepared for spraying the lining adhesive

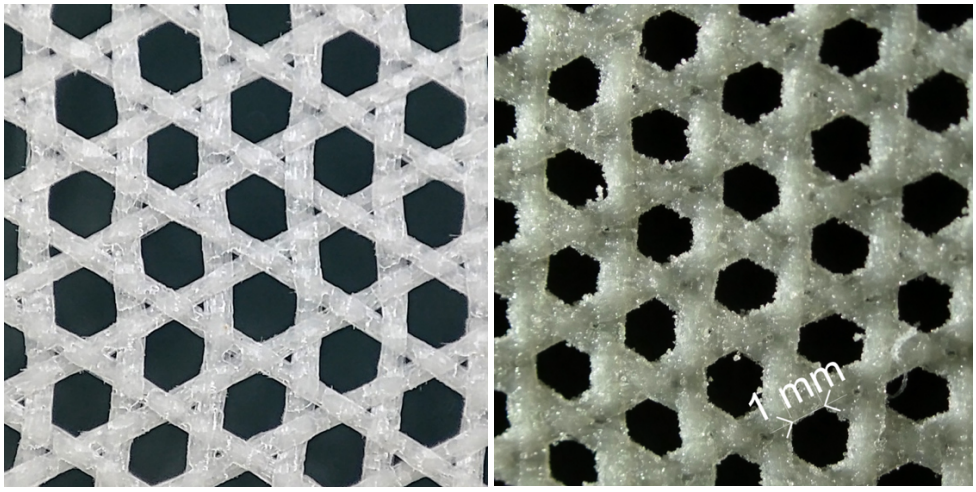

Figure 98 The epoxy-impregnated triaxial fabric, before and after spraying the lining adhesive, dried in spherules on the surface

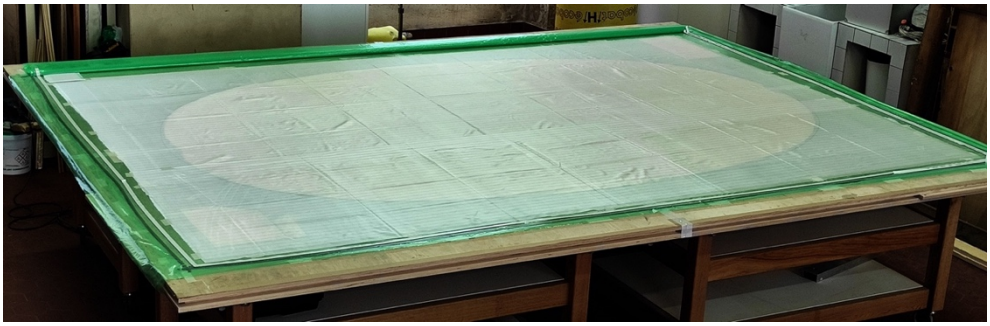

Figure 99 Preparing the vacuum bag for reactivation with methyl ethyl ketone vapors. The mockup in the lower left corner

The painting mockup was placed in the vacuum bag and lined at the same time as the Tiepolo, on a corner of the lining canvas left free from the oval shape of the painting (lower left in the image), which had been prepared by spraying the adhesive in the same way and in the same quantities.

Peel tests[139] were used to evaluate the adhesion strength obtained on the mockup (Figure 100). The average adhesion value measured with the dry peel tests, 31 N/25 mm, is suitable for long-term conservation and reliable, with no risk of spontaneous delamination. The system will therefore ensure stable transmission of forces between the painting and the lining fabric. Numerous studies have been carried out in the past to define a peel test resistance value suitable for the conservation of a lined painting. The speed of the testing machine has a major influence on the result obtained and has been chosen on the basis of various considerations. Among the first peel tests, Mehra's used a speed of 305 mm/min [Mehra, 1975]; a few years later the very low speed of 2 mm/min was used in other studies [Phenix and Hedley, 1984; Katz, 1985]; Roche used 100 mm/min [Roche, 1996]. The value of 100 mm/min seemed to be the most appropriate for simulating the mechanical removal of a lining fabric, and was therefore chosen as the reference in [Iaccarino Idelson and Garofalo, 2019]. In the latter study, in order to compare the values obtained with previous research, a theoretical conversion factor was to be calculated, comparing dedicated tests on the same materials with different speeds. In absolute terms, a peel strength of between 12.5 N/25 mm and 20 N/25 mm is commonly recognized as a reference value for a reliable lining that can still be removed mechanically without imposing excessive mechanical stress on the painting [Phenix and Hedley, 1984; Daly et al, 1993; Roche, 2003].

[139] Tests carried out on cut specimens (25x 245 mm) of the lined model, and peeled according to ASTM D903-49, at a speed of 100 mm/min using the uniaxial tester as in Figure 46, chapter 4.

Recent tests carried out as part of the Getty Conserving Canvas Initiative[140] compared 25 different traditional and "modern" lining techniques, using the same prepared canvas as a common reference substrate[141], at the common peeling speed of 100 mm/min. The different paste-glue techniques produced peel values between 15 N/25 mm and 20 N/25 mm; with heat reactivated brush applied BEVA, the value was doubled: 40 N/25 mm. This confirms that the value of 31 N/25 mm cm is too high for a mechanical removal, as predicted by previous research. However, it was chosen because it would never be advisable to remove the new support by purely mechanical means. Peel tests after a short time reactivation of the adhesive with a small amount of acetone vapor[142] show that the forces required for reversibility become very low. A force of only 3.65 N/25 mm (Figure 100) poses no risk to the painting and such value is not far from a spontaneous delamination. The tests also showed that during mechanical removal using the described reactivation the lining textile separates from the reinforcement polyester fabric adhered to the cotton gauze, which remain securely attached to the painting.

[140] The above-mentioned comparative study conducted by the author in May 2023 at the National Gallery of Ireland, Dublin.

[141] Claessens Canvas 15/2,10 m. https://www.claessenscanvas.com/en/products/canvas/detail/15-2-10-m

[142] Reactivation lasting 30 seconds, with barely dampened cotton gauze, wrung out well to prevent liquids from being absorbed directly, placed on the lining fabric. Acetone does not reach the paint layers.

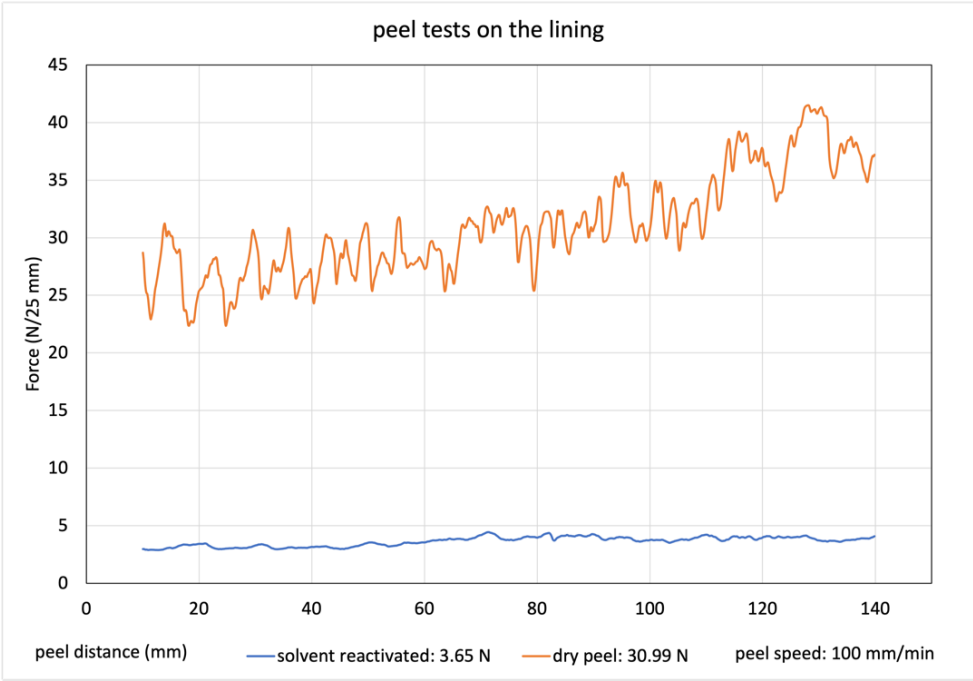

Figure 100 Peel tests on the lined painting model, carried out when dry and after reactivation of the adhesive with acetone vapor. With average values

8.5 The elastic system

Along the edges of the restored and cleaned strainer, small chamfered wooden strips were added to the front and back in order to distance the painting from the strainer and to create the necessary space for the springs. The edges were covered with Teflon-treated fiberglass fabric to reduce friction and help the canvas slide along the perimeter (Figure 101). The influence of friction on the forces involved was measured between a textile and the same Teflon coated surface, and was found to be between 0.3 N/cm and 0.6 N/cm[143]. The perimeter being an irregular ellipse, a CAD model of the shape was required, in order to draw all the parts of the elastic system, including small segments on the excess lining fabric that could be bent backwards to make the connection with the springs (Figure 102). The whole CAD design was then transferred to laser-cut and incised cardboard elements used to draw on the lining textile (Figure 103). After cutting

[143] Friction influences the transfer of forces, introducing an accumulation plateau, which must be reached before movement is possible. The measurement of friction was carried out for a similar case, the elastic tensioning of Frank Stella's large-format mixed-line perimeter painting "Isfahan 3", at the Museo de Solidaridad Salvador Allende in Santiago, Chile. The intervention was carried out as part of the Getty Conserving Canvas Initiative between 2019 and 2022.

and closing the small pockets along the perimeter with heat-seal adhesive[144], and installing the springs on the strainer, the connection was made with rods [145], corresponding to seven pockets, each distributing the tension of two springs[146]. On the 29 rods, 58 springs transmit an evenly distributed force to the lining fabric.

Within the theoretical framework for the choice of tension given in chapter 2, and given the high tensile modulus and resistance to creep of the lining fabric, the value of 2.4 N/cm was chosen, which enables to better manage the limitations due to friction (Figure 104). In fact, as we have seen, all the forces are borne by the lining fabric, which acts as a flat support on which the paint layers are laid without receiving any tension.

Figure 101 Detail of strainer perimeter, with chamfered wooden edging on both sides and Teflon coating

[144] BEVA film turns out very useful in similar cases, and it is not in contact with the painting.
[145] AISI 304 stainless steel rods with a 5 mm diameter, bent to the shape of the perimeter.
[146] Springs, with an elastic constant of 1.02 N/mm, are custom made for Equilibrarte in stainless steel AISI 302, by Mollificio Ciullo s.r.l., Roma Italy. https://www.mollificiociullo.com.

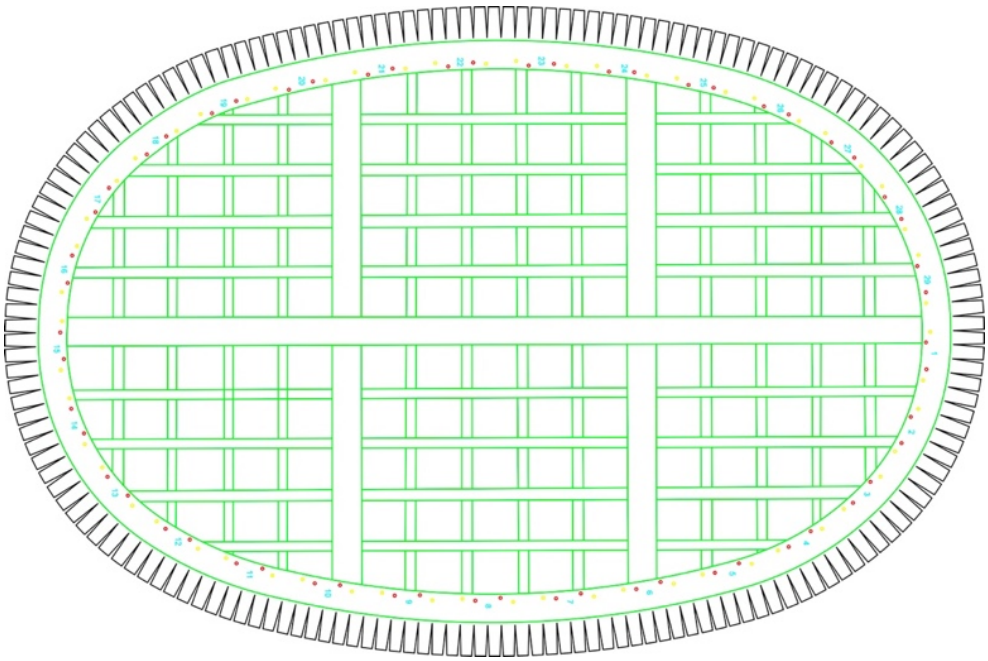

Figure 102 CAD drawing of the strainer with the position of the springs and the layout of the cuts to be made around the perimeter of the lining fabric

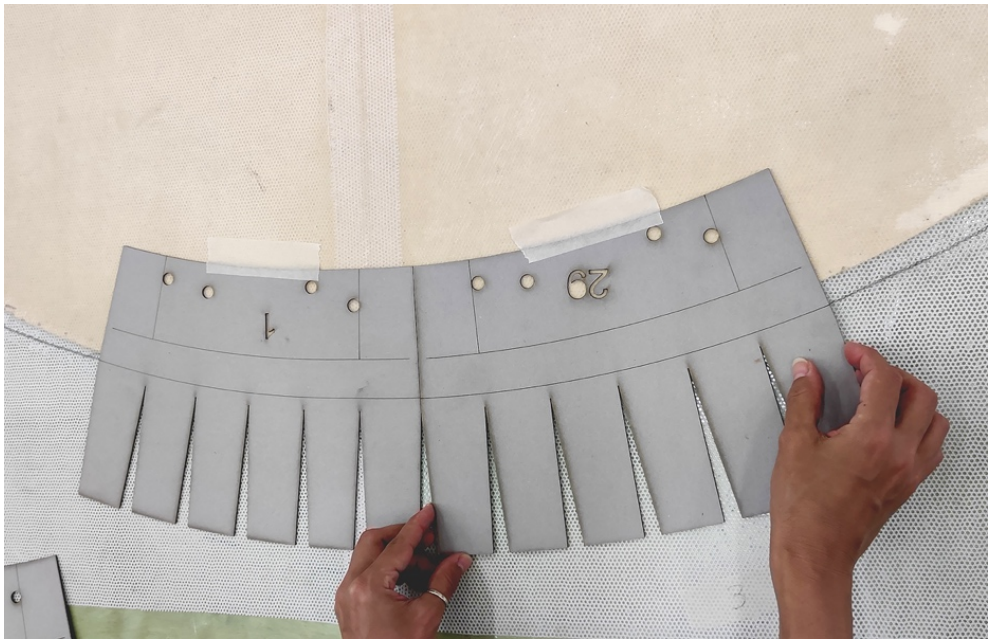

Figure 103 Transfer of CAD design to lining fabric using laser-cut cardboard

Figure 104 A stainless steel rod element with two springs, and force measurement

8.6 Conclusions

The structural intervention on the painting responds to the need of providing the paint layers with a planar support with adequate mechanical properties. The new support was made from a fabric with a high elastic modulus, using an elastic system that ensures evenly distributed tension over the entire surface, and a predetermined value of force. The techniques used for the structural conservation of the painting have the considerable advantage of allowing the preservation of the existing historic strainer, while at the same time protecting the painting from risks in the event of bending of the support.

The mechanical tests used to characterize the materials and the adhesion bond of the lining enabled a better understanding of the forces at play and to adapt them to the needs of the painting. Furthermore, the quantitative data contained in this paper will constitute an explicit reference for the conservation community, enabling to judge its long-term effects on a reproducible basis. Drawing attention to the aspects of repeatability and a certain level of predictability of structural conservation treatments, as is usual in materials engineering, seems to be achievable by fairly simple means also in the structural conservation of paintings on canvas.

Chapter 9 Conclusions and future work

9.1 Conclusions

The research in this thesis was triggered by an awareness of the limited knowledge about the structure of paintings from the mechanical point of view. The amount and depth of knowledge available about the chemical composition of the paint and preparation layers, their manufacturing techniques and the ability of performing a reliable risk assessment are incomparably higher.

The evaluation of tension on stretcher is the first approach to a painting when a conservator is assessing its structural stability or state of conservation, and is a prerequisite to speculating about structural treatments. This value is important because it represents the "fundamental" force acting on the painting and regulating a significant part of its response to external loads and environmental changes, and its quantification is hardly ever possible. The recognition of this simple fact was the starting point of my research in 1992. In the early 2000s, I measured the value of tension of a group of paintings on their traditional stretchers. The same procedure allowed to calculate the MUT (Figure 8), and subsequent research corroborated these values (Figure 9).

The initial objective of my Ph.D. research was to conduct mechanical tests on historical painting samples to develop and implement a predictive FE model. This model would allow for the calculation of the value of tension of a painting on stretcher using a fully non-destructive technique. This method would become increasingly accurate by adding the mechanical information corresponding to different paintings structures to the reference database. For this reason, I collected about a hundred historical specimens.

The first step for the definition of such complexity was the construction of the mockup of a lined historical painting (chapter 6), which was described in precise detail, and its structure subjected to full mechanical analysis with a stratigraphical approach. *The Night Watch* (chapter 7) was considered to be a perfect example, because if permitted a complete description of the boundary conditions thanks to the new elastic strainer. The objective of attempting the calculation of the tension it had on the previous wooden stretcher seemed to be within reach. However, a critical obstacle emerged during the process: the definition of the tensile and flexural elastic moduli needed for the FEM proved to be too complex, and the underlying theoretical background revealed to be insufficient.

The support canvas, the simplest material in a painting's stratigraphy, was chosen as the starting point to build the missing theoretical foundations, in the awareness of the insufficient knowledge about the structure of historical textiles. Their typical description

is generally rather uncertain on most of the key information, and the dimensions of the yarns, their twist and crimp are not considered measurable data. The overall ability to quantify the morphological characteristics of an historical textile was found to be missing in conservation science. In textile engineering studies the quantification of such parameters allows the prediction of the mechanical response of modern textile structures. This revealed to be completely impossible for historical textiles, because of the lack of quantitative morphological data and of the complete absence of mechanical test data. No correlation was possible, because critical information was missing on both sides.

The reasons behind such striking insufficient knowledge are solid and related to the very nature of the materials object of investigation in conservation science, when compared with those in textile engineering. The first is that conservation deals with historical artifacts that are rare, and that studies for their conservation conflict with the idea of destructive sampling, while engineering studies have mostly unlimited access to the materials under observation. The second is that historical artifacts have complex and unpredictable conservation histories, are damaged and contaminated, and were produced with technologies whose details need to be deduced through observation, as they belong to the past[147]. Such reasons are solid enough to have led to a sort of resignation, and conservation science studies are dealing with lacking or extremely simplified data. Instead, for modern textiles, unlimited sampling also allows for destructive mechanical testing, and the correlation between morphology and mechanics is given, or is within hand reach for researchers. Moreover, technological studies for the production of targeted textiles have plenty of applications, and dedicated testing equipment is available, and or continuously adapted to the needs of the research.

My competencies as a senior painting conservator and a broad network of collaborations allowed me access to historical specimens. The experience in the construction of CNC machines used to process the construction of artifacts related to conservation, and the long-standing collaboration with Ph.D. computer scientist Miguel Sanchez, allowed me to face the need for dedicated testing machines. The research done for this Ph.D. has allowed me to produce data about the morphology of historical or conservation-related textiles, that is comparable to that available in textile engineering. These were also mechanically characterized with biaxial tests.

The first outcome of this thesis research was to organize a full set of methods and use it to quantify all the key features of a group of 22 historical specimens. Four modern

[147] The Nicas project “Canvassing” is intended to face exactly this problem.
https://www.nicas-research.nl/projects/canvassing-the-making/

textiles were added to the set of specimens because their presence allowed for comparisons and verifications to be made, and they offered unlimited and uncontaminated sampling. This preliminary database was used to find correlations between characteristics and to define and quantify the differences between warp and weft yarns, highlighting recurring associations. An interesting by-product of the knowledge acquired is that the possibility of recognizing warp from weft, when a selvedge is not available, appears now to be considerably increased. The absence of a selvedge is the most common situation for historical textiles, and finding alternative ways to identify the loom direction has important implications in the understanding of the mechanics of the paintings, and in technical art history.

As the morphological data collected in chapter 3 and the mechanical data in chapter 5 demonstrate (see Table 8), the identification of the loom direction allows defining the orthotropy of the unpainted textile in an unprecedented way. Knowing which direction corresponds to the warp allows us to assume the presence of yarns with higher crimp, lower twist, and a more elliptical cross-section. This, in turn, implies a lower tensile and mechanical response, particularly within the conservation range of tensions. From the perspective of the assessment of the future structural integrity of the textile and of the paint layers it carries, a good example is that a painting exposed to the gravity load along the warp yarns will be more prone to creep. This kind of information will become very useful in the assessment of the conservation needs and intervention protocols for a specific painting, once they will become more widespread knowledge.

From the perspective of technical art history, the methods exposed in chapter 3 allow a relatively straightforward identification of the loom direction, compared to the more complex and costly specialist approaches based on X-ray imaging of the painting [van de Wetering, 1997]. This is allowing a simplified approach to the problem, but not the acquisition of the great wealth of detailed information on the overall textile when the analysis of the Xray images is based on the use of algorithms [Johnson et al., 2013; Noble et al., 2018] and the measures of the yarn density, weaving angle and recurring patterns over the entire surface of the textile become possible.

Nevertheless, the information gathered using the methods developed in this thesis is fully quantitative and repeatable, enabling the calculation of fundamental engineering parameters—such as the effective loaded cross-section of the textile—necessary for determining the tensile elastic modulus, which is a prerequisite for predictive finite element (FE) models.

The second outcome of this thesis research was the design, development and construction of a multi-purpose biaxial tensile testing machine. This was highly needed, because mechanical testing for conservation purposes is done using Universal Testing

Machines (UTM), normally on modern textiles because of the scarce availability of historical samples and of the large dimensions defined by the standards. Moreover, UTM tests are performed along a single axis, be it the warp or the weft, and then extrapolated to define the overall tensile behavior of the textile. Still, the yarns in a textile are interrelated, and tension in one direction influences the properties of the other. Moreover, textiles are made to sustain loads acting in more than the single direction isolated using the UTM, as it is the normal case for a painting on its stretcher. To reconstruct the behavior of the textile under a biaxial load, mathematical parameters need to be applied to the uniaxial tests to obtain realistic estimations. Biaxial testing machines produce a tensile characterization under a biaxial load, thus much closer to the reality. Loading happens simultaneously in the two directions, allowing the interaction between warp and weft to be evaluated and measured.

The biaxial tensile tester is designed to obtain precision measurements on small samples (25x25 mm or 10x10 mm), thus it is more compatible with the dimensions of historical specimens. It is possible to use it in a wide range of speeds and it can also perform standard uniaxial tests, and peel and shear tests, like a UTM. A flexural tower was built to perform 3-point bending tests on paintings using a single actuator of the biaxial tester, a device producing unprecedented data in conservation science because flexural tests are unusual on paintings. The goal of keeping construction not too complex nor expensive was considered crucial because research in painting conservation would benefit from the availability of biaxial tensile testing, and in general from the data or mechanical tests performed on historical samples. For the same reason, we chose to publish in a high-impact, open-access journal with an open-source license to promote the construction and dissemination of similar machines, and to learn from the feedback of potential future users. The design of the biaxial tester proved to be modular enough to allow the use of the same firmware and software for the construction of a portable testing device, using only one of the four actuators. This is dedicated to more standard uniaxial tests, including peel and shear.

The mechanical response of the 26 specimens to biaxial loading was correlated with their quantitative morphological descriptions, opening up new possibilities in the analysis of the influence of the structure of historical textiles on their tensile response. A few preliminary correlations between key features, like twist and crimp, and the mechanical response under biaxial testing were established. The value of the tensile elastic modulus is rarely calculated for canvas paintings materials, and it is needed for engineering Finite Elements Models predictive simulations. Young's modulus is based on the assumption that materials have homogeneous structure, what complicates its calculation for canvas paintings, or even simple textiles, as this requires the mathematical removal of the empty spaces to isolate the response of the materials. Over time, different ways to calculate the actual loading section of the materials were proposed, aiming at an

increasing precision and repeatability. The quantified morphological description of the 26 specimens in this research allowed the elaboration of a simple procedure for a standardized approach to the calculation of the loading area of the cross-section of the textile using robust and repeatable data. The definition of the loading section of the layered structure of a lined painting is more complex, and appears to be crucial considering that probably approx. 50% of the historical paintings are lined.
The materials used for the construction of a lined oil painting mock-up inspired to Rembrandt's The Night Watch, investigated using the biaxial tester. This was also equipped with a flexural testing tower, allowing to measure the flexural elastic modulus of the mockup. A non-destructive mechanical testing set up was used on *The Night Watch* to obtain first hand mechanical data from the painting, using the "Displacement Tester" a third custom-built device. This produced reproducible quantitative data on the resistance of the painting to a force acting perpendicular to the plane of the canvas.

The mechanical testing procedures were applied to another rather exceptional case study, provided by the conservation treatment of a detached wall painting by Tiepolo at the Louvre Museum. The mechanical characterization of the layered structure of the painting allowed the transfer of tensions from the elastic tensioning system to the lining canvas and finally to the painting to be defined. The quantification of each step of the treatment allows the reproducibility of the structural conservation. Peel tests defined the force of adhesion established between the painting and the lining canvas, and the forces were compared with previous research, which confirmed that the results are compatible with the long-term conservation and structural integrity of the painting.

In **Appendix 1**, the complete data set on the morphological and mechanical characterization of each of the 26 textiles is provided, as the foundation of a future database. More samples of each specimen are available, and additional information will be collected over time.

In **Appendix 2**, complete data set on the information introduced in the first paragraphs of chapter 5 is presented: individual yarns tensile tests and uniaxial and biaxial tests on the three modern textiles; biaxial tests performed at different speeds.

In **Appendix 3**, the full text of the English translation of the 1973 Italian paper on the determination of the twist in historical yarns, published here thanks to the copyrights kindly granted by the author Mr. Franco Tassinari.

In **Appendix 4**, additional technical information about the open-source biaxial tester is collected.

9.2 Future work

The future directions of this research are outlined below. Several steps have already been initiated, and part of the required equipment is at an advanced stage of implementation.

About the morphological description of historical textiles, the first will be to conduct statistical tests to determine the probability that the observation of one of the "characterizing features" (see Table 8) on a sample will allow identifying the warp from the weft, and how the probability is increased by the simultaneous observation of more than one characterizing features. This will be done after increasing the number of investigated specimens, still working on those bearing a selvedge (to date 35 more historical specimens are available). In order to investigate the distortions acquired by the yarns during weaving, mockups woven from yarns with a well-defined initial diameter and twist will be analyzed. The expected outcome is an insight in the amount of increase of yarn width and reduction of yarn thickness, or z axis compression, in correlation with yarn twist.

The use of Digital Image Correlation, DIC, will allow a better understanding of the interactions between the yarns and a quantification of their relative displacements during the tensile tests. Macro photographs of the textiles during the tensile tests may be used to measure the progression of the untwisting of single yarns due to tension (see Figure 28).

The mechanical characterization of historical canvas paintings supports has more open questions. Additional uniaxial testing on all the 26 specimens will be performed used to further verify the correlations between uniaxial and biaxial testing, in order to complete the data set in Appendix 1 and obtain precious data to study the correlations between uniaxial and biaxial testing beyond the correlations already tentatively established with twist and crimp in the yarns.

A parametrical FE Model of a textile, based on the data from the 26 textiles object of this thesis work, could be validated using the existing mechanical data. Cross checking the uniaxial and biaxial mechanical response of the materials would allow an even stronger validation of the tool, which could become extremely precious to solve the important doubts arisen about the calculation of the tensile modulus. As we have seen in chapters 5 and 6, the methods used to calculate the elastic modulus of a textile have made the object of research and study, but no real validation method was developed for the mathematical choices about the geometries involved, with the area of the cross section as the most problematic one. Asynchronous biaxial testing, using different loading speeds in the two directions, may also be used to further investigate the biaxial behavior through the comparison with the digital model. The flexural tests can also be simulated

in the FEM, and the flexural modulus validated by comparing them to the results of the experimental value.

The very definition of “elastic modulus” for historical textiles seems to be requiring further analysis. This based on the concept that the strains involved, and described by the modulus, are fully reversible. However, this does not appear to be the case, as permanent deformations are clearly visible in the textile even after testing well below its supposed yield point. This is clearly due to a reorganization of the textile, where the first step is some slippage between the yarns, followed by slippage between the fibers, which is clearly a more permanent deformation and should be defined as damage. The biaxial tester was modified so as to memorize the absolute location of the clamps at the beginning of a tensile test, and to enable series of incremental cycles to be performed. Using cycles of tensile tests, always backing to the initial location will possibly allow the definition of the threshold value of tension after which permanent deformations appear. The current idea is that of performing cycles starting from an initial pre-tensioning value of 0.2 N/cm. Each step will involve an increment of 0.1 N/cm, followed by a return to the initial location for an adequate recovery time before proceeding with the following increment.

The mechanical characterization of historical paintings specimens is more difficult due to the complex stratification. A first step will be that of investigating the layered structures of lined paintings, starting from a lot of 11 years naturally aged 1 m^2specimens deriving from a comparative lining workshop in 2014, during which 18 different lining methods were simulated on the same mockup painting. These will be tested for flexion for uniaxial and biaxial tensile tension and then testing the individual layers, and of the adhesive bond by peel and shear. As for naturally aged painting specimens, to date about 60 are already available, they will be also tested for flexion for uniaxial and biaxial tensile tension. The paint and preparation layers will require dedicated material characterization using standard diagnostics (microscopy, XRF, FTIR) and possibly nanoindentation. As a starting point, the mechanical characterization will be object “related”, as in Table 26, chapter 5.

The research on *The Night Watch* will be completed using the FEM simulation of the painting on its elastic strainer. This will be used to replicate the displacement tests already performed and, run in optimization mode cycles, if may be able to validate the values of the tensile and flexural moduli of the painting. Should this be confirmed, as preliminary runs of the FEM seem to promise, the knowledge of validated elastic moduli opens-up for the possibility of attempting a reconstruction of the value of tension it had on the wooden stretcher, before it was transferred to the new elastic strainer.

The first step will be to run the FEM software in the optimization mode, in order to calculate the values of the moduli that provide a good match between the simulated and experimental curves. As the DT plots quantify the mechanical characteristics of the painting, obtaining a correspondence between the simulated and experimental data is a way to support the choice for the values of the elastic moduli. These values will then be compared to those obtained with the work described in chapter 6, providing a relevant contribution to the above-described problem of the determination of the elastic moduli for a painting. The extents and limits of such contribution appear at the moment to be unpredictable. A further step of the future work will be that of calculating the tension *The Night Watch* had on the 1975 wooden stretcher in January 2022, at the moment when the DT tests were carried out.

10 Glossary of engineering terms used in the text

Tensile elastic modulus

Tensile modulus, often referred to as Young's modulus in tension, measures a material's stiffness or resistance to elastic deformation under tensile loading. It represents the ratio of tensile stress to tensile strain in the linear elastic region of a material's stress-strain curve.

It indicates how much a material will stretch (or compress) under a given tensile (or compressive) load while remaining elastic, i.e., returning to its original shape when the load is removed.

Tensile modulus is critical in various industries and engineering applications because of its ability to predict and quantify how materials behave under tensile loads.

Flexural elastic modulus

The flexural modulus of elasticity, also called the flexural modulus, measures the stiffness of a material when subjected to bending (flexural) loading. It quantifies the relationship between bending stress and bending strain within the elastic limit of the material during a flexural test.

It is particularly important for materials used in beams, plates, and structural components that experience bending. For ductile materials such as metals, flexural modulus and tensile modulus are similar, but for composite or anisotropic materials, flexural modulus can differ significantly from tensile modulus.

Secant elastic modulus

Tensile secant modulus is a measure of the stiffness of a material under tensile loading, calculated as the slope of a secant line drawn from the origin to a specific point on the material's stress-strain curve. This point is usually defined by a specific strain level. Unlike the tangent modulus, which represents the slope of the curve at a specific point, the secant modulus considers the slope of a line drawn from the origin (or a specified reference point) to a point on the stress-strain curve. This modulus provides an average stiffness of the material over the specified strain range and is often used for materials that do not exhibit a linear stress-strain relationship (e.g., polymers or biological tissues). It is often used for materials that exhibit significant nonlinearity, such as plastics, elastomers, and composites, to predict performance under specific loading conditions.

Isotropic/anisotropic behavior

An isotropic material is one that has the same properties in all directions. This means that the material behaves the same regardless of the direction in which forces are applied. In an isotropic material, physical properties such as tensile modulus, elastic modulus, thermal conductivity, and strength do not vary with direction. In contrast,

anisotropic materials, such as composites or wood, exhibit direction-dependent properties.

Orthotropic behavior

Orthotropic materials are a special type of anisotropic material in which the material has three mutually perpendicular axes of symmetry, and the properties of the material differ along each of these axes. In essence, orthotropic materials have different mechanical properties along three mutually orthogonal directions, often related to the internal structure of the material or the processing method.

11 Glossary of textile definitions used in the text

- Fibers. Long, thin, flexible strands of material that can be spun into yarn or thread, used in the production of textiles and fabrics.
- Thread. A yarn that is usually thin and highly twisted, adapted for sewing. Thread and yarn can be considered synonyms.
- Yarn. General definition of a long strand of twisted fibers used for weaving. Yarn and thread can be considered synonyms, but yarn was preferred because it is a more general term. For the definition of the number of yarns per unit length of the textile, the term “thread count” was chosen because it is of general use and changing it to “yarn count” sounded unnatural.
- Twist. During the spinning process, the fiber strands are wound around their axis, thereby acquiring twist. High twist means high tensile strength and cohesion of the yarn.
- Warp. The longitudinal yarns that are held in tension on a loom during the weaving process. They run parallel to the length of the fabric and serve as the foundation or backbone of the woven fabric.
- Weft. The transversal yarns that weave in and out of the warp yarns to make fabric during the shedding process.
- Shedding, shed. Process where the warp yarns are divided into sets to create an open space, or shed, through which the weft yarn is passed.
- Crimp. The waviness or bending of yarns within a fabric as they interlace with each other. It describes how much the yarns deviate from a straight line as they bend over and under other yarns. The crimp is usually expressed as the percentage of the extra length of the interlaced yarn in relation to the straight yarn.
- Plain weave. The pattern alternates every row, so the warp and weft interlace 1:1 at right angles, creating a uniform texture.
- Basket weave. The pattern is the same as in plain weave, but multiple warp and weft threads (usually two or more) are woven together as a unit, rather than individually.

12 Acknowledgments

A PhD is, by definition, a life changing experience. When I began mine, as a mature researcher and a conservator, my career had ranged between humanities and science, craftsmanship and a specialized knowledge of the materials. Research was the natural path for a deeper dive, as it represents for me the negotiation between the physical needs of artworks and science, the most advanced collective achievement of humankind. More personally, since I was a student, it has always been a space for creative thinking. I grew up in a family where artists and scientists sat at the same table, staging their fights and misunderstandings. I am grateful to my family of origin for setting me on this course, even if through my young age rebellion, and to my mother and father, who always fed and supported my curiosity with love and care.

I was lucky enough to study at an amazing school of conservation, Istituto Centrale per il Restauro in Rome, where I dealt with extraordinary masterpieces and met the curiosity of Mauro Torre (professor in physics), and the guidance of Mara Nimmo. My gratitude goes to Alain Roche, who firmly believed in me as a researcher since the late 1990s, and was always generous in high profile conversations and shared projects in Paris. After publishing my first research book, in which some of Mecklenburg's work was translated into Italian for the first time, Marion proposed that we meet at a conference in Valencia in 2005. Laura Fuster Lopez invited me to present my results at the same conference, opening my research to a broader international audience.

I need to thank René de la Rie and Hans Poulis, who strongly supported my decision to embark on a path that would require so much energy, seemingly incompatible with my leadership responsibilities as an art conservator. I am grateful to all my colleagues in Equilibrarte, and in particular to my business partner Carlo Serino, for supporting me without hesitation and for accepting that I devote part of my resources to a personal project. I am particularly thankful to Petria Noble, who welcomed my research proposals concerning *The Night Watch* and believed in my project. An open-minded leader with a clear vision and a genuine commitment to her colleagues, she made the difference in the early stages of my PhD. I believe that a well-grounded scientific approach, based on a clear awareness of the contingent needs of an artwork, is a key for the future of both practicing conservation and of conservation science.

My heartfelt thanks go to my main supervisor Roger Groves, for his presence, commitment, guidance, and for our many enriching conversations; and to Otto Bergsma, for generously sharing his expertise on the structure of textiles and for his always smiling and reassuring presence. I am also grateful to Katrien Keune, Lisette Vos, Anna Krekeler and Esther van Duijn, for the work done together, and for the useful revisions of chapters 6 and 7. I wish to express my gratitude to all the members of the defense committee for

critically reviewing the thesis. In particular, Emma Richardson, Łukasz Bratasz, and Emanuela Bosco, for their insightful and inspiring comments on the thesis, constructive criticism, and openness to dialogue and collaboration.

This PhD unfolded largely online, not only because it began during the pandemic, but also because I carried out my work in Rome, building and using my research facilities in my studio. This was possible, efficient, and productive thanks to decades of prior experience and to the support of friends I could rely on, such as Miguel Sanchez, computer scientist based in Valencia. Miguel was a corner stone in the decision to build the testing equipment, and together we spent countless weekends online working on their design, construction, and implementation. Other friends and colleagues, such as Patrick Buti in France, also supported me greatly, and helped me building a collection of historical samples that set this work apart from previous research on the mechanics of canvas paintings. I thank all the wonderful persons with whom I have shared experiences, in a network whose breadth and interconnection I would have never dreamt of. Among them is Luca Cortelli, who shared his expertise in CNC machines and helped make the latest version of the biaxial tester a more user friendly and accurately operating machine. Dr. Enzo Tassinari, for granting me permission to present his full text translated in Appendix 3, for his friendliness, and for the interest he showed in my research. Many more people deserve mention, some of whom appear in the thesis itself, who make life a blessing through their enthusiasm, generosity, and participation.

Finally, I hope I have been able to express all my gratitude to my wonderful wife, Daniela, for sharing passion, debating decisions, supporting me open heartedly and patiently every day of this long and demanding journey. May the conclusion of my PhD bring new openings, more space for the simple things, and new projects pursued in gratitude and partnership.

13 Curriculum Vitae

The author earned a degree in the conservation of paintings, mosaics, and sculptures from the Istituto Centrale per il Restauro in Rome in 1993. Over the course of his career as a conservator, he has worked on outstanding masterpieces and has received international recognition. A Fellow of the IIC and a member of ICOM-CC, he is currently CEO and CTO of Equilibrarte, a conservation company based in Rome, Italy. He was recently awarded a Getty Residential Scholar Grant as an independent scholar, with a project focused on testing lining methods for canvas paintings, aimed at improving reproducibility and achieving greater predictability of treatment results.

He has been actively engaged in research since his student years, primarily focusing on conservation treatment methods and the constituent materials of artworks, paying special attention to the mechanical behavior of canvas paintings. His first research monograph, published in 2004, examined the measurement of tension on stretchers for canvas paintings and its implications for their conservation. Since 1996, he has authored approximately 90 papers on conservation and related research topics.

Highly active in teaching, he has long been responsible for a university course on the structural conservation of canvas paintings. Fluent in five languages, he supervises master's theses and delivers specialized workshops to peers in museums and conservation centers across several countries.

www.antonioiaccarinoidelson.com

Appendix 1 The full tables of the mechanical and morphological data collected on the set of 26 specimens

author	**unknown**
painting	*plain canvas n.1*
date	18th c.

			obs.	
warp yarn width	0,47	mm	9	w. mean
weft yarn width	0,46	mm	9	w. mean
warp yarn thickness	0,20	mm	9	w. mean
weft yarn thickness	0,22	mm	9	w. mean
warp yarn twist	277,1	TPM	9	w. mean
weft yarn twist	238,3	TPM	9	w. mean
warp yarn crimp	7,9	%	3	mean
weft yarn crimp	5,6	%	3	mean
warp count	16,7	yarns/cm	9	mean
weft count	13,5	yarns/cm	9	mean
weaving	hand			
fiber	linen			
pH	6,45			
weight	257	g/sqm	4	mean
textile thickness	0,54	mm	15	mean
n. of samples	4			
sample width	10	mm		
gauge length	10,6	mm		

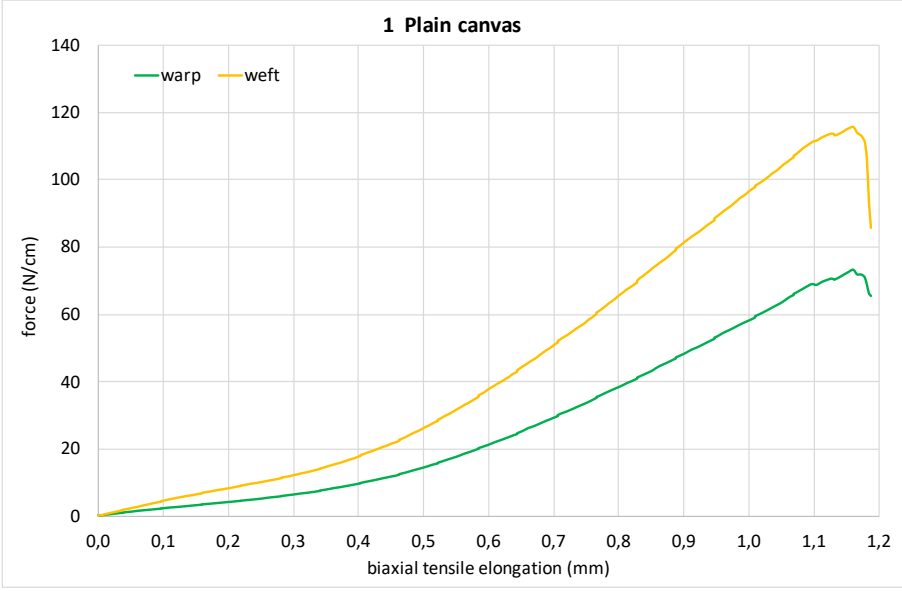

	warp	weft	unit
textile section area	5,40		
yarn section area	0,07	0,08	sqmm
uncrimped length	10,79	10,56	mm
yarn fiber volume	0,72	0,76	cmm
tot yarn vol in RUC	12,06	10,27	cmm
RUC volume	54,00		cmm
volume fraction	0,22	0,19	cmm
Pt (fiber thickness)	0,12	0,10	mm
plate thickness mean	0,11		mm
equiv fiber sect. area	1,21	1,03	sqmm

biax pretension	0,3	N/cm
samples tested	4	
plot is mean of	3	

strain location	**A**	**B**	**C**	**D**
strain value	0,005	0,019	0,047	0,085
warp force value (N/cm)	1,40	4,28	14,53	48,31
weft force value (N/cm)	2,43	8,36	26,25	81,40
textile thickness			**0,54** mm	
strain location	**A**	**B**	**C**	**D**
warp stress	0,26	0,79	2,69	8,95
weft stress	0,45	1,55	4,86	15,07
warp module (Mpa)	**55,1**	**42,0**	**57,0**	**105,4**
weft module (Mpa)	**95,3**	**82,0**	**103,1**	**177,5**
fiber fraction thickness mean			**0,11** mm	
strain location	**A**	**B**	**C**	**D**
warp stress (Mpa)	1,16	3,55	12,05	40,06
weft stress (Mpa)	2,36	8,14	25,55	79,24
warp module (Mpa)	**246,9**	**187,9**	**255,4**	**471,8**
weft module (Mpa)	**501,0**	**431,2**	**541,8**	**933,3**

author	unknown
painting	*plain canvas n.2*
date	18th c.

			obs.	
warp yarn width	0,87	mm	9	w. mean
weft yarn width	0,75	mm	9	w. mean
warp yarn thickness	0,33	mm	9	w. mean
weft yarn thickness	0,41	mm	9	w. mean
warp yarn twist	140,5	TPM	9	w. mean
weft yarn twist	161,7	TPM	9	w. mean
warp yarn crimp	12,1	%	3	mean
weft yarn crimp	4,3	%	3	mean
warp count	11	yarns/cm	9	mean
weft count	8	yarns/cm	9	mean
weaving	hand			
fiber	linen			
pH	6,1			
weight	435	g/sqm	4	mean
textile thickness	0,98	mm	15	mean
n. of samples	4			
sample width	10	mm		
gauge length	10,6	mm		

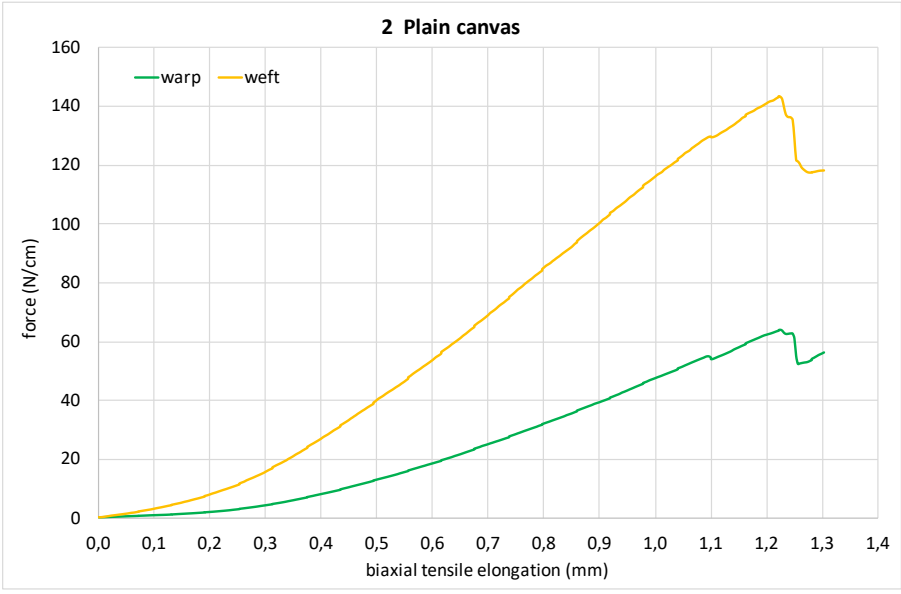

	warp	weft	unit
textile section area	9,80		
yarn section area	0,23	0,24	sqmm
uncrimped length	11,21	10,43	mm
yarn fiber volume	2,29	2,28	cmm
tot yarn vol in RUC	25,21	18,27	cmm
RUC volume	98,00		cmm
volume fraction	0,26	0,19	cmm
Pt (fiber thickness)	0,25	0,18	mm
plate thickness mean	0,22		mm
equiv fiber sect. area	2,52	1,83	sqmm

biax pretension	0,3	N/cm
samples tested	4	
plot is mean of	3	

strain location	**A**	**B**	**C**	**D**
strain value	0,005	0,019	0,047	0,085
warp force value (N/cm)	0,63	2,11	13,11	39,41
weft force value (N/cm)	1,52	8,06	40,16	100,31
textile thickness			**0,98** mm	
strain location	**A**	**B**	**C**	**D**
warp stress	0,06	0,22	1,34	4,02
weft stress	0,16	0,82	4,10	10,24
warp module (Mpa)	**13,7**	**11,4**	**28,4**	**47,4**
weft module (Mpa)	**32,9**	**43,6**	**86,9**	**120,6**
fiber fraction thickness mean			**0,22** mm	
strain location	**A**	**B**	**C**	**D**
warp stress (Mpa)	0,25	0,84	5,20	15,63
weft stress (Mpa)	0,83	4,41	21,98	54,91
warp module (Mpa)	**53,2**	**44,3**	**110,2**	**184,1**
weft module (Mpa)	**176,7**	**233,7**	**466,1**	**646,7**

author	**unknown**
painting	*plain canvas n.3*
date	18 th century

			obs.	
warp yarn width	0,87	mm	9	w. mean
weft yarn width	0,64	mm	9	w. mean
warp yarn thickness	0,28	mm	9	w. mean
weft yarn thickness	0,46	mm	9	w. mean
warp yarn twist	150,4	TPM	9	w. mean
weft yarn twist	229,6	TPM	9	w. mean
warp yarn crimp	7,3	%	3	mean
weft yarn crimp	5,6	%	3	mean
warp count	13,7	yarns/cm	9	mean
weft count	12	yarns/cm	9	mean
weaving	hand			
fiber	linen			
pH	6,4			
weight	278	g/sqm	4	mean
textile thickness	0,35	mm	15	mean
n. of samples	4			
sample width	10	mm		
gauge length	10,6	mm		

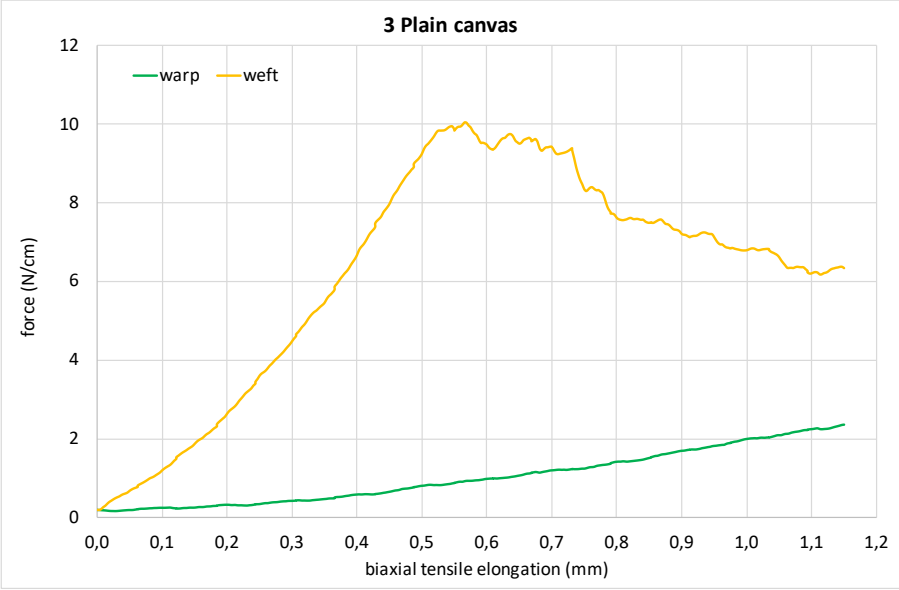

	warp	weft	unit
textile section area	3,50		
yarn section area	0,19	0,23	sqmm
uncrimped length	10,73	10,56	mm
yarn fiber volume	1,87	2,21	cmm
tot yarn vol in RUC	25,58	26,47	cmm
RUC volume	35,00		cmm
volume fraction	0,73	0,76	cmm
Pt (fiber thickness)	0,26	0,26	mm
plate thickness mean	0,26		mm
equiv fiber sect. area	2,56	2,65	sqmm

biax pretension	0,3	N/cm
samples tested	4	
plot is mean of	2	

strain location	**A**	**B**	**C**	**D**
strain value	0,005	0,019	0,047	0,085
warp force value (N/cm)	0,19	0,32	0,80	-
weft force value (N/cm)	0,68	2,64	9,24	-
textile thickness			**0,35**	mm
strain location	**A**	**B**	**C**	**D**
warp stress	0,05	0,09	0,23	-
weft stress	0,19	0,75	2,64	-
warp module (Mpa)	**11,4**	**4,9**	**4,9**	-
weft module (Mpa)	**41,0**	**39,9**	**56,0**	-
fiber fraction thickness mean			**0,26**	mm
strain location	**A**	**B**	**C**	**D**
warp stress (Mpa)	0,07	0,13	0,31	-
weft stress (Mpa)	0,26	1,00	3,49	-
warp module (Mpa)	**15,6**	**6,7**	**6,7**	-
weft module (Mpa)	**54,2**	**52,8**	**74,0**	-

author	unknown
painting	*plain canvas n.4*
date	18th c.

			obs.	
warp yarn width	0,80	mm	9	w. mean
weft yarn width	0,97	mm	9	w. mean
warp yarn thickness	0,49	mm	9	w. mean
weft yarn thickness	0,44	mm	9	w. mean
warp yarn twist	193,5	TPM	9	w. mean
weft yarn twist	134,9	TPM	9	w. mean
warp yarn crimp	11,0	%	3	mean
weft yarn crimp	2,2	%	3	mean
warp count	9	yarns/cm	9	mean
weft count	7	yarns/cm	9	mean
weaving	hand			
fiber	hemp			
pH	7,35			
weight	329	g/sqm	4	mean
textile thickness	0,84	mm	15	mean
n. of samples	5			
sample width	10	mm		
gauge length	10,6	mm		

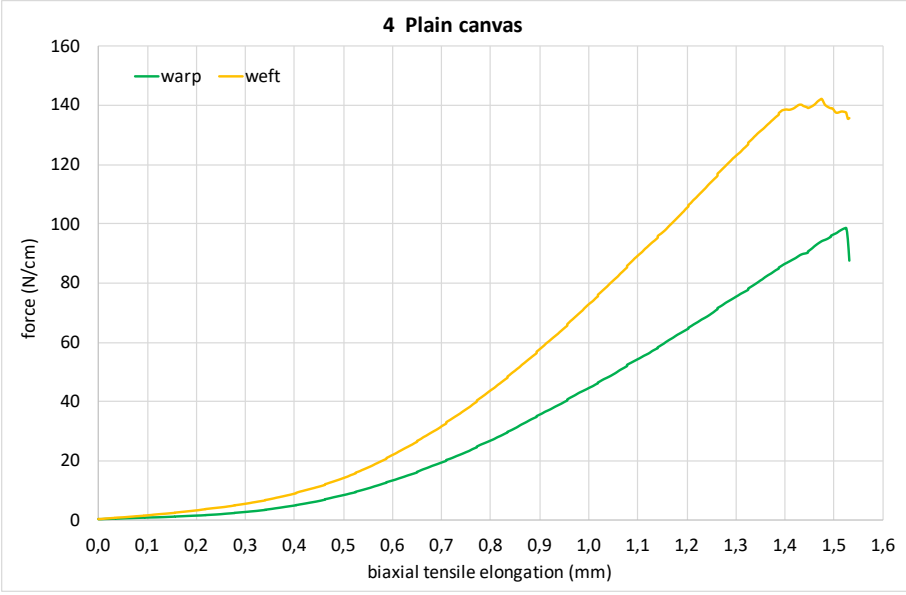

	warp	weft	unit
textile section area	8,40		
yarn section area	0,31	0,34	sqmm
uncrimped length	11,10	10,22	mm
yarn fiber volume	3,10	3,11	cmm
tot yarn vol in RUC	27,88	21,74	cmm
RUC volume	84,00		cmm
volume fraction	0,33	0,26	cmm
Pt (fiber thickness)	0,28	0,22	mm
plate thickness mean	0,25		mm
equiv fiber sect. area	2,79	2,17	sqmm

biax pretension	0,3	N/cm
samples tested	5	
plot is mean of	3	

strain location	**A**	**B**	**C**	**D**
strain value	0,005	0,019	0,047	0,085
warp force value (N/cm)	0,56	1,49	8,41	35,58
weft force value (N/cm)	0,91	3,25	14,17	57,66
textile thickness			**0,84** mm	
strain location	**A**	**B**	**C**	**D**
warp stress	0,07	0,18	1,00	4,24
weft stress	0,11	0,39	1,69	6,86
warp module (Mpa)	**14,1**	**9,4**	**21,2**	**49,9**
weft module (Mpa)	**22,9**	**20,5**	**35,8**	**80,8**
fiber fraction thickness mean			**0,25** mm	
strain location	**A**	**B**	**C**	**D**
warp stress (Mpa)	0,20	0,53	3,02	12,76
weft stress (Mpa)	0,42	1,49	6,52	26,52
warp module (Mpa)	**42,6**	**28,3**	**63,9**	**150,3**
weft module (Mpa)	**88,6**	**79,1**	**138,1**	**312,4**

author	**unknown**
painting	*plain canvas n.5*
date	19th c.

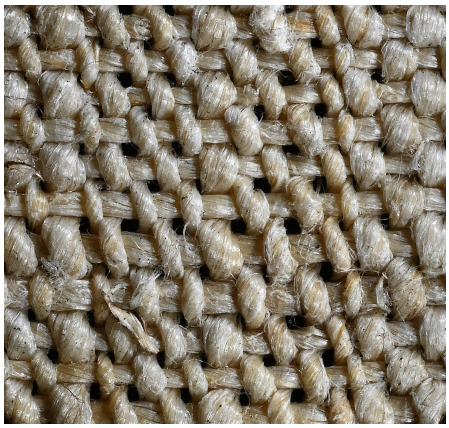

			obs.	
warp yarn width	0,64	mm	9	w. mean
weft yarn width	0,60	mm	9	w. mean
warp yarn thickness	0,27	mm	9	w. mean
weft yarn thickness	0,46	mm	9	w. mean
warp yarn twist	286,2	TPM	9	w. mean
weft yarn twist	175,4	TPM	9	w. mean
warp yarn crimp	21,7	%	3	mean
weft yarn crimp	2,0	%	3	mean
warp count	16,5	yarns/cm	9	mean
weft count	11	yarns/cm	9	mean
weaving	hand			
fiber	hemp			
pH	7,26			
weight	445	g/sqm	4	mean
textile thickness	0,87	mm	15	mean
n. of samples	4			
sample width	10	mm		
gauge length	10,6	mm		

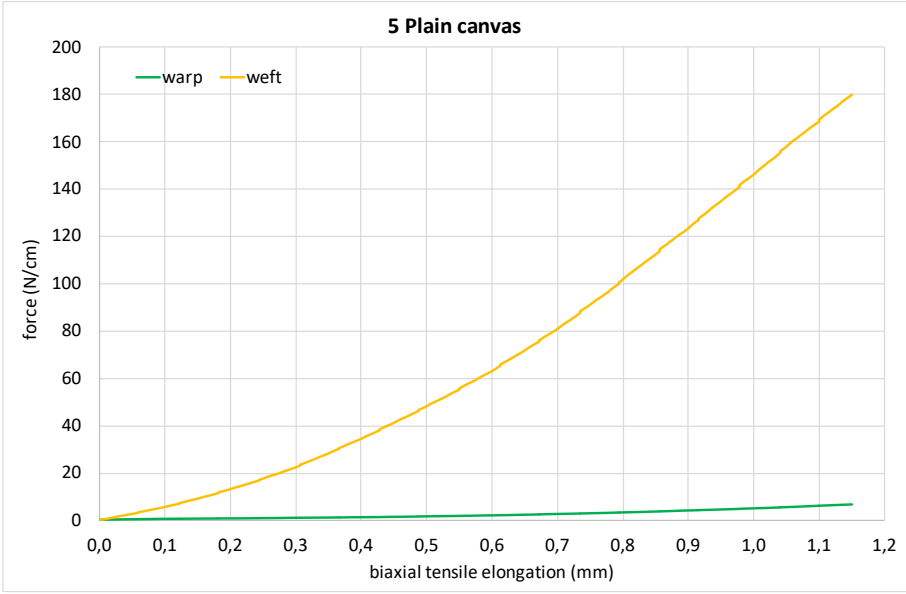

	warp	weft	unit
textile section area	8,70		
yarn section area	0,14	0,22	sqmm
uncrimped length	12,17	10,20	mm
yarn fiber volume	1,50	2,00	cmm
tot yarn vol in RUC	24,71	22,05	cmm
RUC volume	87,00		cmm
volume fraction	0,28	0,25	cmm
Pt (fiber thickness)	0,25	0,22	mm
plate thickness mean	0,23		mm
equiv fiber sect. area	2,47	2,20	sqmm

biax pretension	0,3	N/cm
samples tested	4	
plot is mean of	3	

strain location	**A**	**B**	**C**	**D**
strain value	0,005	0,019	0,047	0,085
warp force value (N/cm)	0,50	0,85	1,72	4,22
weft force value (N/cm)	2,73	13,19	48,26	124,16
textile thickness			**0,87** mm	
strain location	**A**	**B**	**C**	**D**
warp stress	0,06	0,10	0,20	0,48
weft stress	0,31	1,52	5,55	14,27
warp module (Mpa)	**12,3**	**5,2**	**4,2**	**5,7**
weft module (Mpa)	**66,5**	**80,4**	**117,6**	**168,1**
fiber fraction thickness mean			**0,23** mm	
strain location	**A**	**B**	**C**	**D**
warp stress (Mpa)	0,20	0,34	0,70	1,71
weft stress (Mpa)	1,24	5,98	21,89	56,31
warp module (Mpa)	**43,3**	**18,2**	**14,8**	**20,1**
weft module (Mpa)	**262,5**	**317,1**	**464,0**	**663,2**

author	Domenico C. Malinconico
painting	*Incoronazione della vergine*
date	1728

			obs.	
warp yarn width	0,70	mm	9	w. mean
weft yarn width	0,48	mm	9	w. mean
warp yarn thickness	0,24	mm	9	w. mean
weft yarn thickness	0,26	mm	9	w. mean
warp yarn twist	186,5	TPM	9	w. mean
weft yarn twist	197,9	TPM	9	w. mean
warp yarn crimp	11,1	%	3	mean
weft yarn crimp	4,3	%	3	mean
warp count	13	yarns/cm	9	mean
weft count	13,3	yarns/cm	9	mean
weaving	hand			
fiber	hemp			
pH	6,17			
weight	244	g/sqm	3	mean
textile thickness	0,26	mm	15	mean
n. of samples	3			
sample width	10	mm		
gauge length	10,6	mm		

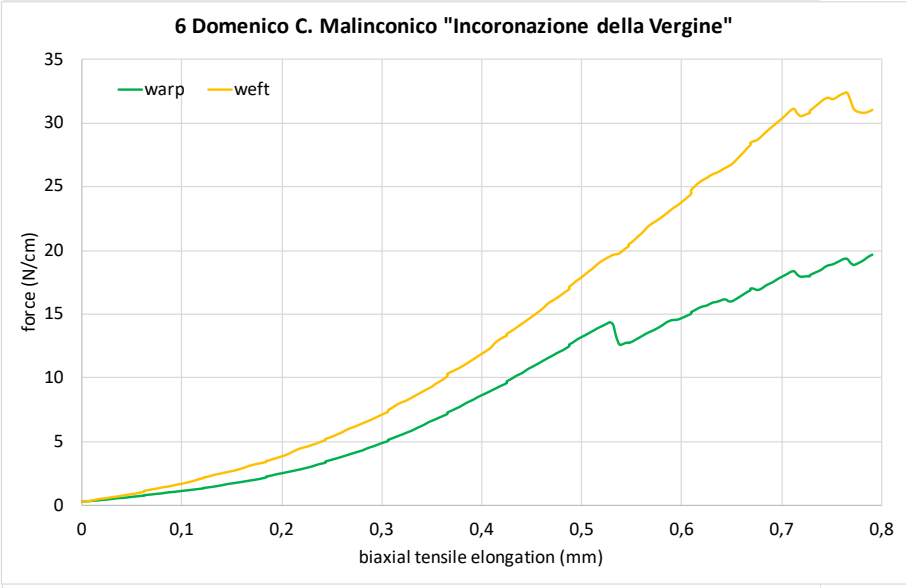

	warp	weft	unit
textile section area	2,65		
yarn section area	0,13	0,10	sqmm
uncrimped length	11,11	10,43	mm
yarn fiber volume	1,33	0,93	cmm
tot yarn vol in RUC	17,28	12,32	cmm
RUC volume	26,45		cmm
volume fraction	0,65	0,47	cmm
Pt (fiber thickness)	0,17	0,12	mm
plate thickness mean	0,15		mm
equiv fiber sect. area	1,73	1,23	sqmm

biax pretension	0,3	N/cm
samples tested	3	
plot is mean of	2	

strain location	**A**	**B**	**C**	**D**
strain value	0,005	0,019	0,047	0,085
warp force value (N/cm)	0,67	2,52	13,21	-
weft force value (N/cm)	0,88	3,85	17,90	-
textile thickness			**0,26** mm	
strain location	**A**	**B**	**C**	**D**
warp stress	0,25	0,95	4,99	-
weft stress	0,33	1,45	6,77	-
warp module (Mpa)	**53,7**	**50,5**	**105,9**	**-**
weft module (Mpa)	**70,7**	**77,1**	**143,5**	**-**
fiber fraction thickness mean			**0,15**	mm
strain location	**A**	**B**	**C**	**D**
warp stress (Mpa)	0,39	1,46	7,64	-
weft stress (Mpa)	0,72	3,12	14,52	-
warp module (Mpa)	**82,2**	**77,3**	**162,1**	**-**
weft module (Mpa)	**151,7**	**165,5**	**307,9**	**-**

author	Bernard d'Agesci
painting	*l'éducation de la vierge*
date	1817

			obs.	
warp yarn width	0,39	mm	9	w. mean
weft yarn width	0,46	mm	9	w. mean
warp yarn thickness	0,27	mm	9	w. mean
weft yarn thickness	0,19	mm	9	w. mean
warp yarn twist	200,1	TPM	9	w. mean
weft yarn twist	252,8	TPM	9	w. mean
warp yarn crimp	6,4	%	3	mean
weft yarn crimp	7,3	%	3	mean
warp count	18,7	yarns/cm	9	mean
weft count	17	yarns/cm	9	mean
weaving	hand			
fiber	linen			
pH	6,8			
weight	334	g/sqm	3	mean
textile thickness	0,41	mm	15	mean
n. of samples	3			
sample width	10	mm		
gauge length	10,6	mm		

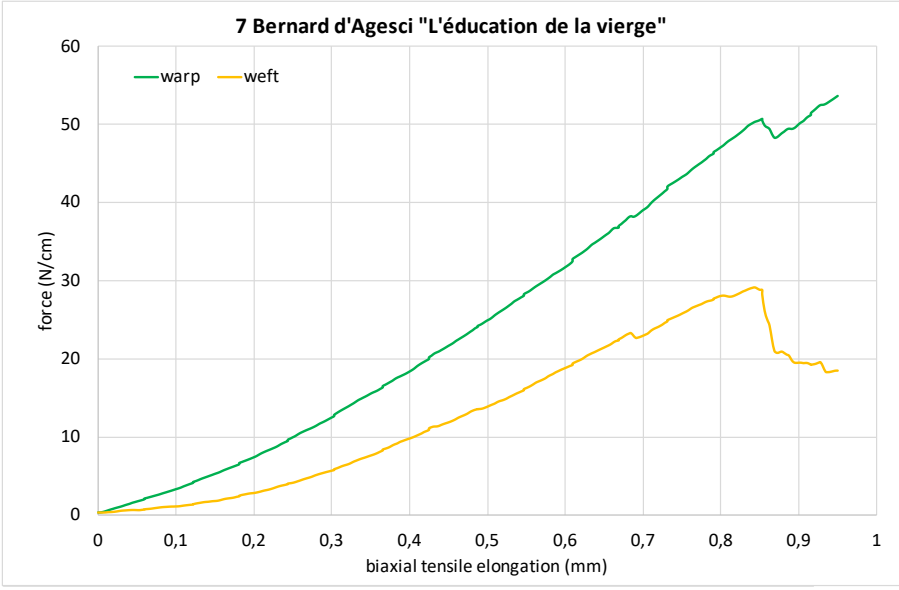

	warp	weft	unit
textile section area	4,10		
yarn section area	0,08	0,07	sqmm
uncrimped length	10,64	10,73	mm
yarn fiber volume	0,79	0,67	cmm
tot yarn vol in RUC	14,76	11,35	cmm
RUC volume	41,00		cmm
volume fraction	0,36	0,28	cmm
Pt (fiber thickness)	0,15	0,11	mm
plate thickness mean	0,13		mm
equiv fiber sect. area	1,48	1,13	sqmm

biax pretension	0,3	N/cm
samples tested	3	
plot is mean of	1	

strain location	**A**	**B**	**C**	**D**
strain value	0,005	0,019	0,047	0,085
warp force value (N/cm)	1,74	7,39	24,91	-
weft force value (N/cm)	0,63	2,82	13,86	-
textile thickness			**0,41** mm	
strain location	**A**	**B**	**C**	**D**
warp stress	0,42	1,80	6,07	-
weft stress	0,15	0,69	3,38	-
warp module (Mpa)	**90,0**	**95,5**	**128,8**	**-**
weft module (Mpa)	**32,5**	**36,4**	**71,7**	**-**
fiber fraction thickness mean			**0,13**	mm
strain location	**A**	**B**	**C**	**D**
warp stress (Mpa)	1,18	5,01	16,88	-
weft stress (Mpa)	0,55	2,48	12,21	-
warp module (Mpa)	**249,9**	**265,4**	**357,8**	**-**
weft module (Mpa)	**117,6**	**131,5**	**258,9**	**-**

author	**unknown**
painting	*medium paste lining canvas*
date	19th c.

			obs.	
warp yarn width	0,79	mm	9	w. mean
weft yarn width	0,77	mm	9	w. mean
warp yarn thickness	0,36	mm	9	w. mean
weft yarn thickness	0,33	mm	9	w. mean
warp yarn twist	231,0	TPM	9	w. mean
weft yarn twist	191,3	TPM	9	w. mean
warp yarn crimp	2,0	%	3	mean
weft yarn crimp	2,5	%	3	mean
warp count	7	yarns/cm	9	mean
weft count	8	yarns/cm	9	mean
weaving	hand			
fiber	hemp			
pH	5,96			
weight	166	g/sqm	4	mean
textile thickness	0,48	mm	15	mean
n. of samples	4			
sample width	10	mm		
gauge length	10,6	mm		

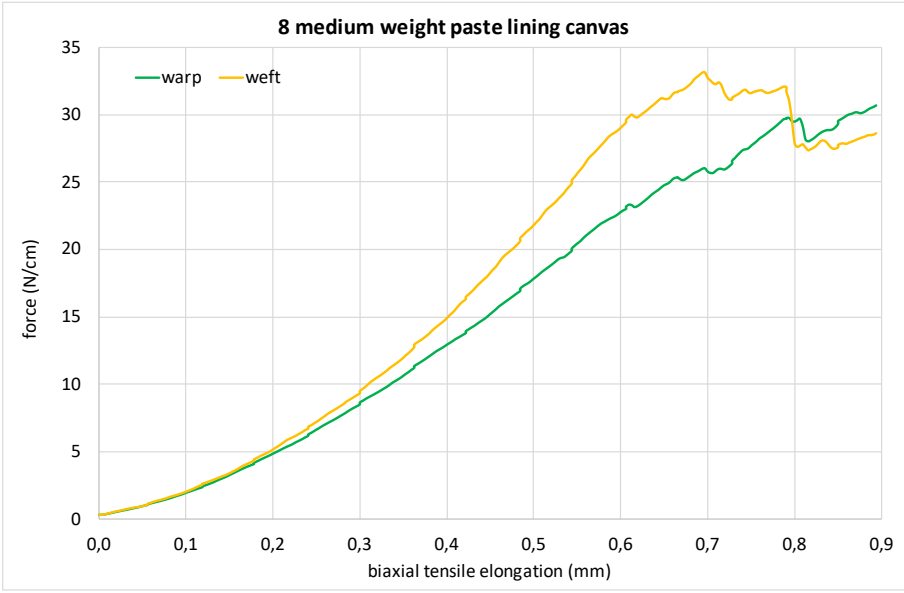

	warp	weft	unit
textile section area	4,80		
yarn section area	0,22	0,20	sqmm
uncrimped length	10,20	10,25	mm
yarn fiber volume	2,07	1,85	cmm
tot yarn vol in RUC	14,46	14,84	cmm
RUC volume	48,00		cmm
volume fraction	0,30	0,31	cmm
Pt (fiber thickness)	0,14	0,15	mm
plate thickness mean	0,15		mm
equiv fiber sect. area	1,45	1,48	sqmm

biax pretension	0,3	N/cm
samples tested	4	
plot is mean of	3	

strain location	**A**	**B**	**C**	**D**
strain value	0,005	0,019	0,047	0,085
warp force value (N/cm)	0,96	4,85	17,85	-
weft force value (N/cm)	0,96	5,16	21,81	-
textile thickness			**0,48** mm	
strain location	**A**	**B**	**C**	**D**
warp stress	0,20	1,01	3,72	-
weft stress	0,20	1,07	4,54	-
warp module (Mpa)	**42,3**	**53,6**	**78,8**	-
weft module (Mpa)	**42,3**	**56,9**	**96,3**	-
fiber fraction thickness mean			**0,15** mm	
strain location	**A**	**B**	**C**	**D**
warp stress (Mpa)	0,66	3,35	12,34	-
weft stress (Mpa)	0,65	3,48	14,70	-
warp module (Mpa)	**140,3**	**177,8**	**261,7**	-
weft module (Mpa)	**136,9**	**184,2**	**311,7**	-

author	**unknown**
painting	*heavy paste lining canvas*
date	19th c.

			obs.	
warp yarn width	1,19	mm	9	w. mean
weft yarn width	0,76	mm	9	w. mean
warp yarn thickness	0,51	mm	9	w. mean
weft yarn thickness	0,52	mm	9	w. mean
warp yarn twist	194,0	TPM	9	w. mean
weft yarn twist	251,2	TPM	9	w. mean
warp yarn crimp	13,2	%	3	mean
weft yarn crimp	9,5	%	3	mean
warp count	8,7	yarns/cm	9	mean
weft count	7	yarns/cm	9	mean
weaving	hand			
fiber	linen			
pH	5,95			
weight	628	g/sqm	4	mean
textile thickness	1,28	mm	15	mean
n. of samples	4			
sample width	10	mm		
gauge length	10,6	mm		

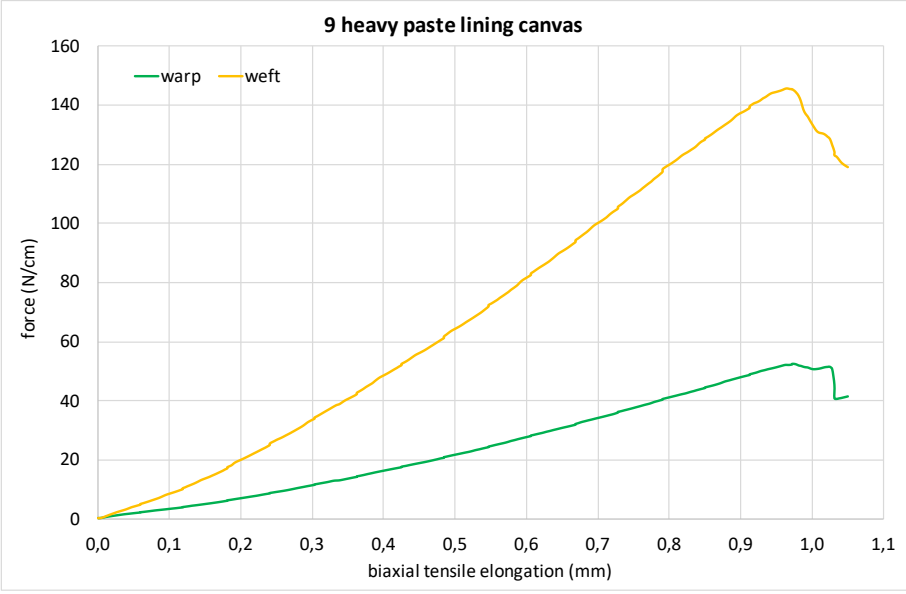

	warp	weft	unit
textile section area	12,80		
yarn section area	0,48	0,31	sqmm
uncrimped length	11,32	10,95	mm
yarn fiber volume	4,89	3,08	cmm
tot yarn vol in RUC	42,56	21,57	cmm
RUC volume	128,00		cmm
volume fraction	0,33	0,17	cmm
Pt (fiber thickness)	0,43	0,22	mm
plate thickness mean	0,32		mm
equiv fiber sect. area	4,26	2,16	sqmm

biax pretension	0,3	N/cm
samples tested	4	
plot is mean of	3	

strain location	**A**	**B**	**C**	**D**
strain value	0,005	0,019	0,047	0,085
warp force value (N/cm)	1,98	7,04	21,75	47,96
weft force value (N/cm)	4,20	20,01	64,30	137,28
textile thickness			**1,28** mm	
strain location	**A**	**B**	**C**	**D**
warp stress	0,15	0,55	1,70	3,75
weft stress	0,33	1,56	5,02	10,73
warp module (Mpa)	**32,8**	**29,1**	**36,0**	**44,1**
weft module (Mpa)	**69,6**	**82,9**	**106,5**	**126,3**
fiber fraction thickness mean			**0,32** mm	
strain location	**A**	**B**	**C**	**D**
warp stress (Mpa)	0,47	1,65	5,11	11,27
weft stress (Mpa)	1,95	9,28	29,81	63,65
warp module (Mpa)	**98,6**	**87,7**	**108,3**	**132,7**
weft module (Mpa)	**413,2**	**491,8**	**632,0**	**749,7**

author	**A. E. Fragonard**
painting	*paste lining canvas*
date	19th c.

			obs.	
warp yarn width	0,72	mm	9	w. mean
weft yarn width	0,70	mm	9	w. mean
warp yarn thickness	0,30	mm	9	w. mean
weft yarn thickness	0,30	mm	9	w. mean
warp yarn twist	196,7	TPM	9	w. mean
weft yarn twist	152,6	TPM	9	w. mean
warp yarn crimp	8,3	%	3	mean
weft yarn crimp	2,8	%	3	mean
warp count	13,7	yarns/cm	9	mean
weft count	11,3	yarns/cm	9	mean
weaving	machine			
fiber	hemp			
pH	6,1			
weight	398	g/sqm	4	mean
textile thickness	0,68	mm	15	mean
n. of samples	4			
sample width	10	mm		
gauge length	10,6	mm		

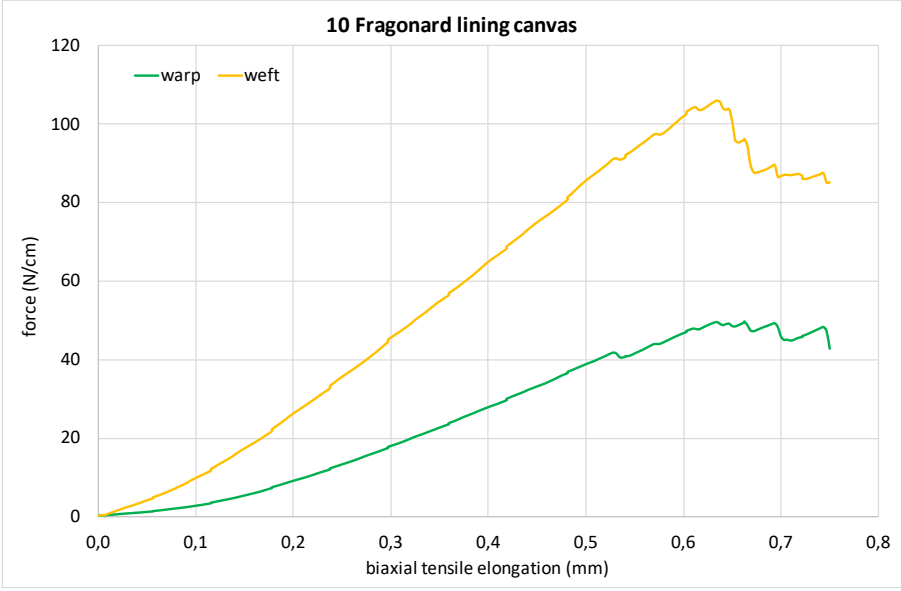

	warp	weft	unit
textile section area	6,80		
yarn section area	0,17	0,16	sqmm
uncrimped length	10,83	10,28	mm
yarn fiber volume	1,67	1,54	cmm
tot yarn vol in RUC	22,82	17,37	cmm
RUC volume	68,00		cmm
volume fraction	0,34	0,26	cmm
Pt (fiber thickness)	0,23	0,17	mm
plate thickness mean	0,20		mm
equiv fiber sect. area	2,28	1,74	sqmm

biax pretension	0,3	N/cm
samples tested	4	
plot is mean of	3	

strain location	**A**	**B**	**C**	**D**
strain value	0,005	0,019	0,047	0,085
warp force value (N/cm)	1,22	9,14	38,83	-
weft force value (N/cm)	4,18	26,29	85,57	-
textile thickness			**0,68**	mm
strain location	**A**	**B**	**C**	**D**
warp stress	0,18	1,34	5,71	-
weft stress	0,62	3,87	12,58	-
warp module (Mpa)	**38,2**	**71,2**	**121,0**	**-**
weft module (Mpa)	**130,4**	**204,9**	**266,8**	**-**
fiber fraction thickness mean			**0,20**	mm
strain location	**A**	**B**	**C**	**D**
warp stress (Mpa)	0,54	4,01	17,02	-
weft stress (Mpa)	2,41	15,14	49,27	-
warp module (Mpa)	**113,7**	**212,3**	**360,7**	**-**
weft module (Mpa)	**510,7**	**802,3**	**1044,5**	**-**

author	Raffaele Postiglione
painting	*Scuola di Atene*
date	1845

			obs.	
warp yarn width	0,60	mm	9	w. mean
weft yarn width	0,96	mm	9	w. mean
warp yarn thickness	0,38	mm	9	w. mean
weft yarn thickness	0,37	mm	9	w. mean
warp yarn twist	229,2	TPM	9	w. mean
weft yarn twist	140,3	TPM	9	w. mean
warp yarn crimp	5,2	%	3	mean
weft yarn crimp	3,3	%	3	mean
warp count	8	yarns/cm	9	mean
weft count	8	yarns/cm	9	mean
weaving	hand			
fiber	linen			
pH	5,2			
weight	265	g/sqm	3	mean
textile thickness	0,66	mm	15	mean
n. of samples	3			
sample width	10	mm		
gauge length	10,6	mm		

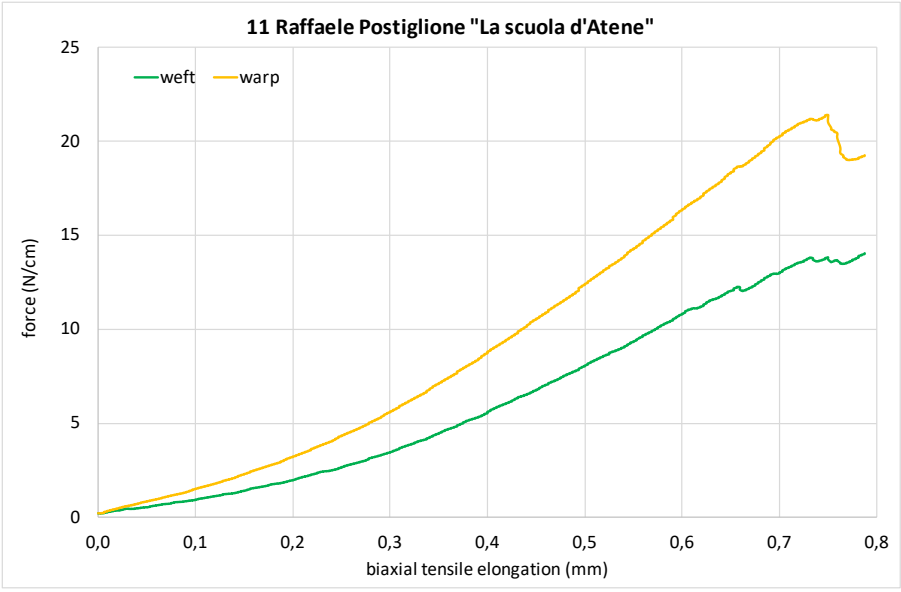

	warp	weft	unit
textile section area	6,60		
yarn section area	0,18	0,28	sqmm
uncrimped length	10,52	10,33	mm
yarn fiber volume	1,71	2,61	cmm
tot yarn vol in RUC	13,66	20,90	cmm
RUC volume	66,00		cmm
volume fraction	0,21	0,32	cmm
Pt (fiber thickness)	0,14	0,21	mm
plate thickness mean	0,17		mm
equiv fiber sect. area	1,37	2,09	sqmm

biax pretension	0,3	N/cm
samples tested	3	
plot is mean of	3	

strain location	**A**	**B**	**C**	**D**
strain value	0,005	0,019	0,047	0,085
warp force value (N/cm)	0,35	1,97	8,02	-
weft force value (N/cm)	0,45	3,22	12,35	-
textile thickness			**0,66**	mm
strain location	**A**	**B**	**C**	**D**
warp stress	0,05	0,30	1,22	-
weft stress	0,07	0,49	1,87	-
warp module (Mpa)	**11,4**	**15,8**	**25,8**	-
weft module (Mpa)	**14,6**	**25,9**	**39,7**	-
fiber fraction thickness mean			**0,17**	mm
strain location	**A**	**B**	**C**	**D**
warp stress (Mpa)	0,26	1,44	5,87	-
weft stress (Mpa)	0,22	1,54	5,91	-
warp module (Mpa)	**55,0**	**76,4**	**124,5**	-
weft module (Mpa)	**46,1**	**81,7**	**125,3**	-

author	**Alfred Dehodencq**
painting	*Fête juive à Tanger*
date	1870

			obs.	
warp yarn width	0,71	mm	9	w. mean
weft yarn width	0,51	mm	9	w. mean
warp yarn thickness	0,38	mm	9	w. mean
weft yarn thickness	0,32	mm	9	w. mean
warp yarn twist	164,0	TPM	9	w. mean
weft yarn twist	212,0	TPM	9	w. mean
warp yarn crimp	15,3	%	3	mean
weft yarn crimp	2,3	%	3	mean
warp count	17	yarns/cm	9	mean
weft count	11	yarns/cm	9	mean
weaving	machine			
fiber	linen			
pH	5,55			
weight	326	g/sqm	4	mean
textile thickness	0,32	mm	15	mean
n. of samples	4			
sample width	10	mm		
gauge length	10,6	mm		

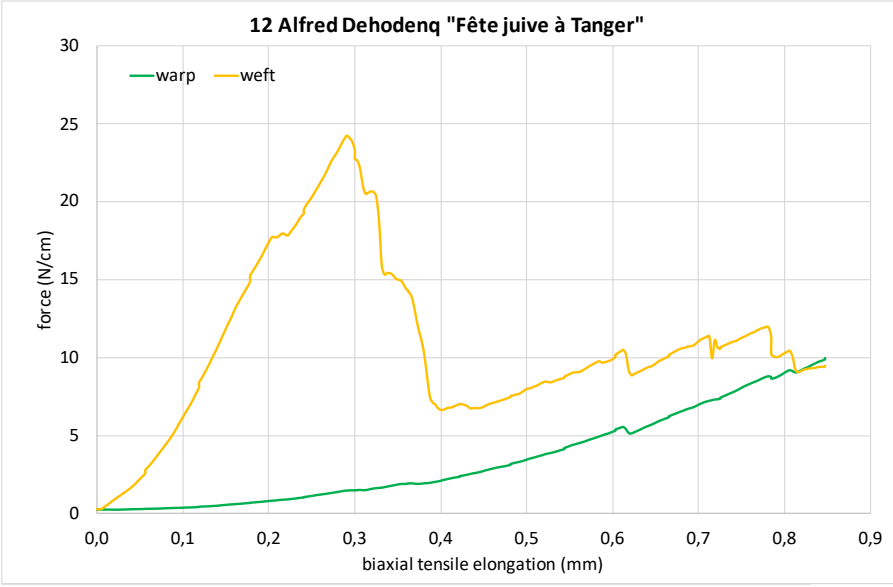

	warp	weft	unit
textile section area	3,24		
yarn section area	0,21	0,13	sqmm
uncrimped length	11,53	10,23	mm
yarn fiber volume	2,21	1,19	cmm
tot yarn vol in RUC	37,65	13,08	cmm
RUC volume	32,40		cmm
volume fraction	1,16	0,40	cmm
Pt (fiber thickness)	0,38	0,13	mm
plate thickness mean	0,25		mm
equiv fiber sect. area	3,77	1,31	sqmm

biax pretension	0,3	N/cm
samples tested	4	
plot is mean of	3	

strain location	**A**	**B**	**C**	**D**
strain value	0,005	0,019	0,047	0,085
warp force value (N/cm)	0,27	0,79	-	-
weft force value (N/cm)	2,38	17,40	-	-
textile thickness			**0,32** mm	
strain location	**A**	**B**	**C**	**D**
warp stress	0,08	0,24	-	-
weft stress	0,73	5,37	-	-
warp module (Mpa)	**17,9**	**12,9**	-	-
weft module (Mpa)	**155,8**	**284,6**	-	-
fiber fraction thickness mean			**0,25** mm	
strain location	**A**	**B**	**C**	**D**
warp stress (Mpa)	0,07	0,21	-	-
weft stress (Mpa)	1,82	13,30	-	-
warp module (Mpa)	**15,4**	**11,1**	-	-
weft module (Mpa)	**385,9**	**704,8**	-	-

author	Jules Gélibert
painting	*Griffons vendéens*
date	1881

			obs.	
warp yarn width	0,49	mm	9	w. mean
weft yarn width	0,41	mm	9	w. mean
warp yarn thickness	0,20	mm	9	w. mean
weft yarn thickness	0,23	mm	9	w. mean
warp yarn twist	244,2	TPM	9	w. mean
weft yarn twist	288,5	TPM	9	w. mean
warp yarn crimp	11,9	%	3	mean
weft yarn crimp	3,6	%	3	mean
warp count	24	yarns/cm	9	mean
weft count	18,7	yarns/cm	9	mean
weaving	machine			
fiber	linen			
pH	5,87			
weight	238	g/sqm	4	mean
textile thickness	0,45	mm	15	mean
n. of samples	4			
sample width	10	mm		
gauge length	10,6	mm		

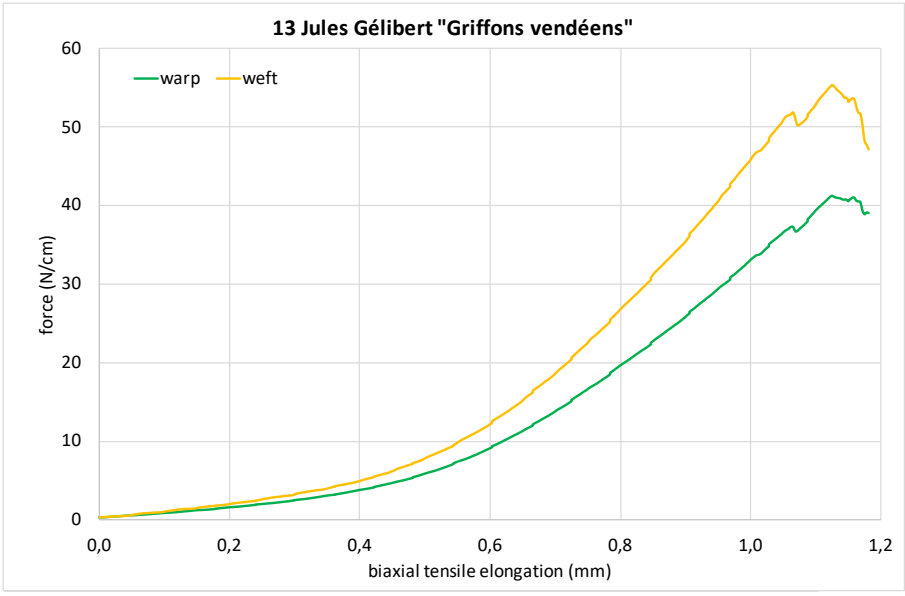

	warp	weft	unit
textile section area	4,50		
yarn section area	0,08	0,07	sqmm
uncrimped length	11,19	10,36	mm
yarn fiber volume	0,78	0,70	cmm
tot yarn vol in RUC	18,74	13,00	cmm
RUC volume	45,00		cmm
volume fraction	0,42	0,29	cmm
Pt (fiber thickness)	0,19	0,13	mm
plate thickness mean	0,16		mm
equiv fiber sect. area	1,87	1,30	sqmm

biax pretension	0,3	N/cm
samples tested	4	
plot is mean of	3	

strain location	**A**	**B**	**C**	**D**
strain value	0,005	0,019	0,047	0,085
warp force value (N/cm)	0,56	1,59	5,87	25,82
weft force value (N/cm)	0,59	2,00	7,81	35,40
textile thickness			**0,45** mm	
strain location	**A**	**B**	**C**	**D**
warp stress	0,12	0,35	1,31	5,74
weft stress	0,13	0,44	1,73	7,87
warp module (Mpa)	**26,3**	**18,7**	**27,7**	**67,6**
weft module (Mpa)	**28,0**	**23,6**	**36,8**	**92,6**
fiber fraction thickness mean			**0,16** mm	
strain location	**A**	**B**	**C**	**D**
warp stress (Mpa)	0,30	0,85	3,13	13,78
weft stress (Mpa)	0,46	1,54	6,00	27,22
warp module (Mpa)	**63,1**	**45,0**	**66,4**	**162,3**
weft module (Mpa)	**96,9**	**81,6**	**127,3**	**320,6**

author	Louis Augustin Auguin
painting	*Mer calme*
date	1885

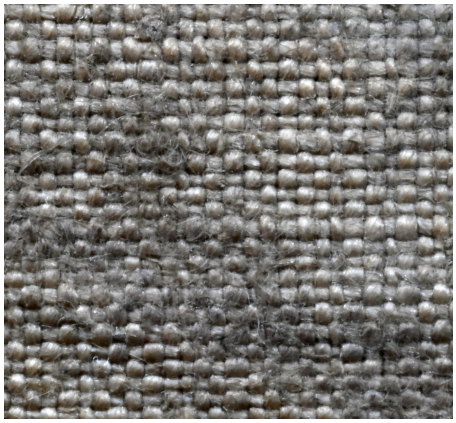

			obs.	
warp yarn width	0,39	mm	9	w. mean
weft yarn width	0,33	mm	9	w. mean
warp yarn thickness	0,24	mm	9	w. mean
weft yarn thickness	0,29	mm	9	w. mean
warp yarn twist	324,5	TPM	9	w. mean
weft yarn twist	464,6	TPM	9	w. mean
warp yarn crimp	13,0	%	3	mean
weft yarn crimp	4,7	%	3	mean
warp count	25,3	yarns/cm	9	mean
weft count	25	yarns/cm	9	mean
weaving	machine			
fiber	linen			
pH	6,08			
weight	296	g/sqm	4	mean
textile thickness	0,22	mm	15	mean
n. of samples	4			
sample width	10	mm		
gauge length	10,6	mm		

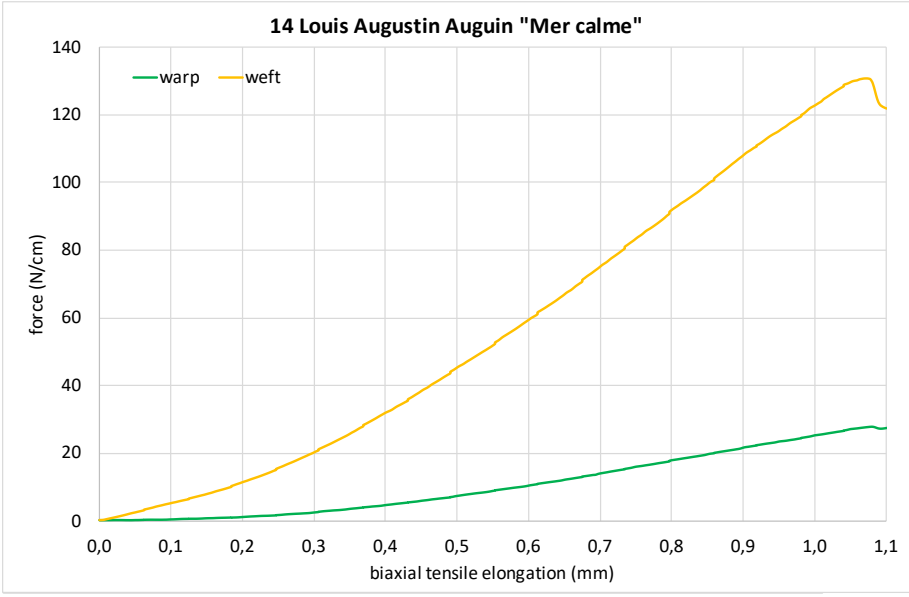

	warp	weft	unit
textile section area	2,16		
yarn section area	0,07	0,08	sqmm
uncrimped length	11,30	10,47	mm
yarn fiber volume	0,75	0,71	cmm
tot yarn vol in RUC	19,05	17,83	cmm
RUC volume	21,64		cmm
volume fraction	0,88	0,82	cmm
Pt (fiber thickness)	0,19	0,18	mm
plate thickness mean	0,18		mm
equiv fiber sect. area	1,90	1,78	sqmm

biax pretension	0,3	N/cm
samples tested	4	
plot is mean of	2	

strain location	**A**	**B**	**C**	**D**
strain value	0,005	0,019	0,047	0,085
warp force value (N/cm)	0,31	1,21	7,44	21,70
weft force value (N/cm)	2,58	11,50	45,36	108,01
textile thickness			**0,22** mm	
strain location	**A**	**B**	**C**	**D**
warp stress	0,15	0,56	3,44	10,03
weft stress	1,19	5,32	20,96	49,91
warp module (Mpa)	**30,8**	**29,8**	**72,9**	**118,1**
weft module (Mpa)	**252,3**	**281,8**	**444,4**	**587,8**
fiber fraction thickness mean			**0,18** mm	
strain location	**A**	**B**	**C**	**D**
warp stress (Mpa)	0,17	0,64	3,91	11,39
weft stress (Mpa)	1,44	6,45	25,44	60,59
warp module (Mpa)	**35,0**	**33,8**	**82,8**	**134,2**
weft module (Mpa)	**306,3**	**342,0**	**539,4**	**713,6**

author	Ludovic Alleaume
painting	*Les Fendeurs d'ardoise*
date	1887

			obs.	
warp yarn width	0,44	mm	9	w. mean
weft yarn width	0,35	mm	9	w. mean
warp yarn thickness	0,16	mm	9	w. mean
weft yarn thickness	0,17	mm	9	w. mean
warp yarn twist	213,3	TPM	9	w. mean
weft yarn twist	250,8	TPM	9	w. mean
warp yarn crimp	11,4	%	3	mean
weft yarn crimp	6,8	%	3	mean
warp count	24	yarns/cm	9	mean
weft count	21,7	yarns/cm	9	mean
weaving	machine			
fiber	linen			
pH	5,17			
weight	248	g/sqm	4	mean
textile thickness	0,44	mm	15	mean
n. of samples	4			
sample width	10	mm		
gauge length	10,6	mm		

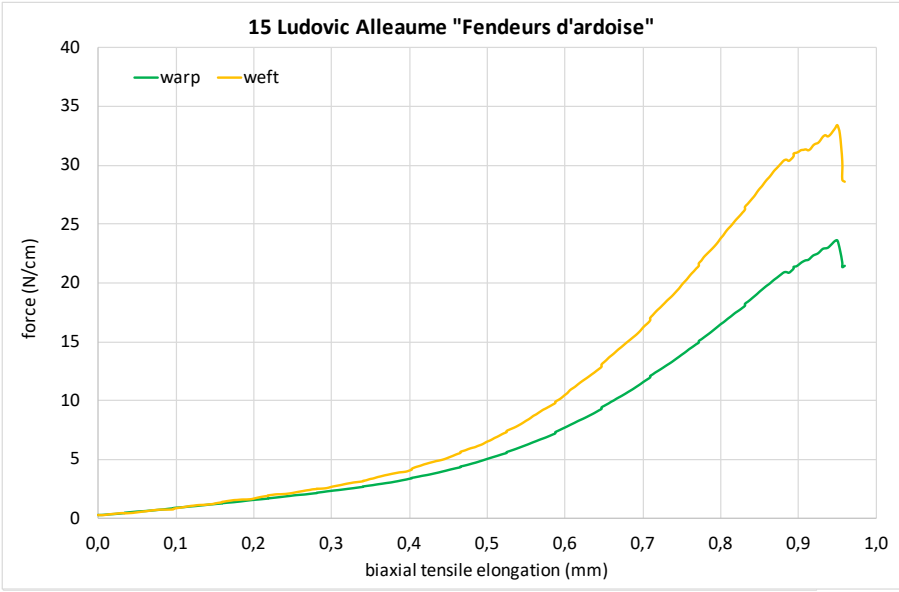

	warp	weft	unit
textile section area	4,44		
yarn section area	0,06	0,05	sqmm
uncrimped length	11,14	10,68	mm
yarn fiber volume	0,56	0,45	cmm
tot yarn vol in RUC	13,40	9,82	cmm
RUC volume	44,37		cmm
volume fraction	0,30	0,22	cmm
Pt (fiber thickness)	0,13	0,10	mm
plate thickness mean	0,12		mm
equiv fiber sect. area	1,34	0,98	sqmm

biax pretension	0,3	N/cm
samples tested	4	
plot is mean of	2	

strain location	**A**	**B**	**C**	**D**
strain value	0,005	0,019	0,047	0,085
warp force value (N/cm)	0,57	1,56	5,04	21,53
weft force value (N/cm)	0,50	1,67	6,51	31,13
textile thickness			**0,44** mm	
strain location	**A**	**B**	**C**	**D**
warp stress	0,13	0,35	1,14	4,85
weft stress	0,11	0,38	1,47	7,02
warp module (Mpa)	**27,1**	**18,6**	**24,1**	**57,1**
weft module (Mpa)	**23,9**	**19,9**	**31,1**	**82,6**
fiber fraction thickness mean			**0,12** mm	
strain location	**A**	**B**	**C**	**D**
warp stress (Mpa)	0,42	1,17	3,76	16,07
weft stress (Mpa)	0,51	1,70	6,63	31,70
warp module (Mpa)	**89,6**	**61,7**	**79,7**	**189,3**
weft module (Mpa)	**108,1**	**90,1**	**140,6**	**373,4**

author	Hubert Sauzeau
painting	*Enfants dans la neige*
date	1893

			obs.	
warp yarn width	0,48	mm	9	w. mean
weft yarn width	0,40	mm	9	w. mean
warp yarn thickness	0,23	mm	9	w. mean
weft yarn thickness	0,23	mm	9	w. mean
warp yarn twist	272,1	TPM	9	w. mean
weft yarn twist	366,5	TPM	9	w. mean
warp yarn crimp	13,7	%	3	mean
weft yarn crimp	5,7	%	3	mean
warp count	22	yarns/cm	9	mean
weft count	20	yarns/cm	9	mean
weaving	machine			
fiber	linen			
pH	6,16			
weight	205	g/sqm	4	mean
textile thickness	0,37	mm	15	mean
n. of samples	4			
sample width	10	mm		
gauge length	10,6	mm		

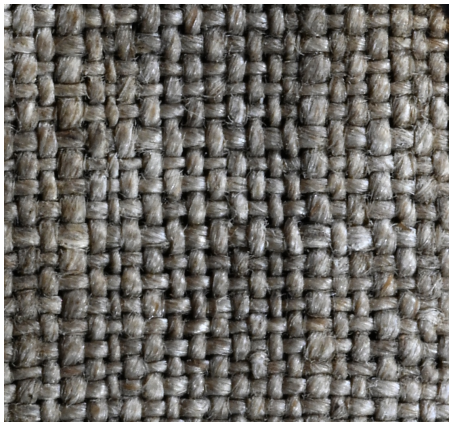

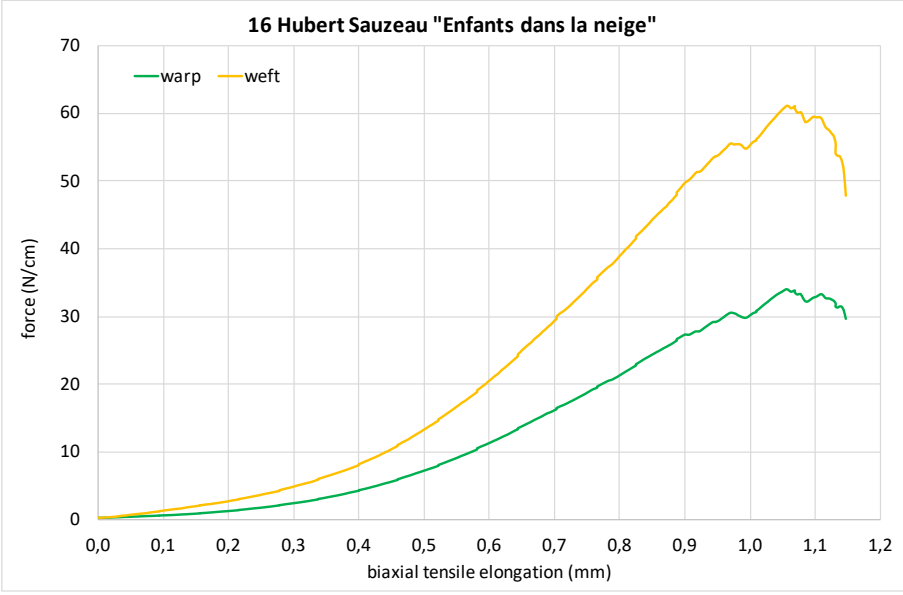

	warp	weft	unit
textile section area	3,70		
yarn section area	0,09	0,07	sqmm
uncrimped length	11,37	10,57	mm
yarn fiber volume	0,89	0,69	cmm
tot yarn vol in RUC	19,66	13,85	cmm
RUC volume	37,00		cmm
volume fraction	0,53	0,37	cmm
Pt (fiber thickness)	0,20	0,14	mm
plate thickness mean	0,17		mm
equiv fiber sect. area	1,97	1,38	sqmm

biax pretension	0,3	N/cm
samples tested	4	
plot is mean of	4	

strain location	**A**	**B**	**C**	**D**
strain value	0,005	0,019	0,047	0,085
warp force value (N/cm)	0,44	1,28	7,25	27,34
weft force value (N/cm)	0,73	2,73	13,31	49,74
textile thickness			**0,37** mm	
strain location	**A**	**B**	**C**	**D**
warp stress	0,12	0,35	1,96	7,39
weft stress	0,20	0,74	3,60	13,44
warp module (Mpa)	**25,1**	**18,3**	**41,5**	**87,0**
weft module (Mpa)	**41,8**	**39,1**	**76,3**	**158,3**
fiber fraction thickness mean			**0,17** mm	
strain location	**A**	**B**	**C**	**D**
warp stress (Mpa)	0,22	0,65	3,69	13,90
weft stress (Mpa)	0,53	1,97	9,61	35,92
warp module (Mpa)	**47,3**	**34,4**	**78,1**	**163,8**
weft module (Mpa)	**111,6**	**104,6**	**203,8**	**423,0**

author	Hubert Sauzeau
painting	*lutteurs*
date	1898

			obs.	
warp yarn width	0,77	mm	9	w. mean
weft yarn width	0,50	mm	9	w. mean
warp yarn thickness	0,32	mm	9	w. mean
weft yarn thickness	0,35	mm	9	w. mean
warp yarn twist	217,7	TPM	9	w. mean
weft yarn twist	219,8	TPM	9	w. mean
warp yarn crimp	19,7	%	3	mean
weft yarn crimp	6,0	%	3	mean
warp count	14	yarns/cm	9	mean
weft count	12	yarns/cm	9	mean
weaving	machine			
fiber	hemp			
pH	6,62			
weight	485	g/sqm	4	mean
textile thickness	0,81	mm	15	mean
n. of samples	5			
sample width	10	mm		
gauge length	10,6	mm		

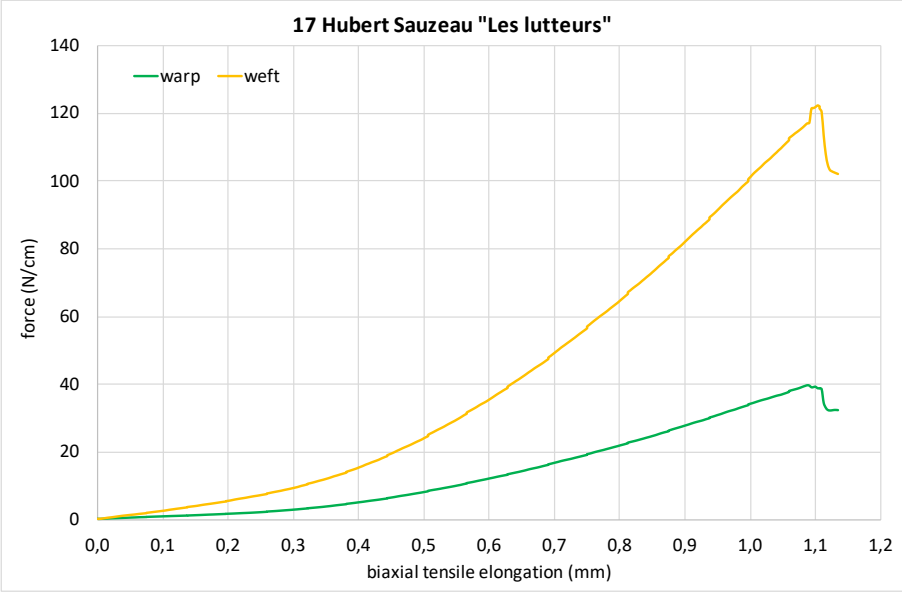

	warp	weft	unit
textile section area	8,10		
yarn section area	0,19	0,14	sqmm
uncrimped length	11,97	10,60	mm
yarn fiber volume	2,10	1,32	cmm
tot yarn vol in RUC	29,39	15,85	cmm
RUC volume	81,00		cmm
volume fraction	0,36	0,20	cmm
Pt (fiber thickness)	0,29	0,16	mm
plate thickness mean	0,23		mm
equiv fiber sect. area	2,94	1,58	sqmm

biax pretension	0,3	N/cm
samples tested	5	
plot is mean of	5	

strain location	**A**	**B**	**C**	**D**
strain value	0,005	0,019	0,047	0,085
warp force value (N/cm)	0,68	1,82	8,22	27,85
weft force value (N/cm)	1,47	5,63	24,11	82,10
textile thickness			**0,81** mm	
strain location	**A**	**B**	**C**	**D**
warp stress	0,08	0,22	1,01	3,44
weft stress	0,18	0,69	2,98	10,14
warp module (Mpa)	**17,9**	**11,9**	**21,5**	**40,5**
weft module (Mpa)	**38,5**	**36,8**	**63,1**	**119,4**
fiber fraction thickness mean			**0,23** mm	
strain location	**A**	**B**	**C**	**D**
warp stress (Mpa)	0,23	0,62	2,80	9,47
weft stress (Mpa)	0,93	3,55	15,21	51,80
warp module (Mpa)	**49,3**	**32,9**	**59,3**	**111,6**
weft module (Mpa)	**196,7**	**188,1**	**322,5**	**610,1**

author	Charles Müller
painting	*Mr de Parseval*
date	late 19th c.

			obs.	
warp yarn width	0,35	mm	9	w. mean
weft yarn width	0,30	mm	9	w. mean
warp yarn thickness	0,14	mm	9	w. mean
weft yarn thickness	0,14	mm	9	w. mean
warp yarn twist	362,4	TPM	9	w. mean
weft yarn twist	381,0	TPM	9	w. mean
warp yarn crimp	10,3	%	3	mean
weft yarn crimp	5,7	%	3	mean
warp count	31,3	yarns/cm	9	mean
weft count	29	yarns/cm	9	mean
weaving	machine			
fiber	linen			
pH	5,62			
weight	150	g/sqm	4	mean
textile thickness	0,26	mm	15	mean
n. of samples	4			
sample width	10	mm		
gauge length	10,6	mm		

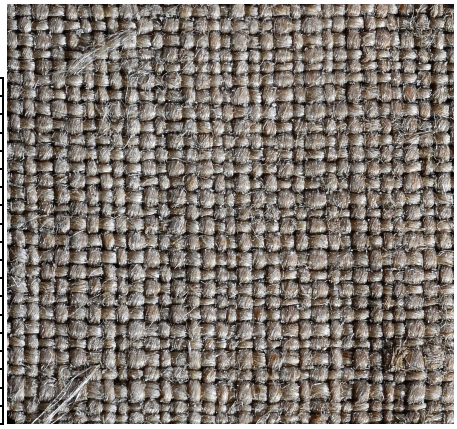

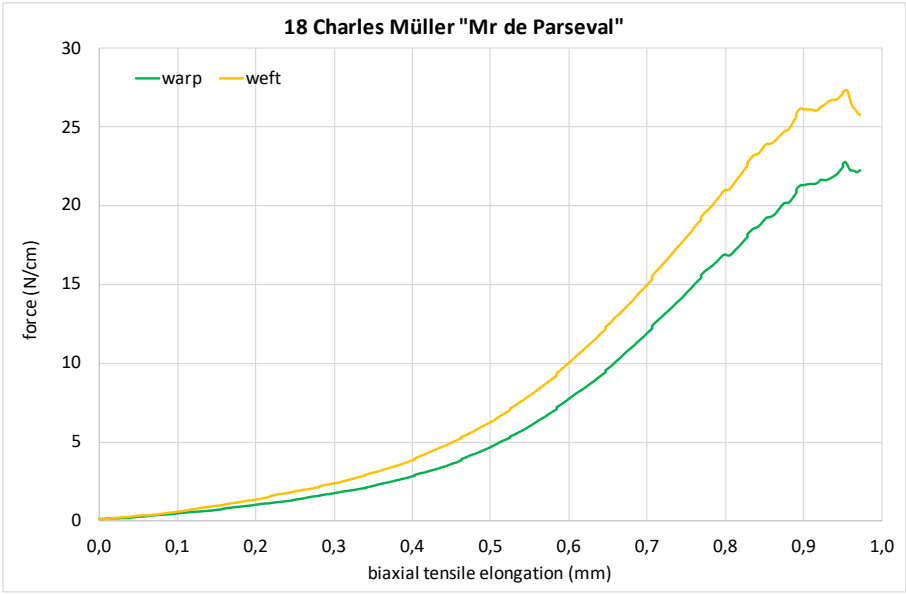

	warp	weft	unit
textile section area	2,60		
yarn section area	0,04	0,03	sqmm
uncrimped length	11,03	10,57	mm
yarn fiber volume	0,38	0,32	cmm
tot yarn vol in RUC	12,04	9,17	cmm
RUC volume	26,00		cmm
volume fraction	0,46	0,35	cmm
Pt (fiber thickness)	0,12	0,09	mm
plate thickness mean	0,11		mm
equiv fiber sect. area	1,20	0,92	sqmm

biax pretension	0,3	N/cm
samples tested	3	
plot is mean of	2	

strain location	**A**	**B**	**C**	**D**
strain value	0,005	0,019	0,047	0,085
warp force value (N/cm)	0,26	1,02	4,68	21,30
weft force value (N/cm)	0,33	1,35	6,27	26,10
textile thickness			**0,26** mm	
strain location	**A**	**B**	**C**	**D**
warp stress	0,10	0,39	1,80	8,19
weft stress	0,13	0,52	2,41	10,04
warp module (Mpa)	**20,9**	**20,8**	**38,2**	**96,5**
weft module (Mpa)	**26,5**	**27,5**	**51,1**	**118,2**
fiber fraction thickness mean			**0,11** mm	
strain location	**A**	**B**	**C**	**D**
warp stress (Mpa)	0,21	0,85	3,89	17,68
weft stress (Mpa)	0,35	1,47	6,84	28,47
warp module (Mpa)	**45,1**	**44,9**	**82,4**	**208,3**
weft module (Mpa)	**75,3**	**78,1**	**144,9**	**335,3**

painting	*Fleurs 'été*
date	late 19th c.

			obs.	
warp yarn width	0,48	mm	9	w. mean
weft yarn width	0,36	mm	9	w. mean
warp yarn thickness	0,17	mm	9	w. mean
weft yarn thickness	0,22	mm	9	w. mean
warp yarn twist	204,4	TPM	9	w. mean
weft yarn twist	339,7	TPM	9	w. mean
warp yarn crimp	14,2	%	3	mean
weft yarn crimp	3,0	%	3	mean
warp count	23,5	yarns/cm	9	mean
weft count	22,3	yarns/cm	9	mean
weaving	machine			
fiber	hemp			
pH	6,02			
weight	228	g/sqm	4	mean
textile thickness	0,38	mm	15	mean
n. of samples	4			
sample width	10	mm		
gauge length	10,6	mm		

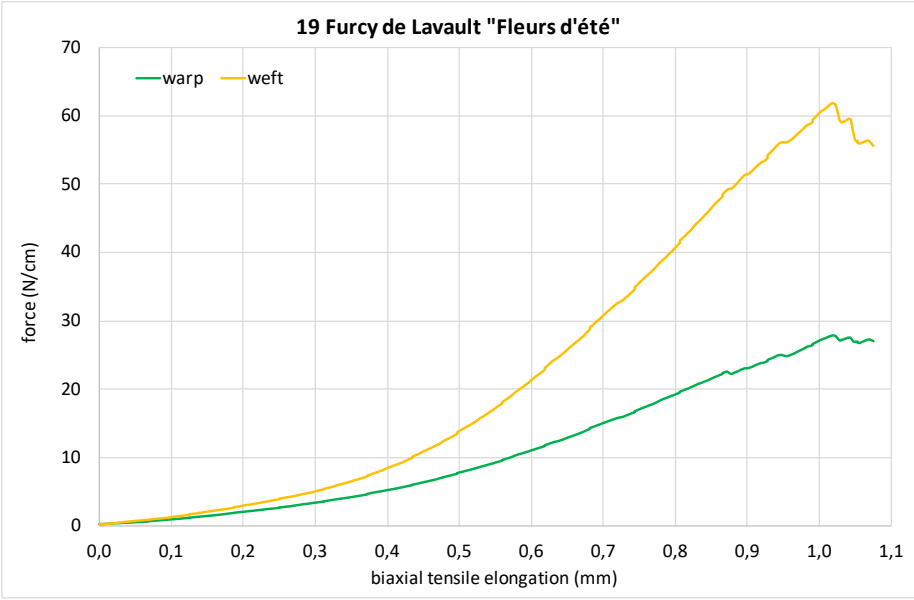

	warp	weft	unit
textile section area	3,80		
yarn section area	0,06	0,06	sqmm
uncrimped length	11,42	10,30	mm
yarn fiber volume	0,66	0,58	cmm
tot yarn vol in RUC	15,59	12,95	cmm
RUC volume	38,00		cmm
volume fraction	0,41	0,34	cmm
Pt (fiber thickness)	0,16	0,13	mm
plate thickness mean	0,14		mm
equiv fiber sect. area	1,56	1,30	sqmm

biax pretension	0,3	N/cm
samples tested	4	
plot is mean of	4	

strain location	**A**	**B**	**C**	**D**
strain value	0,005	0,019	0,047	0,085
warp force value (N/cm)	0,54	2,07	7,82	23,07
weft force value (N/cm)	0,73	2,99	13,90	51,46
textile thickness			**0,38** mm	
strain location	**A**	**B**	**C**	**D**
warp stress	0,14	0,54	2,06	6,07
weft stress	0,19	0,79	3,66	13,54
warp module (Mpa)	**30,1**	**28,9**	**43,6**	**71,5**
weft module (Mpa)	**41,0**	**41,7**	**77,5**	**159,5**
fiber fraction thickness mean			**0,14** mm	
strain location	**A**	**B**	**C**	**D**
warp stress (Mpa)	0,35	1,33	5,02	14,80
weft stress (Mpa)	0,57	2,31	10,73	39,73
warp module (Mpa)	**73,4**	**70,3**	**106,3**	**174,3**
weft module (Mpa)	**120,2**	**122,3**	**227,5**	**467,9**

author	Louis Alexandre Cabié
painting	*La Chaumière*
date	1905

			obs.	
warp yarn width	0,73	mm	9	w. mean
weft yarn width	0,82	mm	9	w. mean
warp yarn thickness	0,38	mm	9	w. mean
weft yarn thickness	0,48	mm	9	w. mean
warp yarn twist	249,2	TPM	9	w. mean
weft yarn twist	168,7	TPM	9	w. mean
warp yarn crimp	10,4	%	3	mean
weft yarn crimp	3,2	%	3	mean
warp count	11,7	yarns/cm	9	mean
weft count	10,8	yarns/cm	9	mean
weaving	machine			
fiber	warp cotton	weft hemp		
pH	5,9			
weight	276	g/sqm	4	mean
textile thickness	0,28	mm	15	mean
n. of samples	4			
sample width	10	mm		
gauge length	10,6	mm		

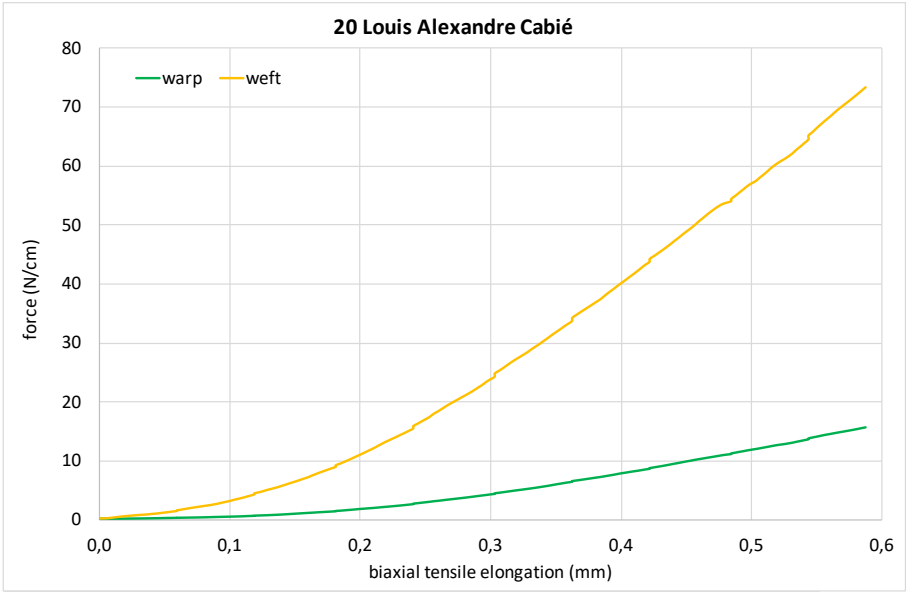

	warp	weft	unit
textile section area	2,80		
yarn section area	0,22	0,31	sqmm
uncrimped length	11,04	10,32	mm
yarn fiber volume	2,18	2,89	cmm
tot yarn vol in RUC	25,51	31,23	cmm
RUC volume	28,00		cmm
volume fraction	0,91	1,12	cmm
Pt (fiber thickness)	0,26	0,31	mm
plate thickness mean	0,28		mm
equiv fiber sect. area	2,55	3,12	sqmm

biax pretension	0,3	N/cm
samples tested	4	
plot is mean of	3	

strain location	**A**	**B**	**C**	**D**
strain value	0,005	0,019	0,047	0,085
warp force value (N/cm)	0,33	1,86	11,90	-
weft force value (N/cm)	1,26	11,07	57,03	-
textile thickness			**0,28**	mm
strain location	**A**	**B**	**C**	**D**
warp stress	0,12	0,67	4,25	-
weft stress	0,45	3,96	20,37	-
warp module (Mpa)	**24,7**	**35,3**	**90,1**	**-**
weft module (Mpa)	**95,1**	**209,6**	**431,8**	-
fiber fraction thickness mean			**0,28**	mm
strain location	**A**	**B**	**C**	**D**
warp stress (Mpa)	0,13	0,73	4,67	-
weft stress (Mpa)	0,40	3,55	18,26	-
warp module (Mpa)	**27,1**	**38,7**	**98,9**	**-**
weft module (Mpa)	**85,3**	**187,9**	**387,1**	**-**

author	Ernest Louis Lessieux
painting	*Sirène*
date	early 20th century

			obs.	
warp yarn width	0,48	mm	9	w. mean
weft yarn width	0,29	mm	9	w. mean
warp yarn thickness	0,14	mm	9	w. mean
weft yarn thickness	0,17	mm	9	w. mean
warp yarn twist	254,8	TPM	9	w. mean
weft yarn twist	371,6	TPM	9	w. mean
warp yarn crimp	13,7	%	3	mean
weft yarn crimp	6,3	%	3	mean
warp count	21	yarns/cm	9	mean
weft count	21	yarns/cm	9	mean
weaving	machine			
fiber	hemp			
pH	6,39			
weight	197	g/sqm	4	mean
textile thickness	0,20	mm	15	mean
n. of samples	4			
sample width	10	mm		
gauge length	10,6	mm		

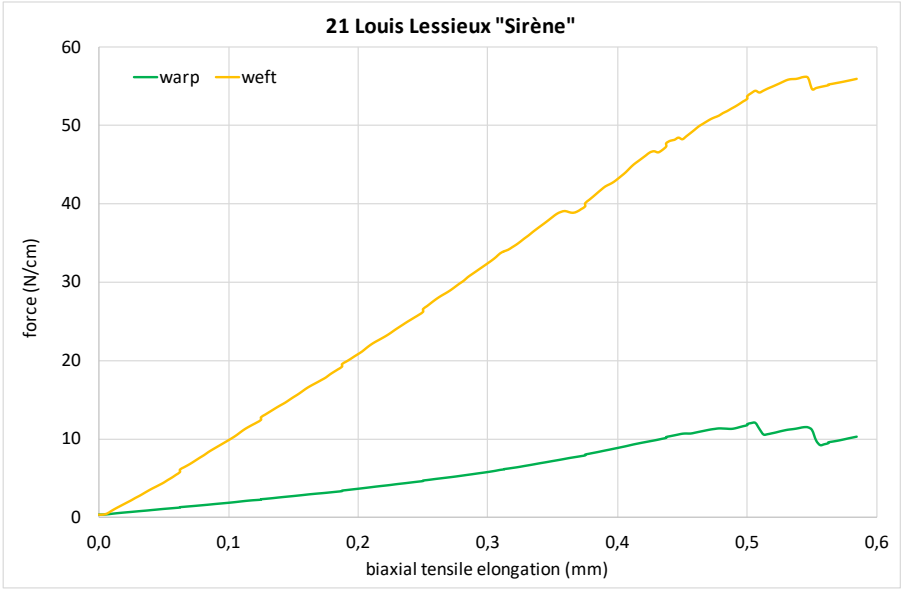

	warp	weft	unit
textile section area	2,00		
yarn section area	0,05	0,04	sqmm
uncrimped length	11,37	10,63	mm
yarn fiber volume	0,54	0,37	cmm
tot yarn vol in RUC	11,42	7,84	cmm
RUC volume	20,00		cmm
volume fraction	0,57	0,39	cmm
Pt (fiber thickness)	0,11	0,08	mm
plate thickness mean	0,10		mm
equiv fiber sect. area	1,14	0,78	sqmm

biax pretension	0,3	N/cm
samples tested	4	
plot is mean of	4	

strain location	**A**	**B**	**C**	**D**
strain value	0,005	0,019	0,047	0,085
warp force value (N/cm)	1,06	3,63	11,88	-
weft force value (N/cm)	4,42	20,83	53,73	-
textile thickness			**0,20**	mm
strain location	**A**	**B**	**C**	**D**
warp stress	0,53	1,82	5,94	-
weft stress	2,21	10,41	26,86	-
warp module (Mpa)	**112,2**	**96,2**	**125,9**	-
weft module (Mpa)	**468,0**	**551,9**	**569,5**	-
fiber fraction thickness mean			**0,10**	mm
strain location	**A**	**B**	**C**	**D**
warp stress (Mpa)	0,93	3,18	10,40	-
weft stress (Mpa)	5,64	26,58	68,57	-
warp module (Mpa)	**196,4**	**168,5**	**220,4**	-
weft module (Mpa)	**1194,6**	**1408,6**	**1453,6**	-

author	Jeannine Gilles-Murique
painting	*Falaises*
date	mid 20th century

			obs.	
warp yarn width	1,08	mm	9	w. mean
weft yarn width	1,14	mm	9	w. mean
warp yarn thickness	0,37	mm	9	w. mean
weft yarn thickness	0,45	mm	9	w. mean
warp yarn twist	125,0	TPM	9	w. mean
weft yarn twist	64,4	TPM	9	w. mean
warp yarn crimp	6,4	%	3	mean
weft yarn crimp	3,9	%	3	mean
warp count	8	yarns/cm	9	mean
weft count	8	yarns/cm	9	mean
weaving	machine			
fiber	hemp			
pH	5,49			
weight	385	g/sqm	4	mean
textile thickness	0,80	mm	15	mean
n. of samples	6			
sample width	10	mm		
gauge length	10,6	mm		

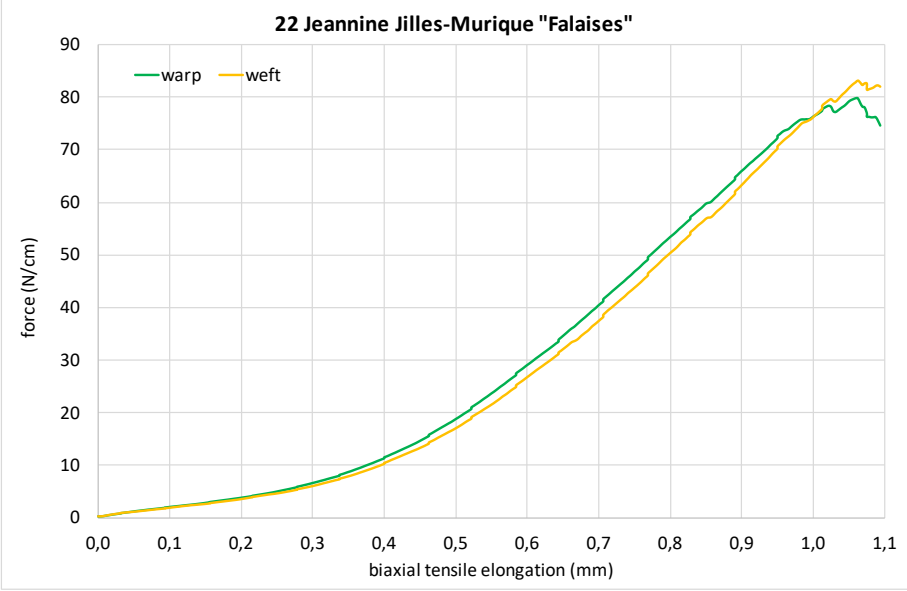

	warp	weft	unit
textile section area	8,00		
yarn section area	0,31	0,40	sqmm
uncrimped length	10,64	10,39	mm
yarn fiber volume	3,03	3,79	cmm
tot yarn vol in RUC	24,22	30,36	cmm
RUC volume	80,00		cmm
volume fraction	0,30	0,38	cmm
Pt (fiber thickness)	0,24	0,30	mm
plate thickness mean	0,27		mm
equiv fiber sect. area	2,42	3,04	sqmm

biax pretension	0,3	N/cm
samples tested	6	
plot is mean of	5	

strain location	**A**	**B**	**C**	**D**
strain value	0,005	0,019	0,047	0,085
warp force value (N/cm)	1,26	3,86	18,81	65,99
weft force value (N/cm)	1,20	3,60	17,06	63,31
textile thickness			**0,80** mm	
strain location	**A**	**B**	**C**	**D**
warp stress	0,16	0,48	2,35	8,25
weft stress	0,15	0,45	2,13	7,91
warp module (Mpa)	**33,5**	**25,6**	**49,9**	**97,1**
weft module (Mpa)	**31,8**	**23,9**	**45,2**	**93,2**
fiber fraction thickness mean			**0,27** mm	
strain location	**A**	**B**	**C**	**D**
warp stress (Mpa)	0,52	1,59	7,77	27,25
weft stress (Mpa)	0,39	1,19	5,62	20,85
warp module (Mpa)	**110,5**	**84,4**	**164,7**	**320,9**
weft module (Mpa)	**83,7**	**62,9**	**119,1**	**245,6**

author	lining canvas
painting	*basket weave*
date	second half 20th c.

			obs.	
warp yarn width	0,69	mm	9	w. mean
weft yarn width	0,46	mm	9	w. mean
warp yarn thickness	0,27	mm	9	w. mean
weft yarn thickness	0,31	mm	9	w. mean
warp yarn twist	181,7	TPM	9	w. mean
weft yarn twist	262,5	TPM	9	w. mean
warp yarn crimp	7,2	%	3	mean
weft yarn crimp	1,6	%	3	mean
warp count	20	yarns/cm	9	mean
weft count	16	yarns/cm	9	mean
weaving	machine			
fiber	linen			
pH	6,24			
weight	380	g/sqm	4	mean
textile thickness	0,72	mm	15	mean
n. of samples	4			
sample width	10	mm		
gauge length	10,6	mm		

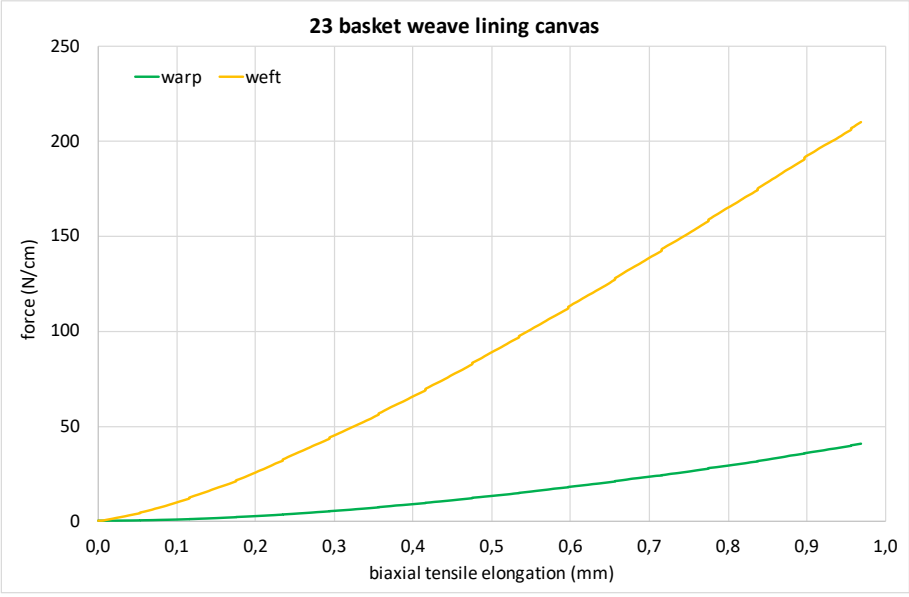

	warp	weft	unit
textile section area	7,20		
yarn section area	0,15	0,11	sqmm
uncrimped length	10,72	10,16	mm
yarn fiber volume	1,42	1,03	cmm
tot yarn vol in RUC	28,43	16,50	cmm
RUC volume	72,00		cmm
volume fraction	0,39	0,23	cmm
Pt (fiber thickness)	0,28	0,17	mm
plate thickness mean	0,22		mm
equiv fiber sect. area	2,84	1,65	sqmm

biax pretension	0,3	N/cm
samples tested	4	
plot is mean of	4	

strain location	**A**	**B**	**C**	**D**
strain value	0,005	0,019	0,047	0,085
warp force value (N/cm)	0,46	2,72	13,34	36,01
weft force value (N/cm)	3,98	25,69	89,03	192,35
textile thickness			**0,72** mm	
strain location	**A**	**B**	**C**	**D**
warp stress	0,06	0,38	1,85	5,00
weft stress	0,55	3,57	12,36	26,72
warp module (Mpa)	**13,5**	**20,1**	**39,3**	**58,9**
weft module (Mpa)	**117,1**	**189,1**	**262,1**	**314,6**
fiber fraction thickness mean			**0,22** mm	
strain location	**A**	**B**	**C**	**D**
warp stress (Mpa)	0,16	0,96	4,69	12,67
weft stress (Mpa)	2,41	15,57	53,95	116,57
warp module (Mpa)	**34,2**	**50,8**	**99,5**	**149,2**
weft module (Mpa)	**511,0**	**825,2**	**1143,7**	**1372,9**

author	lining canvas
painting	*pattina*
date	2015

			obs.	
warp yarn width	0,42	mm	9	w. mean
weft yarn width	0,46	mm	9	w. mean
warp yarn thickness	0,31	mm	9	w. mean
weft yarn thickness	0,32	mm	9	w. mean
warp yarn twist	291,9	TPM	9	w. mean
weft yarn twist	195,4	TPM	9	w. mean
warp yarn crimp	2,9	%	3	mean
weft yarn crimp	1,6	%	3	mean
warp count	9	yarns/cm	9	mean
weft count	9	yarns/cm	9	mean
weaving	machine			
fiber	linen			
pH	6,53			
weight	149	g/sqm	4	mean
textile thickness	0,44	mm	15	mean
n. of samples	4			
sample width	10	mm		
gauge length	10,6	mm		

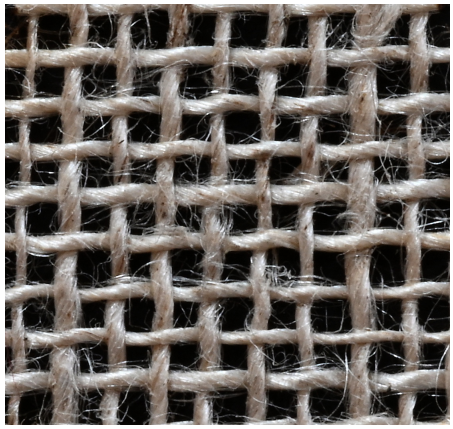

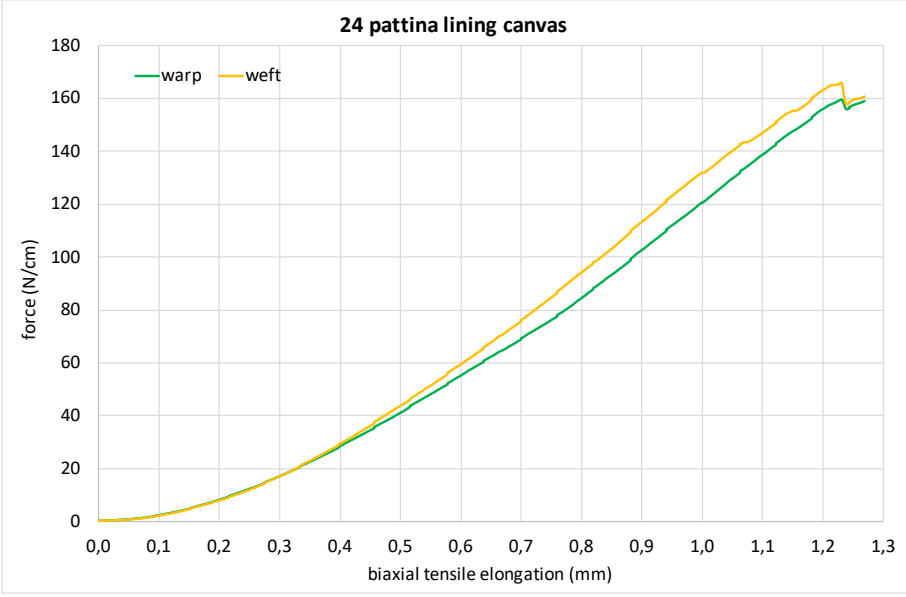

	warp	weft	unit
textile section area	4,40		
yarn section area	0,10	0,12	sqmm
uncrimped length	10,29	10,16	mm
yarn fiber volume	0,95	1,06	cmm
tot yarn vol in RUC	8,59	9,58	cmm
RUC volume	44,00		cmm
volume fraction	0,20	0,22	cmm
Pt (fiber thickness)	0,09	0,10	mm
plate thickness mean	0,09		mm
equiv fiber sect. area	0,86	0,96	sqmm

biax pretension	0,3	N/cm
samples tested	4	
plot is mean of	3	

strain location	**A**	**B**	**C**	**D**
strain value	0,005	0,019	0,047	0,085
warp force value (N/cm)	0,88	8,22	41,11	102,68
weft force value (N/cm)	0,76	7,98	43,73	113,32
textile thickness			**0,44** mm	
strain location	**A**	**B**	**C**	**D**
warp stress	0,20	1,87	9,34	23,34
weft stress	0,17	1,81	9,94	25,75
warp module (Mpa)	**42,6**	**99,0**	**198,1**	**274,9**
weft module (Mpa)	**36,6**	**96,1**	**210,7**	**303,3**
fiber fraction thickness mean			**0,09** mm	
strain location	**A**	**B**	**C**	**D**
warp stress (Mpa)	1,03	9,57	47,89	119,61
weft stress (Mpa)	0,79	8,32	45,64	118,25
warp module (Mpa)	**218,1**	**507,3**	**1015,2**	**1408,7**
weft module (Mpa)	**167,8**	**441,1**	**967,5**	**1392,7**

author	lining canvas
painting	*patta*
date	2015

			obs.	
warp yarn width	0,81	mm	9	w. mean
weft yarn width	0,77	mm	9	w. mean
warp yarn thickness	0,37	mm	9	w. mean
weft yarn thickness	0,41	mm	9	w. mean
warp yarn twist	143,3	TPM	9	w. mean
weft yarn twist	160,3	TPM	9	w. mean
warp yarn crimp	2,3	%	3	mean
weft yarn crimp	2	%	3	mean
warp count	7	yarns/cm	9	mean
weft count	5	yarns/cm	9	mean
weaving	machine			
fiber	linen			
pH	7			
weight	170,70	g/sqm	4	mean
textile thickness	0,56	mm	15	mean
n. of samples	4			
sample width	10	mm		
gauge length	10,6	mm		

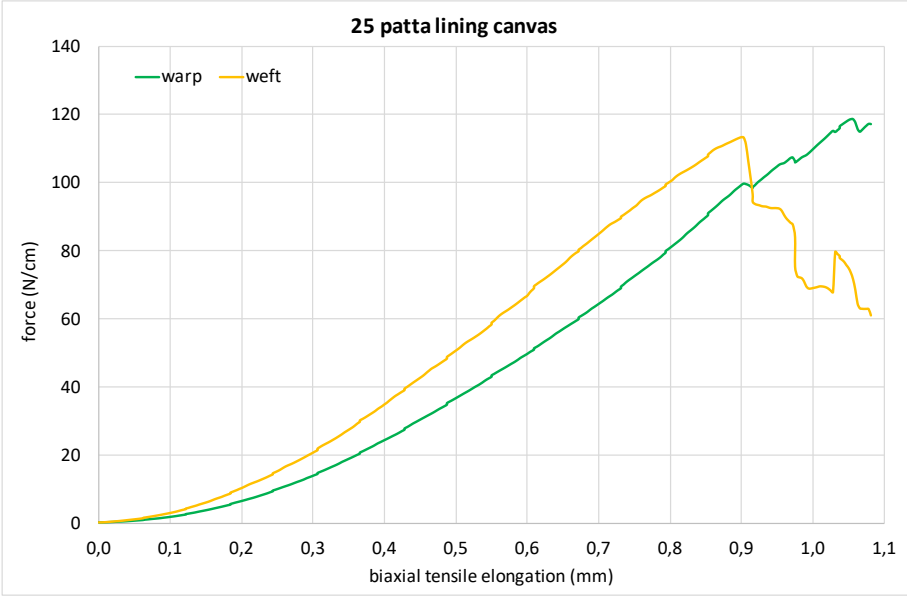

	warp	weft	unit
textile section area	5,60		
yarn section area	0,24	0,25	sqmm
uncrimped length	10,23	10,20	mm
yarn fiber volume	2,18	2,29	cmm
tot yarn vol in RUC	15,28	11,46	cmm
RUC volume	56,00		cmm
volume fraction	0,27	0,20	cmm
Pt (fiber thickness)	0,15	0,11	mm
plate thickness mean	0,13		mm
equiv fiber sect. area	1,53	1,15	sqmm

biax pretension	0,3	N/cm
samples tested	4	
plot is mean of	3	

strain location	**A**	**B**	**C**	**D**
strain value	0,005	0,019	0,047	0,085
warp force value (N/cm)	0,82	6,59	36,78	99,37
weft force value (N/cm)	1,21	10,39	50,74	113,38
textile thickness			**0,56** mm	
strain location	**A**	**B**	**C**	**D**
warp stress	0,15	1,18	6,57	17,75
weft stress	0,22	1,85	9,06	20,25
warp module (Mpa)	**31,1**	**62,4**	**139,2**	**209,0**
weft module (Mpa)	**45,7**	**98,3**	**192,1**	**238,5**
fiber fraction thickness mean			**0,13** mm	
strain location	**A**	**B**	**C**	**D**
warp stress (Mpa)	0,54	4,31	24,07	65,03
weft stress (Mpa)	1,05	9,06	44,26	98,91
warp module (Mpa)	**113,9**	**228,7**	**510,3**	**765,9**
weft module (Mpa)	**223,2**	**480,3**	**938,3**	**1164,9**

author	Canvassing project
painting	*test "03f"*
date	2022

			obs.	
warp yarn width	0,73	mm	9	w. mean
weft yarn width	0,67	mm	9	w. mean
warp yarn thickness	0,50	mm	9	w. mean
weft yarn thickness	0,46	mm	9	w. mean
warp yarn twist	159,5	TPM	9	w. mean
weft yarn twist	162,9	TPM	9	w. mean
warp yarn crimp	5,5	%	3	mean
weft yarn crimp	2,5	%	3	mean
warp count	12	yarns/cm	9	mean
weft count	7	yarns/cm	9	mean
weaving	hand			
fiber	linen			
pH	7,78			
weight	349	g/sqm	4	mean
textile thickness	0,81	mm	15	mean
n. of samples	4			
sample width	10	mm		
gauge length	10,6	mm		

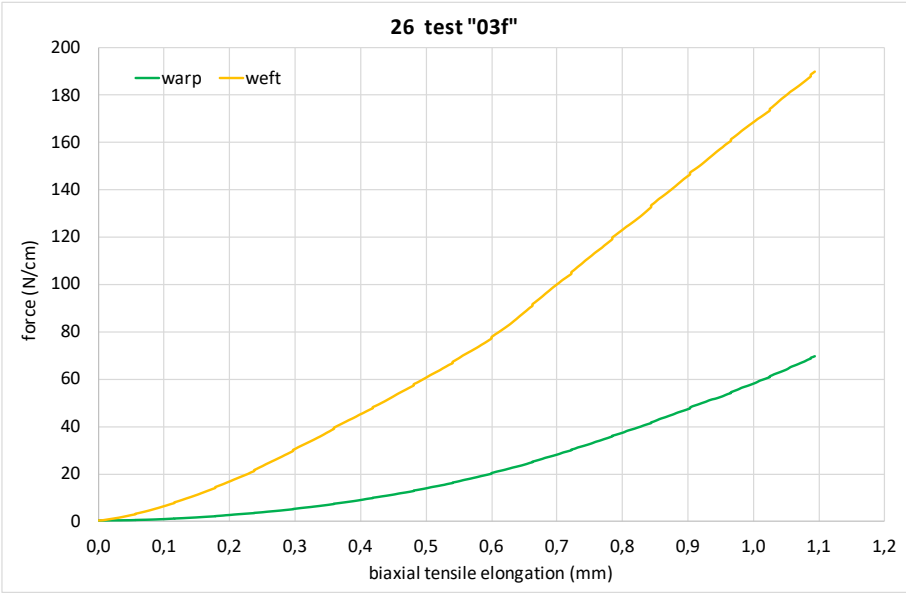

	warp	weft	unit
textile section area	8,10		
yarn section area	0,29	0,24	sqmm
uncrimped length	10,55	10,25	mm
yarn fiber volume	2,74	2,25	cmm
tot yarn vol in RUC	32,89	15,75	cmm
RUC volume	81,00		cmm
volume fraction	0,41	0,19	cmm
Pt (fiber thickness)	0,33	0,16	mm
plate thickness mean	0,24		mm
equiv fiber sect. area	3,29	1,57	sqmm

biax pretension	0,3	N/cm
samples tested	4	
plot is mean of	3	

strain location	**A**	**B**	**C**	**D**
strain value	0,005	0,019	0,047	0,085
warp force value (N/cm)	0,43	2,62	13,86	47,31
weft force value (N/cm)	2,58	16,77	60,61	145,80
textile thickness			**0,81** mm	
strain location	**A**	**B**	**C**	**D**
warp stress	0,05	0,32	1,71	5,84
weft stress	0,32	2,07	7,48	18,00
warp module (Mpa)	**11,1**	**17,1**	**36,3**	**68,8**
weft module (Mpa)	**67,5**	**109,8**	**158,6**	**212,0**
fiber fraction thickness mean			**0,24** mm	
strain location	**A**	**B**	**C**	**D**
warp stress (Mpa)	0,13	0,80	4,21	14,38
weft stress (Mpa)	1,64	10,65	38,49	92,60
warp module (Mpa)	**27,5**	**42,2**	**89,3**	**169,4**
weft module (Mpa)	**347,1**	**564,6**	**816,0**	**1090,6**

Appendix 2 Additional tensile test data

2.1 Individual yarn tests, correlated to uniaxial and biaxial tests of the same textile

The individual yarns provide a highly variable tensile response; therefore 13-15 samples were tested for each and a constant number of 10 were used for their means in order to eliminate the outliers and reduce random variability. A similar approach was used for the 10 mm uniaxial tests, though their variability is much lower.

In Figure 105, we see that the warp yarns in specimen 23 display a very long decrimping phase, as already seen in chapters 5 and 6.

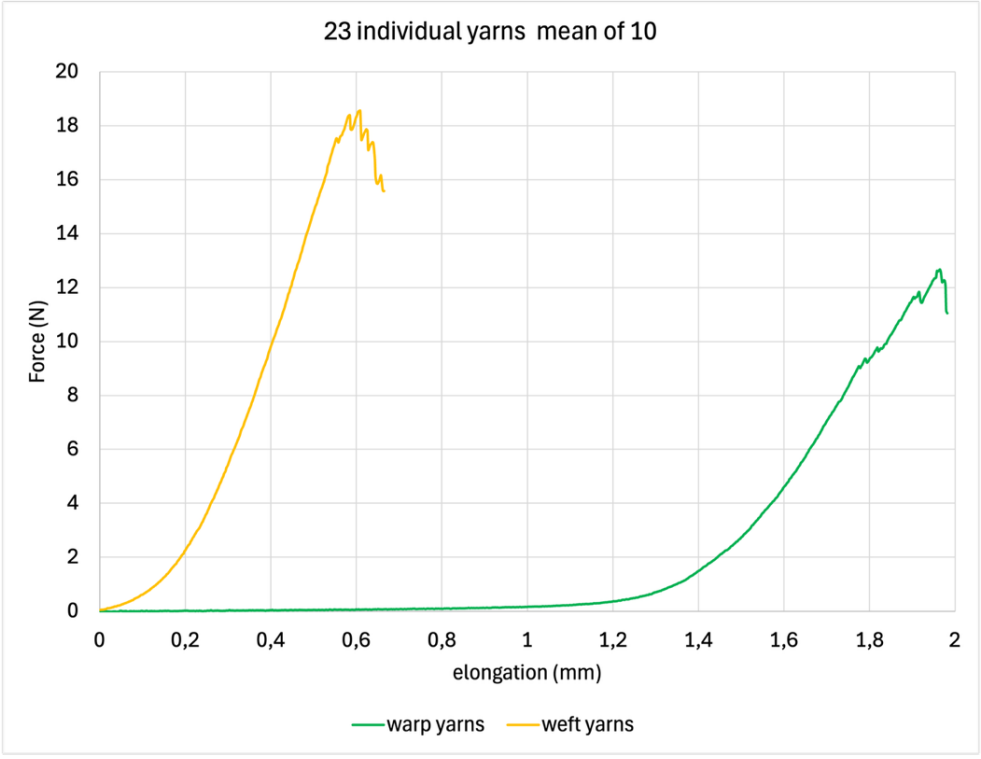

Figure 105 Individual yarns plots from specimen 23, in warp and weft

In Figure 106 and Figure 107, we see the uniaxial and biaxial tensile tests for specimen 23. Plots confirm the roles played by the weft and warp directions, and show that, after the decrimping phase, the ultimate load values become very similar. The slope of the straight-line region of the plot is nevertheless lower for the warp direction. The stiffness transfer in biaxial testing becomes evident looking at the tensile response of the warp under the same elongation value (at about 1 mm, about 22 N in uniaxial and 37 N in biaxial).

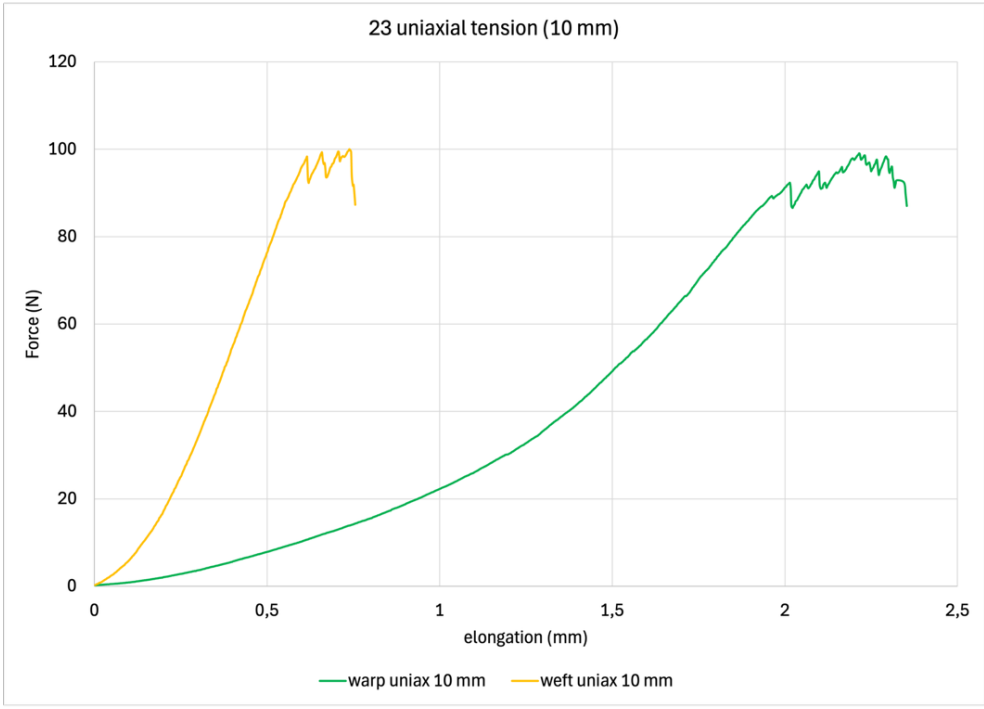

Figure 106 Uniaxial test values for the 10 mm samples of specimen 23

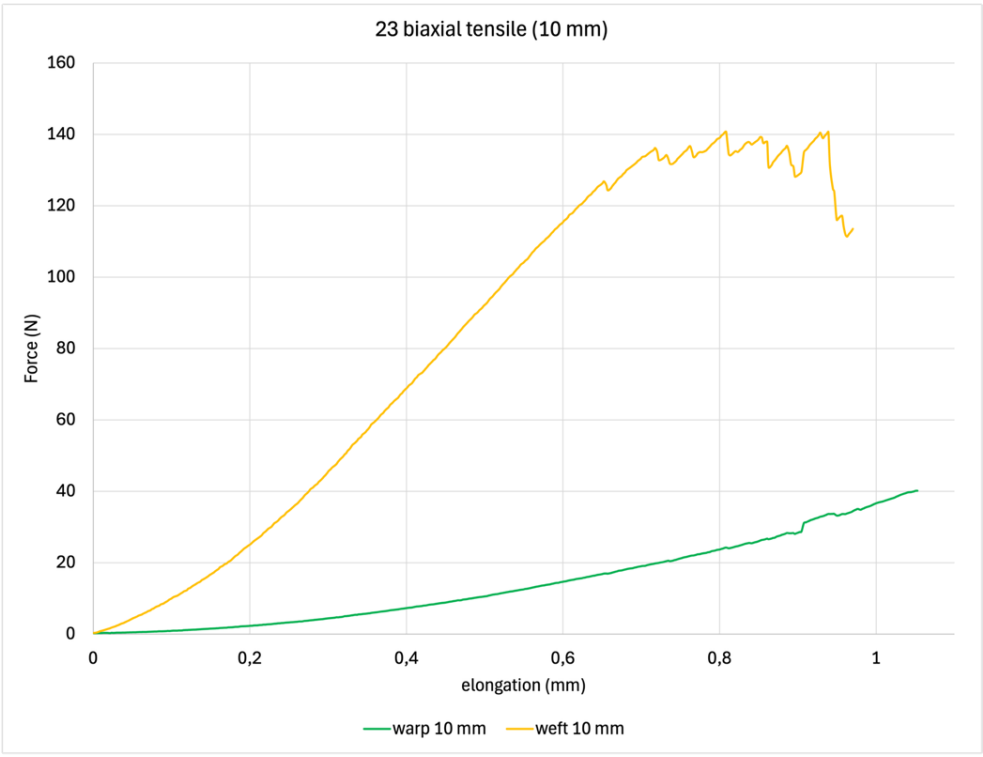

Figure 107 Biaxial test values for the 10 mm samples of specimen 23

In Figure 108 and in Figure 109, we see the uniaxial tensile tests for specimen 23 compared to the individual yarn plots. For the warp direction, we see that the individual yarns face decrimping offering no resistance (force value close to 0), while in the 10 mm uniaxial textile samples some force is recorded, due to the friction with the weft yarns, though they are not under tension. Once the decrimping phase is completed, yarns start a full tensile test and the ultimate load is reached at a slightly lower elongation if compared to the textile. Similar conclusions can be drawn for the weft direction, though the decrimping phase is ended after a much shorter elongation (about 0.12 mm instead of 1.2 mm).

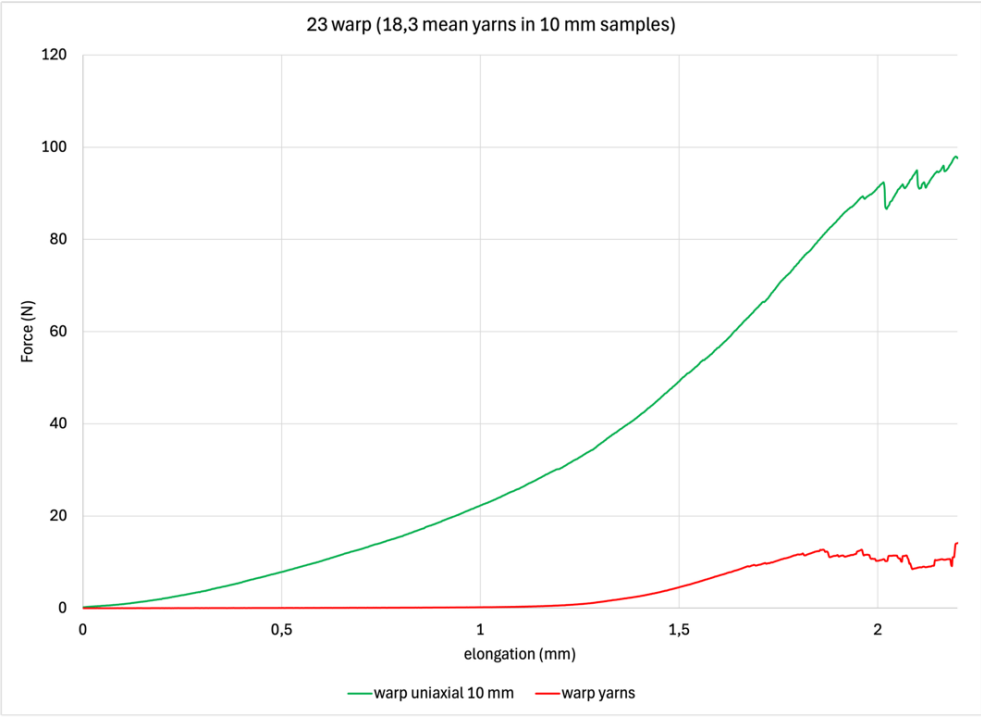

Figure 108 Uniaxial 10 mm warp samples and individual yarns for specimen 23

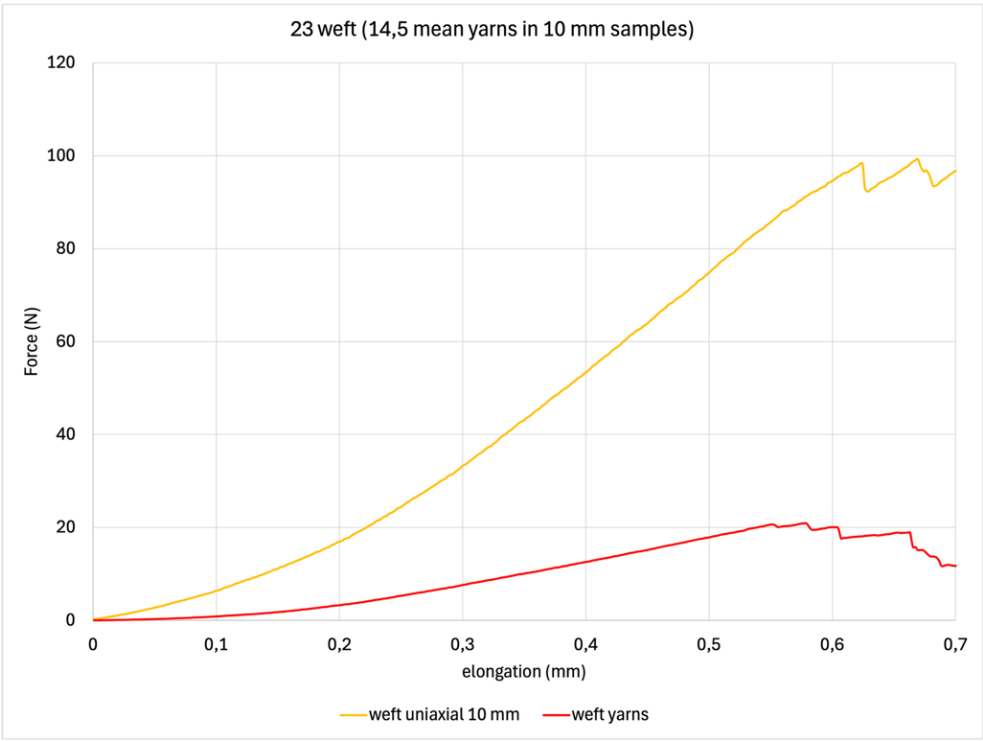

Figure 109 Uniaxial 10 mm weft samples and individual yarns for specimen 23

In Figure 110, we see the plots of the individual yarns from specimen 24. As it could be anticipated looking at the crimp values in Table 7, the decrimping phase is much shorter. Again, the slope of the “elastic region” of the plot in the warp is lower. Though in this case the TPM value is higher in the warp yarns (Table 6), the ultimate load of the weft yarns is about 30% higher.

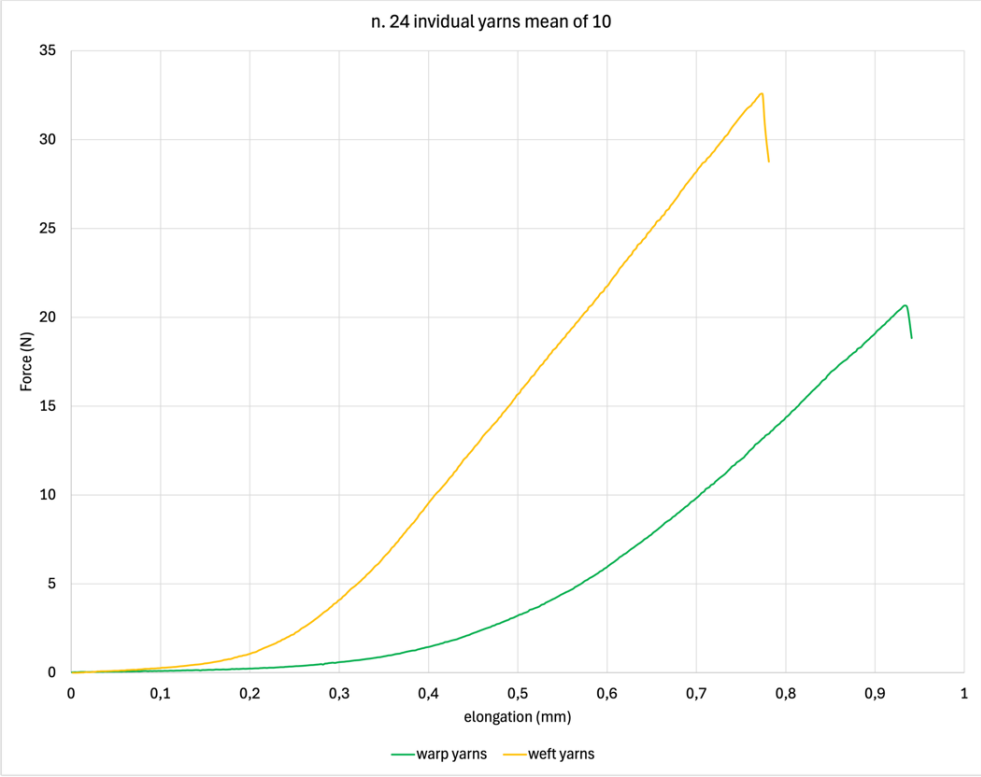

Figure 110 Individual yarns from specimen 24

In Figure 111 and in Figure 112, we see the uniaxial and biaxial tensile tests for specimen 24, clearly demonstrating stiffness transfer in biaxial testing: at 0.8 mm, the warp force is 60 N in uniaxial and 92 N in biaxial). Also, the decrimping phase appears to be completed with a much smaller elongation in both the warp and weft directions under biaxial testing, also because of their low crimp (see Table 7).

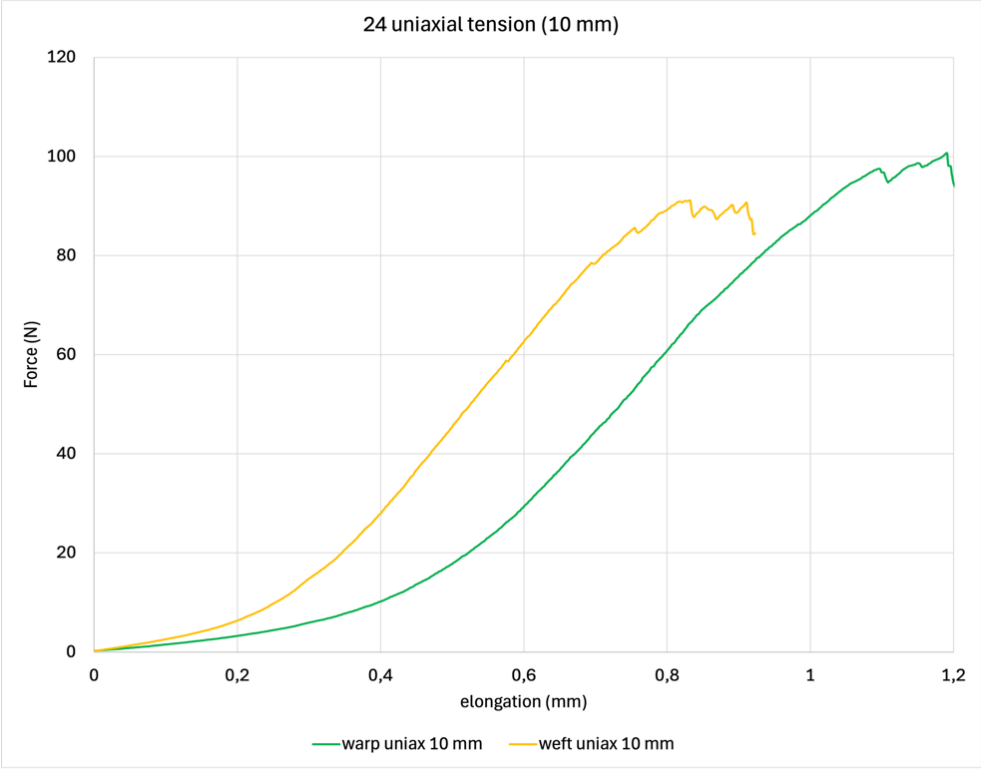

Figure 111 Uniaxial 10 mm samples for specimen 24

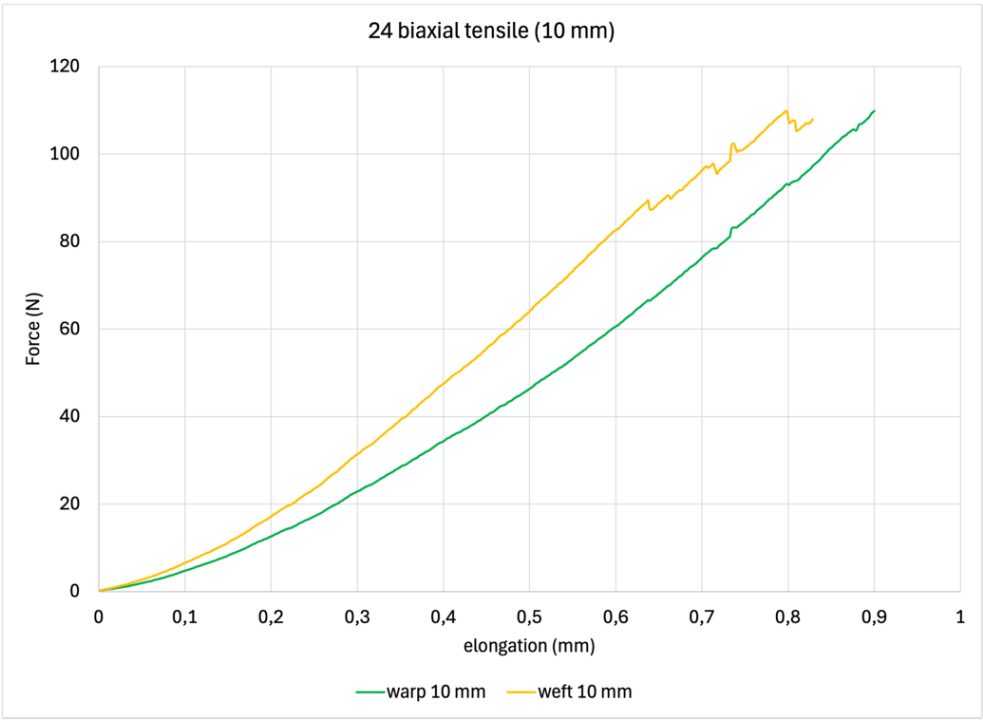

Figure 112 Biaxial 10 mm samples for specimen 24

In, Figure 113 and Figure 114, we see the uniaxial tensile tests for specimen 24 compared to the individual yarn plots. For the warp direction, we see that the individual yarns face decrimping offering no resistance until an elongation of about 0.4 mm, while the same happens until about 0.2 mm in the weft. This follows the same ratio (0.5) as that found in their crimp values: 2.94% in the warp and 1.58% in the weft (see Table 7). In the 10 mm uniaxial textile samples, the friction with the opposite unstretched yarns causes some tensile reaction the decrimping phase in both directions. If compared to textile 23, less difference in the elongation value if found between the ultimate load in the yarns and in the textile.

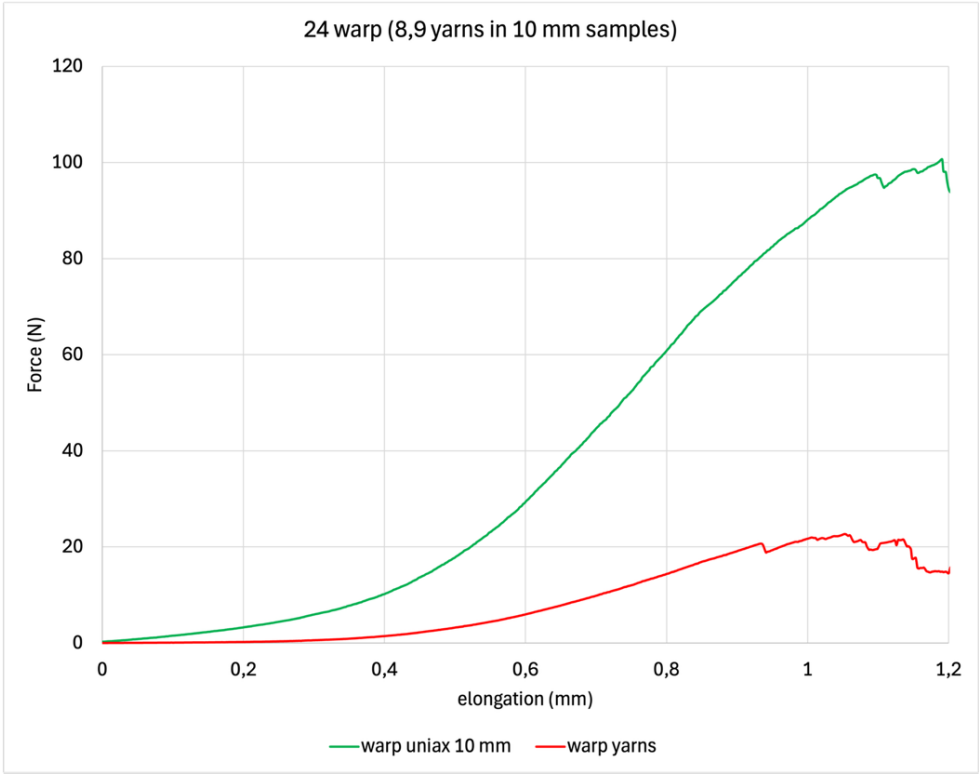

Figure 113 Uniaxial 10 mm warp samples and individual yarns for specimen 24

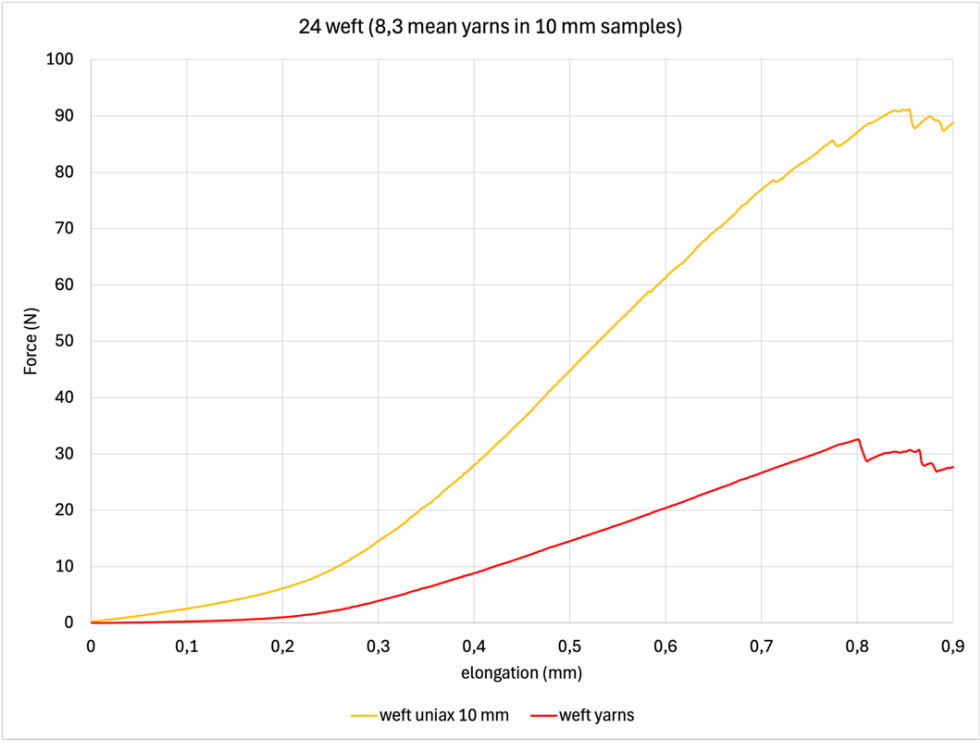

Figure 114 Uniaxial 10 mm weft samples and individual yarns for specimen 24

In Figure 115, we see the individual yarn plots for the textile n. 25. In this case, unexpectedly, the ultimate load of the warp yarns is about 30% higher, though the TPM values are very similar (see Table 6). The slope of the "elastic region" of the plots is substantially parallel, though the two plots appear to be shifted more than the difference in their crimp values would suggest: 2.26 % in the warp and 2.0 % in the weft (see Table 7).

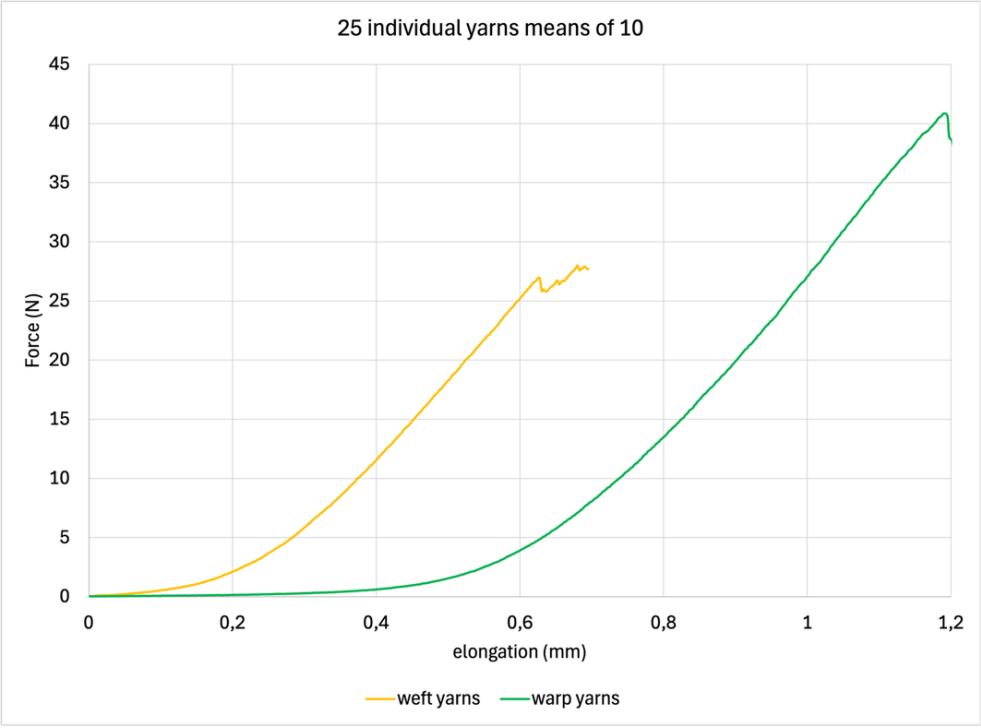

Figure 115 Individual yarns from specimen 25

In Figure 116 and in Figure 117, we see the uniaxial and biaxial tensile tests for specimen 25. In this case, the stiffness transfer seems to be influencing mostly the ultimate load, which is about 20% higher in biaxial testing.

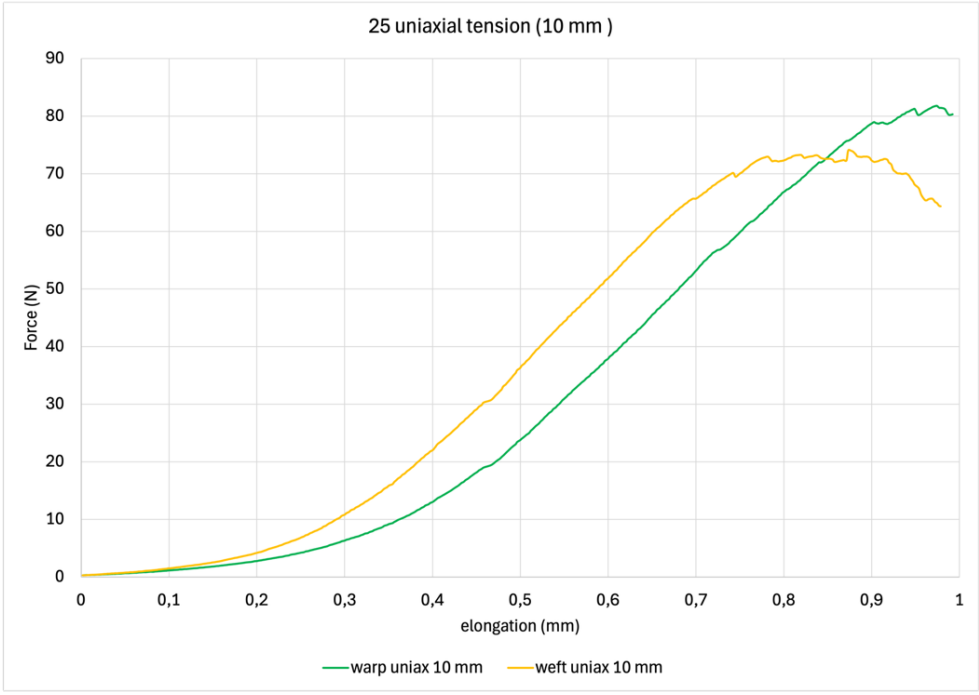

Figure 116 Uniaxial 10 mm samples for specimen 25

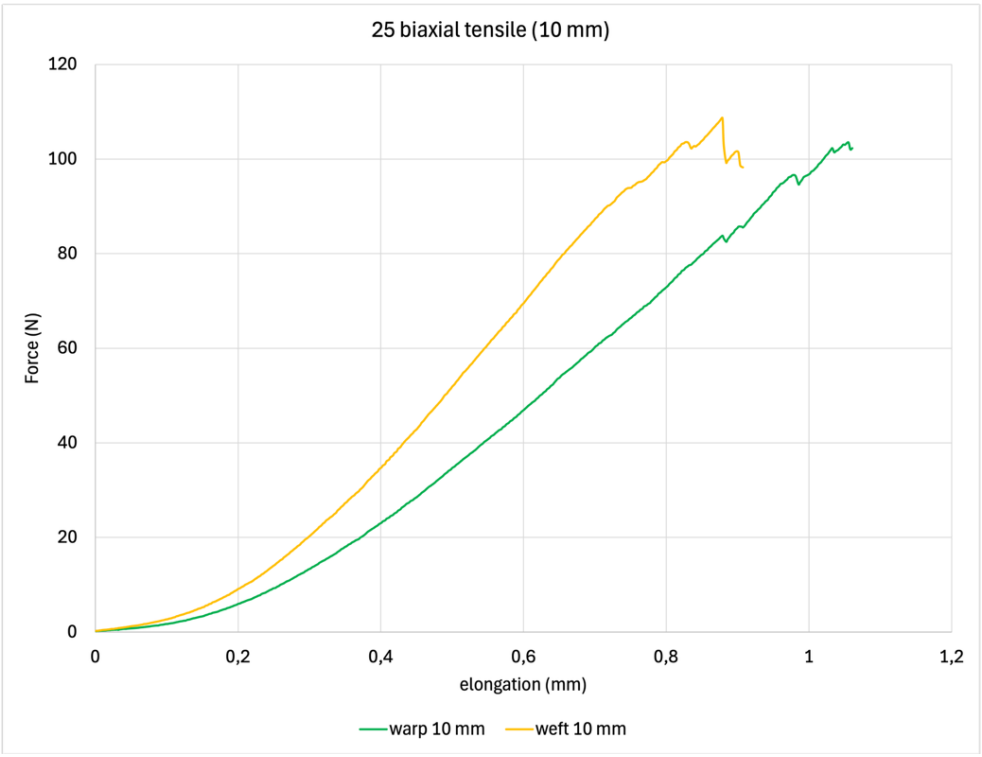

Figure 117 Biaxial 10 mm samples for specimen 25

In Figure 118 and in Figure 119, we see the uniaxial tensile tests for specimen 25 compared to the individual yarn plots. For the warp direction, we see that the individual yarns face decrimping offering no resistance until an elongation of about 0.6 mm, while the same happens until about 0.15 mm in the weft, following a very different ratio if compared with their crimp values: 2.26% in the warp and 2.0 % in the weft (see Table 7). The plot in Figure 118 suggests the possibility that, in this case, the difference in the initial pre-tensioning value between the uniaxial samples (0.3 N) and that in the individual yarns testing (0.03 N), though very small, may have caused a shift in the elongation needed to reach the ultimate load in the individual yarn tests. This would nevertheless appear to be rather surprising, because the choice of the pretension values is correlated to the need of straightening the sample without causing it to start the decrimping process, and a single yarn, not interlaced with cross yarns requires much less force to start decrimping if compared to the full textile. Moreover, no evidence of this problem can be spotted in any of the other five uniaxial/individual yarns plots.

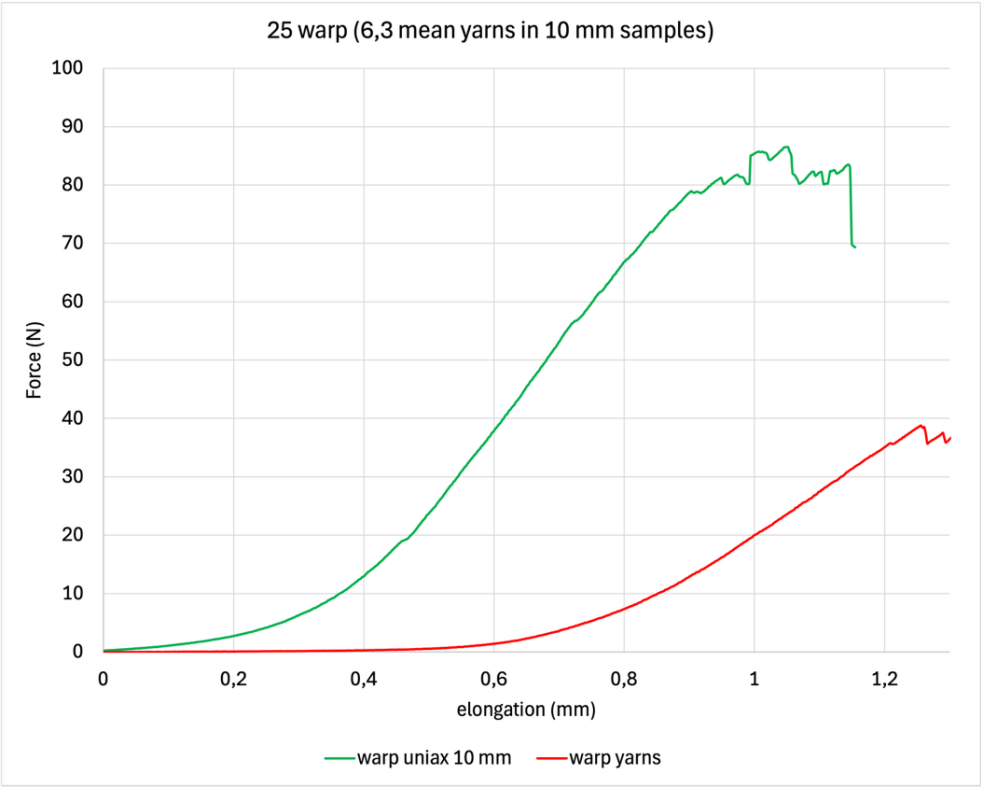

Figure 118 Uniaxial 10 mm warp samples and individual yarns for specimen 25

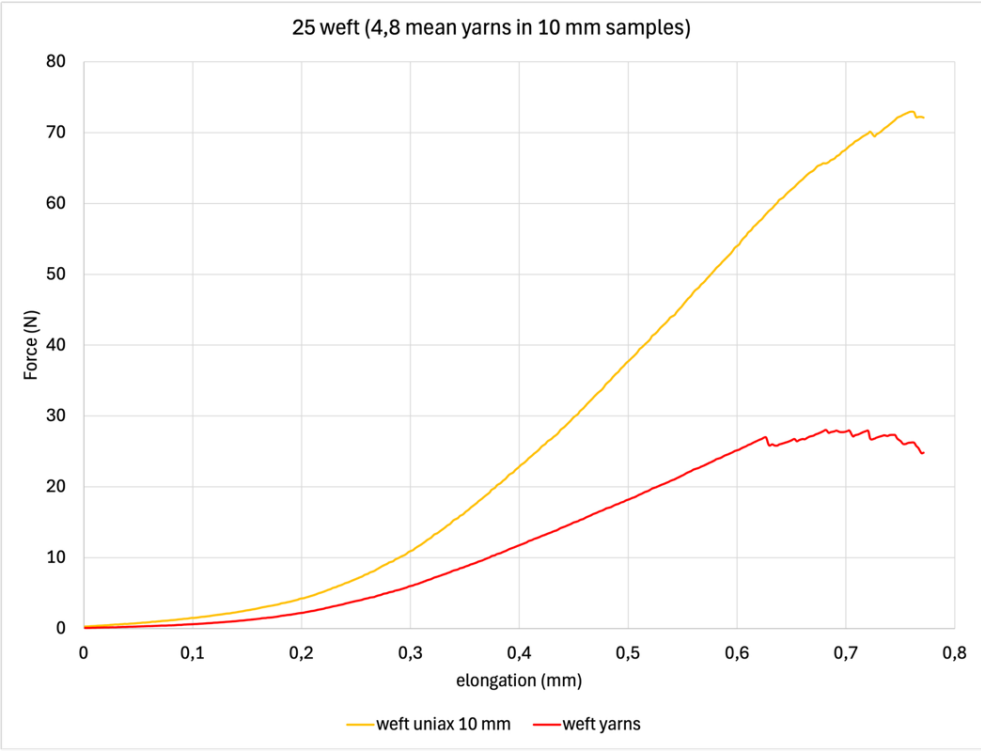

Figure 119 Uniaxial 10 mm weft samples and individual yarns for specimen 25

In Table 31, a summary of the ultimate loads (UL) and ultimate elongation (UE) values for the textiles and individual yarn tests is presented. For the warp direction of the biaxial test of specimen 23, such values are not available because they were too far from those of the weft direction (see Figure 107), and the tests were terminated before reaching them because of an automated procedure.

		textile Ultimate Load and Ultimate Elongation				yarn Ultimate Load and Ultimate Elongation		
specimen		**UL (N) uniaxial**	**UE (mm) uniaxial**	**UL (N) biaxial**	**UE (mm) biaxial**	**yarn UL (N)**	**yarn UE (mm)**	**n of yarns**
23	warp	88,77	1,97			20,35	0,57	18,3
	weft	98,27	0,62	124,32	0,65	9,25	1,79	14,5
24	warp	96,8	1,09	156,44	1,1	20,32	0,92	8,9
	weft	84,8	0,78	118,15	0,87	32,56	0,77	8,3
25	warp	78,69	0,91	145,6	1,35	35,64	1,16	6,3
	weft	69,48	0,73	108,64	0,88	26,95	0,63	4,8

Table 31 Ultimate loads (UL) and ultimate elongation (UE) values for the textiles and individual yarn tests.

2.2 Tests performed at different speeds

Three new series of tests were performed on the textiles 23 and 24, as a preliminary description of the differences that can be found between the chosen value of test speed (2 mm/min) and speeds that differ from it by a factor of 5. The value was therefore divided by 5 (0.4 mm/min) and multiplied by 5 (10 mm/min) and again by 5 (50 mm/min), to obtain a very fast test. As already seen in the introductory section of chapter 5 "Considerations about testing speed", the differences are mostly in the number of samples collected in the test data, that is coherent with the factor regulating the speed as the sampling rate is 18 Hz. Concerning the international standards, the sample number per test needs to be of at least 500 (ISO 6892-1), and the typical density of data (≈400 points/mm) obtained using the speed of 2 mm/min is more than enough to fulfil the requirement of ASTM E8 because the stress-strain plot is complete and well detailed. In some cases, as in Figure 59 (here repeated as Figure 122), some viscoelastic behavior is shown using the low speed of 0.4 mm/min.

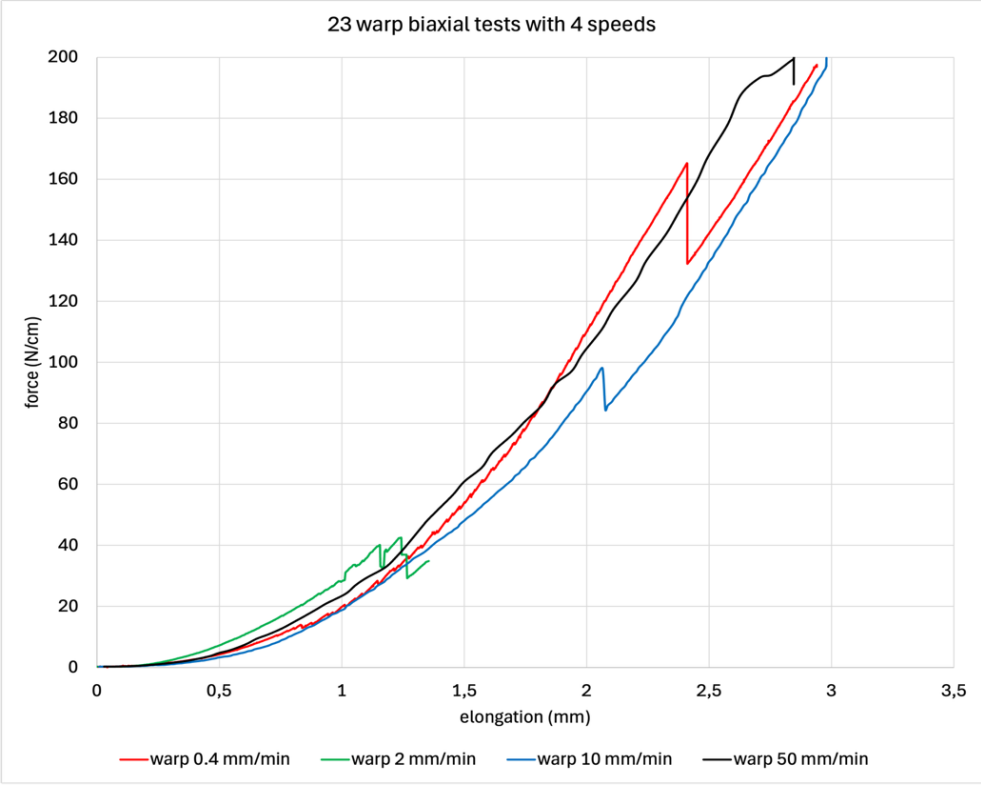

Figure 120 Textile 23, biaxial tensile test - warp direction - comparison between 4 test speeds

The mechanical response of the two textiles under biaxial loading performed with the 4 different speeds is otherwise quite similar, as seen in Figure 120, Figure 122 and Figure 123.

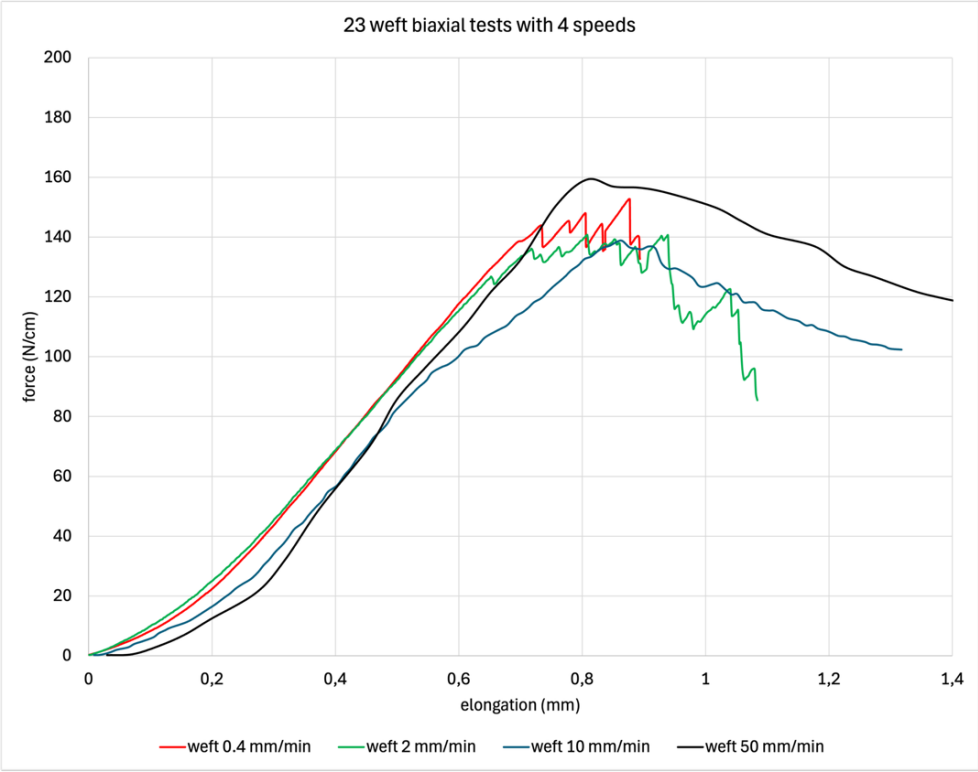

Figure 121 Textile 23, biaxial tensile test - weft direction - comparison between 4 test speeds

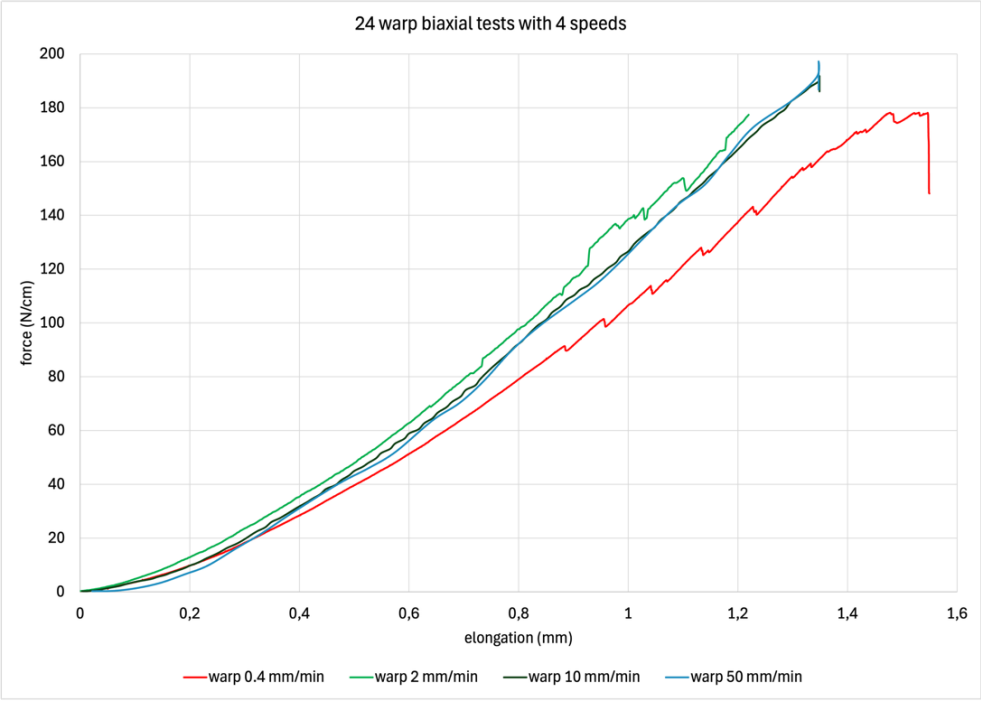

Figure 122 Textile 24, biaxial tensile test - warp direction - comparison between 4 test speeds

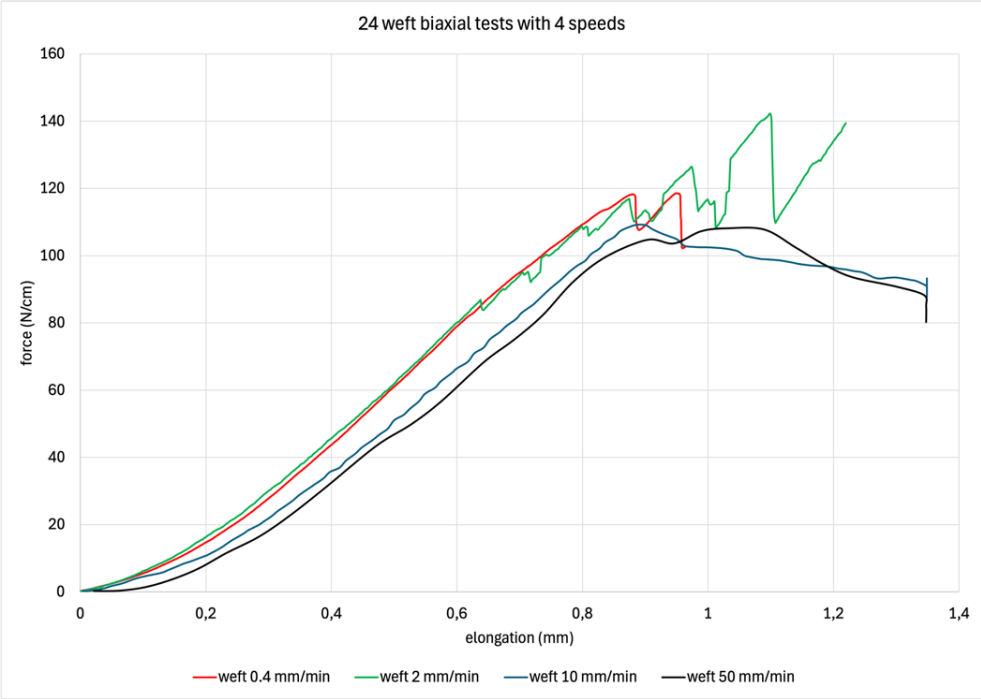

Figure 123 Textile 24, biaxial tensile test - weft direction - comparison between 4 test speeds

Appendix 3 An optical method for the determination of twist in yarns (1973)

This paper appeared in Italian as:

Conti, W., Tassinari, E. Un metodo ottico per la determinazione della torsione dei filati. in: Urbani, G. Problemi di Conservazione Editore Compositori, Bologna 1973b, pag 131.

Original text in Italian available in pdf at: https://doi.org/10.5281/zenodo.13949451

The following translation is by the author, also available in pdf at: https://doi.org/10.5281/zenodo.13949377

An optical method for the determination of twist in yarns.

WALTER CONTI, ENZO TASSINARI
Laboratori Studi e Ricerche SNAM PROGETTI, S. Donato Milanese.

Abstract

The conventional methods to measure yarn twist can be seldom used on painted canvases and antique textiles, both because sampling is unfeasible and because the material is brittle. A non-destructive optical method is described, which proved to be useful to this purpose, whenever the yarn is accessible to visual inspection. All possible motives of error are discussed and the relevant corrections to be made in order to obtain result independent of fabric geometry are calculated.

1. Introduction.

Almost all methods of tissue characterization involve the collection and destruction of samples of a certain size, which makes their application to ancient art textiles, tapestries, painted canvases, etc. problematic. In addition, analyses that could be carried out because they are minimally destructive are often made impossible by the extreme fragility of the aged material, or by the presence of adhesives or consolidants applied to it for restoration purposes.
Such is the case with the method of determining the torsion of threads; a method that normally makes use of a twist meter (or twist tester), whose action of unwinding the twists could hardly be exerted on an antique thread without breaking it at the first few turns. Since, however, that of torsion is one of the most important structural parameters of the fabrics, it was considered useful to attempt its determination on the basis of simple observation of the surface of the threads.
For the time being, we have limited ourselves to experimenting with the new method on the simplest structure: that composed of single ply yarns.

2. Theoretical part.

Let us consider any yarn as consisting of a set of short fibers cohesively joined by twisting. The yarn can be single, that is, composed of a single filament, or twisted, that is, composed of several filaments joined together by successive twisting.

The main characteristics of the yarn are:
a) linear density of the yarn, expressed as length per unit weight;
b) n. of filaments joined together;
c) n. of twists per unit length on the individual strand;
d) n. of twists between yarn ends.

Assimilating a single yarn to a cylinder, and then assuming that its component filaments form cylindrical helices on the surface (Fig. 1). These helices have a pitch *P* that is equal to the inverse of the number of twists per unit length. That is, one has:

$$P = \frac{1}{n}$$

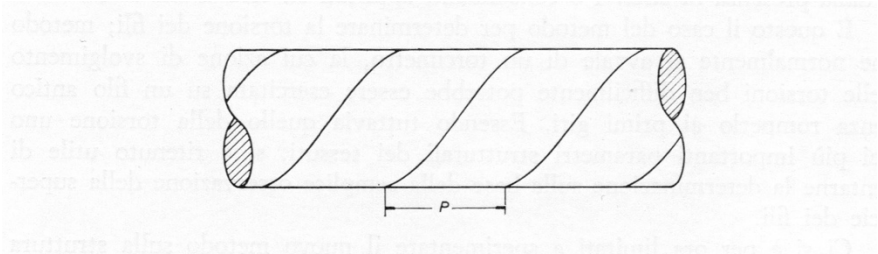

Fig. 1 Ideal appearance of the surface of the yarn (P= pitch of the twist).

Developing the side surface of the cylinder, we obtain (Fig. 2) a rectangle of base πD, where *D* is the diameter of the cylinder (yarn). Let us now consider a single fiber of the yarn; in Fig. 2 it is arranged as a straight line. This straight line forms an angle α with the axis of the cylinder which we shall call as the "twist angle".

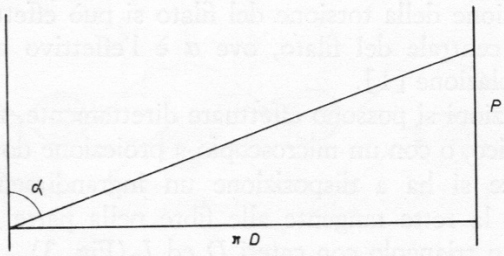

Fig. 2. Surface development of a yarn (*P* = torsion pitch; πD = circumference; α = twist angle).

From the triangle in Fig.2, we obtain:

$$\text{tg } \alpha = \frac{\pi D}{P}$$

thus:

$$n = \frac{\text{tg } \alpha}{\pi \ D}$$

expressing *n* in n. of twists/meter and *D* in mm we obtain:

$$n = \frac{318 \ \text{tg } \alpha}{D} \qquad [1]$$

Observing a yarn, it appears to us as a strand with more or less defined contours, and with its fibers arranged transversely according to a geometry that is the projection of the helix on the plane of observation (Fig. 3).

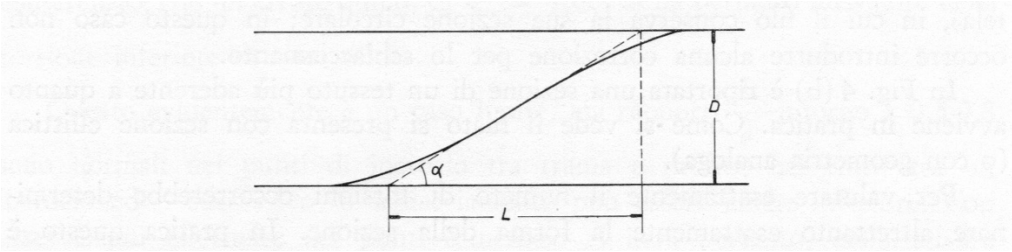

Fig. 3. Determination of twist angle α (*D* = diameter; *L* = segment to be measured for determination of α).

The determination of yarn twist can be made by measuring *D* and α in the central part of the yarn, where α is the effective twist angle, and applying the relationship [1].
These measurements can be made directly, using a suitable goniometric eyepiece, or with a projection microscope equipped with a goniometric scale. If, on the other hand, one has a photographic magnification of the fabric, it will be possible to trace the tangent line to the fibers in the central part of the yarn, and thus obtain a triangle with cathetuses *D* and *L* (Fig. 3).

We thus have:

$$\text{tg } \alpha = \frac{D}{L}$$

and therefore:

$$n = \frac{318 \cdot I}{L}$$

where *L* is the distance shown in Fig. 3, expressed in mm, and *I* is the magnification of the photograph.
By measuring *L* it is therefore easy to backtrack to the twists per meter of the yarn.
Unfortunately, this ideal case rarely occurs in practice; we now want to examine possible deviations from the model adopted so far.
Indeed, the practical interest of the determination is in the yarn contained in a fabric. In this case it is essential to make appropriate corrections for the flattening and bending to which the yarns is subjected in the weave.

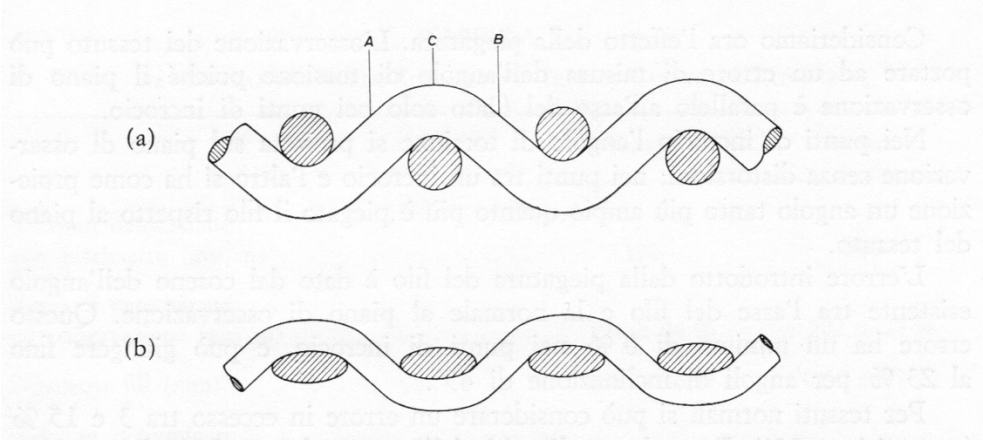

Fig. 4. Ideal section of a canvas (a); real section of a canvas (b).
(ACB = observation points for twist determination).

In Fig. 4 (a) we show the cross-sectional area of a fabric ("plain weave"), in which the yarn retains its circular cross-section; in this case no correction for crushing needs to be introduced.
In Fig. 4 (b) we show a cross section of a more tightly woven fabric, as it is the case in practice. As can be seen, the yarn has an elliptical cross section (or similar geometry).
To estimate exactly the number of twists would require determining just as exactly the shape of the section. In practice this is impossible, but a very good approximation can be obtained by measuring the major axis (*b*) and minor axis (*a*) of the deformed section and applying the following formula, which is derived from the calculation approximate perimeter development of the ellipse:

$$n = \frac{318 \cdot \operatorname{tg} \alpha}{a \sqrt{\frac{1}{2}\left(1 + \frac{b^2}{a^2}\right)}} \qquad [2]$$

Even this is not always possible in practice. It is interesting to see the error made in measuring the twist of a yarn with a fully flattened cross section by measuring only *D*.
The observation gives an "apparent diameter" equal to $\pi/2\ D$ (half circumference), thus with an error of $\pi/2 \cong 1.60$. The calculated twist value is therefore about 60 % smaller.
This evidently is an extreme case, but ratios b/a around 0.5-0.8 are normal at the crossing points between warp and weft; in the stretches between one crossing and the next the crushing may be even less. With observations made at the crossing points, therefore, there will be a default error (around 10-20%) in the twist measurement due to yarn crushing; a lower error at the other points.

Let us now consider the effect of bending. The observation of the fabric can lead to an error in measuring the twist angle because the observation plane is parallel to the yarn axis only at the crossing points.
At the crossing points, the twist angle projects onto the observation plane without distortion; between the crossing points, the projection provides an angle that becomes wider the more the yarn is bent with respect to the plane of the fabric.
The error introduced by yarn bending is given by the cosine of the angle existing between the axis of the yarn and the normal to the observation plane. This error has a minimum of 0 % at the crossing points, and can be as high as 23 % for inclination angles of 45°.
For normal fabrics, an upward error between 3 and 15 % ($\alpha = 14 \div 32°$) can be considered. Therefore, to assess the magnitude of the error and introduce the appropriate correction, it is advisable to evaluate the embedding of the threads in the fabric by observation or measurements.

3. Experimental part.

In order to verify the compliance of the described method, a series of tests has been performed on a sample of a lining canvas with the following characteristics:

Weight of the canvas: 200 g/m^2	Yarn linear density: 10 Ne hemp
Treatment: animal glue	Thread count in warp/cm: 6.4
Glue contents: 50% in weight	Thread count in weft/cm: 5.4

On the yarns taken from the sample before the application of the glue, the twist was determined using a standard "twist meter"; 50 tests were made in the weft direction and 50 in the warp direction to determine the "effective twist."
Determination of twist by simple observation was effectuated by means of a projection microscope (*Projectina*) with 30 magnifications. If it is not possible to obtain samples of the canvas for microscope observation, the measurement is performed by means of a small goniometric eyepiece or using a photographic image.

100 readings of *D* and α were taken at points A and B (Fig. 4). 100 readings were also taken at cross points C to confirm the crush hypotheses.

Results are summarized in Table I.
The distribution of the data was confirmed to be completely random.

TABLE I
DETERMINATION OF TWIST ON HEMP LINING CANVASES

	WEFT	WARP
Twists counted with twist meter (t/meter)	198	209
Twists determined by observation (t/meter)	194 ± 24%	202 ± 27%
Yarn diameter (mm)	0.68 ± 16%	0.66 ± 17%
Twists determined by observation in crossing points (t/meter)	181 ± 25%	185 ± 30%

As it can be seen, a match was obtained between the two torsion measurements that goes over expectations. The error is less than 5 %. The results of the measurements at the crossing points are lower by about 10-15 %.
To determine the extent of crushing, the thickness of the fabric was measured under very small pressure; this thickness is equal to twice the minor axis of the yarn, considered to be of elliptical cross-section.

It was obtained:

Thickness of the canvas = 0.64 mm.
Minor axis of the thread = 0.34 mm.

Since the other axis is the diameter *D*, measured by observation of the tissue, we have a crush ratio of 0.67/0.34, that is about 50 %.
By performing the calculation according to equation [2], a lower torsion of about 20 % (error found experimentally 10-15 %).
For the readings taken outside the crossing points there is a sort of compensation:

error due to crushing:- 10 ÷ 15%
(crushing about 30-40%);
error due to bending: + 5 ÷ 10%
(bending angles ~ 18-25°).

The error of 5 % calculated theoretically is in perfect agreement with that found experimentally.

To verify the validity of the method in a more real-world case, it was used to analyze the following four ancient canvases:

Canvas 1 = Anonymous Neapolitan painter, 18th c. (linen).
Canvas 2 = Anonymous Neapolitan painter, 18th c. (hemp).
Canvas 3 = Painting, 19th c. (hemp).
Canvas 4 = Painting, 20th c. (hemp).

Results are in table 2.

TABLE 2
DETERMINATION OF TWIST ON PAINTED CANVASES

	CANVAS 1		CANVAS 2		CANVAS 3		CANVAS 4	
Direction	*A*	*B*	*A*	*B*	*A*	*B*	*A*	*B*
Twists counted with twist meter (t/meter)	485	440	250	200	300	240	-	-
Twists determined by observation (t/meter)	515	413	211	176	293	245	192	198
Coefficient of variation (%)	54	28	34	32	38	20	29	11
Yarn diameter (mm)	0.44	0.42	0.91	0.71	0.58	0.60	0.60	0.59
Coefficient of variation (%)	16	14	27	23	24	16	12	15
Measurement at the crossing point	yes	yes	yes	yes	no	no	no	no

It should be pointed out that the determination of twist using a twist meter was conducted with difficulty due to the fragility of the yarn and the presence and of adhesives and paint (in the case of canvas 4 it was impossible). The twist value given is to be considered as an approximation.
On the canvas samples it was not possible to identify the warp and weft with certainty; therefore, it was preferred to simply indicate with A and B the directions in which the measurements were taken.

As can be deduced from the data in the table, there is fairly good agreement between the two methods of measuring twist. Corrections can be introduced for crushing where necessary (measurement at the intersection). The important thing is to have established that

it is possible to determine the order of magnitude of the twist by a simple observation of the canvas yarns.

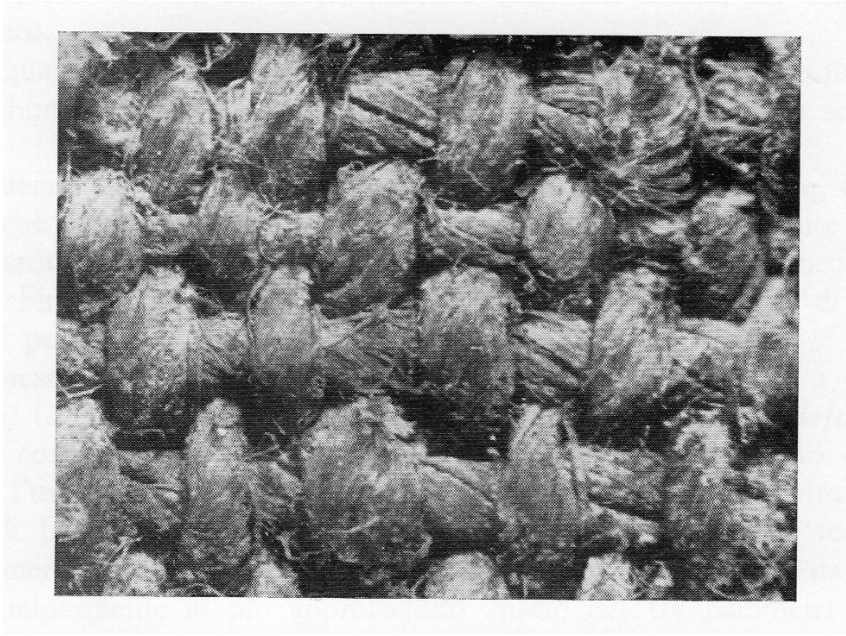

Fig. 5- Canvas 1 = Anonymous Neapolitan painter, 18th c. (linen).

Appendix 4 Design file and bill of materials for the biaxial tester

Design files summary

Descriptor	**File name in repository https://zenodo.org/record/7541996#.Y8Wd1uLMlqs**
Firmware	prototype-4motors-newPreTv2_ver0.13.ino
	biaxialPref.ini
	version_tracker.h
Pc software	speed_increased2.py
Electrical connections in the machine	Schematic_Biaxial_Tester.pdf
Cad of the entire machine	biaxial_tester.stp
Steel cross	steel_cross_holes.stp
Box for the safety switches	switch_box.stp
Sample temporary supports	sample_rest.stp
Manual motion knob	motor_manual_motion_knob.stp
Cable chain support, top	cable_chain_support_top.stp
Cable chain support, bottom	cable_chain_support_bottom.stp
Carriage plate	carriage_plate.stp
Limit switch supports internal	lim_switch_int_support.stp
Limit switch supports external	lim_switch_int_support.stp
Limit switch knobs - internal	lim_switch_int_knobs.stp
Limit switch knobs - external	lim_switch_ext_knobs.stp
Sample clamps – 10mm	10mm_clamps.stp
Sample clamps – 25mm	25mm_clamps.stp
Descriptor	**web link for download**
Ballnut Floating Bearing datasheet	https://www.cnc4you.co.uk/Ballscrew-Support-BF15-TMT-(SYK)?search=ballscrew%20
Ballunt datasheet	https://www.cnc4you.co.uk/Ballscrew-with-Fitted-Anti-Backlash-Ballnut-RM1605-C7-16mm?search=ballnut
Ballscrew support datasheet	https://www.cnc4you.co.uk/BK15-C3-SYK?search=ballscrew%20
CW5045 Driver Wiring Diagram datasheet	https://www.cnc4you.co.uk/Stepper-Motor-Driver-4.5A,-50V-CNC-Microstepping-CW5045?search=CW5045%20
CW5045 Driver datasheet	https://www.cnc4you.co.uk/Stepper-Motor-Driver-4.5A,-50V-CNC-Microstepping-CW5045?search=CW5045%20
Ballscrew support nut datasheet	https://www.cnc4you.co.uk/Ballscrew-Mount-DSG16H-ID-28mm?search=dsg%20
Power Supply Unit datasheet	https://www.cnc4you.co.uk/400W-PSU-36Volt-11Amp?search=power%20supply
Complete linear rails datasheet	https://www.cnc4you.co.uk/Linear-Rail/Supported-Round-Rail-Kits/SBR16LUU-Rail-Kits
Stepper motor datasheet	https://www.cnc4you.co.uk/Stepper-Motor/Nema23-4Nm/Stepper-Motor-4Nm-60BYGH401-03-Nema23

Bill of materials summary

Component	**Units**	**Unit cost**	**subtotal**	**Source of material**	**Model / material type**
Cruciform structure	1		€ 40.00	Hardware shop	Carbon steel
Welding	1		€ 200.00	In studio work facility	TIG welding
Powder coating	1		€ 40.00	Industrial powder coating service	Polyester
Stepper motor, NEMA 23, 4 N/m	4	€ 39.19	€ 156.81	https://www.cnc4you.co.uk/	60BYGH-401-03
Motor Bracket SYK	4	€ 37.49	€ 149.98	https://www.cnc4you.co.uk/	MBA12-C-SYK
Stepper motor driver	4	€ 44.04	€ 176.15	https://www.cnc4you.co.uk/	CW5045
400 W 36V 11A power supply	1	€ 45.57	€ 45.57	https://www.cnc4you.co.uk/	400W36V/11A
5 W 5V 1A power supply	1	€ 87.00	€ 87.00	https://www.oep.co.uk/	PS2125
Ball screw with anti-backlash	4	€ 76.37	€ 305.47	https://www.cnc4you.co.uk/	RM1605-C7
Ball screw support # 1	4	€ 38.26	€ 153.03	https://www.cnc4you.co.uk/	FK12_TMT_(SYK)
Ball screw Support # 2	4	€ 23.78	€ 95.12	https://www.cnc4you.co.uk/	BF12_TMT_(SYK)
Ball screw Mount	4	€ 11.39	€ 45.55	https://www.cnc4you.co.uk/	DSG16H
Supported Rail Kit	4	€ 84.04	€ 336.16	https://www.cnc4you.co.uk/	SBR16LUU_Rail_Kit
XD Coupling	4	€ 13.05	€ 52.21	https://www.cnc4you.co.uk/	XD_30mm_X_35mm
carriage plates	4	€ 9.50	€ 38.00	http://www.inoxcadei.it/	AISI 304 stainless steel
25 mm sample clamp	4	€ 7.00	€ 28.00	https://orrilamiere.it/	AISI 304 stainless steel
10 mm sample clamp	4	€ 5.00	€ 20.00	https://orrilamiere.it/	AISI 304 stainless steel
Cable chain	4	€ 9.00	€ 36.00	https://www.igus.it/	E.2.10.10.038.0
Terminal Block Shield Board	1	€ 21.99	€ 21.99	http://www.amazon.it/	Wingoneer T0339
Load cell amplifier	4	€ 1.60	€ 6.40	http://www.amazon.it/	HX711
Arduino	4	€ 22.00	€ 11.00	https://store.arduino.cc/	Arduino Uno
5 kg load cell	4	€ 23.52	€ 94.08	https://www.aliexpress.com/	C3 class load cell
50 kg load cell	4	€ 23.52	€ 94.08	https://www.aliexpress.com/	C3 class load cell
100 kg load cell	4	€ 29.41	€ 117.64	https://www.aliexpress.com/	C3 class load cell
4-pin connector	9	€ 2.00	€ 18.00	http://www.amazon.it/	
6-pin connector	4	€ 2.75	€ 11.00	http://www.amazon.it/	
Limit switch	4	€ 0.50	€ 2.00	http://www.amazon.it/	GTIWUNG T331
Emergency stop button	1	€ 12.50	€ 12.50	http://www.amazon.it/	Durlclth62egafyswn
Motor disable switch	1	€ 12.50	€ 12.50	http://www.amazon.it/	Tyenazagm375pyku6
Cables		€ 30.00	€ 30.00	Hardware shop	
Limit switch supports - internal	4	€ 0.75	€ 3.00	designed and built in studio	PLA 3D printed part
Limit switch supports - external	4	€ 0.75	€ 3.00	designed and built in studio	PLA 3D printed part
Limit switch knobs - internal	4	€ 0.75	€ 3.00	designed and built in studio	PLA 3D printed part
Limit switch knobs - external	4	€ 0.75	€ 3.00	designed and built in studio	PLA 3D printed part
Manual motion knob	4	€ 0.75	€ 3.00	designed and built in studio	PLA 3D printed part
Cable chain support, top	4	€ 2.50	€ 10.00	designed and built in studio	PLA 3D printed part
Cable chain support, bottom	4	€ 2.75	€ 11.00	designed and built in studio	PLA 3D printed part
Box for the electronics	1	€ 30.00	€ 30.00	designed and built in studio	Laser cut plywood
Total cost of materials and supplies			**€ 2502.20**		

Specifications table

Hardware name	Biaxial tester for canvas paintings samples
Subject area	• Engineering and materials science • Educational tools and open-source alternatives to existing infrastructure • Canvas paintings conservation
Hardware type	• Other: Material testing system
Closest commercial analog	• No commercial analog is available
Open-source license	Creative Commons Attribution 4.0 International
Cost of hardware	• Approximate cost: € 2500
Source file repository	https://zenodo.org/record/7541996#.Y8Wd1uLMIqs

LITERATURE REFERENCES

- Accardo G., Bennici, A., Torre, M. Tensionamento controllato della tela. In Il San Gerolamo del Caravaggio a Malta dal furto al restauro. Istituto Centrale per il Restauro, Roma, 1991. 31–44.
- Accardo G., Santucci G., Torre M. Sollecitazioni meccaniche nei dipinti su tela: ipotesi su alcuni metodi di analisi e di controllo. in 3° Conferenza Internazionale sulle Prove non Distruttive, Metodi Microanalitici e Indagini Ambientali per lo Studio e la Conservazione delle Opere d'Arte, Viterbo 4-8 ottobre 1992: sez. I pp. 37-52.
- Ackroyd, P. The Structural Conservation of Canvas Paintings: Changes in Attitude and Practice since the Early 1970s. *Reviews in Conservation*, 2002, Number.3, pp. 3-14 DOI : 10.1179/sic.2002.47.Supplement-1.3
- Aldemir, E., Özdemir, H., Sarı, Z. An improved gray line profile method to inspect the warp–weft density of fabrics, The Journal of The Textile Institute, 2019. 110:1, 105-116, DOI: 10.1080/00405000.2018.1467743
- Almasian, M., Tiennot, M., Fiske, L.D., Hermens, E. The use of ground glass in red glazes: structural 3D imaging and mechanical behaviour using optical coherence tomography and nanoindentation. *Herit Sci* 9, 66 (2021). https://doi.org/10.1186/s40494-021-00527-y
- Arvind, S. N. Demystifying Lining - The Genesis, Evolution and Historiography of the Mist-Lining Technique developed by SRAL (mid 1990s-current). Master Thesis University of Amsterdam, 2021.
- Bar-Yosef O, Belfer-Cohen A, Mesheviliani T, Jakeli N, Bar-Oz G, Boaretto E, Goldberg P, Kvavadze E, Matskevich Z. Dzudzuana: an Upper Palaeolithic cave site in the Caucasus foothills (Georgia). Antiquity. 2011;85(328):331–349. http://dx.doi.org/10.1017/S0003598X0006779X. doi:10.1017/S0003598X0006779X
- Barella, A., Vigo, J. P., Manich A. M. The relation between the twist and resistance to repeated extensions of man-made-fiber rotor-spun yarns, Journal of the Textile Institute, (1980) 23—71:5, 242-251, DOI: 10.1080/00405008008631561
- Behera, B. K.; Hari, P. K. Woven Textile Structure: Theory and Applications; Woodhead Publishing Series in Textiles, 115; Woodhead Pub: Cambridge, 2010. ISBN: 9781845697815, 1845697812
- Bender Jørgensen, L., Rast-Eicher, A., Wendrich, W. Earliest Evidence for Textile Technologies. Paléorient, 49-1. 2023 -1, 213-228.
- Berger, G. A. A new Adhesive for the Consolidation of Paintings, Drawings and Textiles. Bulletin of the American Group. International Institute for Conservation of Historic and Artistic Works, Oct., 1970, Vol. 11, No. 1 (Oct., 1970), pp. 36-38
- Berger, G. A. Effects of Impregnation on Fibrous Materials. Bulletin of the American Group. International Institute for Conservation of Historic and Artistic Works, Vol. 12, No. 2 (Apr., 1972), pp. 70-71
- Berger, G. The role of tension in the preservation of canvas paintings: a study of panoramas. ICOM-CC, 1981, Ottawa.

- Berger, G. A. A structural solution for the preservation of canvas paintings, Studies in Conservation, 29:3, 1984. 139-142, DOI: 10.1179/sic.1984.29.3.139
- Berger, G. A., Russell W.H. An evaluation of the preparation of canvas paintings using stress measurements, Studies in Conservation, (1988) 33:4, 187-204, DOI: 10.1179/sic.1988.33.4.187
- Berger, G.A., Russell, W.H. Deterioration of Surfaces Exposed to Environmental Changes. Journal of the American Institute for Conservation. (1990) 45-76 https://doi.org/10.1179/019713690806046145
- Berry, G.M., Hersh, S.P., Tucker, P.A., Kerr, N., McElwain, D.M. Properties of some archaeological textiles. ICOM Committee for Conservation 5th Triennial Meeting Zagreb Yugoslavia 1-8 October 1978
- Biddle, J. L. Breasts, bodies, canvas: central desert art as experience. 2007. University of NSW Press Ltd. ISBN 029598712X, 9780295987125
- Bilson, T. Canvas shrinkage: a preliminary investigation into the response of a woven structure. ICOM-CC, 1996 p. 245-252
- Blyth G, Postle R. Measurement and Interpretation of Fabric Dynamic Modulus. *Textile Research Journal*. 1979;49(10):601-608. doi:10.1177/004051757904901008
- Böhme, N., Anders, M., Reichelt, T., Schuhmann, K., Bridarolli, A., Chevalier, A. "New Treatments for Canvas Consolidation and Conservation." Heritage Science 8 (1). 2020 https://doi.org/10.1186/s40494-020-0362-y.
- Booth, J.E. Principles of Textile Testing : An Introduction to Physical Methods of Testing Textile Fibres, Yarns and Fabrics. 3rd ed. London: Heywood Books, 1968.
- Bourriot, A./ Une contribution à l'étude du support de toile au XVème siècle: le cas vénitien. In: Indigo: revue de conservation - restauration, N. 3, 1998 p. 15-21.
- Bräunig, T. A., von Reden, A., Lichtblau, D. A., Herm, C. (2023). A Novel Technique to Determine the Strength of Canvas and Its Correlation with the Degree of Cellulose Polymerization. In: Stoner, J., & Ainsworth, M. (eds.), Conserving Canvas. Getty Conservation Institute. https://www.getty.edu/publications/conserving-canvas/iii-open-questions/16/
- Bridarolli, A., Freeman, A.A., Fujisawa, N., Łukomski, M. Mechanical properties of mammalian and fish glues over range of temperature and humidity. Journal of Cultural Heritage. Vol. 53, 2022, Pages 226-235,ISSN 1296-2074, https://doi.org/10.1016/j.culher.2021.12.005.
- Broecke, L. Cennini Cennnini's *Il libro dell'arte*. A new English translation and commentary with Italian transcription. London, Archetype, 2015. ISBN 9781909492288
- Buckley, B. A., compiler, "PSG - II. "Stretchers and Strainers", 2007.
- Burke, B. From Minos to Midas: Ancient Cloth Production in the Aegean and in Anatolia. Oxbow Books, 2010
- Capriotti, G. Piano e superpiano come luogo della raffigurazione pittorica, cultura della conservazione dei materiali e semiotica del linguaggio visivo. in Il tensionamento dei dipinti su tela. a cura di Capriotti, G. and Iaccarino Idelson, A. Nardini Firenze 2004.
- Cardinali, M., De Ruggieri M. B, Falcucci, C. "Diagnostica artistica tracce materiali per la storia dell'arte e per la conservazione", Palombi Editore, Roma 2007.

- Carità R. Considerazioni sui telai per affreschi trasportati su tela. In Bollettino dell'Istituto Centrale per il Restauro, n. 19-20, 1954. page 131
- Carità, R. Aggiunta sui telai per affreschi trasportati. In Bollettino dell'Istituto Centrale per il Restauro, n. 31-32, 1955. page 170
- Carità R. Il restauro dei dipinti caravaggeschi della Cattedrale di Malta. In Bollettino dell'Istituto Centrale per il Restauro, n. 29-30, 1957, pages 41-82.
- Carr, D.J., Young, C.R.T., Phenix, A., Hibberd, R.D. Development of a Physical Model of a Typical Nineteenth-Century English Canvas Painting, Studies in Conservation, 48:3, 2003, 145-154, DOI: 10.1179/sic.2003.48.3.145
- Cassini, A., Redmond, J. "Models and Idealizations in Science: Artifactual and Fictional Approaches". Springer International Publishing, 2022.
- Chiriboga, P. Finite Element Modeling of Vibrations in Canvas Paintings, 2013. Printed in The Netherlands by Uitgeverij BOXPress, Oisterwijk. ISBN: 978-90-8891-581-9
- Ciatti, M., Conti, L., Conti, S., Iaccarino Idelson, A., Martini, L., Rossi, D., Serino, C., Sostegni, L. Ancora un restauro "impossibile": la Madonna del Rosario del Sodoma. In OPD Restauro n. 21, 2009.
- Cieta. Vocabulaire français. Centre international d'étude des textiles anciens. Lyon 2020. www.cieta.fr
- Clulow, E.E., Taylor H. M. An experimental and theoretical investigation of biaxial stress–strain relations in a plain-weave cloth. Journal of the Textile Institute Transactions. 1963. 323-347. DOI: 10.1080/19447026308660186
- Coarelli, F. (ed.) Pompeji. Hirmer, München 2002.
- Colville, J., Kilpatrick, W., Mecklenburg, M.F. A finite element analysis of multi-layered orthotropic membranes with application to oil paintings on fabric, Studies in Conservation. 1982. 27:sup1, 146-150, DOI: 10.1179/sic.1982.27.Supplement-1.146
- Conti, A. Storia del restauro e della conservazione delle opere d'arte. Electa 1988.
- Conti, W., Tassinari, E. Analysis of creep curves on lining canvas. ICOM CC, Madrid Conference 1972.
- Conti, W., Tassinari, E. Misure di creep su tele da rifodero. in: Urbani, G. Problemi di Conservazione Editore Compositori, Bologna 1973 (**a**), pag 167.
- Conti, W., Tassinari, E. Un metodo ottico per la determinazione della torsione dei filati. in: Urbani, G. Problemi di Conservazione Editore Compositori, Bologna 1973 (**b**), pag 131. Original text in Italian available at: https://doi.org/10.5281/zenodo.13949451 ; English translation available at: https://doi.org/10.5281/zenodo.13949377
- Corti, A., Shameen, T., Sharma, S., De Paolis, A., Cardoso, L. Biaxial testing system for characterization of mechanical and rupture properties of small samples. HardwareX 12. 2022. e00333 https://doi.org/10.1016/j.ohx.2022.e00333
- Czaplicki, Z. A new method of measuring twist of yarn. Fibers and textiles in Eastern Europe vol 14. 2006. Pages 27-29.
- Daly Hartin, D., Michalsky, S. Pacquet, C. Ongoing Research in the CCI Lining Project: Peel Testing of BEVA 371 and Wax-Resin Adhesives with Different Lining support. In:

Preprints of the 10th Triennial Meeting ICOM - Committee for Conservation, Washington. International Council of Museum. 1993. 128-134.

- dePolo, G., Walton, M., Keune, K., Shull, K. R. After the paint has dried: a review of testing techniques for studying the mechanical properties of artists' paint. Journal of Heritage Science 9, 68. 2021. https://doi.org/10.1186/s40494-021-00529-w
- Dings, L. Deformations of The Night Watch canvas under relative humidity fluctuations. Master thesis Eindhoven University of Technology, 2022.
- Doxiadis, E. The Mysterious Fayum Portraits: Faces from Ancient Egypt. Thames & Hudson. 2000. ISBN 050028217X, 9780500282175
- Edwards, Howell G. M., Nik F. Nikhassan, Dennis W. Farwell, Paul Garside, and Paul Wyeth. 2006. "Raman Spectroscopic Analysis of a Unique Linen Artefact: The HMS Victory Trafalgar Sail." *Journal of Raman Spectroscopy* 37 (10): 1193–1200. https://doi.org/10.1002/jrs.1609.
- Erhardt, D., Tumosa, C.S., Mecklenburg, M.F. Can artists' oil paints be accelerated aged? In Polymer preprints. 2000, 41 (2), 1790
- Flock, H., Ph.D thesis. "Einzelfadenverklebung in der Gemälderestaurierung: Klebstoffe, Prüfsystematik und Ergebnisse". Saarbrücken University, 2020.
- Flock, H., Diebels, S., Jägers, E., Demuth, P. New Investigations of Adhesives for Tear Repair of Canvas Paintings, Studies in Conservation. 2020. 66-6 321-341. https://doi.org/10.1080/00393630.2020.1827185
- Freeman, A. Łukomski, M., Beltran, V. Mechanical characterization of a cross-sectional TiO2 acrylic-based paint by nano-indentation. Journal of the American Institute for Conservation, 2019. https://doi.org/10.1080/01971360.2019.1603062
- Fujisawa, N., Łukomski, M. Nanoindentation near the edge of a viscoelastic solid with a rough surface. Materials & Design, Volume 184. 2019. https://doi.org/10.1016/j.matdes.2019.108174.
- Garside, P., and P. Wyeth. 2003. "Identification of Cellulosic Fibres by FTIR Spectroscopy: Thread and Single Fibre Analysis by Attenuated Total Reflectance." *Studies in Conservation* 48: 269–75.
- Giorgiutti-Dauphiné, F., Pauchard, L. Painting cracks: A way to investigate the pictorial matter. *J. Appl. Phys.* 14 August 2016; 120 (6): 065107. https://doi.org/10.1063/1.4960438
- Gorjanc, D.Š.; Sukič, N. Determination of Optimum Twist Equation for the Long Staple Combed Cotton Ring-Spun Yarn. *Fibers* 2020, *8*, 59. https://doi.org/10.3390/fib8090059
- Gregers-Høegh, C., Mortensen, M. N., Christensen, M. E., Andersen, C. K. Distorted Oil Paintings and Wax-Resin Impregnation - A Kinetic Study of Moisture Sorption and Tension in Canvas. Journal of Cultural Heritage 40, 2019: 43–48. https://doi.org/10.1016/j.culher.2019.05.017.
- Guy, J., Britschgi, J. Wonder of the Age: Master Painters of India, 1100-1900. Metropolitan Museum of Art. 2011. ISBN 1588394301, 9781588394309

- Hackney, S. On Canvas. Preserving the structure of paintings. The Getty conservation institute. Los Angeles. 2020
- Hagan, E.W.S., Charalambides, M.N., Young, C.R.T., Learner, T.J.S The effects of strain rate and temperature on commercial acrylic artist paints aged one year to decades. *Appl. Phys. A* 121, 823–835. 2015. https://doi-org.tudelft.idm.oclc.org/10.1007/s00339-015-9423-6
- Hagan, E. Applied Mechanics and the Structural Treatment of Paintings on Canvas. In Conserving Canvas. Los Angeles: Getty Conservation Institute. 2023. https://www.getty.edu/publications/conserving-canvas/
- Hallett, E.Y., Leonardi, M., Cerasoni, J.N., Will, M., Beyer, R., Krapp, M., Kandel, A. W., Manica, A., Scerry, E. M. Major expansion in the human niche preceded out of Africa dispersal. Nature 644, 115–121. 2025 https://doi.org/10.1038/s41586-025-09154-0
- Hardy, B.L., Moncel, M.H., Kerfant, C., Lebon, M., Berlot-Gurlet, L., Mélard, N. Direct evidence of Neanderthal fibre technology and its cognitive and behavioral implications. Sci Rep 10, 4889. 2020
- Hedley, G. Some empirical determinations of the strain distribution in stretched canvases. Icom CC triennial meeting Venice. 1975 (**a**)
- Hedley, G. The effect of beeswax/resin impregnation on the tensile properties of canvas. Icom CC triennial meeting Venice. 1975 (**b**)
- Hedley, G. The stiffness of lining fabrics: theoretical and practical considerations. ICOM Committee for Conservation 7th Triennial Meeting Ottawa Canada 21-25 September. 1981
- Hedley, G., Villers, C. Polyester sailcloth fabric: a high-stiffness lining support, Studies in Conservation. 1982. 27:sup1, 154-158, DOI: 10.1179/sic.1982.27.Supplement-1.154
- Hosseini Ravandi S. A., Toriumi, K. Fourier Transform Analysis of Plain Weave Fabric Appearance Textile Research Journal, 1995 65:11, 676-683
- Iaccarino, A. Dipinti su tela, una proposta per conservare i telai originali. Materiali e Strutture, anno VI n. 2, 1996.
- Iaccarino Idelson, A. La materia dell'opera d'arte, rapporto tra dipinto e telaio e origine dei danni meccanici. In: Capriotti, G., Iaccarino Idelson, A. Tensionamento dei dipinti su tela. Nardini Editore, Firenze. 2004 **(a)**. pages 15-55.
- Iaccarino Idelson, A. Studio del comportamento del sistema dipinto-telaio elastico. In Tensionamento dei dipinti su tela, ed. Capriotti, G. Iaccarino Idelson, A. Nardini editore Firenze. 2004 **(b)**. pages 57-90
- Iaccarino Idelson, A., Torre, M. Sviluppi della ricerca in collaborazione con l'ICR. In Tensionamento dei dipinti su tela, ed. Capriotti, G. Iaccarino Idelson, A. Nardini editore. Firenze. 2004. pages 91-113
- Iaccarino Idelson, A. A study on the correct value of tension for canvas paintings. Atti del Secondo Congresso del Gruppo Spagnolo dell'International Institute for Conservation, "Seminario Internacional de Conservaciòn de Pintura sobre Lienzo". Valencia, Spagna, 9-11 marzo 2005.

- Iaccarino Idelson, A. About the choice of tension for canvas paintings. CeROArt, 4. 2009. URL : http://ceroart.revues.org/index1269.html.
- Iaccarino Idelson, A. Aspetti strutturali della conservazione dei dipinti su tela. in Restauri d'arte. Opere dell'Abruzzo recuperate dopo il sisma. Arbace, L. Baratin, L. (ed.) Gabbiano Editore, Ancona. 2012.
- Iaccarino Idelson, A., Garofalo, V. Aiming at reproducibility in lining canvas paintings. A research on cold lining methods. in CeROArt [Online], 11 | 2019. http://journals.openedition.org/ceroart/6488 ; DOI : 10.4000/ceroart.6488
- Iaccarino Idelson, A., Alba, A., Bonetti, L., Serino, C. The conservation history and treatment of three large-scale paintings by Joan Miró: relieving Canvas distortions in highly reactive paintings with a gliding elastic tensioning system, in AIC Paintings Specialty Group Postprints 32. 47th Annual Meeting of the American Institute for Conservation of Historic and Artistic Works Uncasville, New England May, 2019.
- Iaccarino Idelson, A., Serino, C., Pesso, S., Tranquilli, G., Volpin, S. Davide e Golia, una grande tela di Tiziano danneggiata dall'acqua. Bollettino dell'Istituto Centrale per il Restauro, nuova serie n. 36, 2018. https://doi.org/10.5281/zenodo.14796006
- Iaccarino Idelson, A., Serino, C. The Use of Tension for Double-Sided Paintings, in: Structural treatments on double-sided paintings, Proceedings edited by Centro Conservazione e Restauro "La Venaria Reale", Sagep, Genova 2021.
- Iaccarino Idelson, A., Sánchez López, M., Groves, R. M. An open-source biaxial tensile tester with automated pre-tensioning for mechanical studies of canvas paintings. HardwareX. 2023. doi: https://doi.org/10.1016/j.ohx.2023.e00412
- Iaccarino Idelson, A., Bergsma, O., Groves, R. M. Methodology for measures of twist and crimp in historical textiles and canvas paintings supports, Journal of Cultural Heritage, vol. 71, pages 1-9, 2025 https://doi.org/10.1016/j.culher.2024.10.016 **(a)**
- Iaccarino Idelson, A. Le traitement du support du tableau de Tiepolo « Junon au milieu des nuées ». Techné n. 58, February 2025 **(b)**
- Iaccarino Idelson, A., Bergsma, O., & Groves, R. (2025). Quantitative Morphological Analysis of Warp and Weft Yarns in Historical Woven Structures. Studies in Conservation, 1–17. https://doi.org/10.1080/00393630.2025.2491250 **(c)**
- Janas, A., Fuster-López, L., Andersen, C.K., Escuder, A.V., Kozłowski, R., Poznańska, K., Gajda, A., Scharff, M., Bratasz, L. Mechanical properties and moisture-related dimensional change of canvas paintings–canvas and glue sizing. Herit Sci 10, 160. 2022. https://doi.org/10.1186/s40494-022-00794-3.
- Jiang, M., Sridhar, R.L., Robbins, A.B., Freed, A.D., Moreno, M.R. A versatile biaxial testing platform for soft tissues. Journal of the Mechanical Behavior of Biomedical Materials. 2021. 114. https://doi.org/10.1016/j.jmbbm.2020.104144
- Johnson, D. H., Johnson, C. R., Erdmann, R. G. Weave Analysis of Paintings on Canvas from Radiographs. Signal Processing 93, no. 3 (2013): 527–40. https://doi.org/10.1016/j.sigpro.2012.05.029

- Junhao, X., Zhang, Y., Yu, Q., Zhang, L. Analysis and design of fabric membrane structures: A systematic review on material and structural performance. Thin-Walled Structures 170 (2022) 108619. https://doi.org/10.1016/j.tws.2021.108619
- Kania, K. The spinning experiment: influences on yarn in spinning with a hand-spindle. In Hopkins, H. Ancient textiles, modern science: re-creating techniques through experiments. Proceedings of the First and Second European Textile Forum 2009 and 2010 - Oxford : Oxbow , 2013
- Karpowicz, A. A Study on Development of Cracks on Paintings. Journal of the American Institute for Conservation, Autumn, 1990, Vol. 29, No. 2, pp. 169-180
- Katz, K. B. The Quantitative Testing and Comparisons of Peel and Lap/Shear for Lascaux 360 H.V. and Beva 371. Journal of the American Institute for Conservation, 24:2, 1985. 60-68, DOI: 10.1179/019713685806028097
- Keck, S. Mechanical alteration of the paint film. Stud Conserv. 1969;14(1):9–30.
- Kolcavová Sirková, B., Mertová, I. Prediction of warp and weft crimp in the construction of dobby woven fabrics, The Journal of The Textile Institute, 111:10, 2020. 1401-1409, DOI: 10.1080/00405000.2019.1701967
- Kolcavova Sirkova, B., Vysanska, M. Methodology of evaluation of fabric geometry on the basis of fabric cross-section. Fibers & Textiles in Eastern Europe, 2012. 20, 41–47.
- Kovar, R. Length of the yarn in plain-weave crimp wave, The Journal of The Textile Institute, 102:7 (2011) 582-597, DOI: 10.1080/00405000.2010.498175
- Krarup Andersen, C., Mecklenburg, M., Scharff, M., Wadum, J. With the best intentions. Changed response to relative humidity in wax-resin impregnated lined early-19th-century canvas paintings ICOM-CC 17th triennial conference 2014 Melbourne.
- Kuiper, L., Hesterman, W. Report on the restoration of Rembrandt's Night Watch, Bulletin van het Rijksmuseum, Jaarg. 24, Nr. 1/2 (1976), pp. 14-51 http://www.jstor.org/stable/40381757
- Kvavadze E, Bar-Yosef O, Belfer-Cohen A, Boaretto E, Jakeli N, Matskevich Z, Meshveliani T. 30,000-year-old wild flax fibers. Science (New York, N.Y.). 2009; 325 (5946): 1359. http://dx.doi.org/10.1126/science.1175404. doi:10.1126/science.1175404
- Lee, D.SH., Kim, NS., Scharff, M. Nielsen, A. V., Mecklenburg, M., Fuster-López, L., Bratasz, L., Andersen, C. K. Numerical modelling of mechanical degradation of canvas paintings under desiccation. *Herit Sci* 10, 130 (2022). https://doi.org/10.1186/s40494-022-00763-w
- Lennard, F., Costantini, R. and Philip Harrison Investigating Stitched Support Techniques for Tapestry Using Digital Image Correlation, Studies in Conservation, (2022) DOI: 10.1080/00393630.2022.2083414
- Lewin, M. (Ed.). (2006). Handbook of Fiber Chemistry (3rd ed.). CRC Press. https://doi.org/10.1201/9781420015270
- Lubachevsky, B., Graham, R. Curved Hexagonal Packings of Equal Disks in a Circle. Discrete Comput Geom 18, 179–194 (1997). https://doi-org.tudelft.idm.oclc.org/10.1007/PL00009314

- Lukesova, H., Holst, B. Identifying plant fibres in cultural heritage with optical and electron microscopy: how to present results and avoid pitfalls. *Herit Sci* **12**, 12. 2024. https://doi.org/10.1186/s40494-023-01122-z
- Łukomski M, Bridarolli A, Fujisawa N. Nanoindentation of Historic and Artists' Paints. *Applied Sciences*. 2022; 12(3):1018. https://doi.org/10.3390/app12031018
- Malowany, K., Tymińska-Widmer, L., Malesa, M., Kujawińska, M., Targowski, P., and Rouba, B. Application of 3D digital image correlation to track displacements and strains of canvas paintings exposed to relative humidity changes. Applied Optics 53, 1739-1749 (2014). http://dx.doi.org/10.1364/AO.53.001739
- Maraghechi, S., Bosco, E., Suiker, A.S.J., Hoefnagels, J.P.M. Experimental characterisation of the local mechanical behaviour of cellulose fibres: an in-situ micro-profilometry approach. Cellulose 30, 4225–4245, (2023 a). https://doi.org/10.1007/s10570-023-05151-6
- Maraghechi, S., Dupont, AL., Cardinaels, R. *et al.* Assessing rheometry for measuring the viscosity-average degree of polymerisation of cellulose in paper degradation studies. *Herit Sci* **11**, 15 (2023 b). https://doi.org/10.1186/s40494-022-00855-7
- Markova, I. Textile Fiber Microscopy - A Practical Approach. John Wiley & Sons, 2019. ISBN 978-1-5231-2854-9
- Mecklenburg, M.F. Some Aspects of the Mechanical Behavior of Fabric-Supported Paintings. Report to the Smithsonian Institution, February 1982.
- Mecklenburg, M.F. (ed.) Art in transit: studies in the transport of paintings. International conference on the packing and transportation of paintings, September 9, 10, 11, 1991, London
- Mecklenburg, M.F., Tumosa, C.S., Erhardt, D., Vandiver, P.B., Mass, J.L., Murray, A. The changing mechanical properties of aging oil paints. In Materials Research Society Symposium, eds. P.B. Vandiver, J.L. Mass, and A. Murray, Materials Issues in Art and Archaeology 7, 2005. 13–24. Warrendale: Materials Research Society.
- Mecklenburg, M. F. Failure mechanisms in canvas supported paintings: approaches for developing consolidation protocols. Colour and conservation: materials and methods in the conservation of polychrome artworks: third international conference. Milano, Italy edited by Fuster López, Laura. Il prato, Saonara, Italy 2007
- Mecklenburg, M. An introduction to mechanics and the Giulio Cesare Procaccini double- sided banner. in: Structural treatments on double-sided paintings, Proceedings edited by Centro Conservazione e Restauro "La venaria Reale", Sagep, Genova 2021
- Mehra, V.R. Comparative Study of Conventional Relining Methods and Materials and Research towards their improvement. ICOM Committee for Conservation 3rd Triennial Meeting Madrid Spain 2-7 October 1972
- Mehra, V.R. Further developments in cold lining (nap-bond system). In Icom Committee for Conservation. 4th triennial meeting, Venice, 13-18 October. Preprints, Paris, Icom, 1975. pp. 7511
- Mehra, V. R. The cold lining of paintings In The Conservator, 5: 12-14. 1981. DOI : 10.1080/01410096.1981.9994946

- Mertova, I., Neckář, B., Muzaffar Ishtiaque, S. New method to measure yarn crimp in woven fabric. Textile Research Journal 2016, Vol. 86(10) 1084–1096
- Michalsky, S. Risk analysis of backing boards for paintings: damp climates vs cold climates. In Colore e conservazione: materiali e metodi nel restauro delle opere policrome mobili, congresso internazionale. Thiene, Italy 2004. Il Prato, Saonara, 2005
- Michalsky, S. Climate Guidelines for Heritage Collections: Where We Are in 2014 and How We Got Here. In Proceedings of the Smithsonian Institution Summit on the Museum Preservation Environment Edited by Sarah Stauderman and William G. Tompkins. Washington, D.C. Smithsonian Institution Scholarly Press, 2016. ISBN (online): 978-1-935623-87-8
- Michalski, S. A quantitative review of tensions affecting tear repair decisions. in: Structural treatments on double-sided paintings, Proceedings edited by Centro Conservazione e Restauro "La venaria Reale", Sagep, Genova 2021.
- Mora, P., Mora, L., Philippot, P. Conservation of wall paintings. London, Butterworth Publishers, 1984
- Morris, K., Rosenkranz, A., Seilbert, H., Ringel, L., Diebels, S., Talke, F.E. Uniaxial and biaxial testing of 3D printed hyperelastic photopolymers. Journal of Applied Polymer Science (2019) 137-8. https://doi.org/10.1002/app.48400
- Neckář, B., Das, D. Theory of Structure and Mechanics of Yarns, Woodhead Publishing India in Textiles Series, Woodhead Publishing India PVT. Limited, (2018) ISBN 9385059882, 9789385059889
- Neckář, B., Das, D. Computational methodology for determination of yarn twist and diameter, The Journal of The Textile Institute, (2019) 110:11, 1660-1671, DOI: 10.1080/00405000.2019.1611524
- Nimmo, M.; Paris, M.; Rissotto, L.; Bonetti, F.; Cappa, P. Tensioning gilded and painted leather. ICOM-CC 11th triennial meeting, Edimburg 1996. pp. 751-758.
- Noble, P., van Duijn, E., Hermens, E., Keune, K., van Loon, A., Smelt, S., Tauber, G., Erdmann, R. An Exceptional Commission. The Rijksmuseum Bulletin 66, no. 4, 2018. https://doi.org/10.52476/trb.9762
- Oriola, M., Možir, A., Garside, P., Campo, G., Nualart-Torroja, A., Civil, I., Odlyha, M., Cassar, M., Strlič, M. Looking beneath Dali's paint: non-destructive canvas analysis, Analytical Methods, 2014, 6, 86
- Oriola, M., Campo, G., Ruiz-Recasens, C., Pedragosa, N., Strlič, M. (2015) Collections care scenario appraisal for painting canvases at MuseuNacional d'Art de Catalunya, Barcelona, Spain, Studies in Conservation, 60:sup1, S193-S199, DOI: 10.1179/0039363015Z.000000000224
- Ostergard, E. Woven into the earth: textiles from Norse Greenland. Aarhus University Press, 2004
- Ozkaya, Y. A., Acar, M., Jackson, M. R. Yarn twist measurement using digital imaging. The Journal of The Textile Institute, 101:2, 2010. 91-100, DOI: 10.1080/00405000802263476

- Padfield, T., Borchersen, K. [ed.] Museum microclimates: contributions to the Copenhagen conference, 19-23 November 2007. National Museum of Denmark Museum 2007. ISBN: 9788776020804
- Pan, R., Gao, W., Li. Z, Gou, J., Zhang, J., Zhu, D. Measuring Thread Densities of Woven Fabric Using the Fourier Transform. Fibres & Textiles in Eastern Europe 1, no. 109, 2015.
- Penava, Z., Šimić Penava, D., Tkalec., M. Experimental Analysis of the Tensile Properties of Painting Canvas. AUTEX Research Journal (2015) 16 (4): 182–95. https://doi.org/10.1515/aut-2015-0023
- Percival-Prescott, W. The lining cycle: causes of physical deterioration in oil paintings on canvas: lining from the 17th century to the present day. in Villers, C., ed., Lining Paintings: Papers from the Greenwich Conference on Comparative Lining Techniques (1974). Archetype, London 2003
- Percival-Prescott, W. Report on the Greenwich lining conference. Icom CC triennial meeting Venice 1975
- Pereira, A.B., Fernandes, F.A.O., de Morais, A.B., Maio, J. Biaxial Testing Machine: Development and Evaluation. Machines. 2020. 8, 40. https://doi.org/10.3390/machines8030040
- Pernety, A. J. Dictionnaire portatif de peinture, sculpture et gravure. Paris 1757
- Phenix, A., Hedley, G. Lining without heat or moisture. In: Preprints of the 7th Triennial Meeting ICOM - committee for conservation, Copenhagen 10-14 September 1984. 40-44. DOI : 10.1080/01410096.1985.9995003
- Pierce, F. T. The geometry of cloth structure. Journal of the Textile Institute Transactions, 1937. 28:3, T45-T96, DOI: 10.1080/19447023708658809
- Postle, R., Carnaby, G.A., De Jong, S. The mechanics of wool structures. Chichester: Ellis Horwood Limited Publishers. 1988.
- Reynaud, C., Thoury, M., Dazzi, A., Latour, G., Scheel, M., Li, J., Thomas, A., Moulhérat, C., Didier, A., Bertrand, L. In-place molecular preservation of cellulose in 5,000-year-old archaeological textiles, Proc. Natl. Acad. Sci. U.S.A. 117 (33) 19670-19676, https://doi.org/10.1073/pnas.2004139117 (2020).
- Roche, A. Influence du type de chassis sur le vieillissement mecanique d'une peinture sur toile. Studies in Conservation, (1993) 38:1, 17-24, DOI: 10.1179/sic.1993.38.1.17
- Roche, A. Pressure-sensitive adhesives for the attachment of reinforcing canvases to the back of paintings, Studies in Conservation, 41:1, 1996. 45-54, DOI: 10.1179/sic. 1996. 41.1.45
- Roche A., Approche du principe de réversibilité des doublages des peintures sur toile, in Studies in Conservation, Vol. 48, N° 2, 2003, p. 85
- Roche, A. Comportement mécanique des peintures sur toile. Paris, CNRS Editions, 2003. Page 119

- Roche, A. Comportement mécanique des peintures sur toile : evaluation de la stabilité mechanique aux variations d'humidité et de temperature. International conference on paintings conservation Postprints. Universidad Politécnica de Valencia, Spain, 2005.
- Roche, A. La conservation des peintures modernes et contemporaines. Paris, CNRS Editions. 2016
- Roche A., Soldano A. The Effect of Changes in Environmental Conditions on the Mechanical Behaviour of Selected Paint Systems, Studies in Conservation (2018) 63:sup1, 216-221, DOI: 10.1080/00393630.2018.1504434
- Rota, E., Bozzi, C., Cremonesi, P., Lucchini, A. Study of the Best Methodology for Measuring Surface pH of Linen Canvas, Studies in Conservation, 66:6, 313-320, 2021 DOI: 10.1080/00393630.2020.1838711
- Rouba, B. J. "Die Leinwandstrukturanalyse und ihre Anwendung für die Gemäldekonservierung": Restauratorenblätter Band 13, Malerei und Textil, Wien 1992. p. 79-89
- Russell, W. H., Berger, G. A. The behavior of canvas as a structural support for painting: preliminary report. Studies in Conservation, 27 (1982):sup1, 139-145, DOI: 10.1179/sic.1982.27.Supplement-1.139
- Sauvage, L., Wei, W., Martinez, M. When Conservation Meets Engineering: Predicting the Damaging Effects of Vibrations on Pastel Paintings. Studies in Conservation. (2017) 63-1 418-420. https://doi.org/10.1080/00393630.2018.1504444
- Saville, B. P., and Textile Institute (Manchester, England). Physical Testing of Textiles. Cambridge, England, Boca Raton, Fla.: Woodhead Publishing, Ltd, in association with the Textile Institute; In North and South America by CRC Press, 1999. ISBN: 9781855733671
- Scharff, M., C.K. Andersen, and T. Filtenborg. 2021. Canvas-related microcracks in Danish 19th-century paintings. In Transcending Boundaries: Integrated Approaches to Conservation. ICOM-CC 19th Triennial Conference Preprints, Beijing, 17–21 May 2021, ed. J. Bridgland. Paris: International Council of Museums.
- Scicolone, G., Rossi, E., Sardella, A., Seves, A., Testa, G. Kinetics of cellulose fiber degradation and correlation with some tensile properties to plan consolidation or lining treatments. ICOM-CC, Edinburg 1996
- Seiler-Baldinger, A. Textiles: a classification of techniques. Smithsonian Institution Press, Washington, 1996. 1-56098-509-7
- Settles, G. S., Schlieren and shadowgraph techniques: Visualizing phenomena in transparent media, Berlin:Springer-Verlag, 2001
- Seymour, K. , Van Och, J. De- mystifying mist-lining. An introduction to the lining process and case studies. The picture restorer, 40, 2012. pp. 11-13.
- Shiwarski, D.J., Tashman, J.W., Eaton, A.F., Apodaca, G., Feinberg, A.W. 3D printed biaxial stretcher compatible with live fluorescence microscopy. HardwareX 7 (2020) e00095 https://doi.org/10.1016/j.ohx.2020.e00095
- Sorta, E. Studio preliminare sulla determinazione del modulo elastico di tele dipinte con metodo non distruttivo. In Problemi Di Conservazione / a Cura Di Giovanni Urbani.

Bologna: Editrice Compositori, 1973. The original paper can be found here: https://doi.org/10.5281/zenodo.14834185

- Sozzani, Laurent S., An Economical Design for a Microclimate Vitrine for Paintings Using the Picture Frame as the Primary Housing. Journal of the American Institute for Conservation 36 (1997); 95-107
- Sozzani, L., Iaccarino Idelson, A., Serino, C., Vos, L. Practical application of a constant tension elastic-stretching system. AIC Paintings Specialty Group Postprints 26, 2013.
- Stols-Witlox, M. A perfect ground. Archetype London, 2017
- Stoveland, L.P., Stols-Witlox, M., Ormsby, B. and Streeton N.L.W. 2021. Mock-ups and materiality in conservation research. In Transcending Boundaries: Integrated Approaches to Conservation. ICOM-CC 19th Triennial Conference Preprints, Beijing, 17–21 May 2021, ed. J. Bridgland. Paris: International Council of Museums.
- Tao, N., Anisimov, A. G., van Duijn, E., Vos, L., Steenman, I., Keune, K., Noble, P., Groves, R. M. Application of shearography with thermal loading for structural inspection of Rembrandt's Night Watch. Proceedings Volume 12620, Optics for Arts, Architecture, and Archaeology (O3A) IX; 126200A (2023) https://doi.org/10.1117/12.2673263
- Tassinari, E. Metodi di caratterizzazione delle tele da rifodero. In: Urbani, G. Problemi di Conservazione. Editore Compositori, Bologna 1973, pag 141. (**a**)
- Tassinari, E. Studio preliminare sul tensionamento delle tele da rifodero. in: Urbani, G. Problemi di Conservazione Editore Compositori, Bologna 1973, pag 183. (**b**)
- Tassinari, E. Characterization of lining canvases. In Villers, C., ed., Lining Paintings: Papers from the Greenwich Conference on Comparative Lining Techniques (1974). Archetype, London 2003.
- Te Marvelde, M. How Dutch is 'The Dutch Method'? A History of Wax-resin Lining in its International Context. In *Past Practice – Future Prospects*, A. Oddy and S. Smith (eds.), The British Museum Occasional Paper, 2001, no. 145, 143-149.
- Textile terms and definitions, The textile institute, Manchester 1975.
- Tiennot, M., Paardekam, E., Iannuzzi, D., Hermens, E. Mapping the mechanical properties of paintings via nanoindentation: a new approach for cultural heritage studies. Sci Rep 10, 7924 (2020). https://doi.org/10.1038/s41598-020-64892-7
- Timar-Balazsy, A., Eastop, D. Chemical Principles of Textile Conservation. 1998 Oxford: Butterworth-Heinemann.
- Torrioli, N. Le tele per la pittura. In Maltese, C. (ed), I supporti nelle arti pittoriche. Storia, tecnica e restauro, Mursia, Milano 1990, pp. 49-111.
- Tumosa, C. S., Mecklenburg, M. F. The influence of lead ions on the drying of oils. Studies in Conservation, 50:sup1, 39-47, (2005) DOI: 10.1179/ sic.2005.50.Supplement-1.39
- Urbani, G. Proposition pour un programme de recherche sur la conservation des peintures sur toile. Comité de l'ICOM pour la conservation Amsterdam, 14-19 septembre 1969.
- Urbani, G. (ed) Problemi di Conservazione. Editore Compositori, Bologna 1973.

- Usman, A., Hussain, T., Jabbar, A. (2014) Effect of cotton fiber and yarn characteristics on color variation in woven fabric dyed with vat dyes, The Journal of The Textile Institute, 105:12, 1287-1292, DOI: 10.1080/00405000.2014.887239
- Van Craenenbroeck, M., Mollaert, M., De Laet, L. The influence of test conditions and mathematical assumptions on biaxial material parameters of fabrics. Engineering Structures. (2019) 200: 109691. https://doi.org/10.1016/j.engstruct.2019.109691
- van de Wetering, E. Rembrandt: The Painter at Work. Amsterdam University Press, 1997
- van der Maaten, L., Erdmann, R. Automatic Thread-Level Canvas Analysis. A Machine-Learning Approach to Analyzing the Canvas of Paintings. Signal Processing Magazine, July 2015, pp. 38-45.
- Van Och, J., Hoppenbrouwers, R. Mist-lining and low-pressure envelopes: an alternative lining method for the reinforcement of canvas paintings. Zeitschrift für Kunsttechnologie und Konservierung, 2003, Vo.17, Number 1, pp. 116 – 128
- Vandivere, A., van Loon, A., Dooley, K.A., Haswell, R., Erdmann, R. G., Leonhardt, E., Delaney, J.K. Revealing the painterly technique beneath the surface of Vermeer's Girl with a Pearl Earring using macro- and microscale imaging. Herit Sci 7, 64 (2019). https://doi.org/10.1186/s40494-019-0308-4
- Vasari, G./ le Vite dei più eccellenti pittori, scultori e architetti. Roma, Newton 2002.
- Villers, C. Introduction. In Villers, C., ed., Lining Paintings: Papers from the Greenwich Conference on Comparative Lining Techniques. Archetype, London 2003 (**a**), pages XII-XV.
- Villers, C., ed., Lining Paintings: Papers from the Greenwich Conference on Comparative Lining Techniques. Archetype, London 2003 (**b**)
- Wang, Y., Xiaogang, C., Young, R., Kinloch, I. A Numerical and Experimental Analysis of the Influence of Crimp on Ballistic Impact Response of Woven Fabrics. Composite Structures 140, 2016, 44–52. https://doi.org/10.1016/j.compstruct.2015.12.055.
- Wolters, C. The care of paintings: the fabric paint supports. Museum, vol. 13 n. 3, 1960
- Yamamoto, H., Sassus, F., Ninomiya, M., Gril, J. A model of anisotropic swelling and shrinking process of wood. Wood Science and Technology 35, 167–181 (2001). https://doi.org/10.1007/s002260000074
- Young, C. and Hagan, E. (2008) Cold temperature effects of modern paints used for priming flexible supports. In: Townsend, J. H., Doherty, T., Heydenreich, G. and Ridge, J. (eds.) *Preparation for Painting: The Artist's Choice and its Consequences.* Archetype Publications: London, pp. 172-179. ISBN 9781904982326
- Young, C.R.T. Ph.D. Measurement of the biaxial tensile properties of paintings on canvas. University of London 1996 (**a**)
- Young, C.R.T. Biaxial Properties of Sized Cotton-Duck., Edinburgh ICOM-CC 11th triennial meeting, 1996 (**b**). ISBN: 1-873936-50-8

- Young, C. Measurement of the biaxial properties of nineteenth century canvas primings using electronic speckle interferometry. Optics and Lasers in Engineering 31 (1999) 163-170. https://doi.org/10.1016/S0143-8166(99)00007-X
- Young, C. R. T., Hibberd, R. D. Biaxial tensile testing of paintings on canvas. Studies in Conservation, 1999, 44(2). 129–141. https://doi.org/10.1179/sic.1999.44.2.129
- Young, C., Ackroyd, P., Hibberd, R., Gritt, S. 'The Mechanical Behaviour of Adhesives and Gap Fillers for re-joining Panel Paintings'. National Gallery Technical Bulletin Vol 23, 2002, pp 83–96.
- Young, C., Jardine, S. Fabrics for the Twenty-First Century: As Artist Canvas and for the Structural Reinforcement of Easel Paintings on Canvas. Studies in Conservation, 2012, 57(4):237–25. DOI: 10.1179/2047058412Y.0000000007

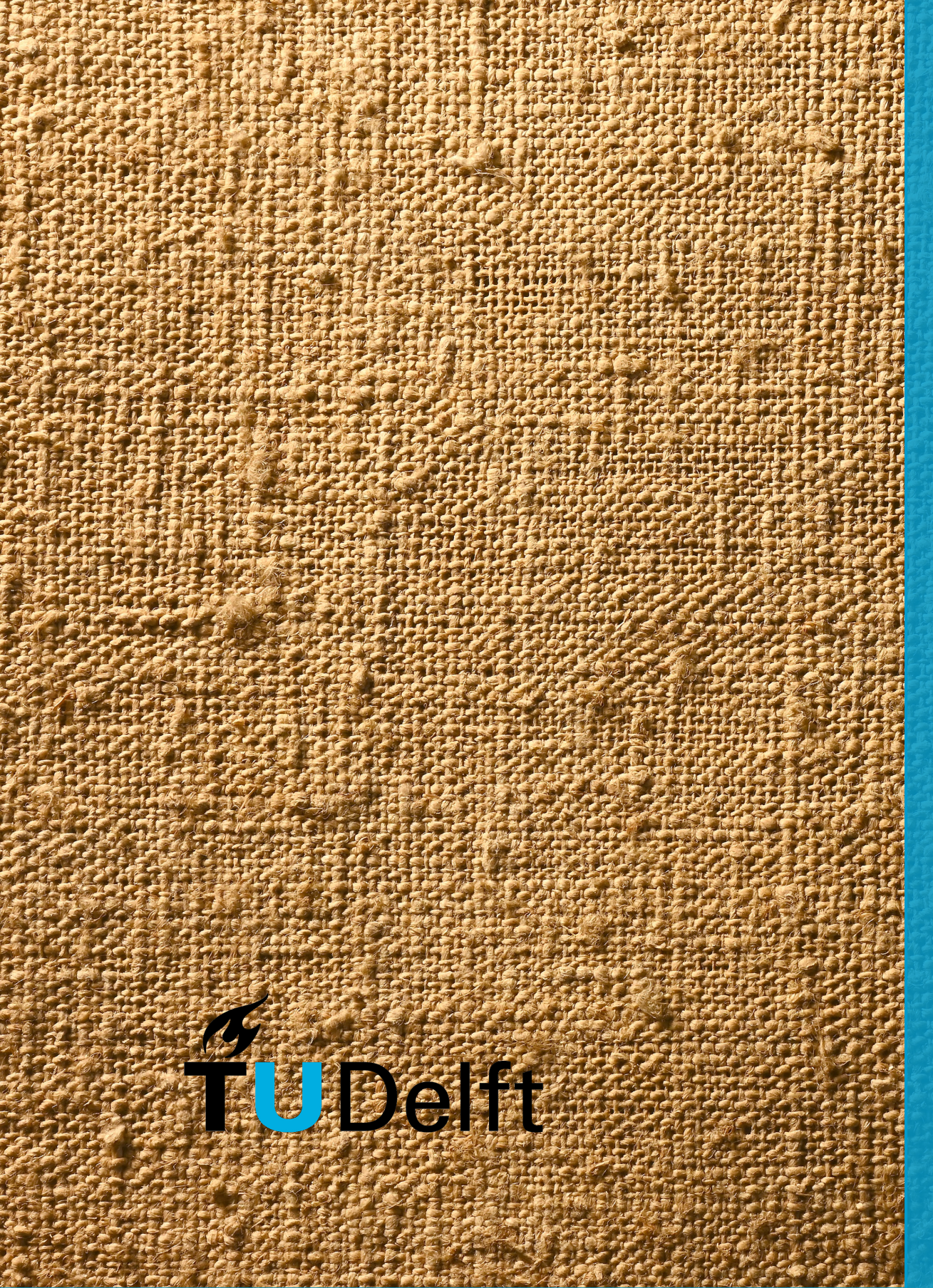
TU Delft